Uncertainty Quantification and Prediction for Non-autonomous Linear and Nonlinear Systems

by

Akash Phadnis

M.Tech. and B.Tech, Indian Institute of Technology Bombay (2011)

Submitted to the Department of Mechanical Engineering
in partial fulfillment of the requirements for the degree of

Master of Science in Mechanical Engineering

at the

MASSACHUSETTS INSTITUTE OF TECHNOLOGY

September 2013

Author .....
Department of Mechanical Engineering
July 31, 2013

Certified by .....
Pierre F. J. Lermusiaux
Associate Professor of Mechanical Engineering
Thesis Supervisor

Accepted by .....
David E. Hardt
Chairman, Department Committee on Graduate Theses

Uncertainty Quantification and Prediction for Non-autonomous Linear and Nonlinear Systems

by

Akash Phadnis

Submitted to the Department of Mechanical Engineering
on July 31, 2013, in partial fulfillment of the
requirements for the degree of
Master of Science in Mechanical Engineering

Abstract

The science of uncertainty quantification has gained a lot of attention over recent years. This is because models of real processes always contain some elements of uncertainty, and also because real systems can be better described using stochastic components. Stochastic models can therefore be utilized to provide a most informative prediction of possible future states of the system. In light of the multiple scales, nonlinearities and uncertainties in ocean dynamics, stochastic models can be most useful to describe ocean systems.

Uncertainty quantification schemes developed in recent years include order reduction methods (e.g. proper orthogonal decomposition (POD)), error subspace statistical estimation (ESSE), polynomial chaos (PC) schemes and dynamically orthogonal (DO) field equations. In this thesis, we focus our attention on DO and various PC schemes for quantifying and predicting uncertainty in systems with external stochastic forcing. We develop and implement these schemes in a generic stochastic solver for a class of non-autonomous linear and nonlinear dynamical systems. This class of systems encapsulates most systems encountered in classic nonlinear dynamics and ocean modeling, including flows modeled by Navier-Stokes equations. We first study systems with uncertainty in input parameters (e.g. stochastic decay models and Kraichnan-Orszag system) and then with external stochastic forcing (autonomous and non-autonomous self-engineered nonlinear systems). For time-integration of system dynamics, stochastic numerical schemes of varied order are employed and compared. Using our generic stochastic solver, the Monte Carlo, DO and polynomial chaos schemes are intercompared in terms of accuracy of solution and computational cost.

To allow accurate time-integration of uncertainty due to external stochastic forcing, we also derive two novel PC schemes, namely, the reduced space KLgPC scheme and the modified TDgPC (MTDgPC) scheme. We utilize a set of numerical examples to show that the two new PC schemes and the DO scheme can integrate both additive and multiplicative stochastic forcing over significant time intervals. For the final example, we consider shallow water ocean surface waves and the modeling of these waves by deterministic dynamics and stochastic forcing components. Specifically, we time-integrate the Korteweg-de Vries (KdV) equation with external stochastic forcing, comparing the performance of the DO and Monte Carlo schemes. We find that the DO scheme is computationally efficient to

integrate uncertainty in such systems with external stochastic forcing.

Thesis Supervisor: Pierre F. J. Lermusiaux
Title: Associate Professor of Mechanical Engineering

Acknowledgments

I would like to express my sincere gratitude towards my advisor, Prof. Pierre Lermusiaux, for introducing me to this fascinating topic and for providing invaluable guidance and support throughout the course of this work. His enthusiasm and energy, along with his helpful comments and words of encouragement, have been instrumental in producing this thesis. I would also like to thank Wayne, Pat, Marcia and Leslie for all their help during my stay at MIT.

I am also grateful to the rest of the MSEAS group, and in particular to Matt, Tapovan and Jing for their support and for the numerous exciting and informative discussions I had with them, without which, this thesis would not have been possible.

Finally, I would like to thank my family and friends, for always being there for me and for constantly showering me with everlasting love and affection.

Contents

List of Figures

List of Tables

Chapter 1

Introduction

1.1 Background and Motivation

Over recent years, stochastic modeling and uncertainty quantification (UQ) have become essential means of study in a wide variety of application areas. Today, stochastic models play a prominent role in studying systems in many diverse fields such as biology, mechanics, economics and finance, weather, ocean and climate predictions and so forth. These stochastic models take into account system and input variability as well as modeling and data errors, and hence provide a more comprehensive understanding of the system when compared to their deterministic counterparts. They also provide a more informative prediction of the future state of the system. These attributes make them very well suited for applications involving systems with high amount of variability and uncertainty. One such field of study where stochastic modeling is starting to be used extensively is ocean modeling.

Oceans are highly dynamical and complex environments with countless physical and biological processes taking place simultaneously. These processes, many of which are nonlinear, take place over a wide range of temporal and spatial scales and often interact with one another, making them difficult to observe and study individually (Lermusiaux, 2006). Due to such challenges, the models formulated to study these coupled nonlinear ocean systems are often imperfect. There are several sources of uncertainties in ocean models. These include, but are not limited to, modeling of a restricted range of tempo-

ral and spatial scales (Nihoul and Djenidi, 1998), limited knowledge of processes within this modeled scale window, limited coverage and accuracy of measurement data, approximations in interactions between various processes and miscalculations due to numerical implementations (Lermusiaux et al., 2006). To account for these uncertainties, in most systems, it is a common practice to assume random components for some parameters of the dynamical equations and/or for some of the initial and boundary conditions. This type of randomness is called uncertainty in input parameters. It has drawn considerable attention over the last few years and substantial progress has been made in modeling such systems, especially to account for initial input uncertainties. Although this type of approach to modeling uncertainty is suitable for a large number of ocean systems, there are many cases where considering randomness only in the form of input parameters is not enough. For example, for studying systems where multiple scales are involved, the effect of unresolved processes outside the modeled scale window needs to be incorporated into the governing dynamical equations. Often times, it is not possible to parameterize such effects in terms of the initial input parameters of the dynamical equations. Sometimes, these unresolved sub-scale processes may have a dependence on a phenomenon not directly related to the main process being studied. In such cases, it is suggested that the resulting uncertainty be modeled in the form of additional stochastic terms in the governing dynamical equations of the system (Müller and Henyey, 1997). This type of randomness is known as uncertainty due to external stochastic forcing or stochastic noise, and the resulting dynamical equations are known as stochastic partial differential equations (SPDEs).

The easiest way to model stochastic systems is through Monte Carlo simulations. However, Monte Carlo schemes can have a high computational cost and may become inefficient or even infeasible to implement for high dimensional systems. As a result, alternate methods for uncertainty quantification and prediction have been developed and significant progress has been made for systems with uncertainty in input parameters. Some of these schemes include generalized Polynomial Chaos (gPC) (for e.g., see the works of (Ghanem and Spanos, 1991), Xiu and Karniadakis (2002), Debusschere et al. (2002), Le Maitre et al. (2002), Knio and Le Maitre (2006)) and its several variations

(Wan and Karniadakis, 2005, Gerritsma et al., 2010, Hou et al., 2006, Le Maitre et al., 2004a), as well as Proper Orthogonal Decomposition (POD) (Berkooz et al., 1993, Holmes et al., 1998, Gay and Ray, 1995).

For modeling systems with external stochastic forcing, a major challenge stems from the difficulties in solving stochastic partial differential equations, in part due to lack of regularities with respect to time. Additionally, modeling stochastic noise involves dealing with a constant influx of randomness, which becomes very expensive to handle over larger time scales, especially for most of the aforementioned methods. Monte Carlo simulations have thus been the method of choice for such larger time simulations with external stochastic forcing. However, in the past fifteen years, methodologies that aim to optimally and dynamically capture most of the uncertainty have been derived and utilized. Such methodologies utilize the property that many nonlinear systems concentrate most of their stochastic energy in a subspace of dimension much smaller than the true dimension of the system. In other words, they consider stochastically forced nonlinear systems of probability measure that decays rapidly away from the mean or that is sufficiently localized by nonlinear effects. In these situations, focusing on capturing uncertainty in the dynamical stochastic subspace is efficient. One such method is the Error Subspace Statistical Estimation (ESSE) scheme (Lermusiaux and Robinson, 1999, Lermusiaux, 1999) developed for optimal state estimation and data assimilation. ESSE aims to adaptively predict the dominant eigenvalue decomposition of the system covariance, using a Monte Carlo scheme for the nonlinear evolution of this error subspace and a learning scheme for adapting the subspace. It was utilized for systems with uncertain parameters, with uncertain initial and boundary conditions, and with stochastic forcing. More recently, Dynamically Orthogonal (DO) equations (Sapsis and Lermusiaux, 2009, Sapsis, 2010) were obtained, aiming to predict the dominant uncertainty of nonlinear systems. These differential equations govern the mean and a reduced time-dependent Karhunen-Loève (K-L) expansion of the system state. Applications of DO equations have so far mostly focused on uncertainty arising due to initial and boundary conditions only. One of the motivations of this thesis is thus uncertainty quantification and prediction for nonlinear systems with stochastic forcing.

The present research is concerned with the development, implementation and evaluation of uncertainty quantification and prediction schemes for dynamical systems of a general class. Existing schemes are first applied to a range of specific dynamics systems belonging to that class and the results are intercompared. These schemes are then modified and improved so as to be able to deal with additive and multiplicative stochastic forcing of varied types over significant periods of time. The implementation of the general class of stochastic dynamical systems and varied solution methods is generic. The resulting computational framework allows the incubation of methods and the scientific and engineering investigation of varied questions related to stochastic dynamical systems, including more realistic ocean systems. The specific ocean science application considered in this thesis is shallow water ocean surface waves and the modeling of these waves by deterministic dynamics and stochastic forcing components. As mentioned above, such stochastic forcing would then model the statistics of the waves not governed by the deterministic components, for example, the smaller-scale surface waves and the remotely forced (incoming) waves.

The governing equations for the class of non-autonomous linear and nonlinear stochastic dynamical systems that we consider is defined by the general stochastic differential system of equations of the form

$$dX(r,t;\omega) = A(X(r,t;\omega),t)\,X(r,t;\omega)dt + B(X(r,t;\omega),t)\,dW(t;\omega) \qquad (1.1)$$

where $X(r,t;\omega)$ represents an N-dimensional *stochastic field*, $W(t;\omega)$ represents an m-dimensional *Brownian motion*, r is a multi-dimensional spatial variable, t is time, and ω are elementary events representing the uncertainty. $A(X(r,t;\omega),t)$ and $B(X(r,t;\omega),t)$ represent the deterministic and stochastic components of the system dynamics respectively. The above system (1.1) is said to be non-autonomous when A and B are explicitly dependent on t, because this dependence is then not modeled within the system (1.1) but is provided from an external (and possibly dynamical) influence. When t represents time (as is the case here), the non-autonomous system is then also simply said to be time-variant.

In order to develop an efficient generic solver, we only consider systems where A and B

have at most a linear dependence in $X(r,t;\omega)$. We note that this is not a strong limitation since many highly nonlinear and high-dimensional ocean systems directly belong to this class when their governing equations are discretized in space or when they can be simplified to systems of that class. For example, fluid flows modeled by Navier-Stokes equations and classic conservation equations, and thus most ocean circulation and wave models, when discretized in space, fall under this class of nonlinear systems. Most (low dimensional) systems that are the hallmarks of strongly nonlinear or chaotic dynamical system theory (Strogatz, 2001) also fall under this class (e.g., the Lorenz system, Rössler attractor etc). As we will see, the resulting quadratic nonlinearities in $X(r,t;\omega)$ (due to the linear-in-$X(r,t;\omega)$ assumption on A and B) restrict the computation of statistics to third moments. For this assumption, we can re-write the matrices A and B as

$$\begin{aligned} A(X(r,t;\omega),t) &= A_0(r,t;\omega) + A_1(X(r,t;\omega),t) \\ B(X(r,t;\omega),t) &= B_0(r,t;\omega) + B_1(X(r,t;\omega),t) \end{aligned} \tag{1.2}$$

where $A_0(r,t;\omega)$ and $B_0(r,t;\omega)$ are functions in time, space and uncertainty (ω) only and $A_1(X(r,t;\omega),t)$ and $B_1(X(r,t;\omega),t)$ are linear in $X(r,t;\omega)$. This assumption has been used to develop a computationally efficient solver which can be utilized for studying uncertainty in a large variety of nonlinear systems.

As discussed earlier, most ocean models involve multi-scale, nonlinear and high dimensional systems. Computational cost is often the limiting factor in modeling such systems, especially when they involve stochastic inputs and forcing. In this work, we utilize the property that for a subset of the dynamical systems described by (1.1) or (1.2), the computational cost of uncertainty quantification schemes can be reduced significantly. This occurs when the system's deterministic and stochastic dynamics (represented by matrices A and B respectively) have singular value decompositions (SVDs) with rapidly decaying singular values. This is the case with most high-dimensional ocean models. Of course, these singular values vary in general with X and with time (as both A and B vary with time), such that the reduction approach needs to adapt.

In what follows, we first state our problem statement and research objectives and summarize the work accomplished. Then, we provide an outline of the thesis.

1.2 Problem Statement and Research Objectives

The problem statement for the present work is to evaluate existing and develop new uncertainty quantification and prediction schemes for a class of non-autonomous linear and nonlinear stochastic dynamical systems, which are represented by equations (1.1) and (1.2), and to implement a computationally efficient framework for the resolution of these generic equations (1.2) such that it can be utilized for future incubation of methodologies and future scientific and engineering inquiries involving such stochastic systems.

The specific objectives of the present research are twofold. The first is to study dynamically orthogonal field equations and polynomial chaos schemes and to compare their performance. The new focus is on studying the applicability of these schemes for modeling uncertainty due to external stochastic forcing, specifically for ocean systems. Since generalized polynomial chaos has limitations in modeling stochastic forcing over large time intervals, two new schemes using the polynomial chaos framework are developed. These schemes are capable of modeling stochastic noise over arbitrarily large time intervals. The second objective is to develop a generic solver for future incubation of methods for uncertainty quantification and prediction for a wide class of systems, and to utilize the solver to study the stochastic characteristics of coupled nonlinear ocean systems. Towards this goal, a computationally efficient solver for the solution of the general stochastic differential equations (1.2) is developed and is used for studying shallow water ocean surface waves governed by the Korteweg-de Vries (KdV) equation with stochastic noise.

For the existing uncertainty quantification and prediction methods, we focus on the dynamically orthogonal equations and polynomial chaos schemes. The corresponding equations for evolution of uncertainty for systems (1.2) are derived using these stochastic modeling schemes. First, uncertainty in input parameters is studied using the example of a one-dimensional stochastic ODE and later using the Kraichnan-Orszag three mode problem. The accuracy and computational cost of the UQ schemes are examined and some limitations are discussed. Next, uncertainty due to external stochastic forcing is analyzed. It is seen that all the existing classic polynomial chaos schemes have an inherent limitation in modeling stochastic noise over large time intervals. Two novel polynomial chaos methods (KLgPC and modified TDgPC) for modeling stochastic noise over an arbitrarily

large time interval are introduced. A few self-engineered model test cases are integrated using dynamically orthogonal field equations and the new polynomial chaos schemes, and their performance is investigated. In order to investigate the likely performance of the UQ schemes at modeling more realistic ocean systems, a 20-dimensional time-dependent test case with external stochastic forcing has been engineered. The results of the different schemes are compared and their relative merits and limitations are explained. Subsequently, a stochastic ocean system (Korteweg de-Vries equation with external stochastic forcing) is considered and integrated with different schemes, and the resulting uncertainty characteristics are examined.

1.3 Thesis Outline

Chapter 2 develops the background for uncertainty quantification of dynamical systems. The first part reviews the concepts of stochastic processes and stochastic differential equations (SDEs). A basic understanding of Brownian motion is developed, and the Itô and Stratonovich form of stochastic integrals are defined. Next, the notions of strong and weak convergence are presented and numerical integration schemes for the weak approximation of solutions of Itô form of stochastic differential equations are studied. The later part of chapter 2 deals with uncertainty quantification methods for non-autonomous dynamical systems. Monte Carlo simulations, dynamically orthogonal (DO) field equations and polynomial chaos schemes are described in greater detail. In chapter 3, dynamically orthogonal field equations and polynomial chaos schemes have been applied to stochastic non-autonomous systems described by equations (1.1) and (1.2), and the evolution equations for the stochastic field have been derived. Building on an existing time-dependent generalized polynomial scheme, a new modified TDgPC (MTDgPC) scheme is developed in such a way as to enable it to handle time-integration of stochastic forcing. Furthermore, a novel reduced space and reduced order scheme in the polynomial chaos framework (KLgPC) capable of integrating stochastic noise over arbitrarily large time intervals is introduced. Chapter 4 focuses on systems with uncertainty in input parameters. The examples studied in this chapter include a one-dimensional stochastic decay model and the Kraichnan-Orszag three mode problem. Solutions of these systems have been presented,

followed by a discussion on the performance of UQ schemes. Chapter 5 addresses uncertainty due to external stochastic forcing. A basic limitation of existing polynomial chaos schemes in modeling stochastic noise is discussed. The two new polynomial chaos schemes introduced in chapter 3, namely the MTDgPC and KLgPC schemes, are used for integrating systems with uncertainty due to external stochastic forcing of both additive and multiplicative nature. Chapter 6 deals with uncertainty quantification of stochastic ocean systems. The implementation of DO and KLgPC schemes on a reduced subspace is studied using a 20-dimensional self-engineered test case with external stochastic forcing and the performance of the two schemes is compared. Next, the Korteweg-de Vries (KdV) equation is introduced and its deterministic solutions are obtained using the Zabosky-Kruskal (Z-K) numerical scheme. Then, using our computationally efficient stochastic solver, KdV equation with uncertainty due to external stochastic forcing is time-integrated and its uncertainty characteristics are examined. Conclusions and directions for future research are presented in chapter 7.

Chapter 2

Background

In this chapter, we review the background theory for studying uncertainty quantification and prediction of dynamical systems. We begin with an overview of the basic theory and definitions related to stochastic algebra. Next we study numerical integration schemes for the solution of stochastic differential equations (SDEs), and intercompare their accuracy and computational costs. In the later part of the chapter, we present a literature review on existing methods for uncertainty quantification, including a detailed description of the generalized polynomial chaos (gPC) scheme, time-dependent generalized polynomial chaos (TDgPC) scheme, Wiener chaos using sparse truncation and dynamically orthogonal (DO) equations.

2.1 Basic Theory and Definitions

2.1.1 Stochastic processes and random fields

Let $(\Omega, \mathcal{F}, \mathcal{P})$ be a *probability space*. Ω is the sample space, which is a set of all possible outcomes of a random experiment. An event $\mathcal{A}$ is a subspace of the sample space Ω. It is a set of outcomes to which a probability is assigned. $\mathcal{F}$ is the σ-algebra associated with Ω. It is a set consisting of measurable subsets of Ω. Its elements are events about which it is possible to obtain information. $\mathcal{P}$ is the probability measure, $\mathcal{P} : \mathcal{F} \to [0, 1]$ such that

1. $\mathcal{P}(\Omega) = 1$

2. $0 \leq \mathcal{P}(\mathcal{A}) \leq 1$

3. $\mathcal{P}(\mathcal{A}_i \cup \mathcal{A}_j) = \mathcal{P}(\mathcal{A}_i) + \mathcal{P}(\mathcal{A}_j)$, if $\mathcal{A}_i \cap \mathcal{A}_j = \emptyset$

A function Y is said to be $\mathcal{F}$-measurable if $Y^{-1}(B) \in \mathcal{F}$, for every Borel set $B \in \mathcal{B}$ in $\mathbb{R}$. A *random variable* $X(\omega)$ defined on the probability space $(\Omega, \mathcal{F}, \mathcal{P})$ is a real valued $\mathcal{F}$-measurable function $X : \Omega \to \mathbb{R}$. In simple words, a random variable is a real-valued measurable quantity, whose value is based on the outcome $\omega \in \Omega$ of a random experiment.

A *stochastic process* or *random process* $X(t;\omega)$ is a real-valued measurable function $X : [0,\infty) \times \Omega \to \mathbb{R}$, where t is the time variable $t \in [0,\infty)$. One can also consider stochastic processes based on finite time intervals. Often times, when the dependence on ω is not required to be shown explicitly, the stochastic processes are represented simply as $X(t)$. Stochastic processes can be thought of in two ways (Hunter, 2009). If we fix $\omega \in \Omega$, we have $X^\omega : t \mapsto X(t;\omega)$. X^ω is called a sample path or realization of the stochastic process. Similarly, if we fix $t \in [0,\infty)$, we have $X_t : \omega \mapsto X(t;\omega)$. From this viewpoint, a stochastic process may also be thought of as a collection of random variables $\{X_t\}$ indexed by the time variable $0 \leq t < \infty$. Consider a spatial domain $D \subseteq \mathbb{R}^3$ and a time domain $\mathcal{T} \subseteq [0,\infty)$. A *stochastic field* or *random field* $X(r,t;\omega)$ is defined as a real-valued measurable function $X : D \times \mathcal{T} \times \Omega \to \mathbb{R}^m$.

2.1.2 Brownian motion and stochastic differential equations

In order to model and study uncertainty due to external stochastic forcing, it is imperative to understand Stochastic Differential Equations (SDEs). These are differential equations consisting of a deterministic part and an additional stochastic part described by a Brownian motion (see Jazwinski (1970), Øksendal (2010) for detailed theory). In 1827, biologist Robert Brown, while studying pollen particles floating in water in the microscope, observed minute particles in the pollen grains executing jittery motion but was not able to determine the theory behind this motion (Brown, 1828). This random jittery motion later came to be known as Brownian motion, named after the biologist. The first theory of Brownian motion was given by Louis Bachelier in his PhD thesis "The theory of speculation" in 1900 (Bachelier, 1900). It was later in 1905, when Albert Einstein used

a probabilistic model to sufficiently explain Brownian motion, that it came to be recognized as an important topic of research (Einstein, 1905). The construction and existence of Brownian motion as it is known today, was established by Norbert Wiener in 1923 (Wiener, 1923), who was a professor of mathematics at MIT. One-dimensional Brownian motion also came to be known as a Wiener process, in honor of the great mathematician.

A scalar *standard Brownian motion*, also known as a one-dimensional *standard Wiener process*, defined over time period $t \in [t_0, T]$, is a random variable $W(t)$ that depends continuously on t. For t', t such that $t_0 \leq t' < t \leq T$, the random variable $\Delta W(t, t') = W(t) - W(t')$ is Gaussian with mean $\mu = 0$ and variance $\sigma^2 = t - t'$. Equivalently, $\Delta W(t, t') \sim \sqrt{t - t'}\mathcal{N}(0, 1)$ (Higham, 2001). In order to be called a standard Brownian motion, the random variable $W(t)$ should satisfy the following three conditions:

1. $W(0) = 0$ (with probability 1)
2. For $t_0 \leq t' < t \leq T$, $\Delta W(t, t') = W(t) - W(t')$ is Gaussian with mean $\mu = 0$ and variance $\sigma^2 = t - t'$, i.e., $\Delta W(t, t') \sim \sqrt{t - t'}\mathcal{N}(0, 1)$
3. For $t_0 \leq t' < t < u < v \leq T$, the increments $\Delta W(t, t') = W(t) - W(t')$ and $\Delta W(v, u) = W(v) - W(u)$ are independent random variables

It is useful to consider discretized Brownian motion for computational purposes, where $W(t)$ is specified at discrete values of time t. Let us consider the time interval $[0, T]$ and divide it into n steps by setting $h = T/n$, for some positive integer n. Let us denote $W(t_j)$ by W_j, where $t_j = jh$ $(j = 0, 1, 2, ..., n - 1)$. We have $W_0 = 0$ from condition 1 for Brownian motion. Also, from conditions 2 and 3, we get

$$W_j = W_{j-1} + dW_j \qquad j = 1, 2, ..., n \tag{2.1}$$

where each dW_j is an independent random variable such that $dW_j \sim \sqrt{h}\mathcal{N}(0, 1)$.

A scalar stochastic differential equation is of the form

$$dX(t) = a(X(t), t)dt + b(X(t), t)dW(t) \qquad X(0) = X_0, \ t \in [0, T] \tag{2.2}$$

where $a(X(t), t)$ and $b(X(t), t)$ are scalar functions of the continuously time-dependent

scalar stochastic process $X(t)$, and the initial condition $X(0) = X_0$ is a random variable. Here, $W(t) = \int_0^t dW(\tau)$ represents a standard Brownian motion path over the time domain [0,T]. The function $a(X(t), t)$ characterizes the deterministic part of the SDE and is called the *drift coefficient.* On the other hand, the function $b(X(t), t)$ characterizes the stochastic part and is known as the *diffusion coefficient.* In its integral form, equation (2.2) is written as

$$X(t) = X(0) + \int_0^t a(X(\tau), \tau)d\tau + \int_0^t b(X(\tau), \tau)dW(\tau) \qquad t \in [0, T] \tag{2.3}$$

The first integral on the right hand side of the equation is an ordinary Riemann integral, whereas the second integral is a stochastic integral along the Brownian motion path, which will be discussed in greater detail in section 2.1.3. A general N-dimensional SDE with an m-dimensional driving Wiener process is given as

$$X(t) = X(0) + \int_0^t a(X(\tau), \tau)d\tau + \sum_{j=1}^{m} \int_0^t b_j(X(\tau), \tau)dW_j(\tau) \qquad t \in [0, T] \tag{2.4}$$

where $X(t)$ is an N-dimensional stochastic process and $b_j(X(t), t)$ $(j = 1, 2, ..., m)$ are m diffusion coefficients corresponding to the m independent Brownian motion paths $W_j(t) = \int_0^t dW_j(\tau)$ represented in equation (2.4). From here onwards, we will omit the explicit time-dependence of $a(X(t), t)$ and $b_j(X(t), t)$, i.e., as if the systems were time-invariant or autonomous, in order to simplify the notation. However, all numerical properties and schemes discussed later still apply to the non-autonomous case.

2.1.3 Stochastic integrals and their convergence

Brownian motion is complex mathematically because it is not differentiable at any point and hence the rules of ordinary calculus are not applicable to it. For a given ordinary function $f(t)$, the integral $\int_0^T f(t)dt$ can be approximated by a Reimann sum as

$$\int_0^T f(t)dt = \sum_{j=0}^{n-1} f(t_j)(t_{j+1} - t_j) \tag{2.5}$$

where $t_j = jh$ $(j = 0, 1, 2, ..., n-1)$ and $h \to 0$. However, the stochastic integrals used in equations (2.3) and (2.4) represent integrals over non-differentiable Brownian

motion paths, and hence cannot be approximated by a Reimann Sum. The first version of stochastic calculus was developed by the Japanese mathematician K. Itô in 1940s (Itô, 1944). The Itô approximation of the stochastic integral $\int_0^T f(t)dW(t)$ is given as

$$\int_0^T f(t)dW(t) = \sum_{j=0}^{n-1} f(t_j)(W(t_{j+1}) - W(t_j)) \tag{2.6}$$

This is known as the *Itô stochastic integral.* An alternative approximation for the stochastic integral was proposed by the Russian physicist R.L. Stratonovich in the 1960s (Stratonovich, 1966). This integral is known as the *Stratonovich stochastic integral* and is represented as

$$\int_0^T f(t) \circ dW(t) - \sum_{j=0}^{n-1} f\left(\frac{t_j + t_{j+1}}{2}\right)(W(t_{j+1}) - W(t_j)) \tag{2.7}$$

The symbol "$\circ$" is used to distinct Stratonovich integral approximation from its corresponding Itô integral approximation. The Stratonovich form of a general N-dimensional SDE with an m-dimensional driving Wiener process, represented by equation (2.4) in its Itô form, is given as

$$X(t) = X(0) + \int_0^t a(X(s))ds + \sum_{j=1}^{m} \int_0^t b_j(X(s)) \circ dW_j(s) \qquad t \in [0, T] \tag{2.8}$$

Both Itô and Stratonovich forms of stochastic integrals are popular and each form has its own advantages and disadvantages. The choice of stochastic calculus used is a matter of convenience and depends on the problem at hand, with several existing guidelines (for e.g., see (Øksendal, 2010)). It is possible to convert an Itô form of an SDE into its Stratonovich form and vice-a-versa quite easily. The present work focuses exclusively on the Itô form of stochastic differential equations, represented by equation (2.4).

The definitions of strong and weak convergence of stochastic processes are adopted from Kloeden and Platen (Kloeden and Platen, 2011). Assume that Y_n is a discrete time approximation of a stochastic process $X(t)$ at time $t = T$ using some discrete numerical time integration scheme. In many situations, it is required that the sample paths of the approximation Y_n be close to those of the stochastic process $X(t)$. The notion of strong

convergence is useful in such cases. A numerical time integration method is said to have a *strong convergence* of order $\gamma \in (0, \infty)$ if there exists a finite constant K and a positive constant h_0 such that

$$\mathbb{E}^{\omega}[|X(T) - Y_n|] \leq Kh^{\gamma} \tag{2.9}$$

for any time discretization with maximum step size $h \in (0, h_0)$, where $\mathbb{E}^{\omega}[X(t)]$ is the Expectation Operator and is defined as the mean value or the expected value of the random variable X. For the deterministic case, when diffusion coefficients b_j of equation (2.4) are zero, the strong convergence criterion reduces to the usual deterministic convergence criterion for ordinary differential equations (ODEs).

In many practical situations, it is not necessary to have a close pathwise approximation of a stochastic process. Often times, only the expectation of a certain function of the stochastic process might be of interest. The type of convergence criterion required in this case is much weaker than the strong convergence criterion discussed above. In order to have such a functional approximation, it suffices to have a good approximation of the probability distribution of the stochastic process $X(t)$ rather than a close approximation of its sample paths. The notion of weak convergence is useful in such cases. The strong convergence criterion asks for the difference in trajectory, whereas the weak convergence criterion asks for a difference in distribution. Consider a function $g(X(t))$ of the stochastic process $X(t)$ at time $t = T$. A numerical time integration scheme is said to have a *weak convergence* of order β if for any polynomial function g, there exists a finite constant K and a positive constant h_0 such that

$$|\mathbb{E}^{\omega}[g(X(T))] - \mathbb{E}^{\omega}[g(Y_n)]| \leq Kh^{\beta} \tag{2.10}$$

for any time discretization with maximum step size $h \in (0, h_0)$. For the deterministic case, when diffusion coefficients b_j of equation (2.4) are zero, the weak convergence criterion also reduces to the usual deterministic convergence criterion for ordinary differential equations (ODEs) when we set $g(X(T)) = X(T)$. In ocean modeling applications, one is often interested in the statistics of the random fields and not so much in their individual sample paths. Hence, the weak convergence criterion is often more relevant. The present work

thus focuses primarily on the weak convergence criterion.

2.2 Numerical Integration Schemes for the Solution of SDEs

In order to model stochastic processes and random fields and to study the evolution of uncertainty with time, SDEs need to be numerically integrated. The presence of Brownian motion renders the deterministic numerical integration schemes incapable of integrating SDEs. Almost all algorithms that are used for the solution of ODEs display very poor numerical convergence when applied to SDEs. Numerical solution of SDEs is a relatively new topic of research when compared to regular ODEs or PDEs. The development of numerical time integration schemes for SDEs began with the Euler-Maruyama scheme developed by Maruyama in 1955 (Maruyama, 1955). This scheme is the first order Taylor approximation of an SDE. Subsequently, higher order Taylor approximations were developed, but these required the evaluation of derivatives of drift and diffusion coefficients (defined in section 2.2), making the algorithms inefficient and cumbersome. This shifted the focus to development of derivative-free approximations to these higher order Taylor expansions. This has become a major topic of research in the last few decades and several derivative-free higher order numerical schemes for solution of SDEs have been developed for both the strong and weak approximation of solutions of SDEs (defined in section 2.3), for e.g. Giles (2008a), Kloeden and Platen (2011), Milstein and Tretyakov (2004) and the references therein. In particular, derivative-free Runge-Kutta schemes for strong approximation of solutions of SDEs have been proposed by Burrage and Burrage (1996), Burrage and Burrage (2000), Kloeden and Platen (2011), Milstein and Tretyakov (2004), Newton (1991), Rößler (2010) and Rümelin (1982). Similarly, Runge-Kutta schemes for weak approximation of solution of SDEs have been developed by Kloeden and Platen (2011), Komori et al. (1997), Komori (2007a), Komori (2007b), Küpper et al. (2007), Rößler (2007), Rößler (2009), Talay (1990) and Tocino and Vigo-Aguiar (2002). Next, we discuss in greater detail, some of these numerical integration schemes for weak approximation of solutions of SDEs.

2.2.1 Euler-Maruyama (EM) method

The Euler-Maruyama scheme is the simplest Taylor approximation of the stochastic differential equation (2.4), and was proposed by Maruyama (Maruyama, 1955). It attains a strong order of convergence of $\gamma = 0.5$ and a weak order of convergence of $\beta = 1.0$. The Euler-Maruyama method has the form

$$Y_{n+1} = Y_n + a(Y_n)h + \sum_{j=1}^{m} b_j(Y_n)\Delta W_j \tag{2.11}$$

where

$$\Delta W_j = W_j(t_{n+1}) - W_j(t_n) \tag{2.12}$$

Higher order Taylor approximations of equation (2.4) require the evaluation of derivatives of diffusion coefficients $b_j(Y_n)$, which are often non-existent or too difficult to evaluate. Hence, higher order Taylor approximations are not very useful as numerical integration methods for SDEs. However, several derivative-free integration schemes have been developed in recent years by substituting appropriate approximations for the derivatives in these higher order Taylor expansions.

2.2.2 Extrapolated Euler-Maruyama (ExEM) method

The Extrapolated Euler-Maruyama scheme, proposed by Talay and Tubaro (Talay and Tubaro, 1990) is based on Euler-Maruyama approximations Y_n^h and $Y_n^{h/2}$, calculated with step sizes h and $h/2$ respectively. It attains a weak order of convergence of $\beta = 2.0$ and has the form

$$Y_{n+1}^1 = Y_n + a(Y_n)h + \sum_{j=1}^{m} b_j(Y_n)\Delta W_j \tag{2.13}$$

$$Y_{n+1}^{2,\text{temp}} = Y_n + a(Y_n)(h/2) + \sum_{j=1}^{m} b_j(Y_n)\Delta W_j^1 \tag{2.14}$$

$$Y_{n+1}^2 = Y_{n+1}^{2,\text{temp}} + a(Y_{n+1}^{2,\text{temp}})(h/2) + \sum_{j=1}^{m} b_j(Y_{n+1}^{2,\text{temp}})\Delta W_j^2 \tag{2.15}$$

$$Y_{n+1} = 2Y_{n+1}^2 - Y_{n+1}^1 \tag{2.16}$$

where

$$\Delta W_j = \Delta W_j^1 + \Delta W_j^2 \tag{2.17}$$

$$\Delta W_j^1 = W_j(t_{n+1/2}) - W_j(t_n) \tag{2.18}$$

$$\Delta W_j^2 = W_j(t_{n+1}) - W_j(t_{n+1/2}) \tag{2.19}$$

2.2.3 Stochastic Runge-Kutta method by Kloeden and Platen (RKKP)

An explicit derivative-free stochastic Runge-Kutta method has been proposed by Kloeden and Platen (Kloeden and Platen, 1989, 2011). This method attains a weak order of convergence of $\beta = 2.0$. It has the form

$$\begin{aligned} Y_{n+1} =& Y_n + 0.5\left(a(Y_n) + a(H^{(0)})\right)h \\ &+ 0.25\sum_{k=1}^{m}\left(b_k(H_+^{(k)}) + b_k(H_-^{(k)}) + 2b_k(Y_n)\right)\hat{I}_{(k)} \\ &+ 0.25\sum_{\substack{k,l=1 \\ k\neq l}}^{m}\left(b_k(\hat{H}_+^{(l)}) + b_k(\hat{H}_-^{(l)}) - 2b_k(Y_n)\right)\hat{I}_{(k)} \\ &+ 0.25\sum_{k=1}^{m}\left(b_k(H_+^{(k)}) - b_k(H_-^{(k)})\right)\frac{\hat{J}_{(k,k)}}{\sqrt{h}} \\ &+ 0.25\sum_{\substack{k,l=1 \\ k\neq l}}^{m}\left(b_k(\hat{H}_+^{(l)}) - b_k(\hat{H}_-^{(l)})\right)\frac{\hat{J}_{(k,l)}}{\sqrt{h}} \end{aligned} \tag{2.20}$$

where

$$H^{(0)} = Y_n + a(Y_n)h + \sum_{k=1}^{m} b_k(Y_n)\hat{I}_{(k)} \tag{2.21}$$

$$H_\pm^{(k)} = Y_n + a(Y_n)h \pm b_k(Y_n)\sqrt{h} \tag{2.22}$$

$$\hat{H}_\pm^{(k)} = Y_n \pm b_k(Y_n)\sqrt{h} \tag{2.23}$$

for $k = 1, 2, ..., m$. The random variables $\hat{I}_{(k)}$ are distributed with $P(\hat{I}_{(k)} = \pm\sqrt{3h}) = \frac{1}{6}$ and $P(\hat{I}_{(k)} = 0) = \frac{2}{3}$ for $k = 1, 2, ..., m$. Also, $\hat{J}_{(k,l)} = \hat{I}_{(k)}\hat{I}_{(l)} + V_{k,l}$ with $P(V_{k,l} = \pm h) = \frac{1}{2}$ for $l = 1, 2, ..., k-1$, $V_{k,k} = -h$ and $V_{k,l} = -V_{l,k}$ for $l = k+1, ..., m$.

2.2.4 Stochastic Runge-Kutta method by Rössler (RKR)

Recently, a new class of stochastic Runge-Kutta methods for weak approximation of solutions of SDEs has been developed by Rössler (Rößler, 2009) in 2009. The novelty of this class of Runge-Kutta methods is that the number of stages does not depend on the dimension m of the driving Wiener process. The Stochastic Runge-Kutta method by Rössler has the form

$$\begin{aligned} Y_{n+1} = Y_n &+ \sum_{i=1}^{s} \alpha_i a(t_n + c_i^{(0)}h, H_i^{(0)})h \\ &+ \sum_{i=1}^{s}\sum_{k=1}^{m} \beta_i^{(1)} b_k(t_n + c_i^{(1)}h, H_i^{(k)})\hat{I}_{(k)} \\ &+ \sum_{i=1}^{s}\sum_{k=1}^{m} \beta_i^{(2)} b_k(t_n + c_i^{(1)}h, H_i^{(k)})\frac{\hat{I}_{(k,k)}}{\sqrt{h}} \\ &+ \sum_{i=1}^{s}\sum_{k=1}^{m} \beta_i^{(3)} b_k(t_n + c_i^{(2)}h, H_i^{(k)})\hat{I}_{(k)} \\ &+ \sum_{i=1}^{s}\sum_{k=1}^{m} \beta_i^{(4)} b_k(t_n + c_i^{(2)}h, H_i^{(k)})\sqrt{h} \end{aligned} \tag{2.24}$$

where s is the number of stages and

$$\begin{aligned} H_i^{(0)} = Y_n &+ \sum_{j=1}^{s} A_{ij}^{(0)} a(t_n + c_j^{(0)}h, H_j^{(0)})h \\ &+ \sum_{j=1}^{s}\sum_{l=1}^{m} B_{ij}^{(0)} b_l(t_n + c_j^{(1)}h, H_j^{(l)})\hat{I}_{(l)} \end{aligned} \tag{2.25}$$

$$\begin{aligned} H_i^{(k)} = Y_n &+ \sum_{j=1}^{s} A_{ij}^{(1)} a(t_n + c_j^{(0)}h, H_j^{(0)})h \\ &+ \sum_{j=1}^{s} B_{ij}^{(1)} b_k(t_n + c_j^{(1)}h, H_j^{(k)})\sqrt{h} \end{aligned} \tag{2.26}$$

$$\begin{aligned} \hat{H}_i^{(k)} = Y_n &+ \sum_{j=1}^{s} A_{ij}^{(2)} a(t_n + c_j^{(0)}h, H_j^{(0)})h \\ &+ \sum_{j=1}^{s}\sum_{\substack{l=1 \\ l\neq k}}^{m} B_{ij}^{(2)} b_l(t_n + c_j^{(1)}h, H_j^{(l)})\frac{\hat{I}_{(k,l)}}{\sqrt{h}} \end{aligned} \tag{2.27}$$

Table 2.1: Butcher tableau for RKR methods

$c^{(0)}$	$A^{(0)}$	$B^{(0)}$	
$c^{(1)}$	$A^{(1)}$	$B^{(1)}$	
$c^{(2)}$	$A^{(2)}$	$B^{(2)}$	
	α^T	${\beta^{(1)}}^T$	${\beta^{(2)}}^T$
		${\beta^{(3)}}^T$	${\beta^{(4)}}^T$

Table 2.2: Butcher tableau for RKR scheme RI5

0									
1	1			$\frac{1}{3}$					
$\frac{5}{12}$	$\frac{25}{144}$	$\frac{35}{144}$		$-\frac{5}{6}$	0				
0									
$\frac{1}{4}$	$\frac{1}{4}$			$\frac{1}{2}$					
$\frac{1}{4}$	$\frac{1}{4}$	0		$-\frac{1}{2}$	0				
0									
0	0			1					
0	0	0		-1	0				
	$\frac{1}{10}$	$\frac{3}{14}$	$\frac{24}{35}$	1	-1	-1	0	1	-1
				$\frac{1}{2}$	$-\frac{1}{4}$	$-\frac{1}{4}$	0	$\frac{1}{2}$	$-\frac{1}{2}$

for $i = 1, 2, ..., s$ and $k = 1, 2, ..., m$. The random variables $\hat{I}_{(k,l)}$ are defined as

$$\hat{I}_{(k,l)} = \begin{cases} \frac{1}{2}(\hat{I}_{(k)}\hat{I}_{(l)} - \sqrt{h}\tilde{I}_{(k)}) & \text{if } k < l \\ \frac{1}{2}(\hat{I}_{(k)}^2 - h) & \text{if } k = l \\ \frac{1}{2}(\hat{I}_{(k)}\hat{I}_{(l)} + \sqrt{h}\tilde{I}_{(l)}) & \text{if } k > l \end{cases} \tag{2.28}$$

for $1 \leq k, l \leq m$. The random variables $\hat{I}_{(k)}$ are distributed with $P(\hat{I}_{(k)} = \pm\sqrt{3h}) = \frac{1}{6}$ and $P(\hat{I}_{(k)} = 0) = \frac{2}{3}$ for $k = 1, 2, ..., m$ and the random variables $\tilde{I}_{(k)}$ are distributed with $P(\tilde{I}_{(k)} = \pm\sqrt{h}) = \frac{1}{2}$ for $k = 1, 2, ..., m-1$.

The coefficients of these Stochastic Runge-Kutta methods can be represented by an extended Butcher Tableau as shown in table (2.1). The order of the schemes varies

Table 2.3: Butcher tableau for RKR scheme RI6

0									
1	1			1					
0	0	0		0	0				
0									
1	1			1					
1	1	0		-1	0				
0									
0	0			1					
0	0	0		-1	0				
	$\frac{1}{2}$	$\frac{1}{2}$	0	$\frac{1}{2}$	$\frac{1}{4}$	$\frac{1}{4}$	0	$\frac{1}{2}$	$-\frac{1}{2}$
				$-\frac{1}{2}$	$\frac{1}{4}$	$\frac{1}{4}$	0	$\frac{1}{2}$	$-\frac{1}{2}$

depending on the actual values of the coefficients used. The values of the coefficients must satisfy the corresponding order conditions based on the colored rooted tree analysis (Rößler, 2004, 2006). Two schemes of this class have been studied in the present work. The coefficients for RKR schemes RI5 and RI6 derived by Rößler (2009) are shown in tables (2.2) and (2.3) respectively. Both these schemes have $s = 3$ stages and attain a weak order of convergence of $\beta = 2.0$.

2.2.5 Computational cost of numerical integration schemes

In this section, we investigate the computational cost of implementing the numerical schemes, in terms of number of floating point operations (flops) required per iteration of the scheme. We utilize theoretical results to compute the number of flops and intercompare the numerical solutions obtained by using the aforementioned numerical schemes.

Theoretical estimates. We consider an N-dimensional SDE with an m-dimensional driving Wiener process, as given by equation (2.4). Consider a numerical implementation by Monte Carlo simulations using M_r realizations. Since the number of flops required for evaluating the drift and diffusion coefficients depends on the problem at hand, assume that the computational cost of evaluating the drift coefficient $a(X)$ (for M_r realizations of X) is n_a and for evaluating diffusion coefficients $b_k(X)$ is n_{b_k}, for $k = 1, 2, ..., m$. Also

assume that the number of flops required for generating M_r realizations of a Gaussian random variable are n_{w_G}, and the number of flops required for generating M_r realizations of the two-point distributed random variable $V_{k,l}$ (used in RKKP scheme) and three-point distributed random variable $\hat{I}_{(k)}$ (used in RKKP and RKR schemes) are n_{w_2} and n_{w_3} respectively. We evaluate the number of flops per iteration for all the schemes in terms of $N, m, M_r, n_a, n_{b_k}, n_{w_G}, n_{w_2}$ and n_{w_3} ($s = 3$ for RKR scheme) and present them in table (2.4).

We observe that the number of flops required for the evaluation of the diffusion coefficient in the RKKP scheme depends on the dimension m of the driving Wiener process, which is also true of most other stochastic Runge-Kutta schemes. However, this is not the case for the schemes RKR and ExEM. Also, the number of random variables that need to be generated for implementing RKR and ExEm schemes is $O(m)$, whereas for RKKP scheme it is $O(m^2)$. For SDEs with higher dimensional driving Wiener processes, these two computations have a major share in the computational cost of the algorithm and hence, RKR and ExEM schemes are expected to be computationally cheaper than other stochastic Runge-Kutta schemes like RKKP, especially for more complex and higher dimensional SDEs with large m. Additionally, although the Extrapolated Euler-Maruyama scheme (ExEM) may be computationally cheap and easy to implement, there are situations in which extrapolation methods only have limited value (Milstein and Tretyakov, 2004). One example of this is the case of *stiff problems*, which have restricted stability regions for the ExEM scheme (Kloeden et al., 1995). Thus, the recently developed Runge-Kutta scheme by Rössler has additional importance for calculating higher order weak approximation of SDEs in a computationally cheap manner.

We estimate the number of flops in generating the required random variables with using the theory on numerical computing with MATLAB given by Moler (Moler, 2004). Two-point and three-point distributed random variables can be generated using the "*if*" condition on uniform random variables. MATLAB generates uniform random variables using the "subtract-with-borrow" step, which requires 2 flops per random variable. Hence, generation of M_r uniform random variables requires $2M_r$ flops. Also, the generation of two-point and three-point random variables using M_r uniform random variables would

Table 2.4: Computational cost of numerical integration schemes

S. No.	Scheme	Flops per iteration
1.	EM	$2(m+1)M_rN + mM_r + n_a + \sum_{k=1}^{m} n_{b_k} + mn_{w_G}$
2.	ExEM	$2(3m+4)M_rN + 2mM_r + 3n_a + 3\sum_{k=1}^{m} n_{b_k} + 2mn_{w_G}$
3.	RKKP	$(11m^2+14m+5)M_rN + 3m^2M_r + 2n_a + (2m+1)\sum_{k=1}^{m} n_{b_k}$ $+mn_{w_3} + 0.5m(m-1)n_{w_2}$
4.	RKR	$(9m^2+48m+12)M_rN + (4m^2+2m-2)M_r + 3n_a + 6\sum_{k=1}^{m} n_{b_k}$ $+mn_{w_3} + (m-1)n_{w_2}$

require additional M_r and $2M_r$ flops respectively. Thus, we have $n_{w_2} = 3M_r$ and $n_{w_3} = 4M_r$. All algorithms for generating Gaussian (normal) random variables are based on transformations of uniform random variables. The simplest way to generate an a by b matrix with approximately normally distributed random variables is to use the expression $sum(rand(a, b, 12), 3) - 6$. This expression requires $12ab$ additional flops for generating ab Gaussian random variables from $12ab$ uniform random variables. Hence, the number of flops for generating M_r Gaussian random variables using this expression is $36M_r$ ($24M_r$ for generating $12M_r$ uniform random variables and $12M_r$ additional flops for doing the required transformations). A more sophisticated table lookup algorithm called the *ziggurat* algorithm is used by MATLAB to generate Gaussian random variables, but for simplicity, we assume $n_{w_G} = 36M_r$.

Numerical Estimates. In order to verify the theoretical results and estimates, we implement the numerical integration schemes discussed in section 2.2.4 for three different systems of stochastic differential equations from Rößler (2009). We compare the schemes using an ensemble of M_r Monte Carlo simulations for each schemes and the sample averages are thus approximated by using M_r independently simulated realizations. The mean error for the numerical integration schemes is computed as $\hat{\mu} = \mathbb{E}^{\omega}[f(X_T)] - \frac{1}{M_r}\sum_{k=1}^{M_r} f(Y_{T,k})$. All errors have been computed for the final time $T = 1.0s$ and are plotted on a log-log scale in order to see the convergence results clearly.

As a first example, a linear SDE system ($d = m = 2$) with commutative noise has

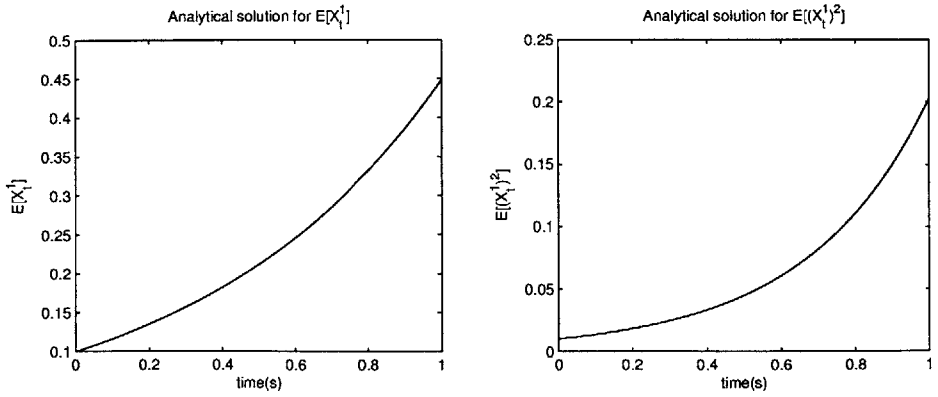

Figure 2-1: Analytical solutions for the first moment $\mathbb{E}^{\omega}[X_t^1]$ (left) and the second moment $\mathbb{E}^{\omega}[(X_t^1)^2]$ (right) for SDE (2.29)

been considered. The governing stochastic differential equation for this system is given as

$$\begin{pmatrix} X_t^1 \\ X_t^2 \end{pmatrix} = \begin{pmatrix} \frac{3}{2}X_t^1 \\ \frac{3}{2}X_t^2 \end{pmatrix} dt + \begin{pmatrix} \frac{1}{10}X_t^1 \\ 0 \end{pmatrix} dW_t^1 + \begin{pmatrix} 0 \\ \frac{1}{10}X_t^2 \end{pmatrix} dW_t^2 \tag{2.29}$$

with the initial condition $X_0 = (\frac{1}{10}, \frac{1}{10})^T$. The analytical solutions for the first and second moments are given as $\mathbb{E}^{\omega}[X_t^i] = \frac{1}{10}\exp(\frac{3}{2}t)$ and $\mathbb{E}^{\omega}[(X_t^i)^2] = \frac{1}{100}\exp(\frac{301}{100}t)$ respectively, for $i = 1, 2$. The analytical solutions for the first and second moments for $i = 1$ are shown in figure (2-1). For this case, we choose $M_r = 1 \times 10^8$. The mean errors $|\hat{\mu}|$ for the first and second moments are shown in figure (2-2). It is observed from figure (2-2) that the EM scheme does display a weak order of convergence of $\beta = 1.0$, whereas the other schemes display an order of convergence of $\beta = 2.0$. The calculated empirical variances corresponding to the mean errors are reasonably small, and hence our results are consistent. Also, we observe that the mean errors for the scheme RI5 are significantly lower than the other schemes.

In order to estimate the computational effort involved in implementing the numerical schemes, the number of flops required for each scheme are shown in figure (2-3). For a fair comparison of the accuracy and computational efforts, figure (2-3) also shows a plot of mean error vs. computational effort for all the schemes considered for their estimates of $\mathbb{E}^{\omega}[X_t^1]$ for the system of SDEs (2.29). It is observed that although in terms of implementation, the EM scheme is the simplest, its error and convergence characteristics

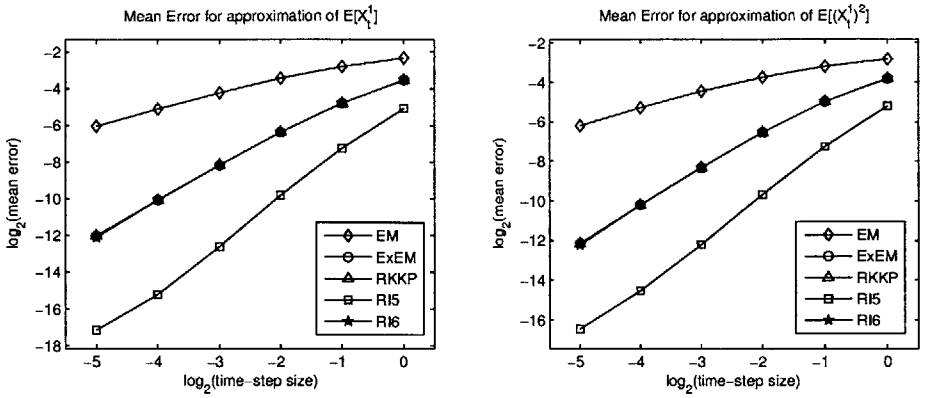

Figure 2-2: Mean errors in the approximation of first moment $\mathbb{E}^{\omega}[X_t^1]$ (left) and second moment $\mathbb{E}^{\omega}[(X_t^1)^2]$ (right) for SDE (2.29)

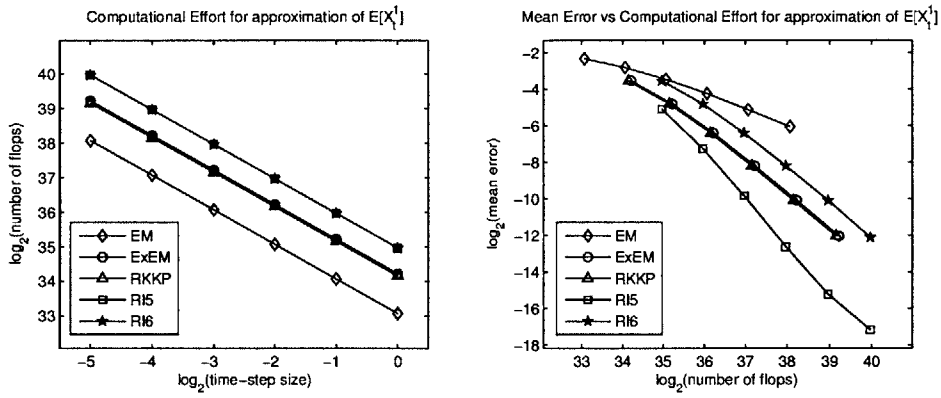

Figure 2-3: Total computational effort vs time-step size (left) and mean error vs total computational effort (right) for the approximation of $\mathbb{E}^{\omega}[X_t^1]$ for SDE (2.29)

make it the most expensive scheme for a fixed desired mean error. Also, we observe that the schemes ExEM, RKKP and RI6 have similar slopes in the plot of mean error vs. computational effort (figure (2-3)). This means that in order to improve the accuracy of approximation, a proportionally similar increase in the computational effort would be required for all the three schemes. It is also observed that the scheme RI5 shows the most desirable characteristics in terms of accuracy and computational cost for this example.

The second example considered is a nonlinear SDE system ($d = m = 2$) with non-commutative noise. The governing stochastic differential equation for this system is given

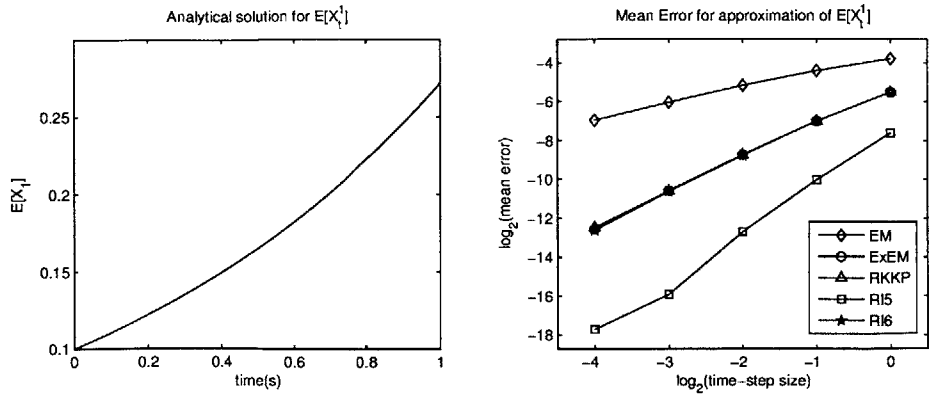

Figure 2-4: Analytical solution (left) and mean errors (right) in the approximation of the first moment $\mathbb{E}^\omega[X_t^1]$ for SDE (2.30)

as

$$
\begin{aligned}
d\begin{pmatrix} X_t^1 \\ X_t^2 \end{pmatrix} = &\begin{pmatrix} -\frac{1}{2}X_t^1 + \frac{3}{2}X_t^2 \\ \frac{3}{2}X_t^1 - \frac{1}{2}X_t^2 \end{pmatrix} dt + \begin{pmatrix} \sqrt{\frac{3}{4}(X_t^1 - X_t^2)^2 + \frac{3}{20}} \\ 0 \end{pmatrix} dW_t^1 \\
&+ \begin{pmatrix} -\sqrt{\frac{1}{4}(X_t^1 - X_t^2)^2 + \frac{1}{20}} \\ \sqrt{(X_t^1 - X_t^2)^2 + \frac{1}{5}} \end{pmatrix} dW_t^2
\end{aligned}
\tag{2.30}
$$

with initial condition $X_0 = (\frac{1}{10}, \frac{1}{10})^T$. The analytical solution for the first moment in this case is given as $\mathbb{E}^\omega[X_t^i] = \frac{1}{10}\exp(t)$, for $i = 1, 2$. Here, we choose $M_r = 1 \times 10^9$. The analytical solution for $\mathbb{E}^\omega[X_t^1]$ and the mean errors $|\hat{\mu}|$ in its approximation for various numerical integration schemes are presented in figure (2-4). We observe that the results are similar to those obtained in the previous example. Because of the non-commutative nature of the noise and the increased complexity of the system, the empirical variances are higher than in the previous example, and hence a larger number of realizations are required to keep them at their acceptable levels. We also observe that again the error characteristics of the schemes ExEM, RKKP and RI6 are similar whereas the mean errors of the scheme RI5 are lower than the others.

A plot of mean error vs. total computational effort is shown in figure (2-5) on the left side. Again, trends very similar to the previous example are observed. For complex SDEs with stochastic forcing from higher dimensional Wiener processes, the generation of

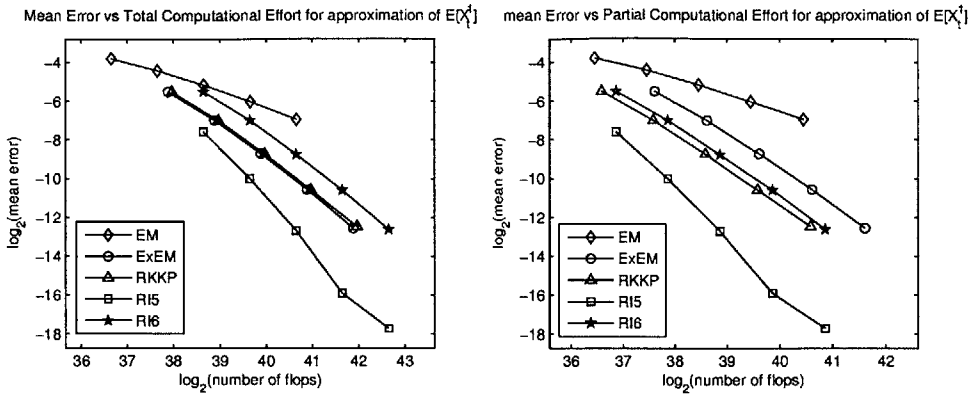

Figure 2-5: Total computational effort vs time-step size (left) and partial computational effort vs time-step size (right) for the approximation of $\mathbb{E}^{\omega}[X_t^1]$ for SDE (2.30)

random variables and the evaluation of drift and diffusion coefficients become the major computational costs. Hence, it is useful to study these partial computational costs for the schemes considered. Such a comparison between mean errors and partial computational costs of the numerical schemes is also shown in figure (2-5) on the right side. By a comparison of the two plots shown in figure (2-5), we observe that the costs of evaluating the drift and diffusion coefficients and generating random variables are relatively lower for the Runge-Kutta schemes as compared to EM and ExEM schemes. Also, since this system has a relatively small dimensional driving Wiener process $m = 2$, the advantages of the RKR schemes over other Runge-Kutta schemes (like RKKP) in terms of computational costs, which have been mentioned earlier in section 5.5, are not evident here. In order to see the advantages of RKR scheme over other Runge-Kutta schemes, we need an SDE system with a higher dimensional driving Wiener process.

Next, we consider a nonlinear SDE with non-commutative noise and a higher dimension $d = 4$. For given $\lambda, \mu \in \{0, 1\}$, the governing stochastic differential equation for this

example is given as

$$
\begin{aligned}
d\begin{pmatrix} X_t^1 \\ X_t^2 \\ X_t^3 \\ X_t^4 \end{pmatrix} = & \begin{pmatrix} \frac{243}{154}X_t^1 - \frac{27}{77}X_t^2 + \frac{23}{154}X_t^3 - \frac{65}{154}X_t^4 \\ \frac{27}{77}X_t^1 - \frac{243}{154}X_t^2 + \frac{65}{154}X_t^3 - \frac{23}{154}X_t^4 \\ \frac{5}{154}X_t^1 - \frac{61}{154}X_t^2 + \frac{162}{77}X_t^3 - \frac{36}{77}X_t^4 \\ \frac{61}{154}X_t^1 - \frac{5}{154}X_t^2 + \frac{36}{77}X_t^3 - \frac{162}{77}X_t^4 \end{pmatrix} dt \\
& + \frac{1}{9}\sqrt{(X_t^2)^2 + (X_t^3)^2 + \frac{2}{23}} \begin{pmatrix} \frac{1}{13} \\ \frac{1}{14} \\ \frac{1}{13} \\ \frac{1}{15} \end{pmatrix} dW_t^1 + \frac{1}{8}\sqrt{(X_t^4)^2 + (X_t^1)^2 + \frac{1}{11}} \begin{pmatrix} \frac{1}{14} \\ \frac{1}{16} \\ \frac{1}{16} \\ \frac{1}{12} \end{pmatrix} dW_t^2 \\
& + \frac{\lambda}{12}\sqrt{(X_t^1)^2 + (X_t^2)^2 + \frac{1}{9}} \begin{pmatrix} \frac{1}{6} \\ \frac{1}{5} \\ \frac{1}{5} \\ \frac{1}{6} \end{pmatrix} dW_t^3 + \frac{\lambda}{14}\sqrt{(X_t^3)^2 + (X_t^4)^2 + \frac{3}{29}} \begin{pmatrix} \frac{1}{8} \\ \frac{1}{9} \\ \frac{1}{8} \\ \frac{1}{9} \end{pmatrix} dW_t^4 \\
& + \frac{\mu}{10}\sqrt{(X_t^1)^2 + (X_t^3)^2 + \frac{1}{13}} \begin{pmatrix} \frac{1}{11} \\ \frac{1}{15} \\ \frac{1}{13} \\ \frac{1}{11} \end{pmatrix} dW_t^5 + \frac{\mu}{11}\sqrt{(X_t^2)^2 + (X_t^4)^2 + \frac{2}{25}} \begin{pmatrix} \frac{1}{12} \\ \frac{1}{13} \\ \frac{1}{16} \\ \frac{1}{13} \end{pmatrix} dW_t^6
\end{aligned}
\tag{2.31}
$$

with initial condition $X_0 = (\frac{1}{8}, \frac{1}{8}, 1, \frac{1}{8})^T$. Thus, we have $m = 2 + 2\lambda + 2\mu$ as the dimension of the driving Wiener process. In this case, the first moment of solution can be calculated as $\mathbb{E}^\omega[X_t^i] = \frac{1}{8}\exp(2t)$, for $i = 1, 2, 4$ and $\mathbb{E}^\omega[X_t^i] = \exp(2t)$, for $i = 3$. The number of realizations are $M_r = 1 \times 10^7$. In this example, the performance of the schemes is compared for the cases $m = 2$ (with $\lambda = \mu = 0$), $m = 4$ (with $\lambda = 1$ and $\mu = 0$) and $m = 6$ (with $\lambda = \mu = 1$). The analytical solution for $\mathbb{E}^\omega[X_t^1]$ and the mean errors $|\hat{\mu}|$ in its approximation by the numerical integration schemes for $m = 2, 4$ and 6 are presented in figures (2-6), (2-7) and (2-8) respectively. From these figures, we observe that the convergence characteristics of the numerical schemes are again similar to those obtained

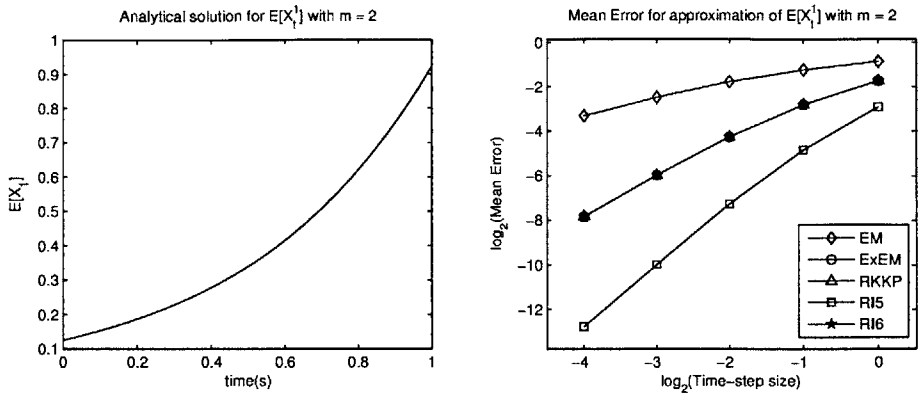

Figure 2-6: Analytical solution (left) and mean errors (right) in the approximation of the first moment $\mathbb{E}^{\omega}[X_t^1]$ for SDE (2.31) with $m = 2$

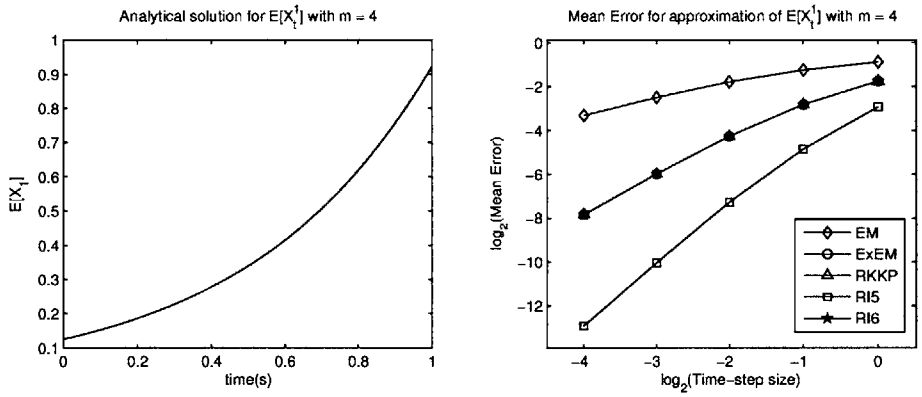

Figure 2-7: Analytical solution (left) and mean errors (right) in the approximation of the first moment $\mathbb{E}^{\omega}[X_t^1]$ for SDE (2.31) with $m = 4$

in the first two examples.

The main purpose of this third example is to observe the change in computational effort of the schemes due to increase in the dimension of the driving Wiener process m. Plots depicting mean error vs. total computational effort and mean error vs. partial computational effort for the approximation of $\mathbb{E}^{\omega}[X_t^1]$ for $m = 2, 4$ and 6 are thus shown in figures (2-9), (2-10) and (2-11) respectively. Comparing figures (2-3), (2-5) and (2-9), we observe that since we are using a smaller number of Monte Carlo realizations, the performance of the EM and ExEM schemes in terms of computational cost is better than in the previous two examples. As m is increased, (figures (2-10) and (2-11)), the computational cost of RKKP scheme increases faster than the other schemes. This is

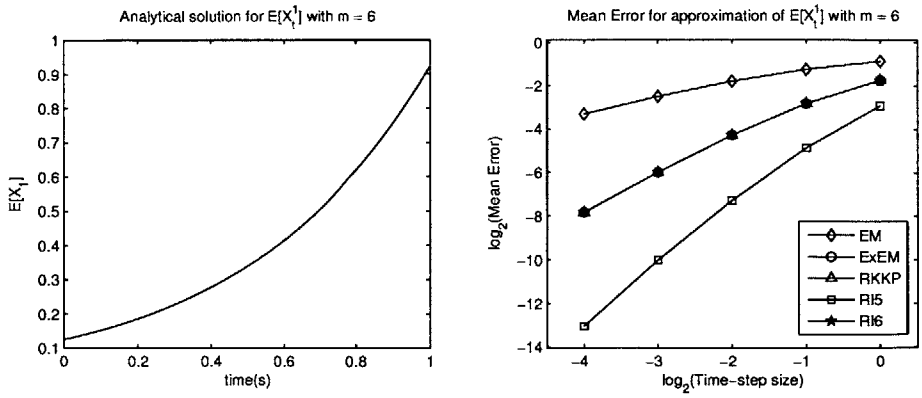

Figure 2-8: Analytical solution (left) and mean errors (right) in the approximation of the first moment $\mathbb{E}^{\omega}[X_t^1]$ for SDE (2.31) with $m = 6$

because in RKKP (and in most other stochastic Runge-Kutta schemes), the number of evaluations of the diffusion coefficients scale linearly with dimension m of the driving Wiener process. Also, the number of random variables that need to be generated for implementing the scheme are $O(m^2)$ for most stochastic Runge-Kutta methods (including RKKP), which add further to the computational cost. However, the family of Runge-Kutta schemes proposed by Rössler does not have this inefficiency and hence we see that the computational cost of the schemes RI5 and RI6 does not increase faster than the schemes EM and ExEM with an increase in m. Moreover, the performance of the scheme RI5, in terms of accuracy of solution and computational cost of implementing the algorithm, is again observed to be better than the other numerical schemes considered here.

In order to minimize statistical error, M_r has to be chosen to be very large (Kloeden and Platen, 2011). In usual practice however, a much smaller M_r is sufficient to get a reasonably good approximation of the solution. In fact, for most ocean modeling applications, due to computational constraints introduced by high dimensionality, M_r cannot be chosen to be very large. For such a choice of M_r, the statistical errors are often dominant and the choice of a higher order numerical scheme does not necessarily improve the accuracy and convergence characteristics of the solution. Hence, for a majority of ocean modeling applications, the Euler-Maruyama method is often the most suitable numerical scheme due to its low computational cost. The EM scheme has been used as the nu-

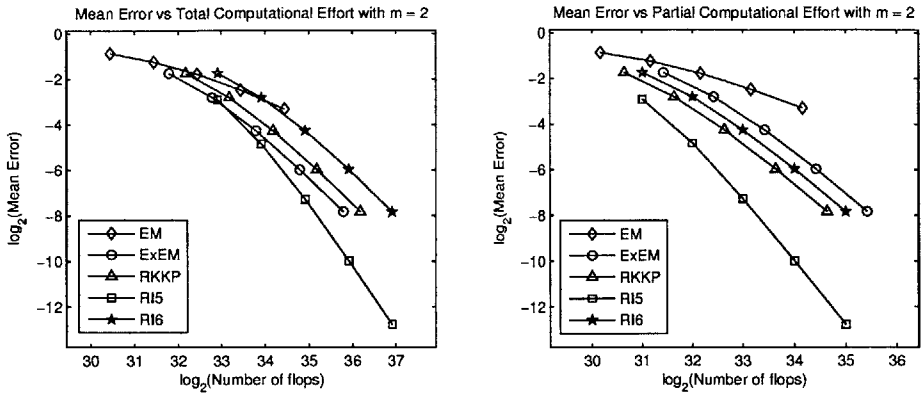

Figure 2-9: Total computational effort vs time-step size (left) and partial computational effort vs time-step size (right) for the approximation of $\mathbb{E}^{\omega}[X_t^1]$ for SDE (2.31) with $m = 2$

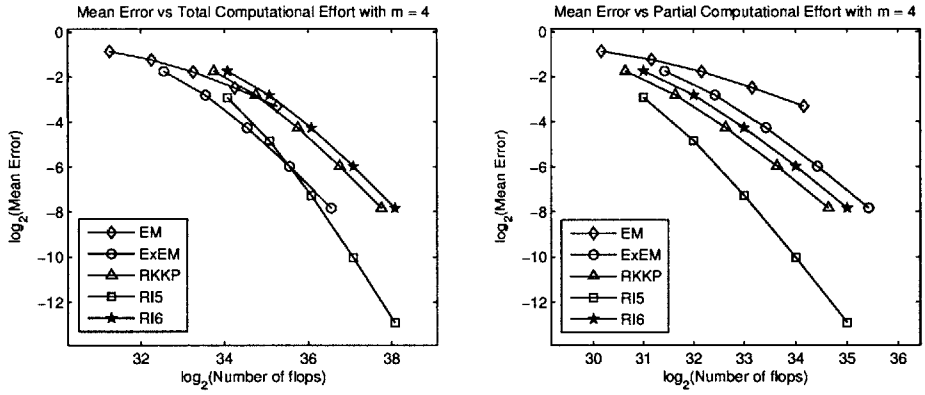

Figure 2-10: Total computational effort vs time-step size (left) and partial computational effort vs time-step size (right) for the approximation of $\mathbb{E}^{\omega}[X_t^1]$ for SDE (2.31) with $m = 4$

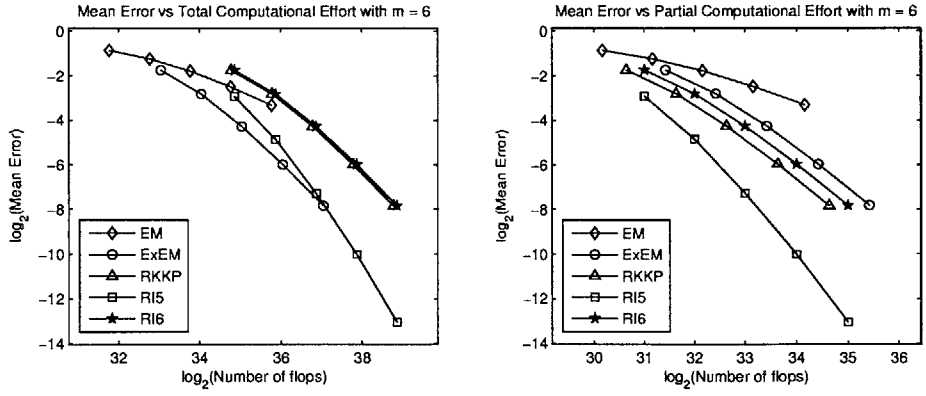

Figure 2-11: Total computational effort vs time-step size (left) and partial computational effort vs time-step size (right) for the approximation of $\mathbb{E}^{\omega}[X_t^1]$ for SDE (2.31) with $m = 6$

merical integration scheme for systems with uncertainty due to stochastic forcing in all the future analysis done in the present work. For the numerical integration of ordinary differential equations and partial differential equations (for studying uncertainty in input parameters), we use the explicit Runge-Kutta scheme (RK-4).

2.3 Methods for Uncertainty Quantification

In this section, we study schemes for uncertainty quantification of stochastic dynamical systems. We consider a general stochastic dynamical system represented by the differential equation

$$\frac{\partial X(r,t;\omega)}{\partial t} = \mathcal{L}\left[X(r,t;\omega),\omega\right] \qquad r \in D, t \in \mathcal{T}, \omega \in \Omega \tag{2.32}$$

where $X(r,t;\omega) \in \mathbb{R}^N$ is an N-dimensional stochastic variable representing the state of the system at any given time $t \in \mathcal{T}$ and $\mathcal{L}$ is any given nonlinear operator. The initial condition is given as

$$X(r,t_0,\omega) = X_0(r,\omega) \qquad r \in D, \omega \in \Omega \tag{2.33}$$

and the boundary conditions are specified as

$$\mathcal{B}\left[X(r_0,t;\omega)\right] = h(r_0,t;\omega) \qquad r_0 \in \partial D, t \in \mathcal{T}, \omega \in \Omega \tag{2.34}$$

We begin with a literature review of existing schemes and methodologies, including Monte Carlo simulations, generalized polynomial chaos, dynamically orthogonal field equations, proper orthogonal decomposition and error subspace statistical estimation. Next, we study generalized polynomial chaos and its derivative schemes, and dynamically orthogonal field equations in greater detail.

2.3.1 Literature review

The Monte Carlo simulation technique is perhaps the simplest and one of the most common methods for uncertainty quantification. This statistical sampling method was first introduced by von Neumann, who used it to study neutron diffusion (Eckhardt, 1987).

The mathematical foundation of Monte Carlo simulations lies in the Law of Large Numbers, which states that the average of a large number of independent samples of a random variable converges to the analytical mean of that random variable (Bertsekas and Tsitsiklis, 2002). Its theoretical basis has been described in detail in Zaremba (1968) and James (2000). Monte Carlo methods can be readily applied to solve problems to an arbitrary degree of accuracy, provided a sufficiently large number of samples is used. Over the years, significant advances have been made to improve the efficiency of these schemes. Some of these include variance reduction (Fishman, 1996, McGrath and Irving, 1973), importance sampling (Hastings, 1970, Gilks et al., 1995), sequential Monte-Carlo (Doucet et al., 2001), quasi-Monte Carlo (Niederreiter, 2010) and multi-level Monte Carlo methods (Giles, 2008b). Monte Carlo methods are easy to implement and are shown to converge without stringent regularity conditions. Another major advantage is that if we have an existing deterministic code for modeling a dynamical system, we do not need to modify it extensively to incorporate uncertainty when implementing the Monte Carlo scheme, as long as we can generate a sufficiently large number of independent samples. Because of its ease of implementation, Monte Carlo scheme has been a preferred method of solution for complex problems which are difficult to model using other stochastic methods. However, Monte Carlo schemes can have a very high computational cost and can become infeasible to implement for high dimensional systems. Hence, several new uncertainty quantification schemes have emerged in recent years, in order to increase the efficiency of modeling stochastic systems.

Development of new uncertainty quantification schemes continues to be a topic of active research. Polynomial chaos is a new approach to model uncertainty which has attracted increasing attention over recent years. The origin of this method is based on the work done by Norbert Wiener on homogeneous chaos theory (Wiener, 1938). Cameron and Martin showed that the expansion of any square-integrable functional in a series of Hermite polynomials of Gaussian random variables is L^2-convergent (Cameron and Martin, 1947). The Cameron-Martin theorem forms the mathematical basis of the polynomial chaos scheme. The polynomial chaos scheme uses polynomial functions as stochastic bases for expanding the uncertainty components of the stochastic field. The Wiener-Hermite

expansions were first used to study Gaussian and other similar stochastic processes in modeling turbulence (Kraichnan, 1963, Orszag and Bissonnette, 1967), but they were found to have some serious limitations (Crow and Canavan, 1970, Chorin, 1974), leading to a decrease of interest in the method. Later, Ghanem and Spanos developed a spectral stochastic finite element method using truncated Wiener-Hermite expansions in a Galerkin framework (Ghanem and Spanos, 1991). This work revived interest in the scheme and led to the development of stochastic Galerkin approach to polynomial chaos. Xiu and Karniadakis generalized the stochastic basis to include non-Gaussian stochastic processes by using Askey-scheme-based orthogonal polynomials (Xiu and Karniadakis, 2002), introducing the generalized polynomial chaos (gPC) scheme. The gPC scheme has been used in a variety of applications to study uncertainty, including transport in porous media (Ghanem, 1998), solid mechanics (Ghanem, 1999a,b), electrochemical flow (Debusschere et al., 2002, 2003), fluid flow (Le Maitre et al., 2002, Xiu and Karniadakis, 2003) and computational fluid dynamics (Knio and Le Maitre, 2006, Najm, 2009). It has also been extended to include arbitrary random distributions outside the Askey family of orthogonal polynomials (Soize and Ghanem, 2004, Wan and Karniadakis, 2006b). Although the gPC scheme has been used successfully to model uncertainty in many diverse applications, there are certain situations in which it is not very effective. These include modeling of parametric uncertainty in nonlinear systems with complex dynamics (limit cycles, strange attractors etc.) and long time integration of systems with external stochastic forcing (Branicki and Majda, 2012). Several new polynomial chaos schemes have been introduced in recent years which try to alleviate the shortcomings of gPC by using a dynamically adaptive polynomial chaos basis. Examples include the multi-element polynomial chaos (ME-gPC) scheme (Wan and Karniadakis, 2005, 2006a), time-dependent polynomial chaos (TDgPC) scheme (Gerritsma et al., 2010), Wiener chaos using sparse truncation (Hou et al., 2006, Luo, 2006), polynomial chaos using Wiener-Haar expansions (Le Maitre et al., 2004a) and multi-resolution polynomial chaos schemes (Le Maitre et al., 2004b, Le Maître et al., 2007, Najm et al., 2009). Some of these schemes are described in detail in section 3.2. Despite the success of these schemes in specific applications, long time integration of unsteady dynamics and uncorrelated stochastic noise continues to be a

significant challenge for polynomial chaos schemes (Debusschere et al., 2004, Ernst et al., 2012, Branicki and Majda, 2012).

Order reduction methods have also been utilized for uncertainty quantification. A classical order reduction method is Proper Orthogonal Decomposition (POD) scheme (Berkooz et al. (1993), Holmes et al. (1998)). This method uses a family of orthogonal spatial functions as bases to capture the dominant components of the stochastic processes. The POD scheme has been applied for uncertainty quantification in a wide range of applications such as turbulence (Sirovich (1987), Berkooz et al. (1993), Holmes et al. (1998), Lumley (2007)) and control of chemical processes (Gay and Ray (1995), Zhang et al. (2003), Shvartsman and Kevrekidis (2004)). However, the basis functions of POD scheme need to be chosen a priori and hence may not always be able to model the evolution of nonlinear dynamical processes accurately. Other examples of uncertainty quantification schemes include those mentioned in the works of Majda et al. (2001), Borcea et al. (2002), Schwab and Todor (2006), Babuška et al. (2007), Majda et al. (2008), Ma and Zabaras (2009), Owhadi et al. (2010), Dashti and Stuart (2011), Doostan and Owhadi (2011) and Majda and Branicki (2012).

Another approach to predict uncertainty for data assimilation is the Error Subspace Statistical Estimation scheme (ESSE) (Lermusiaux and Robinson, 1999, Lermusiaux, 1999). The motivation behind this scheme are multi-scale, intermittent, non-stationary and non-homogeneous uncertainty fields for ocean dynamics (Lermusiaux, 2006). This method uses adaptive and time-varying basis functions to represent the stochastic field. It focuses on the subspace where most of the uncertainty is concentrated as measured by a dominant decomposition of the time-variant covariance of the system, i.e., a time-dependent dominant Karhunen-Loève (K-L) expansion. This dominant decomposition and its basis eigenfunctions are evolved using ensemble predictions through a Monte Carlo approach. The advantage of this scheme is that it does not make any explicit assumption on the form of the stochastic field. A drawback is that the evolution of the basis functions uses Monte Carlo simulations.

Dynamically Orthogonal (DO) equations are new equations to predict uncertainty for dynamical systems (Sapsis and Lermusiaux, 2009, Sapsis, 2010). The DO method is

based on a time-dependent dominant K-L expansion and a Dynamical Orthogonality (DO) condition. The DO condition simply imposes that the rate of change of the dominant K-L expansion basis is orthogonal to the basis itself. This DO condition eliminates redundancy in the representation of the solution field, without imposing additional restrictions. As in ESSE, a major advantage is that the basis functions evolve in time, and are thus able to follow the dominant uncertainty in nonlinear dynamical systems in an efficient manner. The DO equations are a generalization of proper orthogonal decomposition (POD) and generalized polynomial chaos (gPC) schemes, and the governing equations of these schemes can be recovered from the DO equations with additional assumptions, a steady (spatial) basis or a steady stochastic basis, respectively. A closely linked scheme is the Dynamically Bi-Orthogonal (DyBO) method (Cheng et al., 2012). The DO equations have been used for uncertainty quantification in fluid and ocean-relevant flows (Sapsis, 2010, Sapsis and Lermusiaux, 2012, Ueckermann et al., 2013) and extended for use in non-Guassian data assimilation (Sondergaard, 2011, Sondergaard and Lermusiaux, 2013a,b).

2.3.2 Generalized polynomial chaos

A polynomial chaos expansion is an expansion of the stochastic field in terms of polynomial functions of stochastic random variables. A uni-variate polynomial chaos expansion of a stochastic field $X(r,t;\omega)$ has the form

$$X(r,t;\omega) = \sum_{i=0}^{p} \tilde{x}_i(r,t)\psi_i(\xi(\omega)) \tag{2.35}$$

where p is the polynomial order of the expansion, $\psi_i(\xi(\omega))$ are the stochastic basis functions of the random variable $\xi(\omega)$ and $\tilde{x}_i(r,t)$ are the corresponding deterministic coefficients. For optimal convergence, the choice of polynomial basis functions depends on the expected form of the uncertainty in the dynamical system. For example, if it is known that the random variable ξ is a uniform random variable, the basis functions ψ are chosen to be Legendre polynomials, i.e., $\psi_i(\xi) = L_i(\xi)$. Legendre polynomials are given by the

Table 2.5: Basis functions for polynomial chaos expansions

	Random variables (ξ)	Polynomial basis functions $\psi(\xi)$	Support
Continuous	Gaussian	Hermite	$(-\infty, \infty)$
	Gamma	Laguerre	$[0, \infty)$
	Beta	Jacobi	$[a, b]$
	Uniform	Legendre	$[a, b]$
Discrete	Poisson	Charlier	$\{0, 1, 2, ...\}$
	Binomial	Krawtchouk	$\{0, 1, 2, ..., N\}$
	Negative Binomial	Meixner	$\{0, 1, 2, ...\}$
	Hypergeometric	Hahn	$\{0, 1, 2, ..., N\}$

where $a, b \in \mathbb{R}$ and $N \geq 0$ is a finite integer

recurrence relation

$$\begin{aligned} L_0(\xi) &= 1 \\ L_1(\xi) &= \xi \\ L_{i+1}(\xi) &= \frac{(2i+1)\xi L_i(\xi) - iL_{i-1}(\xi)}{i+1} \qquad \text{for } i = 1, 2, 3, ... \end{aligned} \tag{2.36}$$

Similarly, for Gaussian uncertainty, the basis functions ψ are chosen to be Hermite polynomials, i.e., $\psi_i(\xi) = H_i(\xi)$. Hermite polynomials are given by the recurrence relation

$$\begin{aligned} H_0(\xi) &= 1 \\ H_1(\xi) &= \xi \\ H_{i+1}(\xi) &= \xi H_i(\xi) - iH_{i-1}(\xi) \qquad \text{for } i = 1, 2, 3, ... \end{aligned} \tag{2.37}$$

The choice of polynomial basis functions corresponding to various forms of uncertainty is presented in table (2.5). For the multi-variate stochastic case, the generalized polynomial chaos expansion has the form

$$\begin{aligned} X(r, t; \omega) &= \sum_{|\alpha| \leq p} \tilde{x}_\alpha(r, t) \Psi_\alpha(\xi_1(\omega), \xi_2(\omega), .., \xi_{\bar{r}}(\omega)) \\ &= \sum_{i=0}^{s-1} \tilde{x}_i(r, t) \Psi_i(\omega) \end{aligned} \tag{2.38}$$

where α is a multi-index $\alpha = (\alpha_1, \alpha_2, ..., \alpha_{\bar{r}})$, $|\alpha| = \sum_{j=1}^{\bar{r}} \alpha_j$, $\bar{r}$ is the number of random variables (stochastic dimension) and p is the order of the multi-variate polynomial chaos expansion. In addition, in equation (2.38), the multi-variate polynomial basis functions are defined as

$$\Psi_\alpha = \prod_{j=1}^{\bar{r}} \psi_{\alpha_j}(\xi_j(\omega)) \tag{2.39}$$

where $\psi_{\alpha_j}(\xi_j(\omega))$ are the uni-variate polynomial basis functions, and the total number of terms in the expansion is given by

$$s = \binom{\bar{r}+p}{\bar{r}} = \frac{(\bar{r}+p)!}{\bar{r}!\,p!} \tag{2.40}$$

As an example, we consider a Hermite chaos expansion with $\bar{r} = 3$ and $p = 2$. The total number of terms in the expansion are $s = \binom{3+2}{3} = 10$. The set of multi-indices α is given as $\{\alpha\} = \{(0,0,0), (1,0,0), (0,1,0), (0,0,1), (2,0,0), (0,2,0), (0,0,2), (1,1,0), (1,0,1), (0,1,1)\}$. The multi-variate basis functions are calculated as

$$\begin{aligned}
\Psi_{(0,0,0)} &= H_0(\xi_1)H_0(\xi_2)H_0(\xi_3) = 1 \\
\Psi_{(1,0,0)} &= H_1(\xi_1)H_0(\xi_2)H_0(\xi_3) = H_1(\xi_1) = \xi_1 \\
\Psi_{(0,1,0)} &= H_0(\xi_1)H_1(\xi_2)H_0(\xi_3) = H_1(\xi_2) = \xi_2 \\
\Psi_{(0,0,1)} &= H_0(\xi_1)H_0(\xi_2)H_1(\xi_3) = H_1(\xi_3) = \xi_3 \\
\Psi_{(2,0,0)} &= H_2(\xi_1)H_0(\xi_2)H_0(\xi_3) = H_2(\xi_1) = \xi_1^2 - 1 \\
\Psi_{(0,2,0)} &= H_0(\xi_1)H_2(\xi_2)H_0(\xi_3) = H_2(\xi_2) = \xi_2^2 - 1 \\
\Psi_{(0,0,2)} &= H_0(\xi_1)H_0(\xi_2)H_2(\xi_3) = H_2(\xi_3) = \xi_3^2 - 1 \\
\Psi_{(1,1,0)} &= H_1(\xi_1)H_1(\xi_2)H_0(\xi_3) = H_1(\xi_1)H_1(\xi_2) = \xi_1\xi_2 \\
\Psi_{(1,0,1)} &= H_1(\xi_1)H_0(\xi_2)H_1(\xi_3) = H_1(\xi_1)H_1(\xi_3) = \xi_1\xi_3 \\
\Psi_{(0,1,1)} &= H_0(\xi_1)H_1(\xi_2)H_1(\xi_3) = H_1(\xi_2)H_1(\xi_3) = \xi_2\xi_3
\end{aligned} \tag{2.41}$$

Finally, the multivariate polynomial chaos expansion for this example is given as

$$\begin{aligned} X(r,t;\omega) &= \sum_{|\alpha|\leq 2} \tilde{x}_\alpha(r,t)\Psi_\alpha(\xi_1(\omega),\xi_2(\omega),\xi_3(\omega)) \\ &= \tilde{x}_{(0,0,0)}(r,t) + \tilde{x}_{(1,0,0)}(r,t)\xi_1 + \tilde{x}_{(0,1,0)}(r,t)\xi_2 + \tilde{x}_{(0,0,1)}(r,t)\xi_3 \\ &\quad + \tilde{x}_{(2,0,0)}(r,t)(\xi_1^2-1) + \tilde{x}_{(0,2,0)}(r,t)(\xi_2^2-1) + \tilde{x}_{(0,0,2)}(r,t)(\xi_3^2-1) \\ &\quad + \tilde{x}_{(1,1,0)}(r,t)\xi_1\xi_2 + \tilde{x}_{(1,0,1)}(r,t)\xi_1\xi_3 + \tilde{x}_{(0,1,1)}(r,t)\xi_2\xi_3 \\ &= \sum_{i=0}^{9} \tilde{x}_i(r,t)\Psi_i(\omega) \end{aligned} \tag{2.42}$$

Next, we consider the stochastic dynamical system (2.32) with the initial and boundary conditions (2.33) and (2.34), respectively. Consider a multi-variate polynomial chaos expansion of $X(r,t;\omega)$ given by

$$X(r,t;\omega) = \sum_{i=0}^{s-1} \tilde{x}_i(r,t)\Psi_i(\omega) \tag{2.43}$$

where $\Psi_i(\omega)$ represent the stochastic polynomial bases functions and $\tilde{x}_i(r,t) \in \mathbb{R}^N$ represent their corresponding N-dimensional deterministic coefficients. To obtain the evolution equations for the polynomial chaos scheme, we substitute the polynomial chaos expansion into the governing equation and take a stochastic Galerkin projection, which is equivalent to multiplying the resultant equation by $\Psi_j(\omega)$ and applying the mean value operator. Substituting the expansion from equation (2.43) into equation (2.32) and multiplying by $\Psi_j(\omega)$, we get (in Einstein notation)

$$\frac{\partial \tilde{x}_i(r,t)}{\partial t}\Psi_i(\omega)\Psi_j(\omega) = \mathcal{L}\left[X(r,t;\omega),\omega\right]\Psi_j(\omega) \tag{2.44}$$

Applying the mean value operator to equation (2.44), we obtain

$$\frac{\partial \tilde{x}_i(r,t)}{\partial t}\mathrm{E}^\omega\left[\Psi_i(\omega)\Psi_j(\omega)\right] = \mathrm{E}^\omega\left[\mathcal{L}\left[X(r,t;\omega),\omega\right]\Psi_j(\omega)\right] \tag{2.45}$$

The evolution equations for the coefficients $\tilde{x}(r,t)$ are given as

$$\frac{\partial \tilde{x}_i(r,t)}{\partial t} = \mathrm{E}^{\omega}\left[\mathcal{L}\left[X(r,t;\omega),\omega\right]\Psi_j(\omega)\right] C^{-1}_{\Psi_i\Psi_j} \qquad 0 \leq i,j \leq s-1 \tag{2.46}$$

where

$$C_{\Psi_i\Psi_j} = \mathrm{E}^{\omega}\left[\Psi_i(\omega)\Psi_j(\omega)\right] \tag{2.47}$$

The initial and boundary conditions for the coefficients are obtained by substituting the polynomial chaos expansion from (2.43) into (2.33) and (2.34), respectively, and then taking Galerkin projections. The initial conditions on the coefficients are given as

$$\tilde{x}_i(r,t_0) = \tilde{x}_{i_0}(r) \qquad 0 \leq i \leq s-1 \tag{2.48}$$

and the associated boundary conditions are of the form

$$\mathcal{B}\left[\tilde{x}_i(r_0,t)\right] = \mathrm{E}^{\omega}\left[h(r_0,t;\omega)\Psi_j(\omega)\right] C^{-1}_{\Psi_i\Psi_j} \qquad 0 \leq i,j \leq s-1 \tag{2.49}$$

2.3.3 Time-dependent generalized polynomial chaos

The time-dependent generalized polynomial chaos scheme (TDgPC), developed by Gerritsma et al. (2010), is a modification of the gPC scheme and is useful for long time integration of nonlinear stochastic systems with uncertainty in input parameters. The TDgPC scheme utilizes a Gram-Schmidt orthogonalization technique to generate a family of orthogonal polynomials, to be used as stochastic bases in the polynomial chaos expansion of the uncertainty field. The basic idea is that as the probability density function (pdf) of the uncertainty field changes as a function of time, it requires a different set of orthogonal polynomials for its representation (as also discussed in section 2.3.1). In the TDgPC scheme of Gerritsma et al. (2010), the basis functions are time-dependent and are generated at every *re-initialization* step. However, the equations for the time evolution of coefficients have the same form as the evolution equations for the gPC scheme.

2.3.4 Wiener chaos using sparse truncation

Hou et al. (2006) have developed a numerical method based on the gPC scheme for uncertainty quantification of dynamical systems with external stochastic forcing. This scheme involves the use of a compression technique to deal with the sustained influx of new random variables, as provided by the sustained stochastic forcing with time. Let us consider the stochastic dynamical system represented by equation (1.1). Also consider any time $T > 0$ and any orthonormal basis $\{\tilde{m}_i(t), i = 1, 2, ...\}$ in $L^2([0, T])$. For example, consider the trigonometric basis defined as

$$\begin{aligned} \tilde{m}_1(t) &= \frac{1}{\sqrt{T}} \\ \tilde{m}_i(t) &= \sqrt{\frac{2}{T}} \cos \frac{(i-1)\pi t}{T} \qquad i = 2, 3, ... \end{aligned} \tag{2.50}$$

We define random variables $\xi_i(\omega)$ as

$$\xi_i(\omega) = \int_0^T \tilde{m}_i(t) dW(t; \omega) \qquad i = 1, 2, ... \tag{2.51}$$

It can be shown that when the stochastic noise is Gaussian, $\xi_i(\omega)$ are independent identically distributed standard Gaussian random variables, i.e., $\xi_i(\omega) \sim \mathcal{N}(0, 1)$. Also the Wiener process can be represented as

$$W(t; \omega) = \sum_{i=1}^{\infty} \xi_i(\omega) \int_0^t \tilde{m}_i(\tau) dW(\tau, \omega) \tag{2.52}$$

and converges in the mean square sense

$$\mathbb{E}^{\omega} \left[W(t; \omega) - \sum_{i=1}^{n} \xi_i(\omega) \int_0^t \tilde{m}_i(\tau) dW(\tau, \omega) \right]^2 \to 0 \qquad \text{as} \qquad n \to \infty \tag{2.53}$$

for $t \leq T$. The mean square convergence is a result of the Cameron-Martin theorem discussed in section 2.3.1. Expanding this representation of the stochastic forcing integrated over time $[0, T]$ instead of the original instantaneous $dW(t; \omega)$ can be more efficient since the number of random variables needed for a good approximation can be reduced by the time-integration. In those cases, using equations (2.51) and (2.52), we can employ an

efficient polynomial chaos expansion in random variables $\xi_i(\omega)$ and derive equations for the evolution of the corresponding deterministic coefficients, similar to the gPC scheme.

Additionally, the scheme utilizes sparse truncation to reduce the number of terms in the polynomial chaos expansion. In the generalized polynomial chaos scheme, for all random variables $\xi_i(\omega), 1 \leq i \leq \bar{r}$, polynomials of all orders are used, with the truncation condition specified as $\sum_{i=1}^{\bar{r}} \alpha_i \leq p$. With the sparse truncation scheme however, it is recognized that it is better to use lower order polynomials for $\xi_i(\omega)$ with higher values of subscript i. Hence, some additional constraints such as $\alpha_i \leq p - i$ have been introduced, which reduce the number of terms required in the polynomial chaos representation of the stochastic field. This idea is similar to the sparse tensor product developed by Schwab for solving random elliptic problems by polynomial chaos methods (Frauenfelder et al., 2005). Moreover, some of the random variables are decoupled from the rest to further reduce the number of terms in the expansion.

The sparse truncation Wiener chaos scheme by Hou et al. (2006) has been used successfully for uncertainty quantification of dynamical systems with Gaussian noise for short time intervals and has been shown to be computationally more efficient than the Monte Carlo scheme. However, the number of random variables $\xi_i(\omega)$ required to accurately represent the dynamics of the system can still increase rapidly with time and quickly grow beyond computationally acceptable limits, making the scheme unsuitable for uncertainty quantification over large time intervals (Branicki and Majda, 2012).

2.3.5 Dynamically orthogonal field equations

A Dynamically Orthogonal (DO) decomposition of the stochastic field $X(r,t;\omega)$ has the form

$$X(r,t;\omega) = \bar{x}(r,t) + \sum_{i=1}^{s} \tilde{x}_i(r,t)\phi_i(t;\omega) \tag{2.54}$$

where $\bar{x}(r,t)$ is the mean of the stochastic field, defined as

$$\bar{x}(r,t) = \mathbb{E}^{\omega}\left[X(r,t;\omega)\right] \tag{2.55}$$

and s is a non-negative integer representing the number of terms in the DO expansion. The basis functions $\tilde{x}_i(r,t)$ are deterministic and are also known as DO *modes*, whereas $\phi_i(t;\omega)$ represent the stochastic *coefficients*. The *stochastic subspace* V_s is the linear space spanned by the s DO modes and is defined as

$$V_s = \text{span}\{\tilde{x}_i(r,t)\} \qquad 1 \leq i \leq s \tag{2.56}$$

It represents a subspace of the physical space where most of the uncertainty (probability measure) of the random field $X(r,t;\omega)$ resides at time t.

It is seen from equation (2.54) that the mean $\bar{x}(r,t)$, modes $\tilde{x}_i(r,t)$ and coefficients $\phi_i(t;\omega)$ are all time-dependent quantities. It is also observed that the simultaneous variation of the modes and the coefficients in time to represent the evolution of uncertainty is a source of redundancy. Therefore, additional constraints can be imposed to derive closed-form evolution equations for these mean, modes and coefficients. The additional constraint is imposed by restricting the time-rate-of-change of the basis $\tilde{x}_i(r,t)$ to be normal to the stochastic subspace V_s itself. This condition on the evolution of modes is known as the dynamically orthogonal (DO) condition and is represented as

$$\frac{dV_s}{dt} \perp V_s \Leftrightarrow \left\langle \frac{\partial \tilde{x}_i(\bullet,t)}{\partial t}, \tilde{x}_j(\bullet,t) \right\rangle = 0 \qquad 1 \leq i,j \leq s \tag{2.57}$$

where "$\langle\ \rangle$" represents an inner product in space (evaluated by an integral) and "$\bullet$" represents the dummy variable for this integration. Using condition (2.57), one can derive a set of independent explicit equations for the evolution of the mean, modes and coefficients.

The DO evolution equations for the stochastic dynamical system represented by (2.32), (2.33) and (2.34) are derived and discussed in Sapsis and Lermusiaux (2009, 2012) and Ueckermann et al. (2013). Next, we summarize some of this previous work.

Consider the DO expansion of the stochastic field $X(r,t;\omega)$ given by equation (2.54). Substituting this expansion into equation (2.32), we obtain

$$\frac{\partial \bar{x}(r,t)}{\partial t} + \frac{d\phi_i(t;\omega)}{dt}\tilde{x}_i(r,t) + \phi_i(t;\omega)\frac{\partial \tilde{x}_i(r,t)}{\partial t} = \mathcal{L}\left[X(r,t;\omega),\omega\right] \tag{2.58}$$

which is the basic equation from which the DO governing equations for the mean, coeffi-

cients and modes are obtained.

Evolution equation for mean field. By applying the mean value operator to equation (2.58), we obtain the evolution equation for the mean of the stochastic field, given as

$$\frac{\partial \bar{x}(r,t)}{\partial t} = \mathbb{E}^{\omega}\left[\mathcal{L}\left[X(r,t;\omega),\omega\right]\right] \tag{2.59}$$

Evolution equation for stochastic coefficients. We first take the inner product of equation (2.58) with each of the modes $\tilde{x}_j(r,t)$ to obtain

$$\begin{aligned}\left\langle \frac{\partial \bar{x}(\bullet,t)}{\partial t}, \tilde{x}_j(\bullet,t)\right\rangle + \frac{d\phi_i(t;\omega)}{dt}\left\langle \tilde{x}_i(\bullet,t), \tilde{x}_j(\bullet,t)\right\rangle \\ + \phi_i(t;\omega)\left\langle \frac{\partial \tilde{x}_i(\bullet,t)}{\partial t}, \tilde{x}_j(\bullet,t)\right\rangle = \left\langle \mathcal{L}\left[X(\bullet,t;\omega),\omega\right], \tilde{x}_j(\bullet,t)\right\rangle\end{aligned} \tag{2.60}$$

The third term on the left hand side vanishes by the DO condition (2.57). Additionally, by orthogonality of the DO modes (if they are orthogonal initially, (2.57) ensures that they are orthogonal for all times), the second term on the left hand side is non-zero only for the term $i = j$. For the first term of the right-hand-side, we take the inner product of (2.59) with $\tilde{x}_j(r,t)$ and obtain

$$\left\langle \frac{\partial \bar{x}(\bullet,t)}{\partial t}, \tilde{x}_j(\bullet,t)\right\rangle = \mathbb{E}^{\omega}\left[\left\langle \mathcal{L}\left[X(\bullet,t;\omega),\omega\right], \tilde{x}_j(\bullet,t)\right\rangle\right] \tag{2.61}$$

Using these facts, equation (2.60) reduces to the evolution equation for the stochastic coefficients, given as

$$\frac{d\phi_i(t;\omega)}{dt} = \left\langle \mathcal{L}\left[X(\bullet,t;\omega),\omega\right] - \mathbb{E}^{\omega}\left[\mathcal{L}\left[X(\bullet,t;\omega),\omega\right]\right], \tilde{x}_i(\bullet,t)\right\rangle \qquad 1 \le i \le s \tag{2.62}$$

Evolution equation for DO modes. Instead of a projection of (2.58) onto the modes and a spatial integration, by duality, we now multiply with stochastic coefficients and take a statistical average. Hence, multiplying (2.58) with $\phi_j(t;\omega)$ and applying the mean

value operator, the first term cancels since $\mathbb{E}^{\omega}\left[\phi_j(t;\omega)\right] = 0$, and we obtain

$$\begin{aligned}\mathbb{E}^{\omega}\left[\frac{d\phi_i(t;\omega)}{dt}\phi_j(t;\omega)\right]\tilde{x}_i(r,t) + \mathbb{E}^{\omega}\left[\phi_i(t;\omega)\phi_j(t;\omega)\right]\frac{\partial\tilde{x}_i(r,t)}{\partial t} \\ = \mathbb{E}^{\omega}\left[\mathcal{L}\left[X(r,t;\omega),\omega\right]\phi_j(t;\omega)\right]\end{aligned} \tag{2.63}$$

To replace $\frac{d\phi_i(t;\omega)}{dt}$ in the first term of (2.63), we multiply (2.62) with $\phi_j(t;\omega)$ and apply the mean value operator to obtain

$$\mathbb{E}^{\omega}\left[\frac{d\phi_i(t;\omega)}{dt}\phi_j(t;\omega)\right] = \mathbb{E}^{\omega}\left[\left\langle\mathcal{L}\left[X(\bullet,t;\omega),\omega\right],\tilde{x}_i(\bullet,t)\right\rangle\phi_j(t;\omega)\right] \tag{2.64}$$

Inserting this expression into (2.63) and simplifying, we obtain the evolution equation for the DO modes, which is given as

$$\frac{\partial\tilde{x}_i(r,t)}{\partial t} = \Pi_{V_s}^{\perp}\left[\mathbb{E}^{\omega}\left[\mathcal{L}\left[X(r,t;\omega),\omega\right]\phi_j(t;\omega)\right]\right]C^{-1}_{\phi_i\phi_j} \qquad 1 \leq i,j \leq s \tag{2.65}$$

where

$$\Pi_{V_s}^{\perp}\left[F(x)\right] = F(x) - \Pi_{V_s}\left[F(x)\right] = F(x) - \left\langle F(\bullet),\tilde{x}_i(\bullet,t)\right\rangle\tilde{x}_i(r,t) \tag{2.66}$$

and

$$C_{\phi_i\phi_j} = \mathbb{E}^{\omega}\left[\phi_i(t;\omega)\phi_j(t;\omega)\right] \tag{2.67}$$

The initial and boundary conditions for the evolution equations can be obtained by substituting the DO expansion in equations (2.33) and (2.34), using a similar analysis as done for the governing equation. The initial conditions are given as

$$\begin{aligned}\bar{x}(r,t_0) &= \bar{x}_0(r) = \mathbb{E}^{\omega}\left[X_0(r,\omega)\right] \\ \phi_i(t_0,\omega) &= \left\langle X_0(\bullet;\omega) - \bar{x}_0(\bullet),\tilde{x}_{i_0}(\bullet)\right\rangle \\ \tilde{x}_i(r,t_0) &= \tilde{x}_{i_0}(r)\end{aligned} \tag{2.68}$$

where $\tilde{x}_{i_0}$ are the s most dominant modes of the initial error covariance of the system

state. The associated boundary conditions are given as

$$\begin{aligned} \mathcal{B}\left[\bar{x}(r_0,t)\right] &= \mathrm{E}^{\omega}\left[h(r_0,t;\omega)\right] \\ \mathcal{B}\left[\tilde{x}_i(r_0,t)\right] &= \mathrm{E}^{\omega}\left[h(r_0,t;\omega)\phi_j(t;\omega)\right] C^{-1}_{\phi_i\phi_j} \end{aligned} \tag{2.69}$$

Chapter 3

Derivation of Evolution Equations

In this chapter, we derive evolution equations for the class of non-autonomous linear and nonlinear systems represented by (1.1) and its special case (1.2), using Dynamically Orthogonal (DO) equations, generalized Polynomial Chaos (gPC) and several polynomial chaos derivative schemes. We also introduce two novel polynomial chaos schemes, namely, the modified TDgPC scheme and the KLgPC scheme, which are capable of modeling dynamical systems with additive and multiplicative stochastic forcing over arbitrarily large time intervals.

3.1 Dynamically Orthogonal Equations

We consider the class of stochastic dynamical systems whose governing equation is (1.1) and derive its DO evolution equations. We then address its special quadratic-nonlinearity case (1.2).

Derivation of DO governing equations for (1.1)

Substituting the DO expansion (2.54) in equation (1.1), we have

$$\begin{aligned} & d\bar{x}(r,t) + d\phi_i(t;\omega)\tilde{x}_i(r,t) + \phi_i(t;\omega)d\tilde{x}_i(r,t) \\ & \quad = A(\bar{x}(r,t) + \tilde{x}_k(r,t)\phi_k(t;\omega),t)\ (\bar{x}(r,t) + \tilde{x}_l(r,t)\phi_l(t;\omega))\,dt \\ & \quad + B(\bar{x}(r,t) + \tilde{x}_m(r,t)\phi_m(t;\omega),t)\,dW(t;\omega) \end{aligned} \tag{3.1}$$

This is again the basic equation from which the DO governing equations for the mean, coefficients and modes are obtained. In the remaining part of the derivation, we omit the arguments (r,t) after the deterministic mean $\bar{x}(r,t)$ and modes $\tilde{x}_i(r,t)$ and the arguments $(t;\omega)$ after the stochastic coefficients $\phi_i(t;\omega)$ and incremental Brownian motion $dW(t;\omega)$.

Evolution equation for mean field:

Applying the mean value operator to (3.1), we obtain the evolution equation for the mean of the stochastic field, given as

$$d\bar{x} = \mathrm{E}^{\omega}\left[A(\bar{x}+\tilde{x}_k\phi_k,t)\ (\bar{x}+\tilde{x}_l\phi_l)\right]dt + \mathrm{E}^{\omega}\left[B(\bar{x}+\tilde{x}_m\phi_m,t)\,dW\right] \tag{3.2}$$

Evolution equation for stochastic coefficients:

Taking the inner product of (3.1) with each of the modes $\tilde{x}_j(r,t)$ and simplifying the resulting equation, we obtain the evolution equation for the stochastic coefficients, given as

$$\begin{aligned} d\phi_i = &\left\langle A(\bar{x}+\tilde{x}_j\phi_j,t)\left[\bar{x}+\tilde{x}_k\phi_k\right] - \mathrm{E}^{\omega}\left[A(\bar{x}+\tilde{x}_l\phi_l,t)\left[\bar{x}+\tilde{x}_m\phi_m\right]\right],\tilde{x}_i\right\rangle dt \\ &+ \left\langle B(\bar{x}+\tilde{x}_n\phi_n,t)dW - \mathrm{E}^{\omega}\left[B(\bar{x}+\tilde{x}_p\phi_p,t)dW\right],\tilde{x}_i\right\rangle \end{aligned} \tag{3.3}$$

Evolution equation for DO modes:

Instead of a projection of (3.1) onto modes and a spatial integration, by duality, we now multiply with stochastic coefficients and take a statistical average. Hence, multiplying (3.1) with $\phi_j(t;\omega)$ and applying the mean value operator, the first term cancels since $\mathrm{E}^{\omega}\left[\phi_j(t;\omega)\right]=0$ and we obtain

$$\begin{aligned} &\mathrm{E}^{\omega}\left[d\phi_i\phi_j\right]\tilde{x}_i + \mathrm{E}^{\omega}\left[\phi_i\phi_j\right]d\tilde{x}_i \\ &\quad = \mathrm{E}^{\omega}\left[A(\bar{x}+\tilde{x}_k\phi_k,t)\left[\bar{x}+\tilde{x}_l\phi_l\right]\phi_j\right]dt + \mathrm{E}^{\omega}\left[B(\bar{x}+\tilde{x}_m\phi_m,t)dW\phi_j\right] \end{aligned} \tag{3.4}$$

The expression for $\mathrm{E}^{\omega}\left[d\phi_i(t;\omega)\phi_j(t;\omega)\right]$ can be obtained by multiplying equation (3.3) by $\phi_j(t;\omega)$ and applying the mean value operator. Substituting this expression in equation

(3.4) and simplifying, we obtain the evolution equation for the DO modes, given as

$$d\tilde{x}_i = \mathrm{E}^{\omega}\Big[A(\bar{x}+\tilde{x}_k\phi_k,t)\,[\bar{x}+\tilde{x}_l\phi_l]\,\phi_j - \Big\langle A(\bar{x}+\tilde{x}_n\phi_n,t)\,[\bar{x}+\tilde{x}_p\phi_p]\,\phi_j,\tilde{x}_m\Big\rangle\tilde{x}_m\Big]C^{-1}_{\phi_i\phi_j}dt$$
$$+\,\mathrm{E}^{\omega}\Big[B(\bar{x}+\tilde{x}_q\phi_q)dW\phi_j - \Big\langle B(\bar{x}+\tilde{x}_z\phi_z)dW\phi_j,\tilde{x}_m\Big\rangle\tilde{x}_m\Big]C^{-1}_{\phi_i\phi_j} \tag{3.5}$$

Summary of DO governing equations for (1.1)

To summarize, we reinsert the arguments (r,t) after the deterministic mean $\bar{x}$ and modes $\tilde{x}_i$, and arguments $(t;\omega)$ after the stochastic coefficients ϕ_i and incremental Brownian motion dW. The DO evolution equations for the mean, coefficients and modes have the final form

$$d\bar{x}(r,t) = \mathbb{E}^{\omega}\left[A(\bar{x}(r,t)+\tilde{x}_k(r,t)\phi_k(t;\omega),t)\;(\bar{x}(r,t)+\tilde{x}_l(r,t)\phi_l(t;\omega))\right]dt$$
$$+\,\mathbb{E}^{\omega}\left[B(\bar{x}(r,t)+\tilde{x}_m(r,t)\phi_m(t;\omega),t)\,dW(t;\omega)\right] \tag{3.6}$$

$$d\phi_i(t;\omega) = \Big\langle A(\bar{x}(\bullet,t)+\tilde{x}_j(\bullet,t)\phi_j(t;\omega),t)\,[\bar{x}(\bullet,t)+\tilde{x}_k(\bullet,t)\phi_k(t;\omega)]$$
$$-\mathrm{E}^{\omega}\left[A(\bar{x}(\bullet,t)+\tilde{x}_l(\bullet,t)\phi_l(t;\omega),t)\right]$$
$$\left[\bar{x}(\bullet,t)+\tilde{x}_m(\bullet,t)\phi_m(t;\omega)\right],\tilde{x}_i(\bullet,t)\Big\rangle dt \tag{3.7}$$
$$+\Big\langle B(\bar{x}(\bullet,t)+\tilde{x}_n(\bullet,t)\phi_n(t;\omega),t)dW(t;\omega)$$
$$-\,\mathrm{E}^{\omega}\left[B(\bar{x}(\bullet,t)+\tilde{x}_p(\bullet,t)\phi_p(t;\omega),t)dW(t;\omega)\right],\tilde{x}_i(\bullet,t)\Big\rangle$$

$$d\tilde{x}_i(r,t) = \mathrm{E}^{\omega}\Big[A(\bar{x}(r,t)+\tilde{x}_k(r,t)\phi_k(t;\omega),t)\,[\bar{x}(r,t)+\tilde{x}_l(r,t)\phi_l(t;\omega)]\,\phi_j(t;\omega)$$
$$-\Big\langle A(\bar{x}(r,t)+\tilde{x}_n(r,t)\phi_n(t;\omega),t)\,[\bar{x}(r,t)+\tilde{x}_p(r,t)\phi_p(t;\omega)]$$
$$\phi_j(t;\omega),\tilde{x}_m(r,t)\Big\rangle\tilde{x}_m(r,t)\Big]C^{-1}_{\phi_i\phi_j}dt$$
$$+\,\mathrm{E}^{\omega}\Big[B(\bar{x}(r,t)+\tilde{x}_q(r,t)\phi_q(t;\omega),t)dW(t;\omega)\phi_j(t;\omega)$$
$$-\Big\langle B(\bar{x}(r,t)+\tilde{x}_z(r,t)\phi_z(t;\omega),t)dW(t;\omega)\phi_j(t;\omega),\tilde{x}_m(r,t)\Big\rangle\tilde{x}_m(r,t)\Big]C^{-1}_{\phi_i\phi_j} \tag{3.8}$$

DO governing equations for quadratic-nonlinear systems (1.2)

For the special case when A and B are at most linear in $X(r,t;\omega)$ as represented by equation (1.2), we can further simplify the equations (3.6), (3.7) and (3.8). After performing these simplifications, the final evolution equation for the mean $\bar{x}(r,t)$ of the stochastic field is given as

$$d\bar{x} = A_0(t)\bar{x}dt + A_1(\bar{x},t)\bar{x}dt + A_1(\tilde{x}_i,t)\tilde{x}_j \mathrm{E}^{\omega}\left[\phi_i\phi_j\right]dt + B_1(\tilde{x}_i,t)\mathrm{E}^{\omega}\left[\phi_i dW\right] \tag{3.9}$$

The evolution equation for the stochastic coefficients $\phi_i(t;\omega)$ has the form

$$\begin{aligned} d\phi_i = {} & \left\langle A_0(t)\tilde{x}_j, \tilde{x}_i\right\rangle \phi_j dt + \left\langle A_1(\bar{x},t)\tilde{x}_j, \tilde{x}_i\right\rangle \phi_j dt + \left\langle A_1(\tilde{x}_k,t)\bar{x}, \tilde{x}_i\right\rangle \phi_k dt \\ & + \left\langle A_1(\tilde{x}_k,t)\tilde{x}_j, \tilde{x}_i\right\rangle \left(\phi_k\phi_j - \mathrm{E}^{\omega}\left[\phi_k\phi_j\right]\right)dt \\ & + \left\langle B_0(t), \tilde{x}_i\right\rangle dW + \left\langle B_1(\bar{x},t), \tilde{x}_i\right\rangle dW \\ & + \left\langle B_1(\tilde{x}_k,t), \tilde{x}_i\right\rangle \left(\phi_k dW - \mathrm{E}^{\omega}\left[\phi_k dW\right]\right) \end{aligned} \tag{3.10}$$

Finally, the evolution equation for the DO modes is given as

$$\begin{aligned} d\tilde{x}_i = {} & \left[A_0(t)\tilde{x}_i - \left\langle A_0(t)\tilde{x}_i, \tilde{x}_j\right\rangle \tilde{x}_j\right] dt + \left[A_1(\bar{x},t)\tilde{x}_i - \left\langle A_1(\bar{x},t)\tilde{x}_i, \tilde{x}_j\right\rangle \tilde{x}_j\right] dt \\ & + \left[A_1(\tilde{x}_k,t)\bar{x} - \left\langle A_1(\tilde{x}_k,t)\bar{x}, \tilde{x}_m\right\rangle \tilde{x}_m\right] \mathrm{E}^{\omega}\left[\phi_k\phi_j\right] C^{-1}_{\phi_i\phi_j} dt \\ & + \left[A_1(\tilde{x}_k,t)\tilde{x}_p - \left\langle A_1(\tilde{x}_k,t)\tilde{x}_p, \tilde{x}_m\right\rangle \tilde{x}_m\right] \mathrm{E}^{\omega}\left[\phi_k\phi_p\phi_j\right] C^{-1}_{\phi_i\phi_j} dt \\ & + \left[B_0(t) - \left\langle B_0(t), \tilde{x}_m\right\rangle \tilde{x}_m\right] \mathrm{E}^{\omega}\left[dW\phi_j\right] C^{-1}_{\phi_i\phi_j} \\ & + \left[B_1(\bar{x},t) - \left\langle B_1(\bar{x},t), \tilde{x}_m\right\rangle \tilde{x}_m\right] \mathrm{E}^{\omega}\left[dW\phi_j\right] C^{-1}_{\phi_i\phi_j} \\ & + \left[B_1(\tilde{x}_k,t) - \left\langle B_1(\tilde{x}_k,t), \tilde{x}_m\right\rangle \tilde{x}_m\right] \mathrm{E}^{\omega}\left[\phi_k dW\phi_j\right] C^{-1}_{\phi_i\phi_j} \end{aligned} \tag{3.11}$$

3.2 Generalized Polynomial Chaos

We consider again the class of stochastic dynamical systems whose governing equation is (1.1) and derive its gPC evolution equations. We then address its special quadratic-nonlinearity case (1.2).

Derivation of gPC governing equations for (1.1)

Substituting the polynomial chaos expansion from equation (2.43) into equation (1.1) and

taking a stochastic Galerkin projection, we have

$$\begin{aligned} d\tilde{x}_i(r,t)\mathrm{E}^{\omega}\left[\Psi_i(\omega)\Psi_k(\omega)\right] = \mathrm{E}^{\omega}\left[A(\tilde{x}_i(r,t)\Psi_i(\omega),t)\tilde{x}_j(r,t)\Psi_j(\omega)\Psi_k(\omega)\right]dt \\ + \mathrm{E}^{\omega}\left[B(\tilde{x}_i(r,t)\Psi_i(\omega),t)dW(t;\omega)\Psi_k(\omega)\right] \end{aligned} \tag{3.12}$$

The evolution equations for the coefficients are then given as

$$\begin{aligned} d\tilde{x}_i(r,t) = \mathrm{E}^{\omega}\left[A(\tilde{x}_k(r,t)\Psi_k(\omega),t)\tilde{x}_j(r,t)\Psi_j(\omega)\Psi_l(\omega)\right]C^{-1}_{\Psi_i\Psi_l}dt \\ + \mathrm{E}^{\omega}\left[B(\tilde{x}_i(r,t)\Psi_i(\omega),t)dW(t;\omega)\Psi_l(\omega)\right]C^{-1}_{\Psi_i\Psi_l} \end{aligned} \tag{3.13}$$

gPC governing equations for quadratic-nonlinear systems (1.2)

For the special case when A and B are at most linear in $X(r,t;\omega)$ as represented by equations (1.2), we can further simplify (3.13). Inserting (2.43) into (1.2) , we first obtain

$$\begin{aligned} A(\tilde{x}_k(r,t)\Psi_k(\omega),t) = A_0(t) + A_1(\tilde{x}_k(r,t),t)\Psi_k(\omega) \\ B(\tilde{x}_k(r,t)\Psi_k(\omega),t) = B_0(t) + B_1(\tilde{x}_k(r,t),t)\Psi_k(\omega) \end{aligned} \tag{3.14}$$

where $A_0(t)$ and $B_0(t)$ are functions in time only and $A_1(\tilde{x}_k(r,t),t)$ and $B_1(\tilde{x}_k(r,t),t)$ are linear in $\tilde{x}_k(r,t)$. Substituting (3.14) into (3.13) and simplifying, we obtain the final evolution equations for this special case, which are given as

$$\begin{aligned} d\tilde{x}_i(r,t) = A_0(t)\tilde{x}_i(r,t)dt + A_1(\tilde{x}_k(r,t),t)\tilde{x}_j(r,t)\,\mathrm{E}^{\omega}\left[\Psi_k(\omega)\Psi_j(\omega)\Psi_l(\omega)\right]C^{-1}_{\Psi_i\Psi_l}dt \\ + B_0(t)\,\mathrm{E}^{\omega}\left[dW(t;\omega)\Psi_l(\omega)\right]C^{-1}_{\Psi_i\Psi_l} \\ + B_1(\tilde{x}_k(r,t),t)\,\mathrm{E}^{\omega}\left[\Psi_k(\omega)dW(t;\omega)\Psi_l(\omega)\right]C^{-1}_{\Psi_i\Psi_l} \end{aligned} \tag{3.15}$$

where $C_{\Psi_i\Psi_l}$ is given by (2.47).

3.3 Time-dependent Generalized Polynomial Chaos

As presented in section 2.3.3, the TDgPC scheme Gerritsma et al. (2010) was derived as a modification of the gPC scheme and is useful for longer time integration of nonlinear dynamical systems with uncertainty in input parameters. It evolves the deterministic coefficients as the gPC scheme does, but with an additional re-initialization of the stochas-

tic basis functions, carried out whenever the nonlinearity effects dominate. Next, we first motivate the need for the TDgPC scheme and then present its re-initialization step.

We still consider the nonlinear stochastic dynamical system represented by (1.1). We begin with the gPC expansion given by (2.43) and time integrate (3.15) to obtain the time evolution of the deterministic coefficients. For nonlinear systems, the magnitude of the coefficients of higher-order polynomials would increase in time, indicating that the stochastic characteristics of the solution are changing. When the magnitude of the nonlinear part reaches a certain threshold level (which is decided heuristically based on the problem at hand), we halt the gPC scheme and perform a change of stochastic variables, which is called *re-initialization*. This is obtained next, following Gerritsma et al. (2010).

Basis re-initialization

Assuming that the threshold for re-initialization is reached at time $t = t_1$, the change of random variables is given by

$$\zeta_i(t_1;\omega) = x^{(i)}(r,t_1;\omega) \qquad 1 \leq i \leq N \tag{3.16}$$

where $\zeta_i(t_1;\omega), 1 \leq i \leq N$ represent the stochastic variables to be used for generating the new polynomial chaos basis and the scalar $x^{(i)}(r,t_1;\omega)$ represents the i^{th} component of the stochastic field $X(r,t_1;\omega)$ in N-dimensional state space, given by

$$x^{(i)}(r,t_1;\omega) = \sum_{k=0}^{s-1} \tilde{x}_k^{(i)}(r,t)\Psi_k(\omega) \tag{3.17}$$

where similarly the scalar $\tilde{x}_k^{(i)}(r,t)$ is the i^{th} component of the N-dimensional deterministic coefficient $\tilde{x}_k(r,t)$ corresponding to the polynomial basis function $\Psi_k(\omega)$. Note that s is the total number of terms in the re-initialized polynomial chaos expansion and is given by equation (2.40) with $\bar{r} = N$.

Next, we use Gram-Schmidt orthogonalization to generate a set of uni-variate poly-

nomial basis functions for each of the stochastic variables $\zeta_i, 1 \leq i \leq N$, given by

$$\begin{aligned}
\psi_0^{\text{new}}(t_1;\omega) &= 1 \\
\psi_k^{\text{new}}(t_1;\omega) &= [\zeta_i(t_1;\omega)]^k - \sum_{j=0}^{k-1} \frac{\left\langle [\zeta_i(t_1;\omega)]^j, \psi_j^{\text{new}}(t_1;\omega) \right\rangle}{\left\langle \psi_j^{\text{new}}(t_1;\omega), \psi_j^{\text{new}}(t_1;\omega) \right\rangle} \qquad 1 \leq k \leq p
\end{aligned} \tag{3.18}$$

Subsequently, we use the uni-variate polynomial basis functions to generate the corresponding multi-variate polynomial basis. We have

$$\Psi_\alpha^{\text{new}}(t_1;\omega) = \prod_{j=1}^{N} \psi_{\alpha_j}^{\text{new}}(\zeta_j(t_1;\omega)) \tag{3.19}$$

Using a single dimensional representation for the multi-index and arranging the basis functions by increasing order, we observe that the first basis function is a constant and the next N multi-variate polynomial basis functions are linear functions of random variables $\zeta_i, 1 \leq i \leq N$, given as

$$\begin{aligned}
\Psi_0^{\text{new}}(t_1;\omega) &= 1 \\
\Psi_k^{\text{new}}(t_1;\omega) &= \psi_1^{\text{new}}(\zeta_k(t_1;\omega)) \\
&= \zeta_k(t_1;\omega) - \mathrm{E}^\omega\left[\zeta_k(t_1;\omega)\right] \qquad 1 \leq k \leq N
\end{aligned} \tag{3.20}$$

The next set of multi-variate polynomial functions are quadratic functions of $\zeta_i, 1 \leq i \leq N$, then cubic and so on. Once we obtain the new polynomial basis, we need to re-initialize the deterministic coefficients. The re-initialized coefficients are given as

$$\begin{aligned}
\tilde{x}_0^{\text{new}} &= \mathrm{E}^\omega\left[X(r,t_1;\omega)\right] \\
\tilde{x}_k^{\text{new}} &= \hat{\mathbf{e}}_\mathbf{k} \qquad\qquad 1 \leq k \leq N \\
\tilde{x}_k^{\text{new}} &= \mathbf{0} \qquad\qquad N+1 \leq k \leq s-1
\end{aligned} \tag{3.21}$$

where $\hat{\mathbf{e}}_\mathbf{k}$ represents an N-dimensional unit vector such that

$$\hat{e}_k^{(i)} = \begin{cases} 1, & \text{if } \; i = k \\ 0, & \text{otherwise} \end{cases} \tag{3.22}$$

and 0 represents an N-dimensional zero vector. The total number of terms in the new polynomial chaos expansion are given (using equation (2.40)) as

$$s = \binom{N+p}{N} = \frac{(N+p)!}{N!\,p!} \tag{3.23}$$

It is observed that in the re-initialized polynomial chaos expansion, the coefficients corresponding to quadratic and other higher-order polynomials are zero, and hence the expansion is linear in terms of the polynomial basis functions. Once the polynomial basis has been re-initialized, the time evolution of the coefficients is continued in the same manner as in the gPC scheme, until the threshold is reached again.

3.4 New Modified TDgPC Scheme for Handling External Stochastic Forcing

All existing PC schemes known to us, including gPC and TDgPC, have fundamental limitations in modeling stochastic noise for long time intervals (as also illustrated in chapter 5). One of our research goals is to evaluate and obtain methodologies that can predict uncertainty in dynamical systems with external stochastic forcing, as employed for oceanic systems (Lermusiaux, 2006). For such predictions, one needs to integrate stochastic noise over sufficiently long time intervals. In this section, we introduce and derive a new Modified TDgPC (MTDgPC) scheme capable of modeling stochastic noise over arbitrarily large time intervals.

We again consider the stochastic dynamical system represented by (1.1). Consider the gPC expansion of the field variable $X(r,t;\omega)$ given by (2.43), with a modification that the polynomial basis functions are now a function of time as well. Thus, we have

$$X(r,t;\omega) = \sum_{i=0}^{s-1} \tilde{x}_i(r,t)\Psi_i(t;\omega) \tag{3.24}$$

The main idea of our new MTDgPC scheme is to modify the polynomial basis functions $\Psi_i(t;\omega)$ in time so as to include the effect of the external stochastic forcing as it occurs. The algorithm is as follows:

1. Evolve the deterministic coefficients $\tilde{x}_i(r,t)$ at each time step using the classic TDgPC scheme, but based on the system dynamics without new stochastic forcing, i.e. neglecting the new stochastic noise $dW(t;\omega)$ in (1.1) during the time step. This involves evolving the coefficients using the gPC scheme, followed by re-initialization of the polynomial basis. Thus, we apply the TDgPC scheme to the differential equation

$$dX(r,t;\omega) = A(X(r,t;\omega),t)X(r,t;\omega)dt \tag{3.25}$$

Let the corresponding time-evolved coefficients obtained by (3.21) be represented as $\tilde{x}_i^{\text{new}}(r,t+dt)$. It is observed from (3.21) that for these coefficients we have

$$\left\langle \tilde{x}_i^{\text{new}}(\bullet,t+dt), \tilde{x}_j^{\text{new}}(\bullet,t+dt) \right\rangle = \hat{\mathbf{e}}_\mathbf{i} \cdot \hat{\mathbf{e}}_\mathbf{j} = \delta_{ij} \qquad 1 \le i,j \le N \tag{3.26}$$

Thus, the set of deterministic coefficients $\{\ \tilde{x}_i^{\text{new}}(r,t+dt) : 1 \le i \le N\ \}$ spans the entire N-dimensional physical space. The intermediate solution of the stochastic field at time $t+dt$ is then represented as

$$X_{\text{int}}(r,t+dt;\omega) = \sum_{i=0}^{s-1} \tilde{x}_i^{\text{new}}(r,t+dt)\Psi_i(t;\omega) \tag{3.27}$$

2. Next, we modify the basis functions so as to add the effect of the new stochastic noise (both multiplicative and additive). We define $\tilde{w}_i$ as the projection of the stochastic noise term on the new set of deterministic coefficients obtained in step 1. We have

$$\tilde{w}_i = \left\langle B(X(\bullet,t;\omega),t)dW(t;\omega)), \tilde{x}_i^{\text{new}}(\bullet,t+dt) \right\rangle \qquad 1 \le i \le N \tag{3.28}$$

The new set of polynomial basis functions $\Psi_i^{\text{new}}(t+dt;\omega)$ is then given as

$$\Psi_i^{\text{new}}(t+dt;\omega) = \begin{cases} 1, & \text{if } \ i=0 \\ \Psi_i(t;\omega) + \tilde{w}_i, & \text{if } \ 1 \le i \le N \\ \Psi_i(t;\omega), & \text{if } \ N+1 \le i \le s-1 \end{cases} \tag{3.29}$$

where s is given by (3.23).

The final form of solution of the stochastic field at time $t + dt$ is represented as

$$X(r, t + dt; \omega) = \sum_{i=0}^{s-1} \tilde{x}_i^{\text{new}}(r, t + dt)\Psi_i^{\text{new}}(t + dt; \omega) \tag{3.30}$$

where the deterministic coefficients $\tilde{x}_i^{\text{new}}(r, t + dt)$ and the stochastic polynomial basis functions $\Psi_i^{\text{new}}(t + dt; \omega)$ are as defined in steps 1 and 2 of the algorithm respectively.

We now show that the final solution of the stochastic field at time $t + dt$ is indeed the solution of (1.1). To do so, we substitute for $\Psi_i^{\text{new}}(t + dt; \omega)$ from equation (3.29) into equation (3.30), and obtain

$$\begin{aligned}
X(r, t + dt; \omega) &= \sum_{i=0}^{s-1} \tilde{x}_i^{\text{new}}(r, t + dt)\Psi_i^{\text{new}}(t + dt; \omega) \\
&= \tilde{x}_0^{\text{new}}(r, t + dt)\Psi_0^{\text{new}}(t + dt; \omega) \\
&\quad + \sum_{i=1}^{N} \tilde{x}_i^{\text{new}}(r, t + dt)\Psi_i^{\text{new}}(t + dt; \omega) \\
&\quad + \sum_{i=N+1}^{s-1} \tilde{x}_i^{\text{new}}(r, t + dt)\Psi_i^{\text{new}}(t + dt; \omega) \\
&= \tilde{x}_0^{\text{new}}(r, t + dt)\Psi_0(t; \omega) \\
&\quad + \sum_{i=1}^{N} \tilde{x}_i^{\text{new}}(r, t + dt)\left[\Psi_i(t; \omega) + \tilde{w}_i\right] \\
&\quad + \sum_{i=N+1}^{s-1} \tilde{x}_i^{\text{new}}(r, t + dt)\Psi_i(t; \omega) \\
&= \sum_{i=0}^{s-1} \tilde{x}_i^{\text{new}}(r, t + dt)\Psi_i(t; \omega) + \sum_{i=1}^{N} \tilde{w}_i\tilde{x}_i^{\text{new}}(r, t + dt) \\
&= X_{\text{int}}(r, t + dt; \omega) + \sum_{i=1}^{N} \tilde{w}_i\tilde{x}_i^{\text{new}}(r, t + dt)
\end{aligned} \tag{3.31}$$

Using the definition of $\tilde{w}_i$ from equation (3.28), we have

$$\begin{aligned} X(r,t+dt;\omega) &= X_{\text{int}}(r,t+dt;\omega) \\ &\quad + \sum_{i=1}^{N} \left\langle B(X(\bullet,t;\omega),t)dW(t;\omega), \tilde{x}_i^{\text{new}}(\bullet,t+dt)\right\rangle \tilde{x}_i^{\text{new}}(r,t+dt) \\ &= X_{\text{int}}(r,t+dt;\omega) \\ &\quad + \sum_{i=1}^{N} \left\langle B(X(\bullet,t;\omega),t)dW(t;\omega), \hat{\mathbf{e}}_\mathbf{i}\right\rangle \hat{\mathbf{e}}_\mathbf{i} \\ &= X_{\text{int}}(r,t+dt;\omega) + B(X(r,t;\omega),t)dW(t;\omega) \end{aligned} \tag{3.32}$$

which is the correct representation of the solution field at time $t+dt$, including the effect of stochastic noise.

Considering computations, the time integration of the system dynamics without the stochastic forcing terms and the integration of these new stochastic forcing terms alone need to be compatible. In the numerical sense, the scheme splits the governing dynamics in two parts (deterministic dynamics and stochastic forcing), which is straightforward to handle for explicit schemes. For implicit or multi-steps time-discretization schemes, there will be numerical choices that will lead to optimum within-time-step coupling, and others that won't.

3.5 New Reduced Space and Reduced Order Polynomial Chaos Scheme

The MTDgPC scheme presented in section 3.4 can model stochastic noise over arbitrarily large time intervals. However, as seen later in chapter 5, it has limited applicability in modeling realistic ocean models due to its high computational cost. Hence, for high-dimensional dynamical systems that concentrate most of their stochastic energy in a time-dependent subspace, we propose another new reduced space and reduced order polynomial chaos scheme. Next, we first review the known concepts of Singular Value Decomposition (SVD) and Karhunen-Loève (K-L) expansion. Then, the algorithm for the new SVD and K-L expansion based generalized polynomial chaos (KLgPC) scheme is presented and the

evolution equations for the stochastic system represented by equation (1.1) using the new KLgPC scheme are derived.

3.5.1 Singular value decomposition

A singular value decomposition (SVD) of a real $m \times n$ matrix A has the form

$$A = U\Sigma V^T \tag{3.33}$$

where U is an $m \times m$ orthogonal matrix, V is an $n \times n$ orthogonal matrix and Σ is an $m \times n$ matrix with elements

$$\Sigma_{i,j} = \begin{cases} \sigma_i, & \text{if } \ 1 \leq i = j \leq r \\ 0, & \text{otherwise} \end{cases} \tag{3.34}$$

where r here is the rank of matrix A. By definition, σ_i^2 are the eigenvalues of AA^T. These σ_i are called the singular values of matrix A and are defined such that $\sigma_1 \geq \sigma_2 \geq ... \geq \sigma_r > 0$. The matrix A can be represented as

$$A = \sum_{i=1}^{r} \sigma_i u_i v_i^T \tag{3.35}$$

where u_i and v_i are the i^{th} column vectors of matrices U and V respectively. A low rank approximation of A is given by a truncated SVD, which is represented as

$$A_{r_{\text{red}}} = \sum_{i=1}^{\bar{r}_{\text{red}}} \sigma_i u_i v_i^T \qquad \text{where} \quad \bar{r}_{\text{red}} \leq r \tag{3.36}$$

Consider an $n \times m$ data matrix X (with stochastic mean removed), representing m observations of a stochastic field $u(x,t;\omega)$ at time $t \in \mathcal{T}$ in a physical domain $D \in \mathrm{R}^n$. The covariance matrix of the random field is then defined as $C_{u(t)u(t)} = XX^T$. The eigenvalues $\lambda_i = \sigma_i^2$ of the covariance matrix (where σ_i are the singular values of the data matrix X) represent the magnitude of the variance of the stochastic field in the directions of the corresponding eigenvectors. This idea is central to the concept of

principal component analysis (PCA) (see, for e.g., Jolliffe (1986)), and is used in several uncertainty quantification schemes, including proper orthogonal decomposition (POD) and error subspace statistical estimation (ESSE).

3.5.2 Karhunen-Loève expansion

The Karhunen-Loève expansion (see Ghanem and Spanos (1991), Le Maître and Knio (2010)), like the polynomial chaos expansion, is a common spectral representation of a stochastic process $u(x;\omega)$. It is analogous to principal component analysis (PCA) in an infinite dimensional setting. Loosely speaking, the Karhunen-Loève theorem states that any square integrable random process $u(x;\omega)$ with a continuous covariance function can be represented as an infinite sum of uncorrelated random variables.

Using the Karhunen-Loève theorem, a stochastic process $u(x;\omega)$ defined on a probability space $(\Omega, \mathcal{F}, \mathcal{P})$ and a finite domain D with a known covariance function $C_{uu}(x_1, x_2)$ can be represented as

$$u(x;\omega) = \bar{u}(x) + \sum_{i=1}^{\infty} \sqrt{\lambda_i} Z_i(\omega) \tilde{u}_i(x) \tag{3.37}$$

where $\bar{u}(x) = \mathrm{E}^{\omega}[u(x;\omega)]$ is the mean value of the stochastic process, $Z_i(\omega)$ are uncorrelated random variables with zero mean, and λ_i and $\tilde{u}_i(x)$ are the eigenvalues and eigenfunctions of the covariance function $C_{uu}(x_1, x_2)$. In short, we have the following properties and definitions,

$$\begin{aligned}
&\int_D C_{uu}(x_1, x_2)\tilde{u}_i(x_2)dx_2 = \lambda_i \tilde{u}_i(x_1) \\
&\int_D \tilde{u}_i(x)\tilde{u}_i(x)dx = \delta_{ij} \\
&Z_i(\omega) = \frac{1}{\sqrt{\lambda_i}} \int_D \left(u(x;\omega) - \bar{u}(x)\right) \tilde{u}_i(x)dx \\
&\mathrm{E}^{\omega}[Z_i(\omega)] = 0 \\
&\mathrm{E}^{\omega}[Z_i(\omega)Z_j(\omega)] = \delta_{ij}
\end{aligned} \tag{3.38}$$

Furthermore, the total variance of $u(x;\omega)$ is given as

$$\int_D \text{Var}\left[u(x;\omega)\right] dx = \sum_{i=1}^{\infty} \lambda_i \tag{3.39}$$

Next, let us consider a random field $u(x,t;\omega)$ defined on the probability space $(\Omega, \mathcal{F}, \mathcal{P})$, spatial domain D and time domain $\mathcal{T}$, with a continuous covariance function $C_{u(t)u(t)}(x_1, x_2)$. For any $t \in \mathcal{T}$, the Karhunen-Loève expansion of the stochastic field is given as

$$u(x,t;\omega) = \bar{u}(x,t) + \sum_{i=1}^{\infty} \sqrt{\lambda_i(t)} Z_i(t;\omega) \tilde{u}_i(x,t) \tag{3.40}$$

The K-L expansion represented by equation (3.40) is exact, but in order to facilitate computations, needs to be truncated to a finite number of terms. The set of $\bar{r}_{\text{red}}$ terms that maximizes the total variance of the stochastic field and hence leads to the most accurate representation (in this variance sense) is given by the first $\bar{r}_{\text{red}}$ terms of the expansion, assuming that the eigenvalues $\{\lambda_i(t)\}_{i\in\mathbb{N}}$ have been arranged in decreasing order of magnitude. Hence, the truncated Karhunen-Loève expansion is given as

$$u_{\text{red}}(x,t;\omega) = \bar{u}(x,t) + \sum_{i=1}^{\bar{r}_{\text{red}}} \sqrt{\lambda_i(t)} Z_i(t;\omega) \tilde{u}_i(x,t) \tag{3.41}$$

The truncated K-L expansion $u_{\text{red}}(x,t;\omega)$ converges to $u(x,t;\omega)$ in the mean square sense (given by Mercer's theorem). Therefore, we have

$$\text{E}^{\omega}\left[\int_D |u_{\text{red}}(x,t;\omega) - u(x,t;\omega)|^2 dx\right] = \sum_{i=\bar{r}_{\text{red}}+1}^{\infty} \lambda_i(t) \to 0 \quad \text{as} \quad \bar{r}_{\text{red}} \to \infty \tag{3.42}$$

3.5.3 KLgPC algorithm and derivation of evolution equations

The main idea of the new KLgPC scheme is to utilize the concepts of SVD and K-L expansion to obtain a reduced space and reduced order representation of the stochastic field at every time step, taking into account the effect of stochastic noise, and to use this truncated representation to implement a polynomial chaos based uncertainty quantification scheme which minimizes the computational effort involved, while solving for the stochastic

field with sufficient accuracy. In some sense, it combines the uncertainty prediction part of ESSE scheme with gPC.

As in section 3.4, we again consider the stochastic dynamical system (1.1) and assume that at time t, the solution field $X(r,t;\omega)$ is represented in the form of a gPC expansion given by (3.24). The algorithm for our KLgPC scheme is as follows:

1. Evolve the deterministic coefficients $\tilde{x}_i(r,t)$ at each time step using the gPC scheme, but based on the system dynamics without the new stochastic forcing, i.e. neglecting the new stochastic noise $dW(t;\omega)$ in (1.1) during the time step. Thus, we apply the gPC scheme to the differential equation (3.25). Let the time evolved coefficients be represented as $\tilde{x}_i(r,t+dt)$. The intermediate or predictor solution field (without including the effect of the new external stochastic forcing) is then represented as

$$X_{\text{int}}(r,t+dt;\omega) = \sum_{i=0}^{s-1} \tilde{x}_i(r,t+dt)\Psi_i(t;\omega) \tag{3.43}$$

which is similar to (3.27) from step 1 of the modified TDgPC algorithm. However, only an optimally truncated version of this expansion will be used in KLgPC. This is developed next in steps 2 and 3.

2. Approximate the intermediate stochastic field $X_{\text{int}}(r,t+dt;\omega)$ using a reduced spectral representation. We have from equation (3.43)

$$\begin{aligned} X_{\text{int}}(r,t+dt;\omega) &= \tilde{x}_0(r,t+dt)\Psi_0(t;\omega) + \sum_{i=1}^{s-1} \tilde{x}_i(r,t+dt)\Psi_i(t;\omega) \\ &= \tilde{x}_0(r,t+dt)\Psi_0(t;\omega) + \tilde{X}(r,t+dt)\tilde{\Psi}(t;\omega) \end{aligned} \tag{3.44}$$

where $\tilde{X}(r,t+dt)$ is an $N \times (s-1)$ matrix with column vectors $\tilde{x}_i(r,t+dt), 1 \leq i \leq (s-1)$ and $\tilde{\Psi}(t;\omega)$ is an $(s-1)$ dimensional column vector with elements $\Psi_i(t;\omega), 1 \leq i \leq (s-1)$. Here, $\Psi_0(t;\omega) = 1$ and $\tilde{x}_0(r,t+dt)$ represents the mean or expected value of the stochastic field, i.e., $\tilde{x}_0(r,t+dt) = \mathrm{E}^{\omega}\left[X_{\text{int}}(r,t+dt;\omega)\right] = \bar{X}_{\text{int}}(r,t+dt)$. Taking the complete SVD of matrix $\tilde{X}(r,t+dt)$ and substituting it

in equation (3.44), we have

$$X_{\text{int}}(r, t+dt;\omega) = \bar{X}_{\text{int}}(r, t+dt) + \sum_{i=1}^{\bar{r}} \tilde{\sigma}_i \tilde{u}_i \tilde{v}_i^T \tilde{\Psi}(t;\omega) \tag{3.45}$$

where $\bar{r}$ is the rank of matrix $\tilde{X}(r, t+dt)$, $\tilde{\sigma}_i$ are its singular values and u_i and v_i are the left and right singular vectors respectively. Truncating the singular value decomposition to $\bar{r}_{\text{red}}$ terms ($\bar{r}_{\text{red}} \leq \bar{r}$), we get

$$X_{\text{int}}(r, t+dt;\omega) \approx \bar{X}_{\text{int}}(r, t+dt) + \sum_{i=1}^{\bar{r}_{\text{red}}} \tilde{\sigma}_i \tilde{u}_i \tilde{v}_i^T \tilde{\Psi}(t;\omega) \tag{3.46}$$

Defining $\tilde{Z}_i(t;\omega) \equiv \tilde{v}_i^T \tilde{\Psi}(t;\omega)$, we rewrite equation (3.46) to get

$$X_{\text{int}}(r, t+dt;\omega) \approx \bar{X}_{\text{int}}(r, t+dt) + \sum_{i=1}^{\bar{r}_{\text{red}}} \tilde{\sigma}_i \tilde{Z}_i(t;\omega) \tilde{u}_i \tag{3.47}$$

which is similar to a truncated K-L expansion, as defined by (3.41).

3. Next, we use the truncated spectral representation (3.47) to obtain a gPC expansion of the intermediate stochastic field. First, we define new random variables $\zeta_i(t+dt;\omega)$ such that

$$\zeta_i(t+dt;\omega) = \tilde{\sigma}_i \tilde{Z}_i(t;\omega) \qquad 1 \leq i \leq \bar{r}_{\text{red}} \tag{3.48}$$

Using these new random variables, we generate a new set of polynomial basis functions $\Psi_i^{\text{new}}(t;\omega), 1 \leq i \leq s_{\text{red}}$ $\left(\text{where } s_{\text{red}} = \frac{(\bar{r}_{\text{red}}+p)!}{\bar{r}_{\text{red}}!\, p!}\right)$ using Gram-Schmidt orthogonalization, following ideas similar to that of the TDgPC scheme, using equations (3.18) and (3.19). The corresponding deterministic coefficients are then similar to (3.21) and are given as

$$\begin{aligned}
&\tilde{x}_0^{\text{new}}(r, t+dt) = \mathrm{E}^{\omega}\left[X_{\text{int}}(r, t+dt;\omega)\right] \\
&\tilde{x}_k^{\text{new}}(r, t+dt) = \tilde{u}_k && 1 \leq k \leq \bar{r}_{\text{red}} \\
&\tilde{x}_k^{\text{new}}(r, t+dt) = \mathbf{0} && \bar{r}_{\text{red}}+1 \leq k \leq s_{\text{red}}-1
\end{aligned} \tag{3.49}$$

Thus, the gPC expansion of the intermediate solution field is given as

$$X_{\text{int}}(r, t+dt; \omega) = \sum_{i=0}^{s_{\text{red}}} \tilde{x}_i^{\text{new}}(r, t+dt) \Psi_i^{\text{new}}(t; \omega) \tag{3.50}$$

where $\tilde{x}_i^{\text{new}}(r, t+dt)$ and $\Psi_i^{\text{new}}(t; \omega)$ are as defined above. This is the KLgPC approximation of equation (3.43) and it is to this equation (3.50) that the new stochastic noise is added to.

4. Modify the stochastic basis functions so as to add the effect of new stochastic noise over dt (both additive and multiplicative noise), using an approach similar to our modified TDgPC scheme. We define

$$\tilde{w}_i = \left\langle B(X(r, t; \omega), t)\, dW(t; \omega), \tilde{x}_i^{\text{new}}(r, t+dt) \right\rangle \qquad 1 \leq i \leq \bar{r}_{\text{red}} \tag{3.51}$$

as the projection of the stochastic noise term on the set of deterministic coefficients. The new set of polynomial bases functions $\Psi_i^{\text{new}}(t+dt; \omega)$ is then given as

$$\Psi_i^{\text{new}}(t+dt; \omega) = \begin{cases} 1, & \text{if} \quad i = 0 \\ \Psi_i^{\text{new}}(t; \omega) + \tilde{w}_i, & \text{if} \quad 1 \leq i \leq \bar{r}_{\text{red}} \\ \Psi_i^{\text{new}}(t; \omega), & \text{if} \quad \bar{r}_{\text{red}} + 1 \leq i \leq s_{\text{red}} - 1 \end{cases} \tag{3.52}$$

The final form of solution of the stochastic field at time $t + dt$ is represented as

$$X(r, t+dt; \omega) = \sum_{i=0}^{s_{\text{red}}-1} \tilde{x}_i^{\text{new}}(r, t+dt) \Psi_i^{\text{new}}(t+dt; \omega) \tag{3.53}$$

where the deterministic coefficients $\tilde{x}_i^{\text{new}}(r, t+dt)$ and the stochastic polynomial basis functions $\Psi_i^{\text{new}}(t+dt; \omega)$ are as defined previously in the algorithm. Using an analysis similar to that represented in equations (3.31) and (3.32), it can be shown that the solution represented by equation (3.53) is indeed the correct representation of the solution field at time $t + dt$, including the effect of stochastic noise, but only considering the dominant components of the two terms in (1.1).

Remarks:

a) We note that the dominant left-singular-vector subspace of $\tilde{X}(r, t+dt; \omega)$ corresponding to the first (deterministic) dynamical term $A(X(r,t;\omega),t)\,X(r,t;\omega)dt$ and the dominant left-singular-vector subspace of the matrix of $\tilde{w}_i$'s corresponding to the second (stochastic) dynamical term $B(X(r,t;\omega),t)\,dW(t;\omega)$ of (1.1) need not to be the same. The two SVDs of these two matrices are not equal. In fact, if one of the matrices requires a smaller/larger basis than the other to represent most of its variance, then the two subspaces have different dimensions. The final subspace that represents the sum of the two dynamical terms is the union of the two subspaces. This union-subspace can be further reduced to maintain a certain percentage of variance (as done in the ESSE scheme). These different versions of combination of subspaces is not discussed in the above, but they clearly allow the size of the subspace to vary with time, in accord with the nonlinear deterministic and stochastic terms of the dynamical system (1.1).

b) A special example of the situation described in remark (a) is the case of zero initial uncertainty in the stochastic field, $\tilde{x}_i(r,0) = 0$ for $1 \leq i \leq (s-1)$. Hence, after step 1 of the algorithm, we have $\tilde{x}_i(r,dt) = 0$ for $1 \leq i \leq s$ and the singular value decomposition of the matrix $\tilde{X}(r,dt)$ in step 2 of the algorithm would not have any non-zero singular values. This situation would also be true for the MTDgPC scheme. There is nothing incorrect with this, the computation simply indicates that over the first time-step, the zero initial uncertainty leads to zero future uncertainty if there is no new external stochastic forcing. However, if there is new stochastic forcing over dt, then it needs to be accounted for and different options are feasible. The best option for KLgPC is to set the initial basis such that the second dynamical term in (1.1), i.e. the noise term over dt, is best represented in the variance sense. That basis is the dominant right singular vectors of the matrix of $\tilde{w}_i$'s corresponding to this second term $B(X(r,t;\omega),t)\,dW(t;\omega)$. Another choice (less efficient) is to select a complete initial basis (which is expensive for large systems) and then represent that second term fully, possibly truncating it for the next time-step. A third choice (less efficient) is to start the scheme with a Monte-Carlo approach. After that first time step, the above KLgPC scheme can be used.

Chapter 4

Uncertainty in Input Parameters

In this chapter, we study stochastic linear and nonlinear dynamical systems with uncertainty in input parameters. These systems involve uncertainty in the form of initial conditions, boundary conditions and model parameters (without sustained stochastic noise). We have studied a set of both self-engineered and classic nonlinear dynamical systems (for e.g., see Strogatz (2001)), but only a summary subset of these results are presented here. As a first example, we consider a one-dimensional stochastic ordinary differential equation and solve it using DO and gPC schemes. Next, we move on to the Kraichnan-Orszag three mode problem (Kraichnan, 1963, Orszag and Bissonnette, 1967), which involves a nonlinear system originally used for modeling fluid turbulence. The long-time integration issues of classic gPC schemes are discussed and the TDgPC scheme introduced by Gerritsma et al. (Gerritsma et al., 2010) is used to obtain improved solutions. These solutions are compared to the solutions obtained using DO and MC schemes and the performance of the uncertainty quantification schemes is analyzed in terms of accuracy of solution and computational cost of implementation. The new MTDgPC and KLgPC schemes derived in chapter 3 are not used in this chapter since for now, only uncertainty in input parameters is considered.

4.1 One-dimensional Decay Model

The one-dimensional decay model is represented by the stochastic ordinary differential equation

$$du(t;\omega) + k(\omega)u(t;\omega)dt = 0 \tag{4.1}$$

where the decay rate $k(\omega)$ is stochastic. We consider a deterministic initial condition, given as

$$u(0,\omega) = 1 \tag{4.2}$$

For this problem, we consider the decay rate to be a uniformly distributed random variable in the interval $[0,1]$. Thus, the decay rate $k(\omega)$ is represented as

$$k(\omega) \sim U[0,1] \tag{4.3}$$

The one-dimensional stochastic ODE represented by equations (4.1), (4.2) and (4.3) has an analytical solution, which is given by the equation

$$u(t;\omega) = e^{-k(\omega)t} \tag{4.4}$$

Using this analytical stochastic solution (4.4), the mean and the variance of $u(t;\omega)$ can be computed analytically. The mean of $u(t;\omega)$ is

$$\bar{u}(t) = \mathrm{E}^{\omega}\left[u(t;\omega)\right] = \frac{1-e^{-t}}{t} \tag{4.5}$$

and the variance is

$$\mathrm{Var}\left[u(t;\omega)\right] = \frac{1-e^{-2t}}{2t} - \left(\frac{1-e^{-t}}{t}\right)^2 \tag{4.6}$$

The one-dimensional stochastic decay model is solved using various uncertainty quantification schemes for $t \in [0,30]$, using a time step of $\Delta t = 0.01$. The stochastic mean and variance of the numerical solution obtained using Monte Carlo simulations with 10000 sample realizations, is plotted in figure (4-1). For comparison, the analytical mean and variance of $u(t;\omega)$ are also shown in the same figure. The relative error in the mean and variance of the stochastic field is depicted in figure (4-2). From figures (4-1) and (4-2),

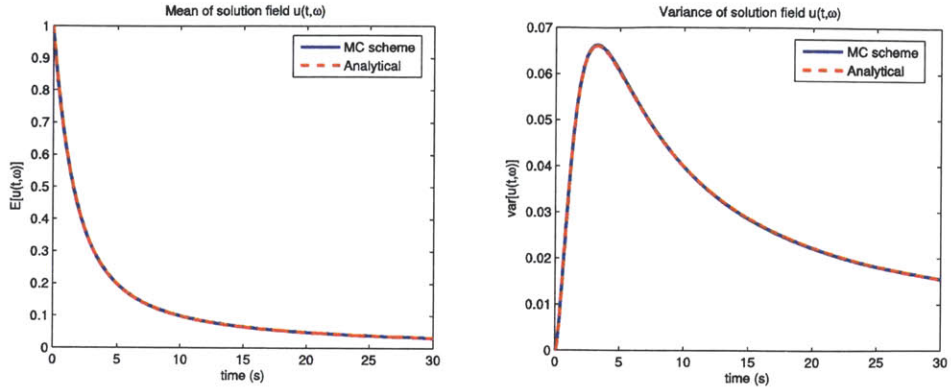

Figure 4-1: Mean and variance of the solution $u(t;\omega)$ for 1-D decay model using the MC scheme

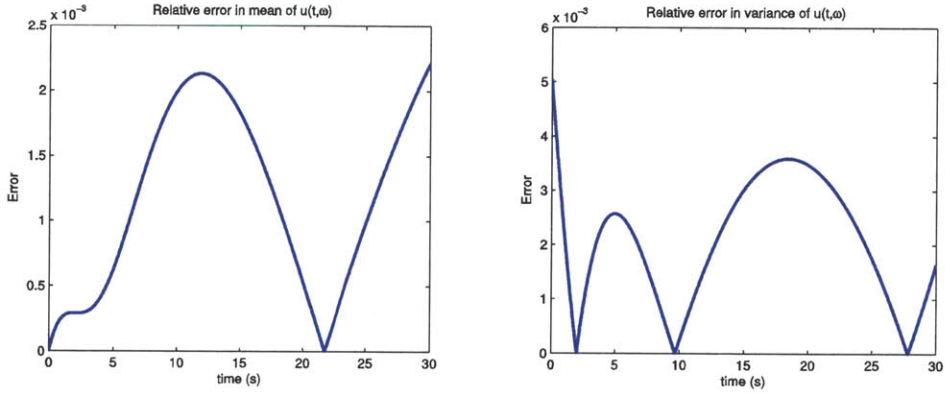

Figure 4-2: Relative error in mean and variance of $u(t;\omega)$ for 1-D decay model using the MC scheme

it is observed that the Monte Carlo scheme with 10000 sample realizations shows a very good agreement with the analytical results. For stochastic systems without analytical solutions, the Monte carlo solution with a sufficiently high number of sample realizations is a good estimate of the true solution.

Next, we solve the stochastic decay model using gPC scheme (described in section 2.3.2), with varying polynomial order. The stochastic mean and variance of the numerical solution obtained with polynomial expansions of order 2, 4, 6, 8 and 10, along with their relative errors, are plotted in figures (4-3), (4-4), (4-5), (4-6) and (4-7) respectively. We observe that the accuracy of the results is dependent on the order of the gPC scheme. The solution of $u(t;\omega)$ using a lower order gPC scheme ($p = 2$ and $p = 4$) is not very accurate. As the order of the polynomial chaos expansion increases, there is a better

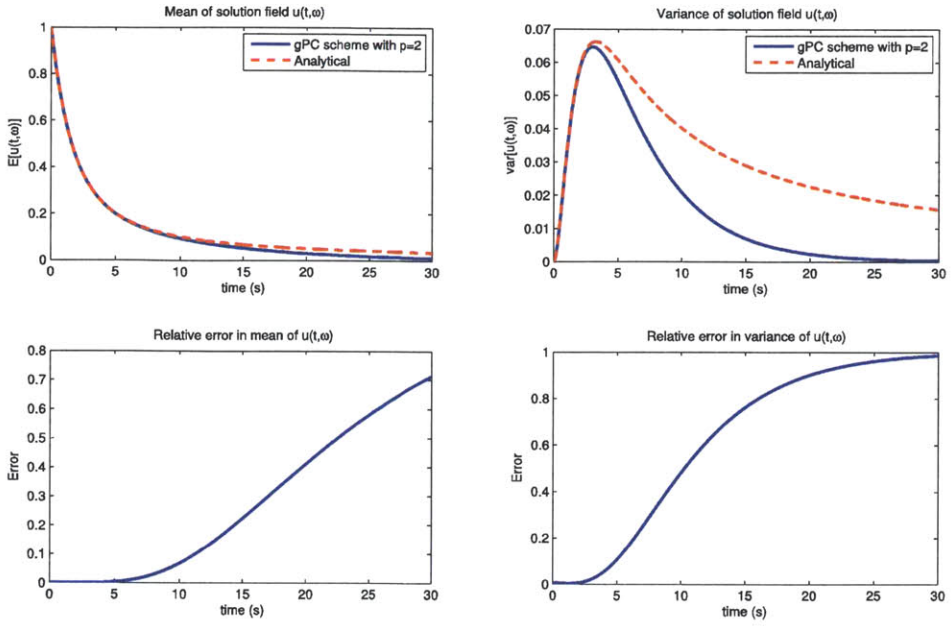

Figure 4-3: (a) Mean and variance of $u(t;\omega)$ for 1-D decay model using the gPC scheme with $p = 2$ (b) Relative error in the mean and variance of $u(t;\omega)$ using the gPC scheme with $p = 2$

agreement between the numerical results obtained using gPC scheme and the analytical solution. The solution obtained using gPC scheme of order $p = 10$, exhibits a fairly good accuracy, similar to that of the Monte Carlo scheme.

Finally, we solve the 1-D decay model using dynamically orthogonal equations (described in section 2.3.5). The stochastic mean and variance of the solution $u(t;\omega)$ using the DO scheme with one stochastic mode, i.e., $s = 1$, and their corresponding relative errors, are plotted in figure (4-8). It is observed that the DO solution with one stochastic mode is identical (up to stochastic realizations) to the Monte Carlo solution, and shows a very good agreement with the analytical results. This is normal since for $s = 1$ the DO scheme captures the whole dynamical system and becomes a Monte Carlo scheme (if the stochastic coefficients are solved for using a Monte Carlo scheme).

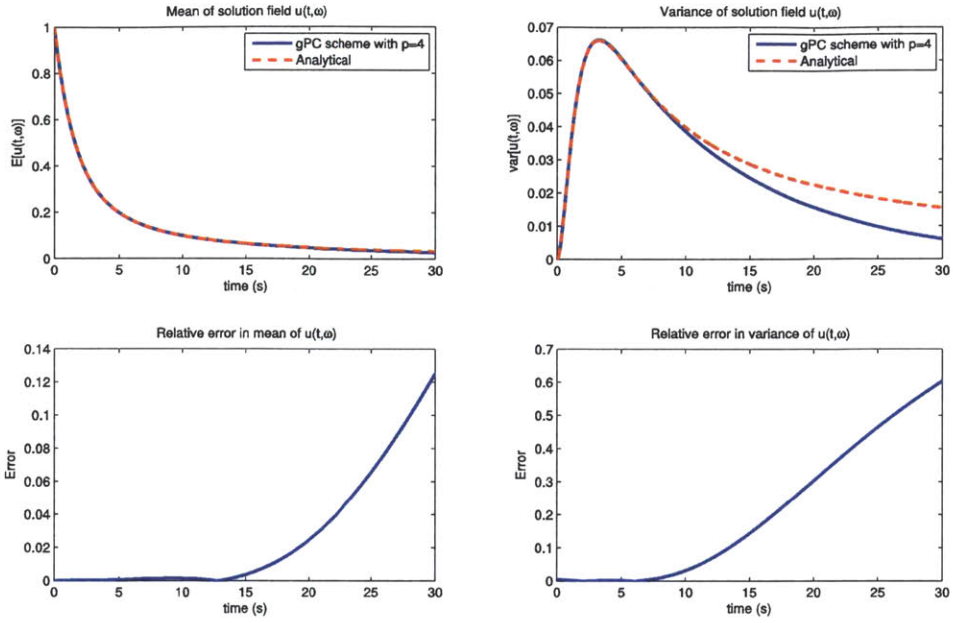

Figure 4-4: As figure (4-3), but using the gPC scheme with $p = 4$

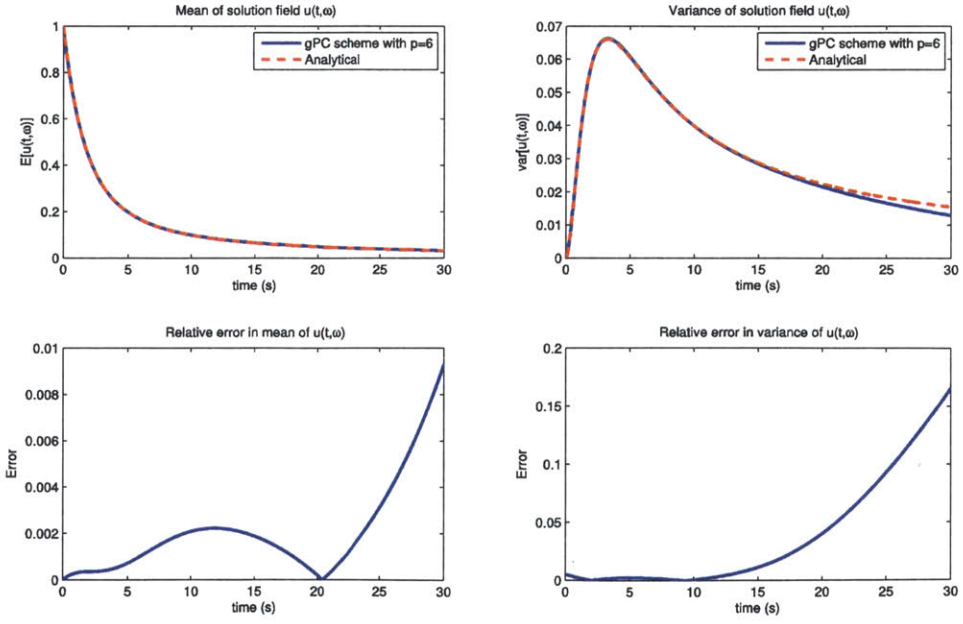

Figure 4-5: As figure (4-3), but using the gPC scheme with $p = 6$

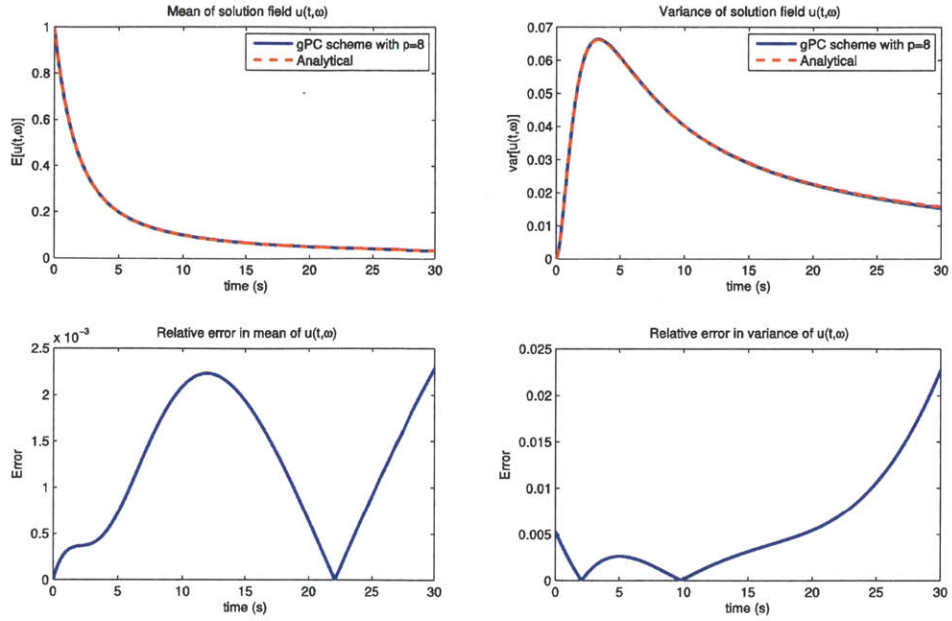

Figure 4-6: As figure (4-3), but using the gPC scheme with $p = 8$

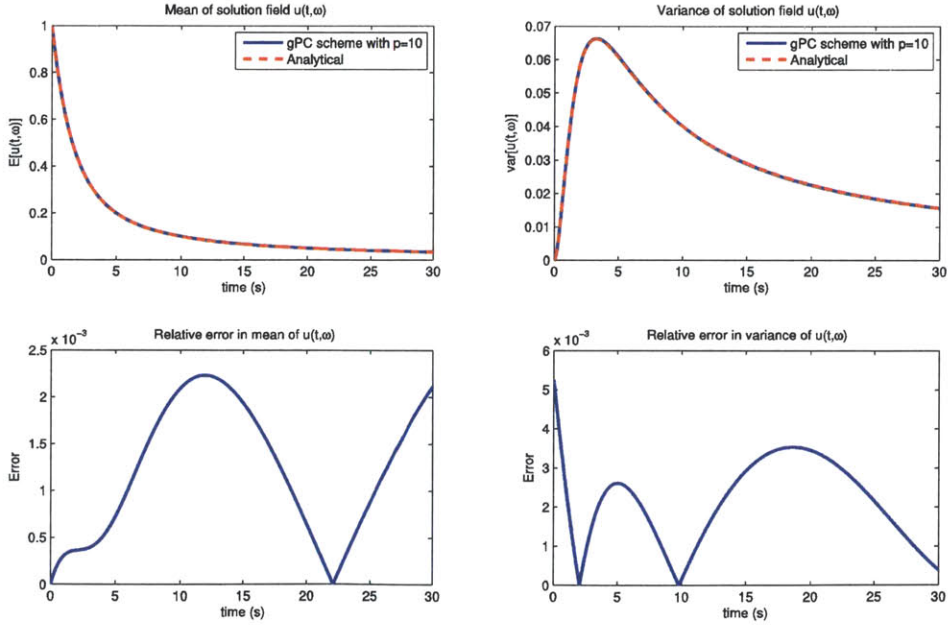

Figure 4-7: As figure (4-3), but using the gPC scheme with $p = 10$

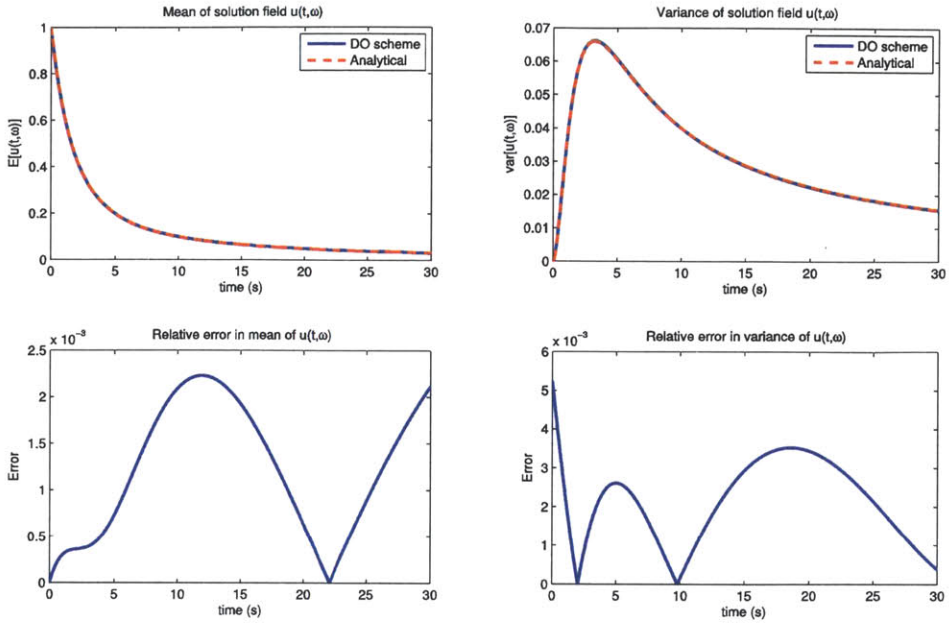

Figure 4-8: (a) Mean and variance of $u(t;\omega)$ for 1-D decay model using the DO scheme with $s = 1$ (b) Relative error in the mean and variance of $u(t;\omega)$ using the DO scheme with $s = 1$

4.2 Kraichnan-Orszag Three Mode Problem

In this section, we study the Kraichnan-Orszag three mode problem, which is a well-known system in literature, used for studying the long time numerical behavior of uncertainty quantification schemes. The Kraichnan-Orszag (K-O) system was first introduced by R. H. Kraichnan (Kraichnan, 1963) and later used by S. A. Orszag (Orszag and Bissonnette, 1967) for studying uncertainties of Gaussian nature in turbulence. It is derived from simplified inviscid Navier-Stokes equations and consists of three coupled nonlinear ordinary differential equations, given as

$$\begin{aligned} \frac{dx_1(t;\omega)}{dt} &= x_2(t;\omega)x_3(t;\omega) \\ \frac{dx_2(t;\omega)}{dt} &= x_3(t;\omega)x_1(t;\omega) \\ \frac{dx_3(t;\omega)}{dt} &= -2x_1(t;\omega)x_2(t;\omega) \end{aligned} \tag{4.7}$$

Uncertainty in the system is introduced through initial conditions. Each of the three state variables $x_1(t;\omega), x_2(t;\omega)$ and $x_3(t;\omega)$, may have an uncertain initial condition. The number of state variables having initial uncertainty determines the stochastic dimension of the system. The solution of the Kraichnan-Orszag system is known to be heavily dependent on the initial state of the system.

First we consider the case with initial uncertainty in just one state variable. In this case, the initial conditions are represented as

$$\begin{aligned} x_1(0,\omega) &= 0.99 + 0.01\xi(\omega) \\ x_2(0,\omega) &= 1.0 \\ x_3(0,\omega) &= 1.0 \end{aligned} \tag{4.8}$$

where $\xi(\omega) \sim U[-1,1]$ is a uniform random variable. We consider the time domain $t \in [0,40]$ and use a time step of $\Delta t = 0.01$. The stochastic mean and variance of the state variable $x_1(t;\omega)$ using Monte Carlo simulations with 10000 sample realizations is plotted in figure (4-9). Since the analytical solution is not available for the Kraichnan-Orszag system, the stochastic solution obtained using the Monte Carlo scheme is assumed to be the true solution. Next we use the gPC scheme to integrate the Kraichnan-Orszag system with initial conditions given by equation (4.8). The mean and variance of $x_1(t;\omega)$ using the gPC scheme with polynomial order $p = 2$ is shown in figure (4-10). For comparison, the Monte Carlo solution is also plotted in the same figure. We observe that the gPC scheme with $p = 2$ is unable to model the evolution of uncertainty in the Kraichnan-Orszag three mode problem. In an attempt to improve the accuracy of solution, we solve the same system with a gPC scheme of higher polynomial order. The stochastic mean and variance using gPC schemes of order $p = 4$ $(s = 5)$ and $p = 6$ $(s = 7)$ are plotted in figures (4-11) and (4-12) respectively. It is observed that even with an increase in the order of polynomial chaos expansion, there is not much improvement in the accuracy of the solution. The inability of the gPC scheme in modeling uncertainty in nonlinear dynamical systems over large time-intervals is well known, and is discussed in detail in section 4.3. The stochastic mean and variance of $x_1(t;\omega)$ using the DO scheme with three stochastic modes, i.e., $s = 3$, is depicted in figure (4-13). As in the case of the one-dimensional decay

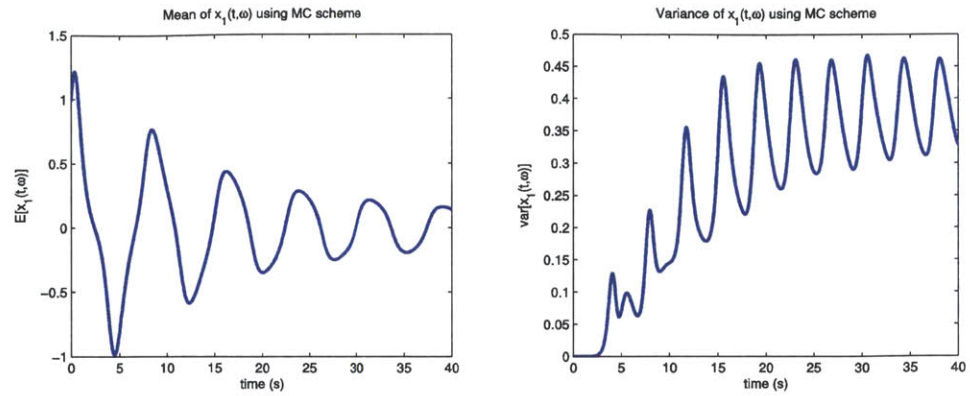

Figure 4-9: Mean and variance of the state variable $x_1(t;\omega)$ for the K-O system with initial uncertainty in one state variable using the MC scheme

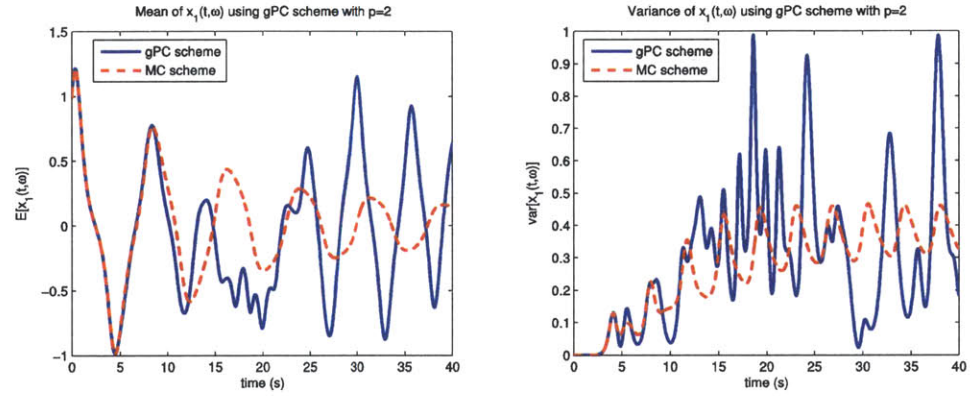

Figure 4-10: Mean and variance of the state variable $x_1(t;\omega)$ for the K-O system with initial uncertainty in one state variable using the gPC scheme with order $p = 2$

problem, the DO solution is found to be identical to the MC solution.

Now, we consider the case with initial uncertainty in all three state variables. The initial conditions are then represented as

$$\begin{aligned} x_1(0,\omega) &= 0.99 + 0.01\,\xi_1(\omega) \\ x_2(0,\omega) &= 1.0 + 0.01\,\xi_2(\omega) \\ x_3(0,\omega) &= 1.0 + 0.01\,\xi_3(\omega) \end{aligned} \tag{4.9}$$

where $\xi_1(\omega), \xi_2(\omega), \xi_3(\omega) \sim U[-1,1]$ are independent and identically distributed (i.i.d.) uniform random variables. We again consider the time domain $t \in [0,40]$ and use a time step of $\Delta t = 0.01$. We use the time-dependent generalized polynomial scheme proposed

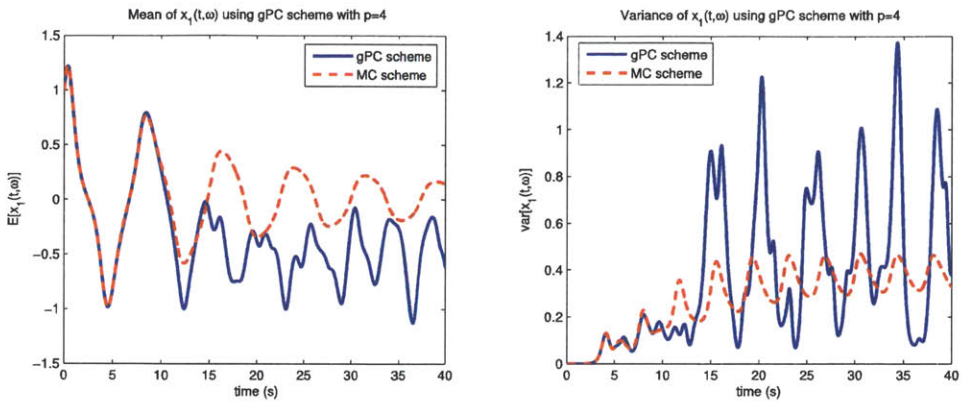

Figure 4-11: As figure (4-10), but using the gPC scheme with order $p = 4$

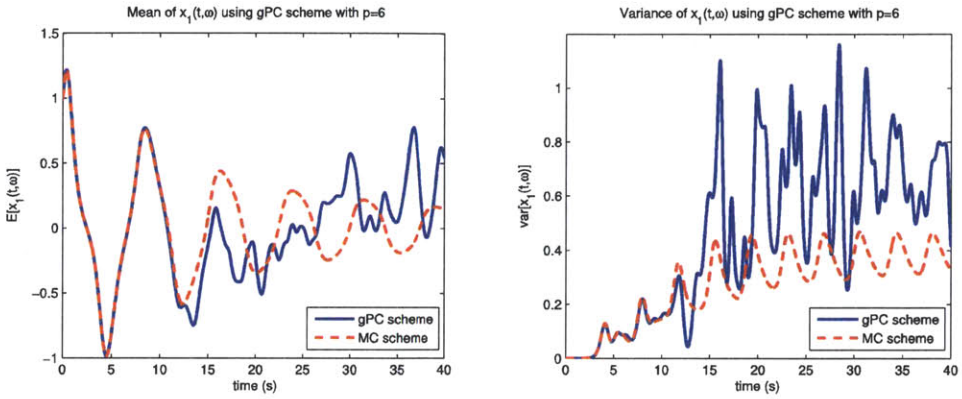

Figure 4-12: As figure (4-10), but using the gPC scheme with order $p = 6$

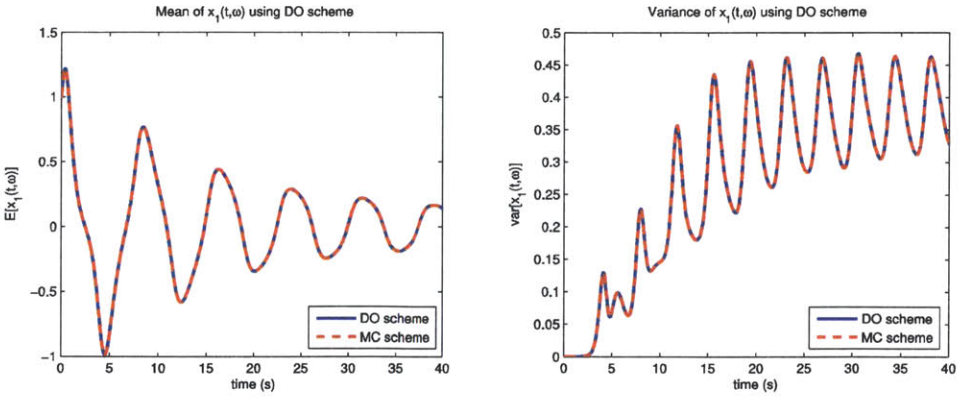

Figure 4-13: Mean and variance of the state variable $x_1(t;\omega)$ for the K-O system with initial uncertainty in one state variable using the DO scheme with $s = 3$

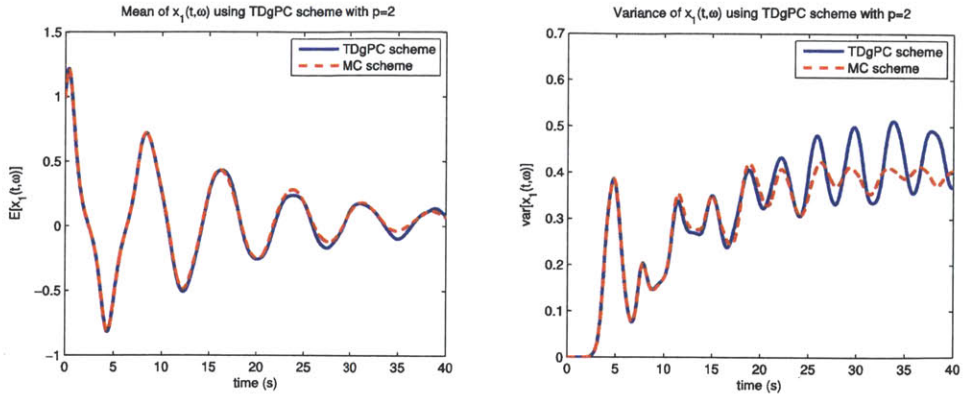

Figure 4-14: Mean and variance of the state variable $x_1(t;\omega)$ for the K-O system with initial uncertainty in all state variables using the TDgPC scheme with order $p = 2$

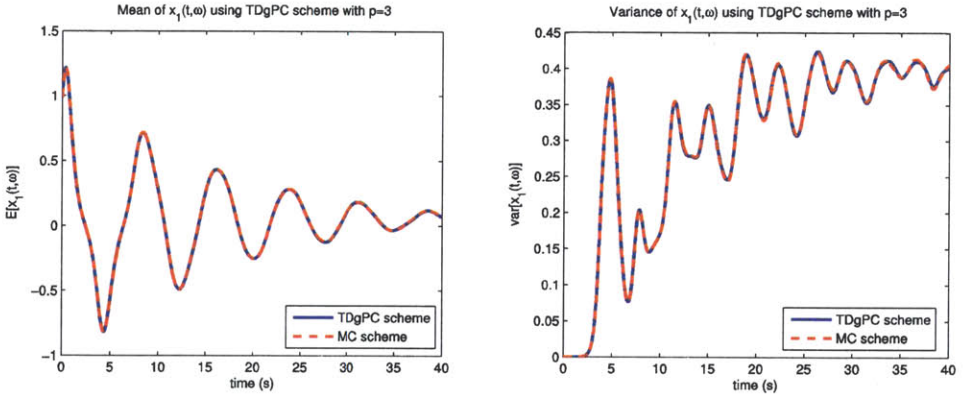

Figure 4-15: As figure (4-14), but using the TDgPC scheme with order $p = 3$

by Gerritsma et al. (2010) to compute the solution. The stochastic mean and variance of the state variable $x_1(t;\omega)$ using the TDgPC scheme with $p = 2$ ($s = 10$) and $p = 3$ ($s = 20$) are plotted in figures (4-14) and (4-15), along with their respective Monte Carlo solutions. From these figures, we observe that the TDgPC scheme, even with relatively low polynomial orders, is able to model uncertainty in nonlinear systems accurately over large time intervals. The mean and variance of $x_1(t;\omega)$ using DO scheme with $s = 3$ is shown in figure (4-16). Once again, the DO solution is found to be identical to the MC solution.

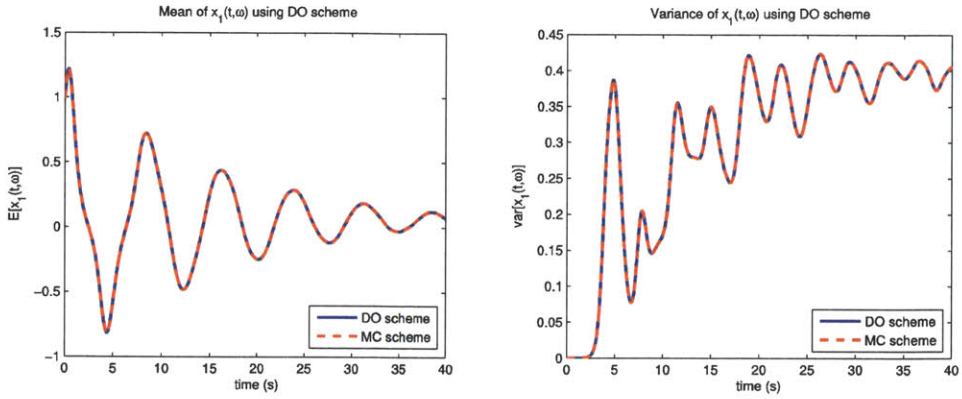

Figure 4-16: Mean and variance of the state variable $x_1(t;\omega)$ for the K-O system with initial uncertainty in all state variables using the DO scheme with $s = 3$

4.3 Long Time Integration of Nonlinear Systems using the gPC Scheme

This section studies in greater detail, the limitation of classic gPC schemes in integrating uncertainties in nonlinear dynamical systems over large time intervals. We begin by revisiting the one-dimensional decay model, studied earlier in section 4.1. We found in section 4.1 that the lower order gPC schemes (with $p = 2$ and $p = 4$) were not effective in integrating the stochastic ODE accurately. As we increased the order of the gPC expansion, the agreement between the numerical results obtained using gPC and the analytical solution increased. However, even for a higher order scheme (for e.g., with $p = 6$), we found that the gPC scheme started to deviate from the analytical solution at a later time. This effect is a consequence of the continuous increase in the magnitude of nonlinearities in the PC expansion of the solution field with time. To see this effect more clearly, the probability density function (pdf) of the numerical gPC solutions $u(t;\omega)$ using different polynomial orders ($p = 2$ and $p = 3$) and at different values of time t is plotted in figures (4-17) through (4-28), along with its stochastic mean and variance. From figures (4-17) and (4-18), it is observed that initially, both the schemes represent the pdf of the solution accurately. At around $t = 1.5$ s, the gPC scheme with order $p = 2$ starts to deviate from the Monte Carlo solution (figure (4-19)). This is due to the inability of the scheme to handle growing nonlinearities. The higher order gPC scheme (with $p = 3$) is

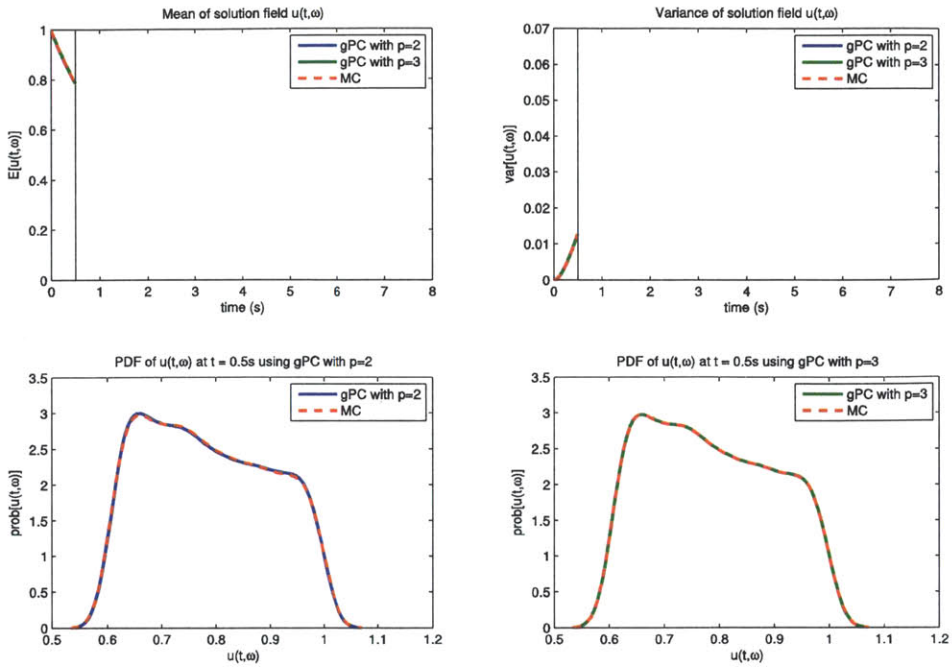

Figure 4-17: Probability density function of $u(t;\omega)$ for the 1-D decay model at $t = 0.5$ s

able to handle the growing nonlinearities better than the lower order scheme, but at a later time $t = 4.0$ s, the higher order scheme also begins to deviate from the true solution (figure (4-24)). From figures (4-25), (4-26), (4-27) and (4-28), it is evident that for $t \geq 4.5$ s, the probability distribution function of $u(t;\omega)$ represented by both the gPC schemes is inaccurate.

To explain this behavior, consider the polynomial chaos expansion of the stochastic field $X(r,t;\omega)$, given by equation (2.43), with $\bar{r}$ stochastic random variables. The first deterministic coefficient of the expansion $\tilde{x}_0(r,t)$ (with $\psi_0(\omega) = 1$) represents the stochastic mean of the solution field. The next $\bar{r}$ terms $(\tilde{x}_i(r,t), 1 \leq i \leq \bar{r})$ represent the coefficients corresponding to the linear terms of the polynomial expansion of the stochastic random variables and subsequent terms $(\tilde{x}_i(r,t), \bar{r}+1 \leq i \leq s-1)$ represent the coefficients corresponding to quadratic and other higher order terms. In many cases, the initial uncertainty is almost always linear, meaning that the magnitude of the coefficients corresponding to quadratic and other higher terms is zero initially $(\tilde{x}_i(r,t) = 0, \bar{r}+1 \leq i \leq s-1)$. As the system is evolved numerically in time, the stochastic characteristics of the solution

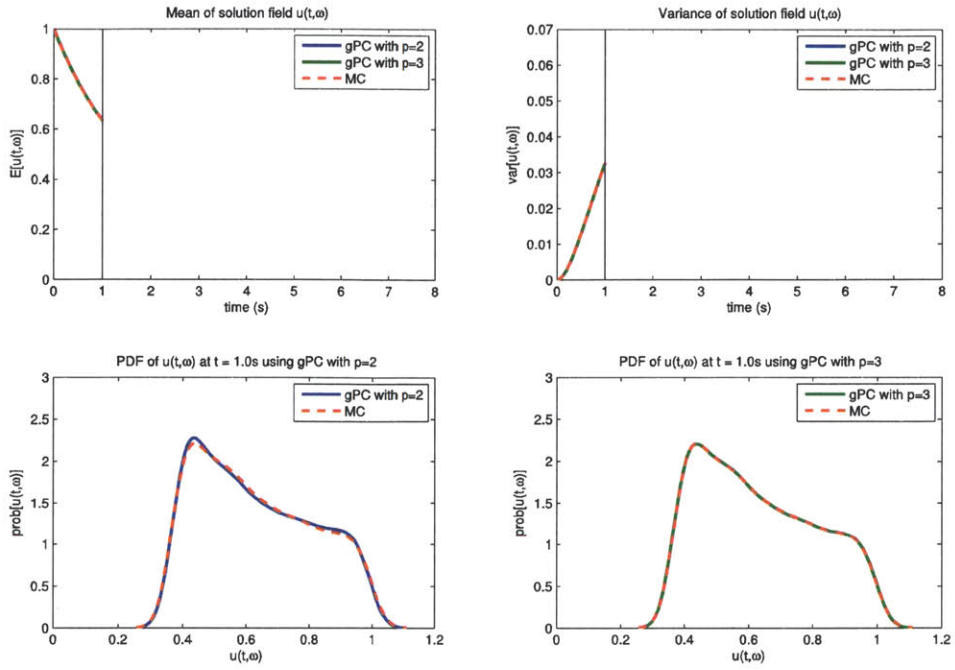

Figure 4-18: As figure (4-17), but at time $t = 1.0$ s

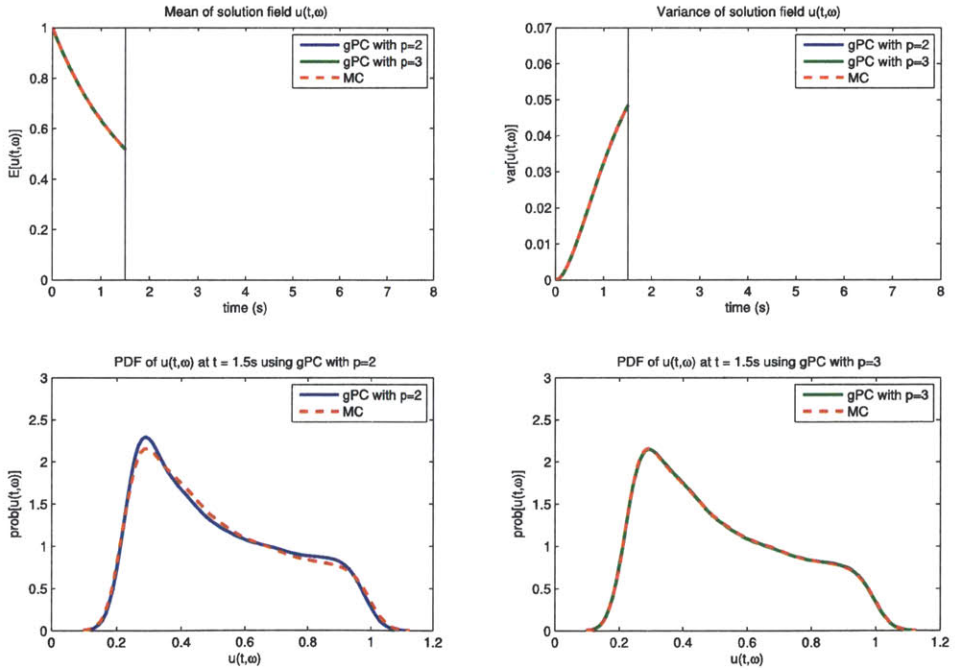

Figure 4-19: As figure (4-17), but at time $t = 1.5$ s

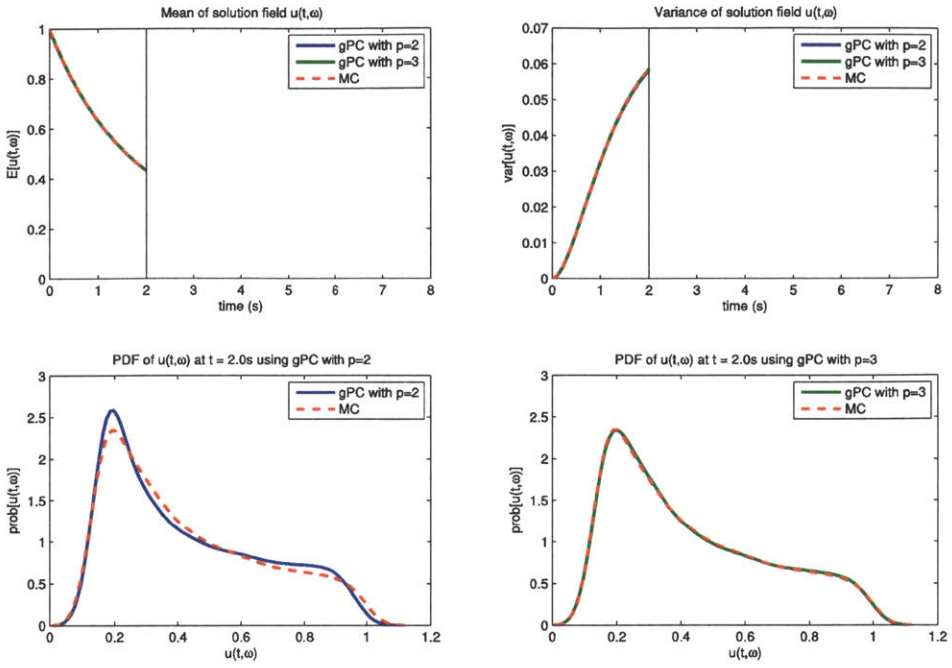

Figure 4-20: As figure (4-17), but at time $t = 2.0$ s

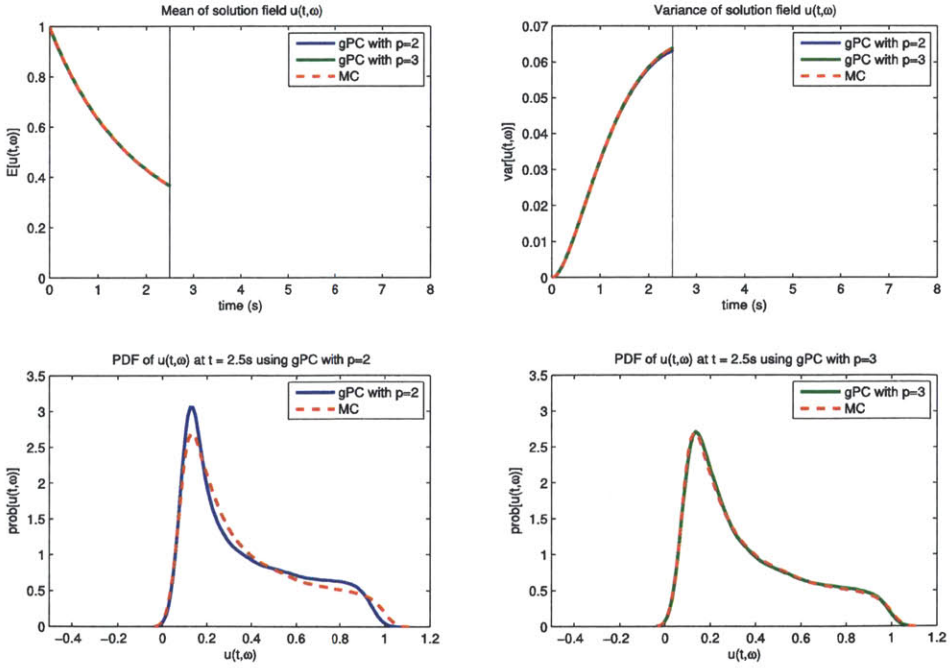

Figure 4-21: As figure (4-17), but at time $t = 2.5$ s

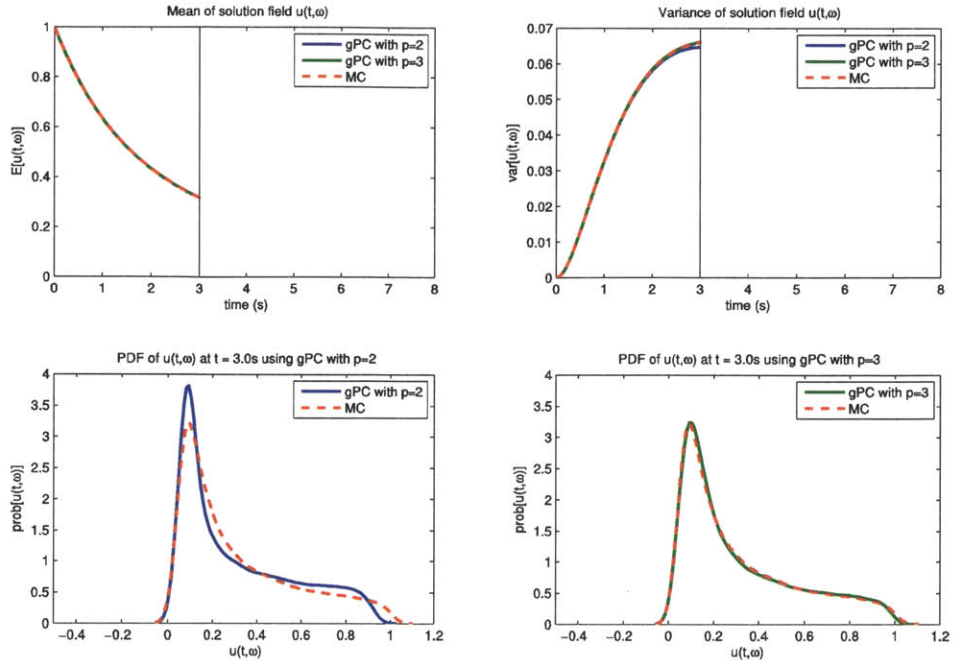

Figure 4-22: As figure (4-17), but at time $t = 3.0$ s

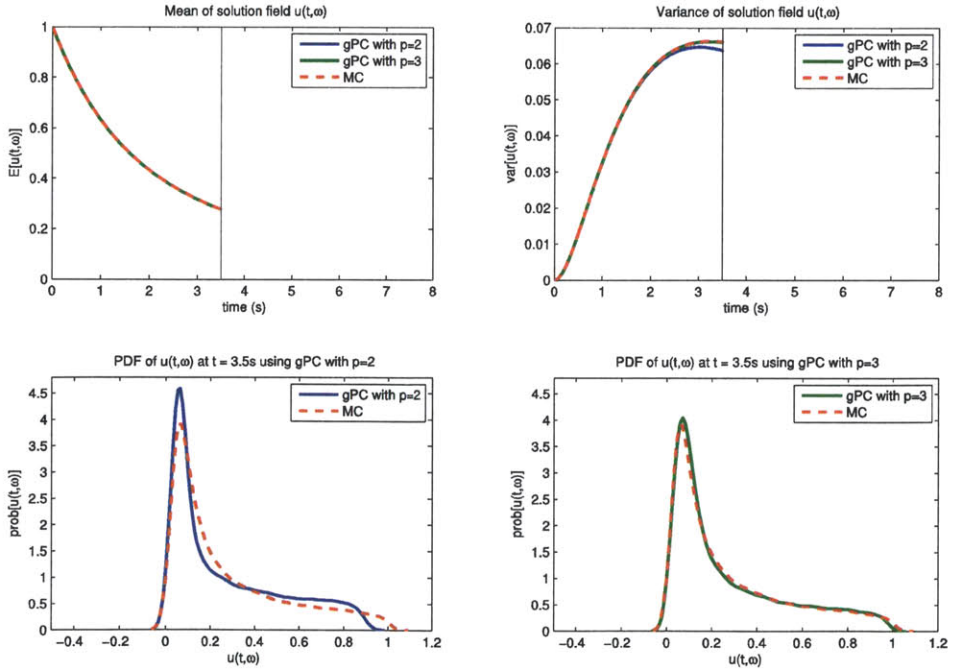

Figure 4-23: As figure (4-17), but at time $t = 3.5$ s

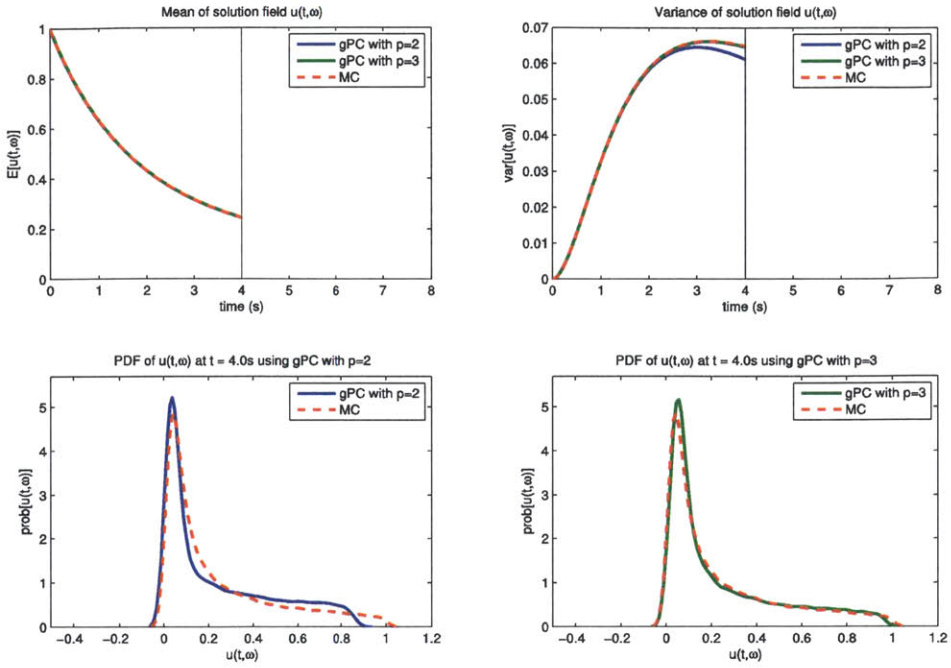

Figure 4-24: As figure (4-17), but at time $t = 4.0$ s

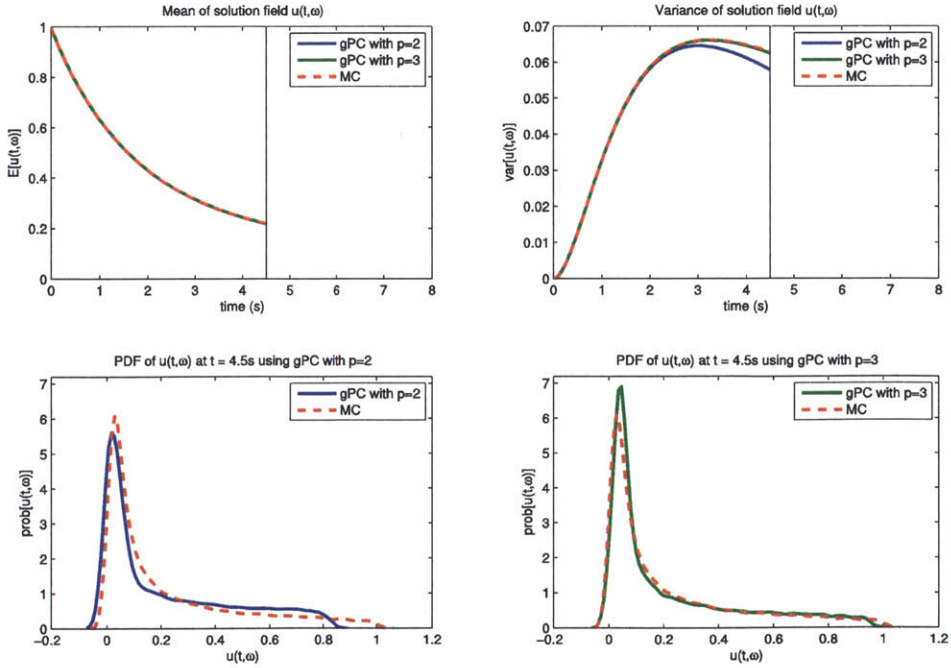

Figure 4-25: As figure (4-17), but at time $t = 4.5$ s

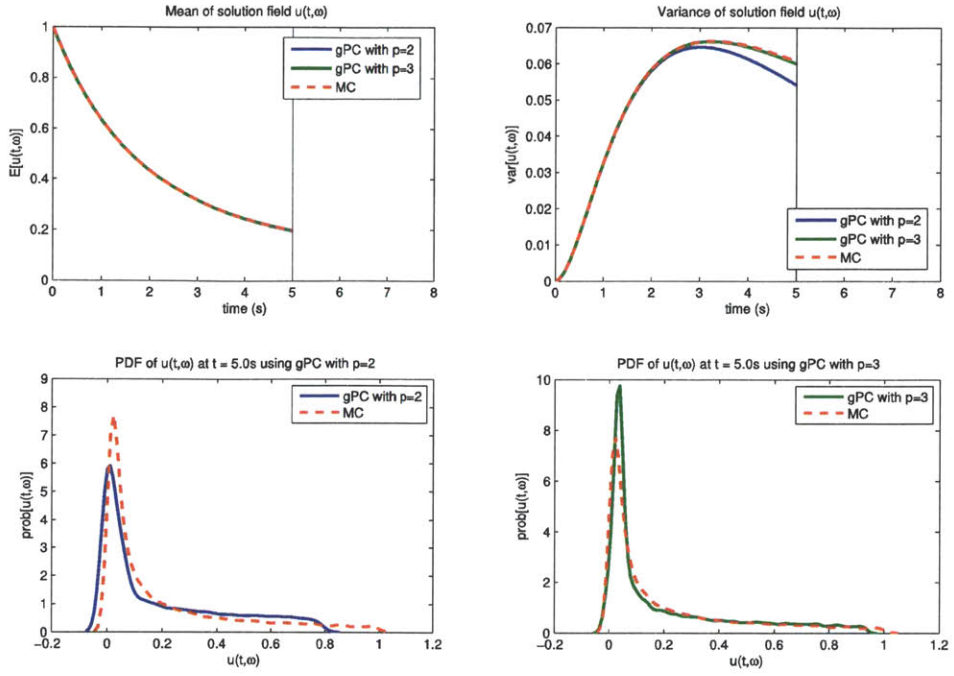

Figure 4-26: As figure (4-17), but at time $t = 5.0$ s

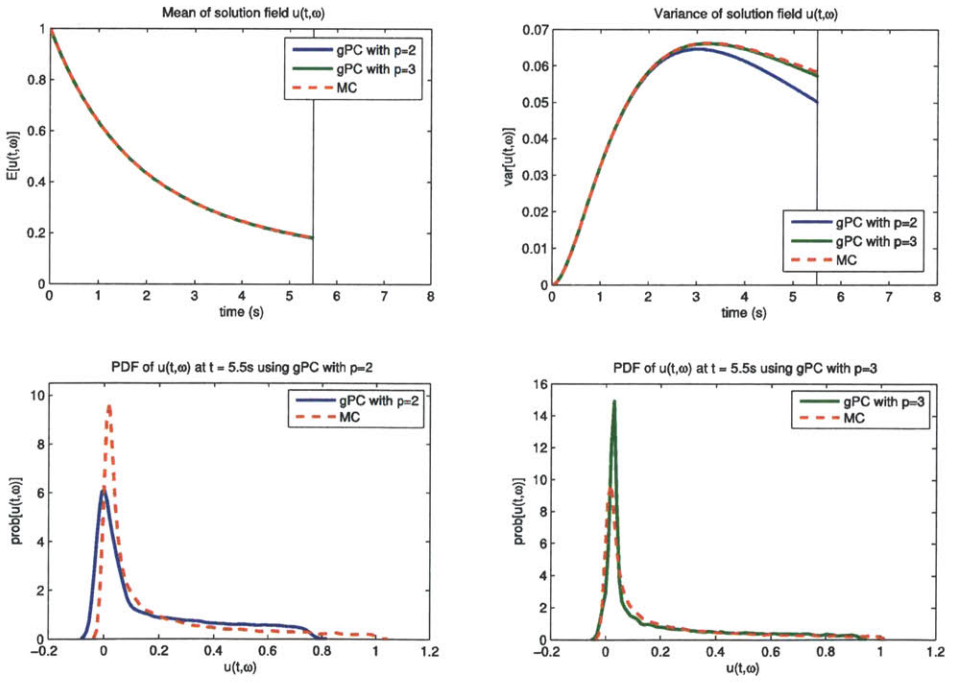

Figure 4-27: As figure (4-17), but at time $t = 5.5$ s

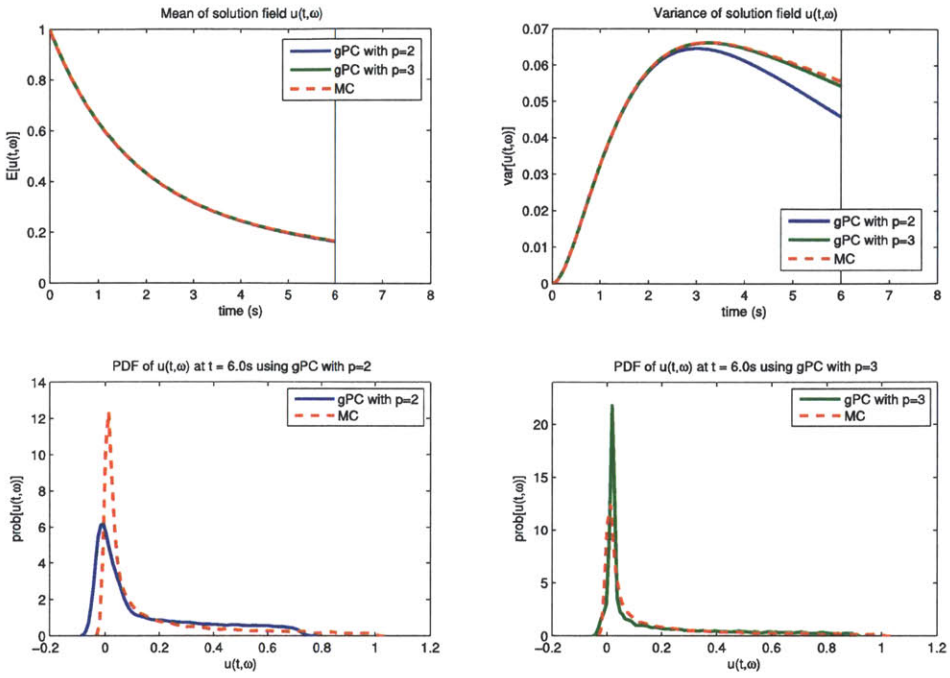

Figure 4-28: As figure (4-17), but at time $t = 6.0$ s

field change. Depending on the extent of nonlinearities in system dynamics, the magnitude of the coefficients corresponding to the higher order terms in the gPC expansion increases with time. With increasing magnitudes of nonlinear terms, the ability of the polynomial chaos expansion to approximate the true pdf of the solution field diminishes, leading to reduction in accuracy of the scheme. A higher order gPC scheme, by virtue of more number of higher order terms, will be able to accurately model the nonlinearities for a larger period of time compared to a lower order scheme, but will tend to lose its accuracy eventually. This causes the gPC scheme to be ineffective in modeling highly nonlinear systems over large time-intervals. The TDgPC scheme proposed by Gerritsma et al. (2010) alleviates this limitation by redefining the polynomial basis so as to make the magnitude of the coefficients corresponding to the higher order terms equal to zero during the re-initialization step, thereby reducing the polynomial chaos expansion to linear terms only.

To further explain the limitation of gPC scheme in integrating nonlinear systems, we consider the highly nonlinear Kraichnan-Orszag three mode problem (from section 4.2).

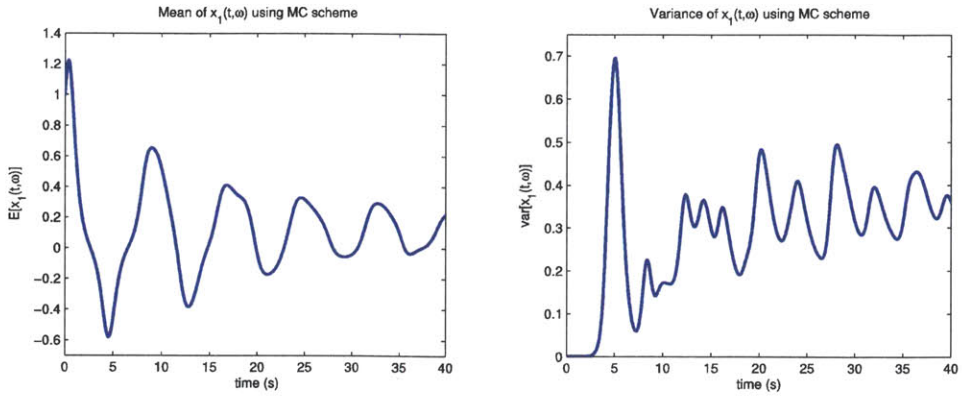

Figure 4-29: Mean and variance of the state variable $x_1(t;\omega)$ for the K-O system with initial uncertainty in one state variable using the MC scheme

Consider the K-O system represented by equation (4.7) with the initial condition given as

$$\begin{aligned} x_1(0,\omega) &= 0.995 + 0.01\xi(\omega) \\ x_2(0,\omega) &= 1.0 \\ x_3(0,\omega) &= 1.0 \end{aligned} \tag{4.10}$$

where $\xi(\omega) \sim U[-1,1]$ is a uniform random variable. We again consider the time domain $t \in [0,40]$ and use a time step of $\Delta t = 0.01$. The stochastic mean and variance of the state variable $x_1(t;\omega)$ using Monte Carlo simulations with 10000 sample realizations is plotted in figure (4-29). The mean and variance of $x_1(t;\omega)$ using gPC scheme with polynomial order $p = 6$ and using TDgPC scheme with polynomial order $p = 3$ are shown in figures (4-30) and (4-31), respectively. From these figures, we find that the gPC scheme is unable to integrate the evolution of uncertainty in the K-O system, whereas the TDgPC scheme is fairly accurate in the chosen example.

For a clearer comparison, we again show the pdf of $x_1(t;\omega)$ at different values of time t using the two schemes, in figures (4-32) through (4-39). The corresponding pdf using Monte Carlo simulations is also depicted in the same figures. The gPC solution is found to be accurate only for smaller values of time t. From figures (4-32) and (4-33), it is observed that initially, the pdf of $x_1(t;\omega)$ is similar in appearance to that of a uniform random variable. As the system evolves in time, the nonlinear characteristics of the gPC

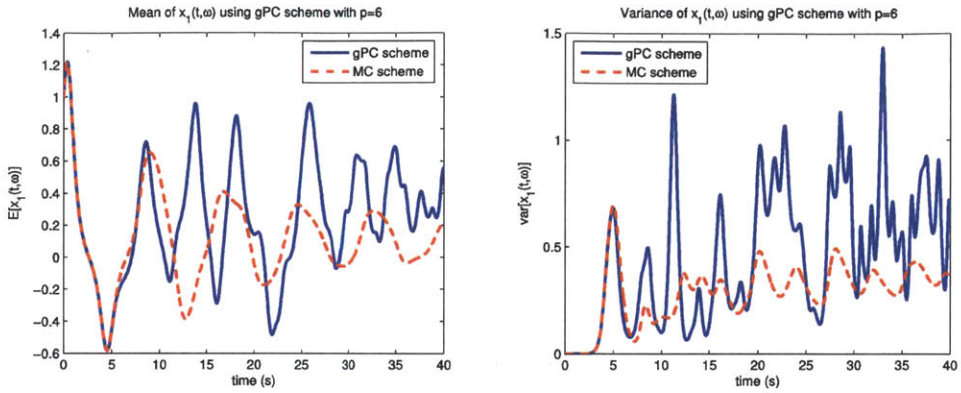

Figure 4-30: Mean and variance of the state variable $x_1(t;\omega)$ for the K-O system with initial uncertainty in one state variable using the gPC scheme with $p = 6$

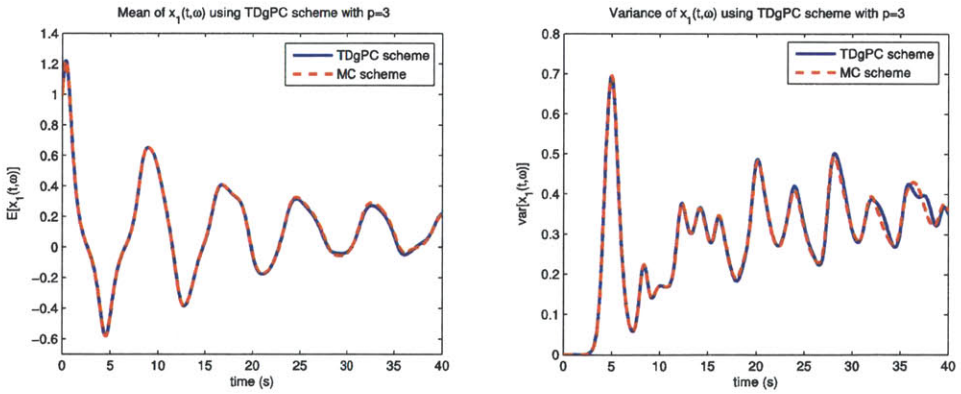

Figure 4-31: Mean and variance of the state variable $x_1(t;\omega)$ for the K-O system with initial uncertainty in one state variable using the TDgPC scheme with $p = 3$

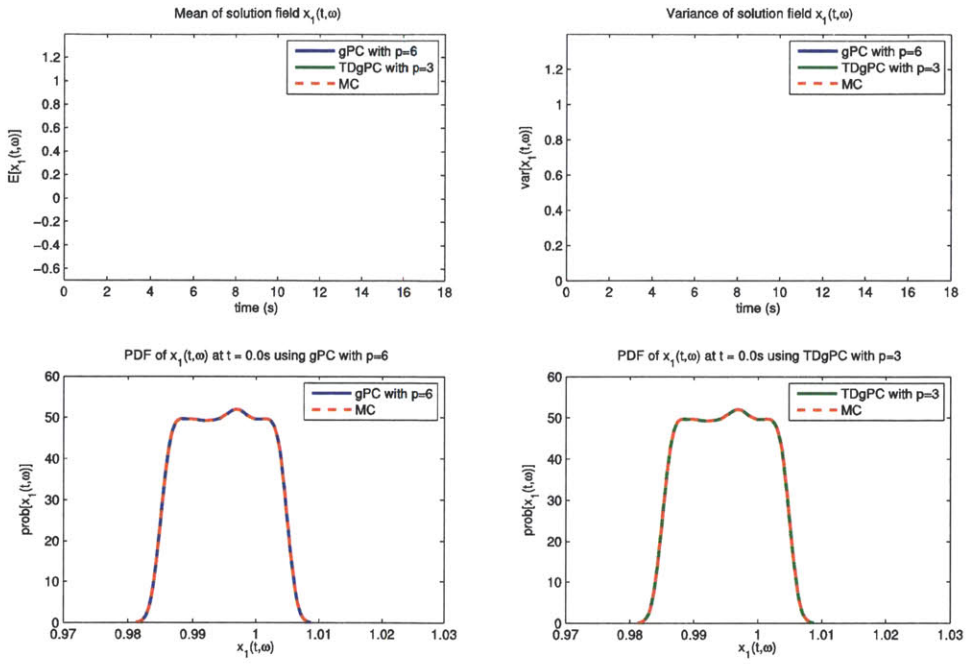

Figure 4-32: Probability density function of $x_1(t;\omega)$ for the K-O system at $t = 0.0$ s

expansion increase, and the pdf of $x_1(t;\omega)$ assumes a shape completely different from that of a uniform random variable (seen in figures (4-35) through (4-39)). As the stochastic characteristics of the solution field change, the gPC scheme loses its ability to represent the pdf of $x_1(t;\omega)$ accurately, and hence deviates from the true solution. On the other hand, the TDgPC scheme is able to represent the pdf of the solution field fairly accurately at all values of time t.

4.4 Discussion on Performance of Uncertainty Quantification Schemes

In this section, we discuss and investigate the performance of uncertainty quantification schemes for integrating uncertainties in input parameters, in terms of accuracy of solution and computational cost. First, we remark that the solution field obtained using the DO scheme implemented over full space is exactly identical to the solution field obtained using Monte Carlo simulations. By studying the DO evolution equations (3.15), (3.16)

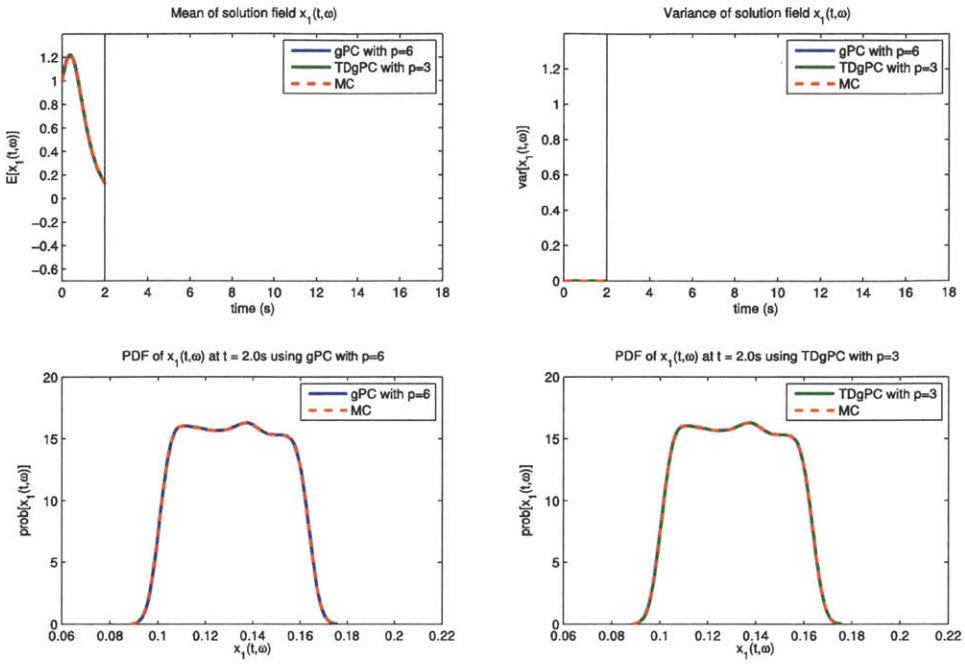

Figure 4-33: As figure (4-32), but at time $t = 2.0$ s

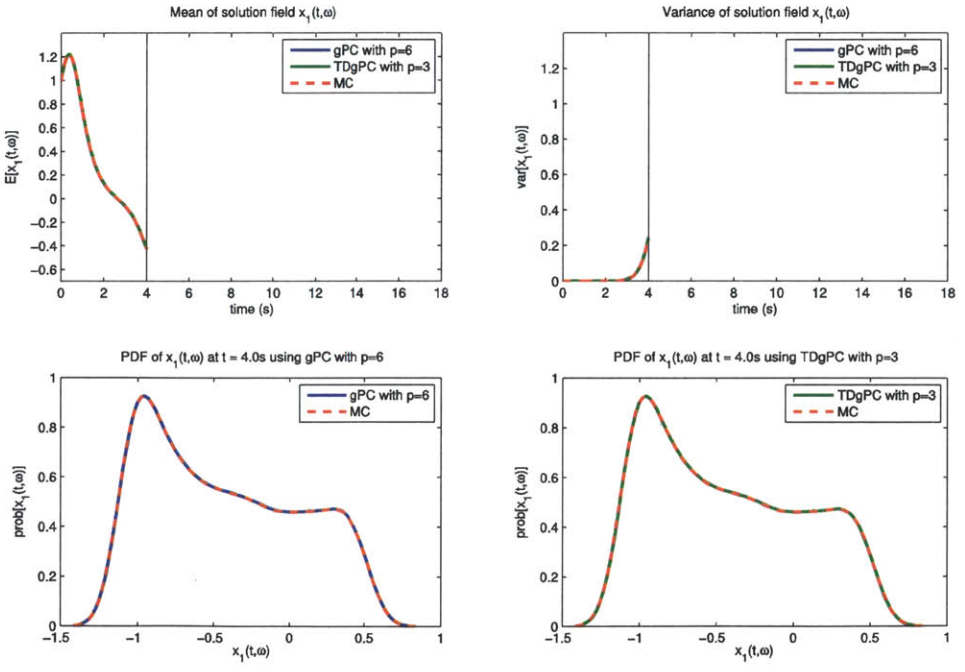

Figure 4-34: As figure (4-32), but at time $t = 4.0$ s

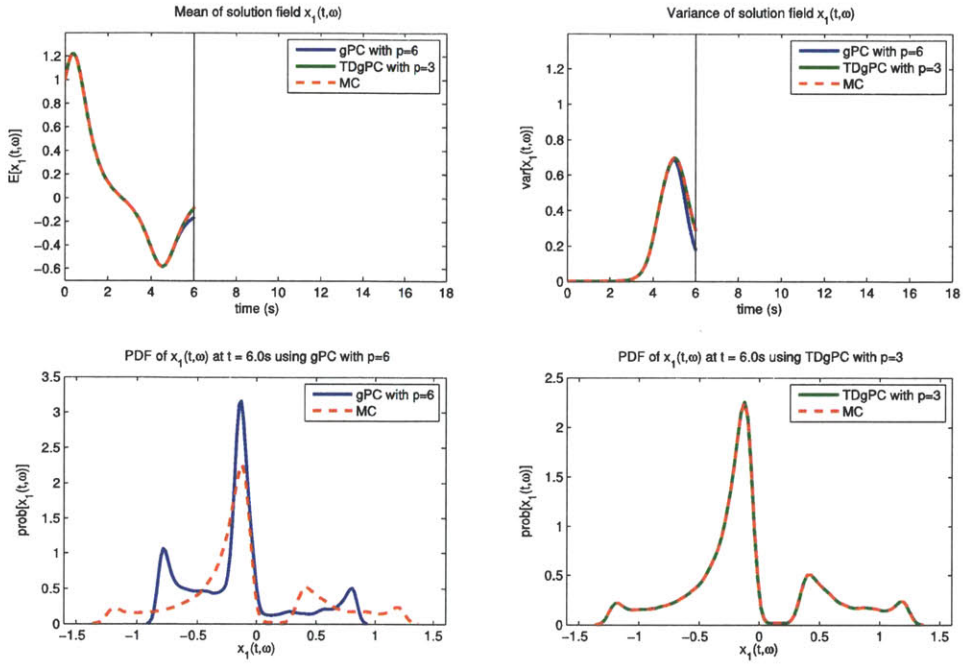

Figure 4-35: As figure (4-32), but at time $t = 6.0$ s

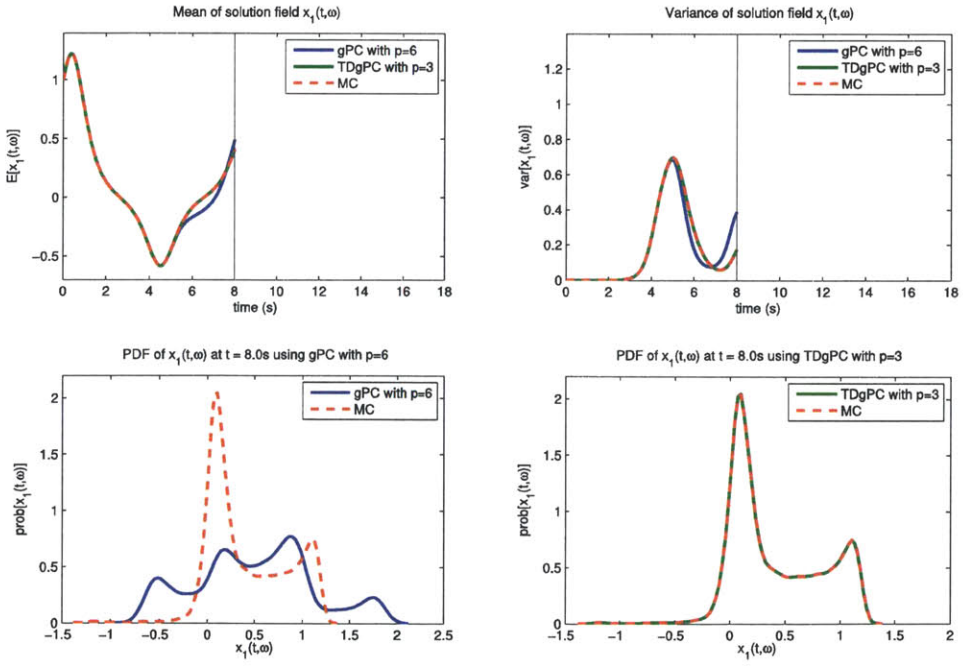

Figure 4-36: As figure (4-32), but at time $t = 8.0$ s

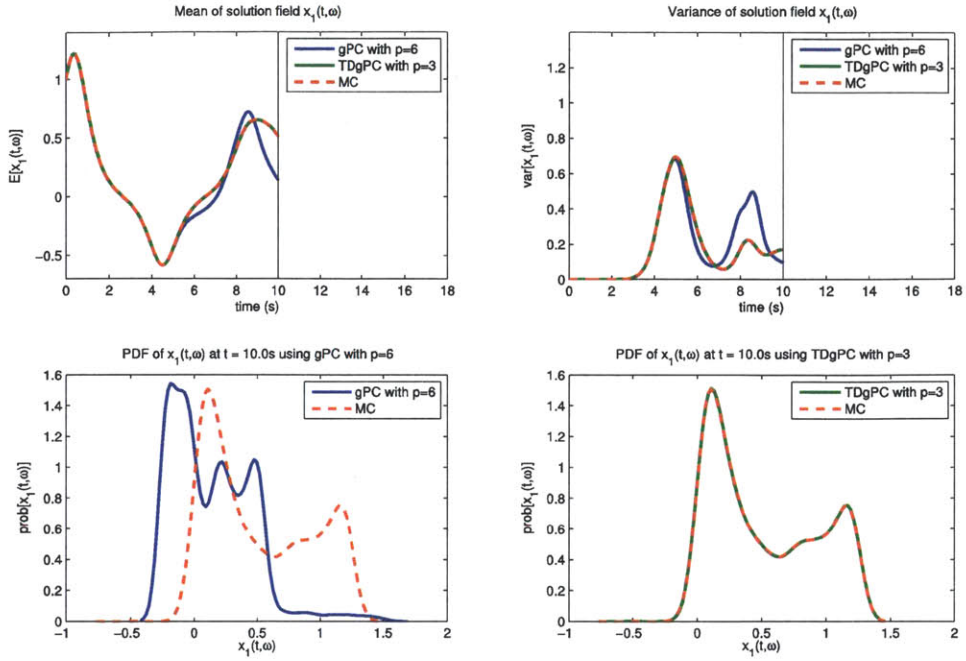

Figure 4-37: As figure (4-32), but at time $t = 10.0$ s

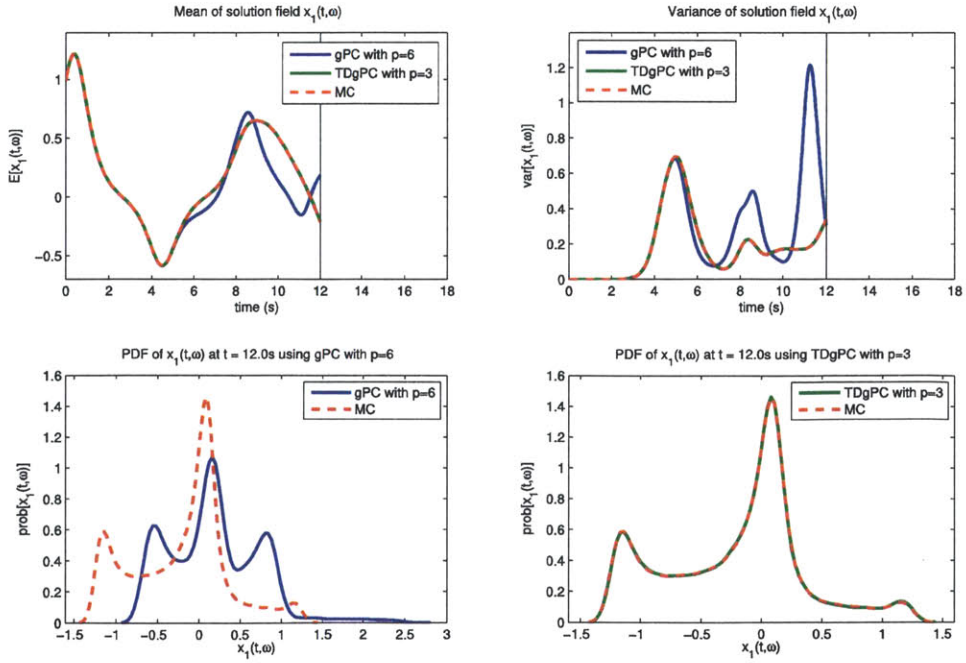

Figure 4-38: As figure (4-32), but at time $t = 12.0$ s

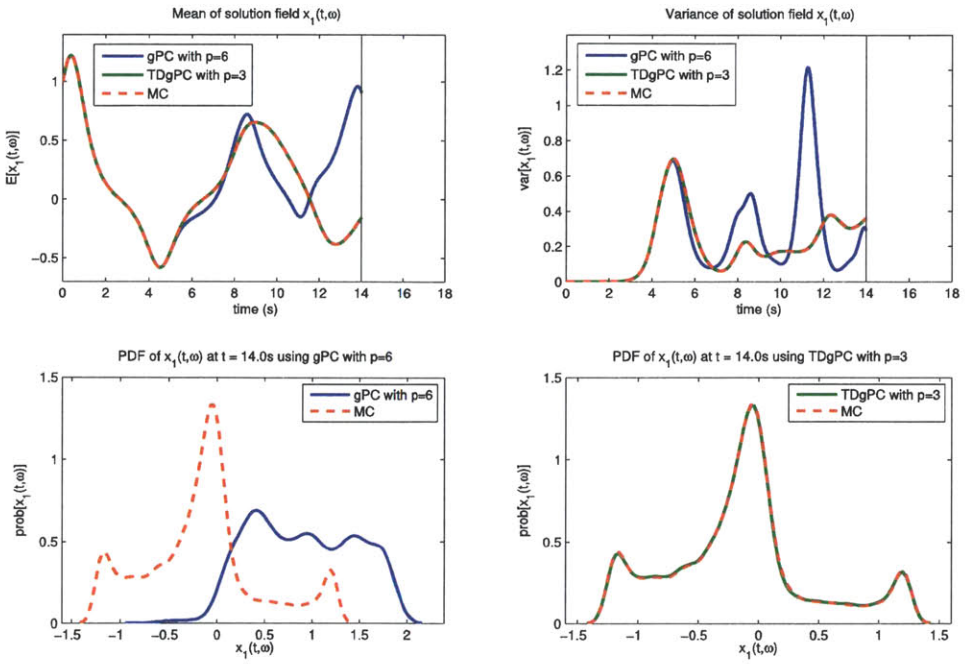

Figure 4-39: As figure (4-32), but at time $t = 14.0$ s

and (3.17) in greater detail, it can be observed that when the DO scheme is implemented over full space, the DO modes do not (need to) evolve in time. As such, a full space DO scheme with MC integration of the stochastic coefficient becomes equivalent to a classic MC scheme.

As was shown in the previous section, the gPC scheme is ineffective in integrating nonlinear dynamical systems over large time intervals. This limitation is removed in the TDgPC scheme by using time-dependent gPC bases. However, re-initializing the bases frequently in time significantly increases the computational cost of the TDgPC scheme. Moreover, since the re-initialization increases the number of random variables ($\bar{r}$) to be equal to the size of the physical space (N), the TDgPC scheme becomes computationally expensive for large dimensional stochastic systems. Hence, it might have limited applicability in integrating uncertainty in realistic ocean models, which typically involve high dimensionality.

The run times for the various examples studied in this chapter using UQ schemes of comparable accuracy are presented in table (4.1). Since the gPC scheme is unable to model

Table 4.1: Run times for uncertainty quantification schemes of comparable accuracy for integrating in time uncertainty in input parameters

S. No.	Test Case	MC	gPC ($p = 10$)	TDgPC ($p = 3$)	DO (full space)
1.	1-D Decay Model Equations (4.1), (4.2), (4.3)	1380.63s	121.26s ($s = 11$)	273.81s ($s = 4$)	62.51s ($s = 1$)
2.	K-O Model with initial uncertainty in x_1 Equations (4.7), (4.8)	1908.48s	Not Applicable	4376.06s ($s = 20$)	196.98s ($s = 3$)
3.	K-O Model with initial uncertainty in x_1 Equations (4.7), (4.10)	1874.08s	Not Applicable	4560.03s ($s = 20$)	157.59s ($s = 3$)
4.	K-O Model with initial uncertainty in x_1, x_2, x_3 Equations (4.7), (4.9)	1895.61s	Not Applicable	5633.97s ($s = 20$)	194.59s ($s = 3$)

the Kraichnan-Orszag three mode problem with sufficient accuracy, its run times are not included. We find from table (4.1) that for the examples studied in this chapter, the run times for the DO scheme are smaller than those of the other schemes. Additionally, the run times for the TDgPC scheme are significantly higher compared to the other schemes, which is a result of the frequent re-initialization of the gPC basis. Thus, the TDgPC scheme compromises computational cost in order to integrate the evolution of uncertainty accurately using a PC framework. It is also evident that increasing the dimensionality of the system leads to a significant increase in run times of all the schemes, as seen here in the case of one-dimensional and three-dimensional examples. Specifically, the DO increase in time is linear in the system size (as is also the case of ESSE or MC integrations). Overall, for integrating uncertainty in high dimensional realistic ocean systems, schemes which may be implemented over a reduced space may have a significant advantage in terms of computational cost.

Chapter 5

Uncertainty due to External Stochastic Forcing

In this chapter, we study stochastic linear and nonlinear dynamical systems with uncertainty due to external stochastic forcing. The type of forcing we consider is given by the second term of our system of equations (1.1), i.e. $B(X(r,t;\omega),t)\,dW(t;\omega)$. It is important to realize that this covers both additive and multiplicative noise since B is in general a function of the stochastic state variable $X(r,t;\omega)$,. The source for the noise is the multi-dimensional $dW(t;\omega)$ which are Brownian motions, defined in section 2.1.2. This Gaussian forcing (also known as white noise) is chosen because our long-term interest is in efficient uncertainty quantification and prediction for realistic ocean systems. Gaussian stochastic forcing is a common and relevant type of forcing to model processes not represented deterministically in classic ocean circulation equations. Of course, the whole stochastic forcing is $B(X(r,t;\omega),t)\,dW(t;\omega)$, which accounts for nonlinear interactions of state variables $X(r,t;\omega)$ with the multi-dimensional Gaussian forcing. In fact, one can show that a large class of statistics can be represented by stochastic forcing of this type (Jazwinski, 1970).

In what follows, we begin by discussing and illustrating a fundamental limitation of existing PC schemes in capturing sustained influx of randomness, resulting in their inability to accurately integrate stochastic forcing over long time intervals. Next, we utilize and study our new MTDgPC scheme (section 3.4) to integerate a stochatic three-dimensional

autonomous system with Gaussian noise and compare the results with those of DO and MC schemes. We then consider again a stochastic three-dimensional system but this time with both autonomous and non-autonomous dynamics, and we compare the results and efficiency of our new reduced space and reduced order KLgPC scheme (section 3.5) to those of our new MTDgPC scheme. Finally, we study the application of our new MTDgPC and KLgPC schemes for integrating multiplicative noise in a four-dimensional autonomous system. We end the chapter with a discussion on the performance of uncertainty quantification schemes for integrating multi-dimensional stochastic forcing.

5.1 Limitations of Existing Polynomial Chaos Schemes

As a first example of a system with stochastic noise, we consider a three-dimensional autonomous system $X(t;\omega) = [x_1(t;\omega) \quad x_2(t;\omega) \quad x_3(t;\omega)]^T$ with a three-dimensional driving Wiener process. Consider the dynamical system represented by equation (1.1), where the matrices A and B are given as

$$A = \begin{bmatrix} -3 & 1 & 1 \\ 2 & -5 & 1 \\ 3 & 1 & -6 \end{bmatrix} \qquad B = \begin{bmatrix} 0 & 2 & 1 \\ 0 & 1 & 0 \\ 2 & 0 & 0 \end{bmatrix} \tag{5.1}$$

In this case, the initial conditions are deterministic and are represented as

$$\begin{bmatrix} x_1(0,\omega) \\ x_2(0,\omega) \\ x_3(0,\omega) \end{bmatrix} = \begin{bmatrix} 1.0 \\ 1.0 \\ 1.0 \end{bmatrix} \tag{5.2}$$

We consider the time domain $t \in [0, 4]$ and use a time step of $\Delta t = 0.01$. The stochastic mean and variance of the state variable $x_1(t;\omega)$ estimated using Monte Carlo simulations with 2×10^5 realizations is shown in figure (5-1). The same result using the DO scheme with three stochastic modes ($s = 3$) is plotted in figure (5-2). For comparison, the analytical results are also depicted in the same figures. It is observed that even for dynamical systems with external stochastic forcing, the solution obtained using the DO

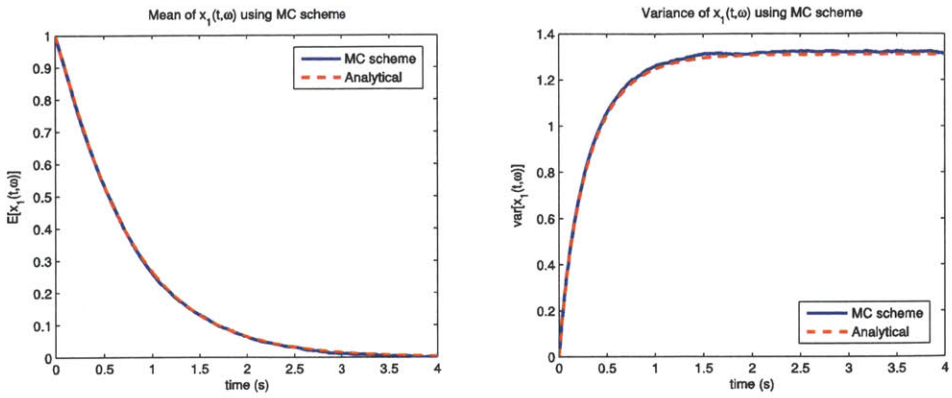

Figure 5-1: Mean and variance of the state variable $x_1(t;\omega)$ for a three-dimensional autonomous system with additive noise using the MC scheme

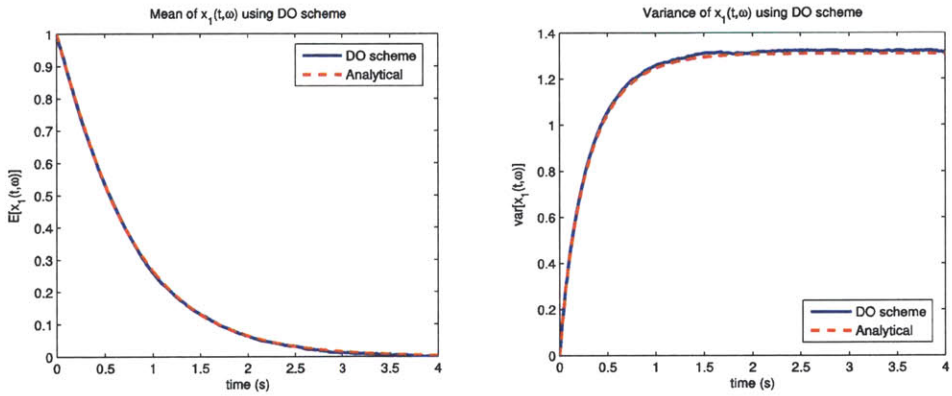

Figure 5-2: Mean and variance of the state variable $x_1(t;\omega)$ for three-dimensional autonomous system with additive noise using the DO scheme with $s = 3$

scheme implemented over the full space is identical to the solution obtained using Monte Carlo simulations.

All existing PC schemes known to us, including the gPC and TDgPC schemes, have inherent limitations in integrating stochastic forcing of dynamical systems. To better understand this limitation, it is useful to revisit the concept of Brownian motion. Let us consider a Brownian motion $W(t)$ over a time interval $t \in [0, T]$, numerically discretized into n steps, by setting $h = T/n$, as discussed in section 2.1.2. Let $dW_j = W(t_j) - W(t_{j-1})$, where $j = 1, 2, ..., n$, be a Brownian motion increment over the time step interval $(\Delta t)_j = t_j - t_{j-1}$. Then, by definition of a Brownian motion, each dW_j is an independent random variable. Thus, in order to represent the solution field over the time interval $[0, T]$ using polynomial chaos, we need to construct a PC expansion of the solution field using all dW_j

as independent random variables. Even in a system with no other form of uncertainty, the total number of random variables needed to model an m-dimensional Wiener process over n time steps turns out to be $\bar{r} = mn$. The total number of terms in the polynomial chaos expansion is then given as

$$s = \binom{\bar{r} + p}{\bar{r}} = \frac{(mn + p)!}{(mn)!\, p!} \tag{5.3}$$

It is clearly seen that the number of terms in the expansion increases very rapidly beyond computational capabilities as the number of time steps n increases or as the modeling duration T increases. As an example, we again consider the three-dimensional autonomous system described by equations (1.1) with dynamics (5.1) and (5.2) and over a duration $t \in [0, 4]$. The number of terms required to represent the solution field using a PC expansion of order $p = 3$ and using a time step of $\Delta t = 0.01$ is given by

$$s = \frac{(1200 + 3)!}{1200!\, 3!} \approx 2.9 \times 10^8 \tag{5.4}$$

which is beyond acceptable computational limits for such a small system. Ideally, with $\Delta t \to 0$, a Brownian motion is represented by an infinite number of random variables.

In order to represent a white noise process numerically using PC schemes, one has to deal with a sustained flux of new random variables, which grows very quickly in time and becomes computationally infeasible. Hou et al. (2006) and a few other authors have accurately intgerated dynamical systems with stochastic noise over short time intervals using PC schemes with sparse truncation methods (described in detail in section 2.3.4). However, even when using sparse truncation methods, the number of terms in the PC approximation of the solution field grows very quickly in time and hence, these schemes lose their effectiveness in integrating uncertainty over longer time intervals. With our interest in modeling realistic ocean systems with external stochastic forcing, we introduced two new PC schemes, the Modified TDgPC scheme (section 3.4) and the reduced space and reduced order KLgPC scheme (section 3.5). As we will show next, these new schemes are capable of integrating stochastic noise over arbitrarily long time intervals.

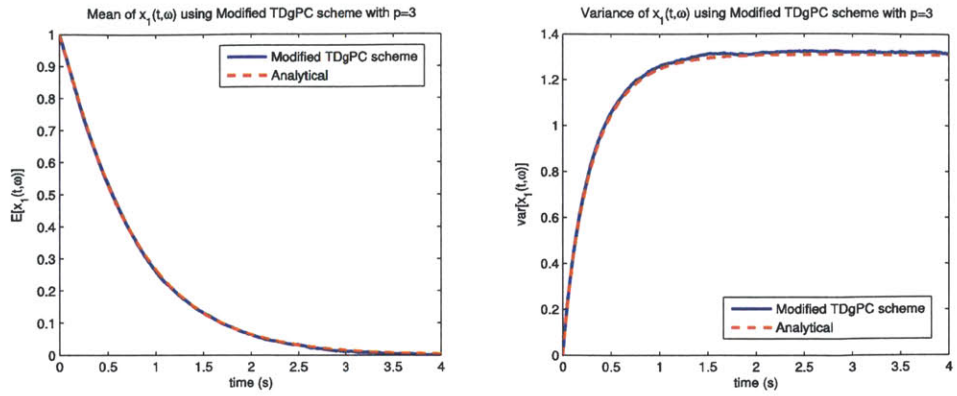

Figure 5-3: Mean and variance of the state variable $x_1(t;\omega)$ for three-dimensional autonomous system with additive noise using the new MTDgPC scheme with $p = 3$

5.2 Modeling Stochastic Noise using our New Polynomial Chaos Schemes

In this section, we utilze our new polynomial chaos schemes, namely, the MTDgPC and the KLgPC schemes to integrate stochastic forcing. First, we consider again the three-dimensional autonomous system represented by equations (1.1) and dynamics (5.1) and (5.2). We again consider the time domain $t \in [0, 4]$ and use a time step of $\Delta t = 0.01$. The stochastic mean and variance of the state variable $x_1(t;\omega)$ using the new MTDgPC scheme with polynomial order $p = 3$ ($s = 20$) is plotted in figure (5-3). The analytical solutions are also depicted in the same figure. Similarly, the mean and variance of state variables $x_2(t;\omega)$ and $x_3(t;\omega)$ using the new MTDgPC scheme with $p = 3$, along with their corresponding analytical solutions are shown in figures (5-4) and (5-5) respectively. It is observed that all the errors are reasonably small over the entire time domain. Thus, the new MTDgPC scheme accurately models stochastic additive noise in the three-dimensional autonomous system. However, it has a relatively high computational cost (discussed in detail in section 5.3).

Next, we study a three-dimensional dynamical non-autonomous system with a three-dimensional driving Wiener process. In this example as well, the external stochastic forcing is additive in nature. Specifically, the system is governed by (1.1), but with

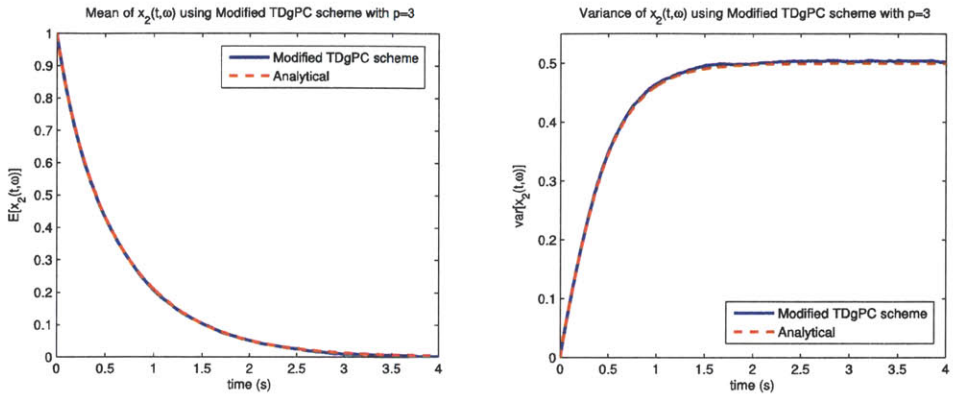

Figure 5-4: Mean and variance of the state variable $x_2(t;\omega)$ for three-dimensional autonomous system with additive noise using the new MTDgPC scheme with $p = 3$

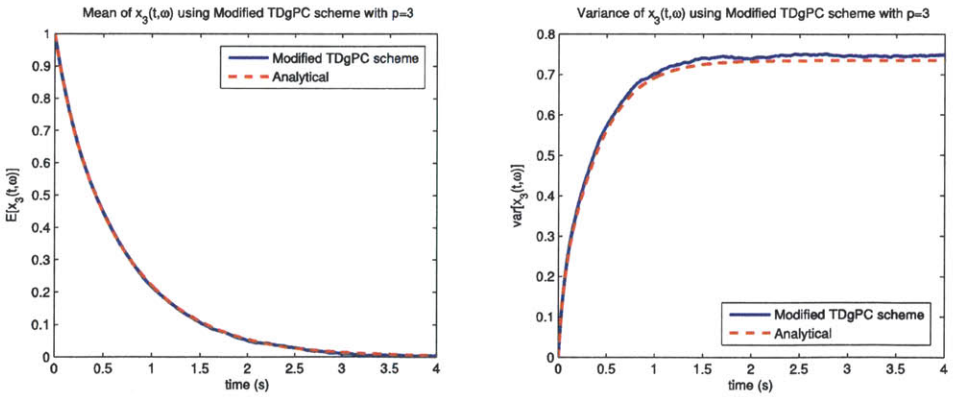

Figure 5-5: Mean and variance of the state variable $x_3(t;\omega)$ for three-dimensional autonomous system with additive noise using the new MTDgPC scheme with $p = 3$

dynamics matrices A and B now given as

$$A = \begin{bmatrix} -3 + 2\cos(2\pi t) & 1 & 1 + 2\sin(2\pi t) \\ 2 & -5 & 1 \\ 3 & 1 + 3\sin(4\pi t) & -6 + +3\cos(4\pi t) \end{bmatrix}$$
$$B = \begin{bmatrix} 0.5\cos(2\pi t) & 2 + 0.5\sin(2\pi t) & 1 \\ 0 & 1 + \sin(2\pi t) & \cos(2\pi t) \\ 2 & 0 & 0 \end{bmatrix} \tag{5.5}$$

The initial conditions are again chosen to be deterministic and are represented by equation (5.2). We still consider the time domain $t \in [0, 4]$ and use a time step of $\Delta t = 0.01$, and we compare the Monte Carlo solution to the MTDgPC and KLgPC solutions.

The three-dimensional non-autonomous system is first integrated using the Monte Carlo scheme, and the stochastic mean and variance of $x_1(t;\omega)$ estimated using the MC scheme with 2×10^5 sample realizations is shown in figure (5-6). The same state variable, but estimated using our new KLgPC scheme with $\bar{r}_{red} = 3$ (full space) and a polynomial order $p = 3$ ($s = 20$) is plotted in figure (5-7). The corresponding analytical solutions are also depicted in the same figures. Similar results for the state variables $x_2(t;\omega)$ and $x_3(t;\omega)$ using the KLgPC scheme are shown in figures (5-8) and (5-9) respectively. From these results, it is observed that the new KLgPC scheme accurately models the three-dimensional non-autonomous system with additive forcing. Note that it is possible to integrate the system using a reduced space KLgPC scheme, for e.g., using $\bar{r}_{red} = 2$. For this case, the results would be accurate if the singular values of dynamics matrices A and B decay rapidly and the dynamics are represented adequately using only the first two singular values (when the third singular value is sufficiently small). We study examples using reduced space KLgPC and DO schemes in chapter 6. For comparison of numerical results, the stochastic mean and variance of the state variables state variables $x_1(t;\omega)$, $x_2(t;\omega)$ and $x_3(t;\omega)$ estimated using the new MTDgPC scheme with polynomial order $p = 3$ ($s = 20$), along with their corresponding analytical solution, are plotted in figures (5-10), (5-11) and (5-12) respectively. It is observed that the new MTDgPC scheme also models the uncertainty with reasonable accuracy.

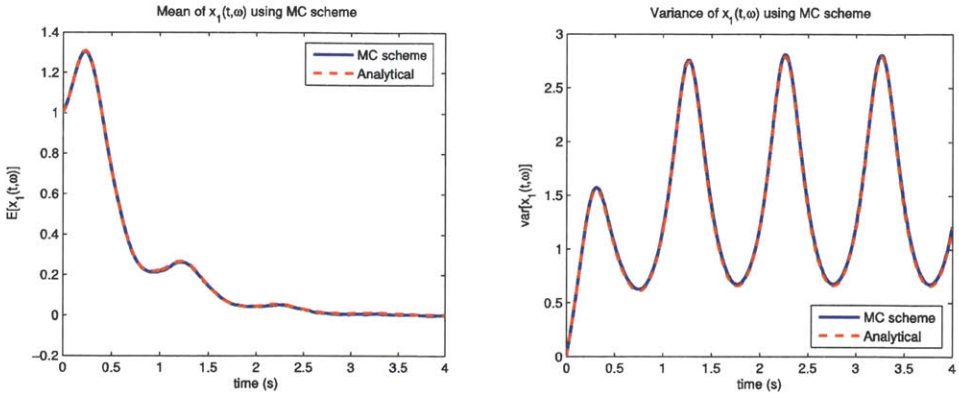

Figure 5-6: Mean and variance of $x_1(t;\omega)$ for the three-dimensional non-autonomous system with additive noise using the MC scheme

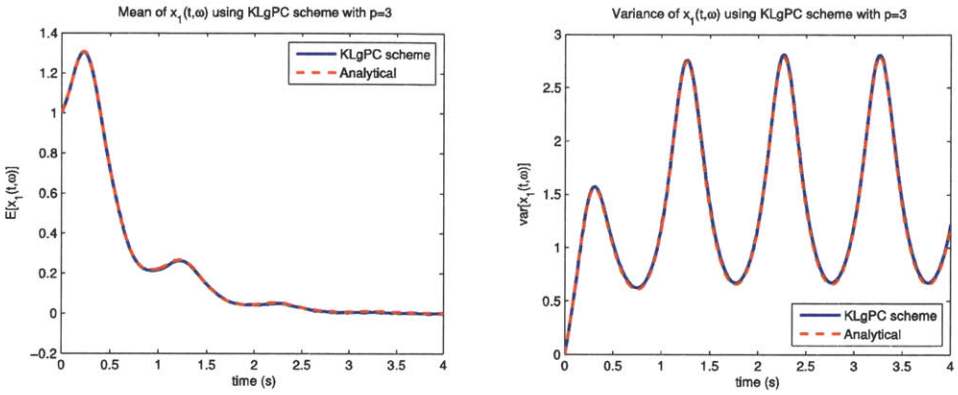

Figure 5-7: Mean and variance of $x_1(t;\omega)$ for the three-dimensional non-autonomous system with additive noise using the new KLgPC scheme with $\bar{r}_{red} = 3$ and $p = 3$

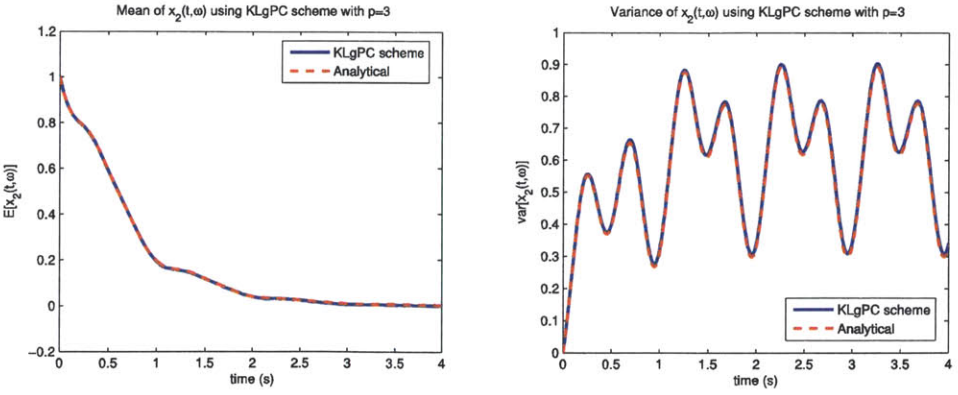

Figure 5-8: Mean and variance of $x_2(t;\omega)$ for the three-dimensional non-autonomous system with additive noise using the new KLgPC scheme with $\bar{r}_{red} = 3$ and $p = 3$

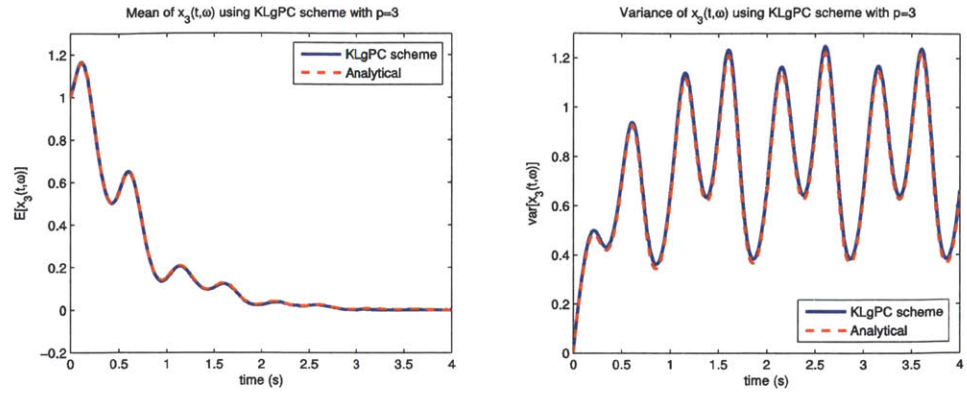

Figure 5-9: Mean and variance of $x_3(t;\omega)$ for the three-dimensional non-autonomous system with additive noise using the new KLgPC scheme with $\bar{r}_{red} = 3$ and $p = 3$

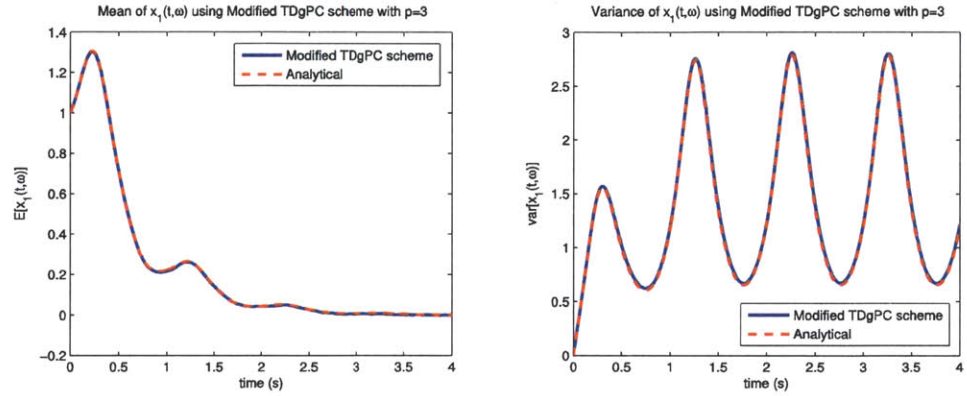

Figure 5-10: Mean and variance of $x_1(t;\omega)$ for the three-dimensional non-autonomous system with additive noise using the new MTDgPC scheme with $p = 3$

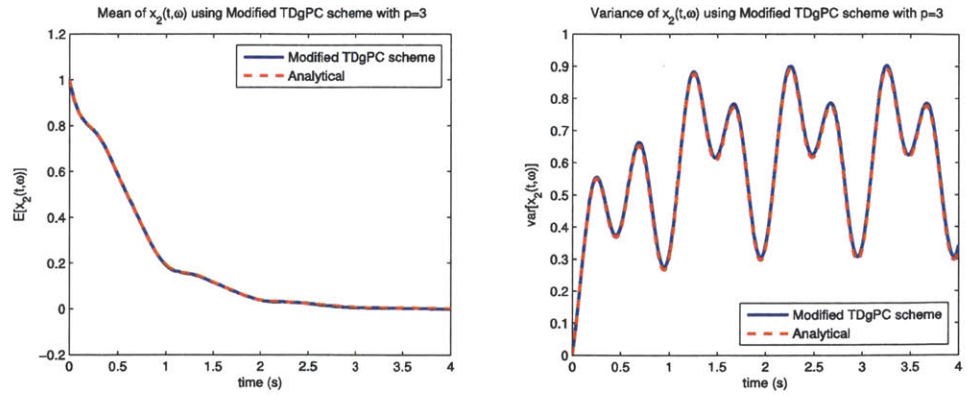

Figure 5-11: Mean and variance of $x_2(t;\omega)$ for the three-dimensional non-autonomous system with additive noise using the new MTDgPC scheme with $p = 3$

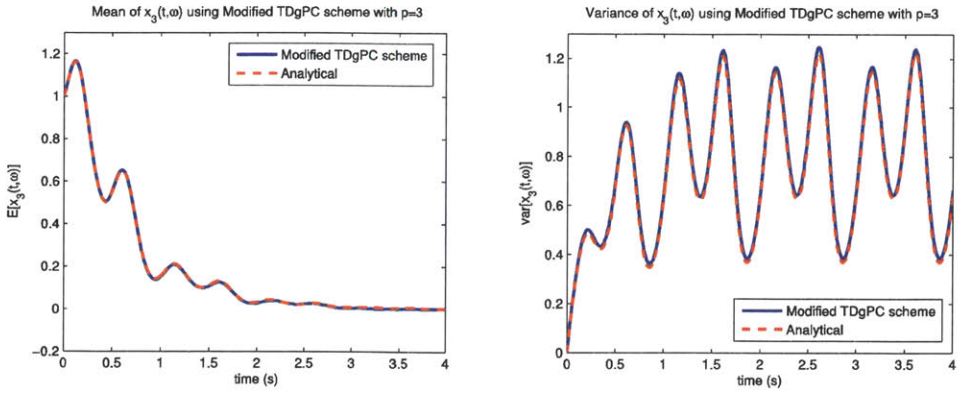

Figure 5-12: Mean and variance of $x_3(t;\omega)$ for the three-dimensional non-autonomous system with additive noise using the new MTDgPC scheme with $p = 3$

Finally, we consider the application of the new KLgPC and MTDgPC schemes for modeling uncertainty due to multiplicative noise. To do so, we consider a four-dimensional autonomous system with a four-dimensional driving Wiener process multiplying dynamical variables via the matrix B. Specifically, the governing equation for this system is again (1.1), where the dynamics matrices A and B are given by

$$A = \begin{bmatrix} \frac{-3}{20} & \frac{1}{20} & \frac{1}{20} & \frac{1}{20} \\ \frac{1}{20} & \frac{-3}{20} & \frac{1}{20} & \frac{1}{20} \\ \frac{1}{20} & \frac{1}{20} & \frac{-3}{20} & \frac{1}{20} \\ \frac{1}{20} & \frac{1}{20} & \frac{1}{20} & \frac{-3}{20} \end{bmatrix} \qquad B = \begin{bmatrix} \frac{1}{5}x_1 & \frac{1}{100}x_2 & \frac{1}{100}x_3 & \frac{1}{100}x_4 \\ \frac{1}{100}x_1 & \frac{1}{5}x_2 & \frac{1}{100}x_3 & \frac{1}{100}x_4 \\ \frac{1}{100}x_1 & \frac{1}{100}x_2 & \frac{1}{5}x_3 & \frac{1}{100}x_4 \\ \frac{1}{100}x_1 & \frac{1}{100}x_2 & \frac{1}{100}x_3 & \frac{1}{5}x_4 \end{bmatrix} \tag{5.6}$$

We use a deterministic initial condition, which is represented as

$$\begin{bmatrix} x_1(0,\omega) \\ x_2(0,\omega) \\ x_3(0,\omega) \\ x_4(0,\omega) \end{bmatrix} = \begin{bmatrix} 1.0 \\ 1.0 \\ 1.0 \\ 1.0 \end{bmatrix} \tag{5.7}$$

We consider the time domain $t \in [0, 3]$ and use a time step of $\Delta t = 0.01$. The stochastic mean and variance of the state variable $x_1(t;\omega)$ estimted using the MC scheme with 5×10^4 sample realizations and using the DO scheme with $s = 4$ (full space) are shown in figures (5-13) and (5-14) respectively. For comparison, the corresponding analytical solutions are

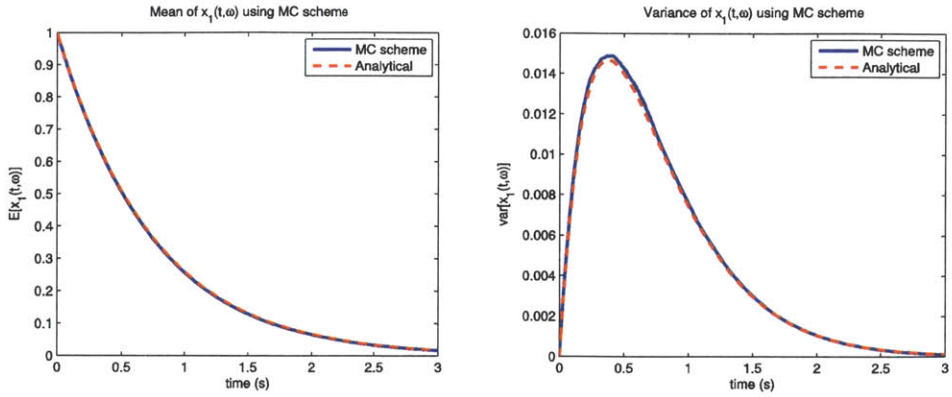

Figure 5-13: Mean and variance of $x_1(t;\omega)$ for four-dimensional autonomous system with multiplicative noise using the MC scheme

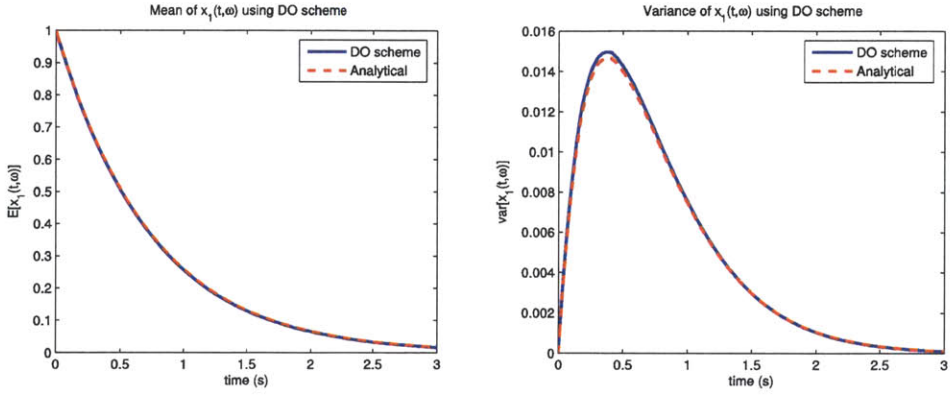

Figure 5-14: Mean and variance of $x_1(t;\omega)$ for four-dimensional autonomous system with multiplicative noise using the DO scheme

also depicted in the same figures. The same results using KLgPC scheme with $\bar{r}_{red} = 4$ (full space) and $p = 3$ ($s = 35$), and using new MTDgPC scheme with $p = 3$ ($s = 35$), along with the corresponding analytical solutions, are plotted in figures (5-15) and (5-16) respectively. It is observed that both the KLgPC and new MTDgPC schemes are able to integrate uncertainty due to multiplicative noise with sufficiently good accuracy.

From the examples discussed in this section, it can be concluded that the new MTDgPC and KLgPC schemes can accurately integrate dynamical systems with external stochastic forcing of additive as well as multiplicative nature over long time intervals. However, as discussed later in section 5.3, the new MTDgPC scheme utilizes the entire physical space for its implementation and hence its computational cost is largely dependent on the dimensionality of the state space. Thus, the new MTDgPC scheme is useful

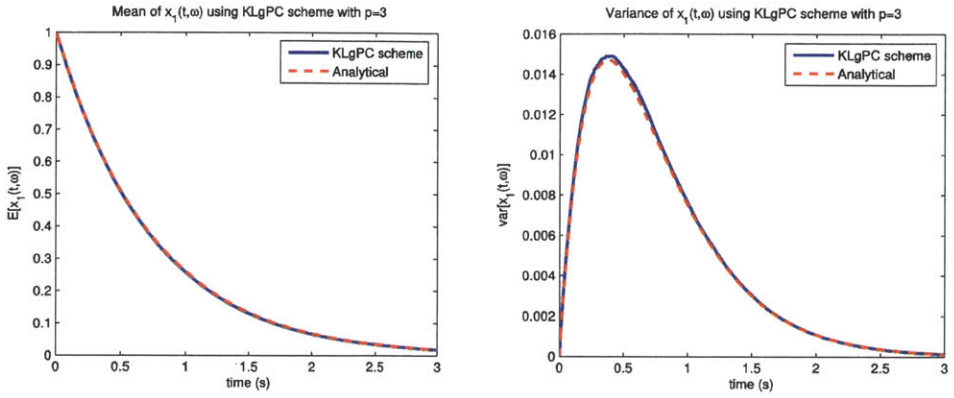

Figure 5-15: Mean and variance of $x_1(t;\omega)$ for four-dimensional autonomous system with multiplicative noise using the new KLgPC scheme with $\bar{r}_{red} = 4$ and $p = 3$

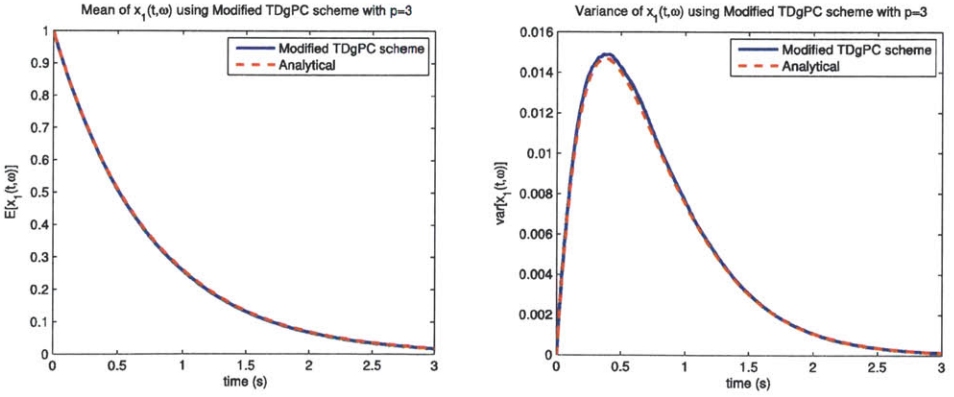

Figure 5-16: Mean and variance of $x_1(t;\omega)$ for four-dimensional autonomous system with multiplicative noise using the new MTDgPC scheme with $p = 3$

for modeling relatively small physical systems, but loses its effectiveness when used for modeling large dimensional systems. The KLgPC scheme, on the other hand, is implemented on an adaptive (time-dependent) reduced space and is computationally effective in integrating uncertainty in large-dimensional nonlinear systems and over long time intervals. Of course, this will work when the systems actually concentrate most of their stochastic energy in a time-dependent subspace. If this is not the case, the whole state space needs to be retained and the KLgPC scheme becomes similar to the MTDgPC scheme.

5.3 Discussion on Performance of Uncertainty Quantification Schemes

We now investigate the efficiency of the UQ schemes in integrating uncertainty due to external stochastic forcing. Specifically, we discuss the schemes in terms of accuracy of solution and computational cost.

As in section 4.4, it is again observed that the solution field obtained using the DO scheme implemented over the full space is exactly identical to the solution field obtained using Monte Carlo simulations. Thus, even for dynamical systems with stochastic noise, the full space DO scheme with the DO coefficients integrated with an MC scheme is equivalent to the MC scheme.

We illustrated in section 5.1 that all existing PC schemes known to us, including the gPC and TDgPC schemes, have an inherent limitation in integrating effects of stochastic noise over long time intervals. We also showed that our new MTDgPC and KLgPC schemes, were capable of integrating dynamical systems with external stochastic forcing of additive as well as multiplicative nature with reasonable accuracy. Next, we discuss the applicability of these new schemes in integrating uncertainty in realistic ocean systems.

The run times for the various examples studied in this chapter using different UQ schemes are presented in table (5.1). It is observed that for the examples shown here, the run times for the test cases with additive noise using the DO scheme are significantly smaller than those of the other schemes. However, in the current framework of implemen-

Table 5.1: Run times for UQ schemes for integrating uncertainty due to external stochastic forcing

S. No.	Test Case	MC	Modified TDgPC ($p = 3$)	KLgPC ($p = 3$) (full space)	DO (full space)
1.	3-D Autonomous System with additive noise Equations (5.1), (5.2)	631.50s	15764.36s ($s = 20$)	19378.66s ($s = 20$)	131.41s ($s = 3$)
2.	3-D Non-autonomous System with additive noise Equations (5.5), (5.2)	613.62s	16435.68s ($s = 20$)	19719.64s ($s = 20$)	137.00s ($s = 3$)
3.	4-D Autonomous System with multiplicative noise Equations (4.7), (4.9)	176.07s	11097.10s ($s = 35$)	14746.56s ($s = 35$)	401.50s ($s = 4$)

tation, the run time for modeling multiplicative noise using the DO scheme is considerably higher than the run time for modeling additive noise, which is not the case with other schemes. It is also seen that the run times for the new gPC schemes are comparable. From the given examples, it appears that the computational cost of our MTDgPC scheme is slightly lower than that of our KLgPC scheme implemented over full space. However, unlike the KLgPC scheme, the MTDgPC scheme cannot be implemented on a reduced subspace. This is because at every re-initialization step of the MTDgPC scheme, the number of random variables ($\bar{r}$) is set to be equal to the size of the physical space (N). Hence, the stochastic dimension of the system in the new MTDgPC scheme is always equal to the dimensionality of the full physical space, i.e., $\bar{r} = N$. Therefore, for high dimensional realistic ocean models where N is large, the computational cost of the MTDgPC scheme would be much higher than that of the reduced space KLgPC scheme. Thus, we anticipate that in comparison to our MTDgPC scheme, our reduced space KLgPC scheme will be much more efficient for integrating realistic ocean systems with external stochastic forcing.

Chapter 6

Uncertainty Prediction for Stochastic Ocean Systems

This chapter focuses on uncertainty prediction schemes that can be used for stochastic models of realistic ocean systems. We first study the application of the DO and the new KLgPC schemes on a stochastic dynamical system that concentrates most of its probability measure in a time-dependent subspace. The system considered is a self-engineered 20-dimensional non-autonomous stochastic dynamical system. Its time integration is used as a test case for the reduced space DO and KLgPC schemes, and the two schemes are analyzed in terms of their solution accuracy and computational efficiency. Next, we employ our computationally efficient stochastic solver to integrate the probability density function and moments of stochastic shallow-water ocean surface waves. We begin with a brief introduction of general surface waves and study a few differential equation models used to describe their dynamical evolution. Then, we focus on shallow water surface waves of limited amplitudes, governed by the weakly nonlinear Korteweg-de Vries (KdV) equation with stochastic forcing. Such stochastic forcing can model the statistics of waves that force the real system but are not solely represented by the deterministic KdV equation. We obtain numerical solutions of the stochastic KdV equation using the DO scheme and study the corresponding probability density function and uncertainty characteristics. The chapter ends with a brief discussion on the application of reduced space DO scheme for the integration of models of real ocean systems that include stochastic forcing.

6.1 A Self-Engineered 20-Dimensional Test Case

In the previous chapter, it was seen that amongst all uncertainty quantification schemes which use the polynomial chaos framework, the KLgPC scheme is most suited for modeling high dimensional realistic nonlinear ocean systems. Here, we utilize the reduced space DO and KLgPC schemes to integrate a stochastically forced 20-dimensional self-engineered test case. The test case is constructed in such a way that it has similar characteristics to that of a realistic nonlinear ocean model which has been observed to concentrate stochastic energy in a reduced subspace of the full state space (for e.g., see the work of Lermusiaux (2006)).

The self-engineered stochastic dynamical system is still within the class of systems governed by (1.1), with the dynamics matrices A and B now constructed using eigenvalue and singular value decompositions, respectively. The system is a 20-dimensional system with an 8-dimensional driving Wiener process. The eigenvalues of matrix A are presented in figure (6-1). The eigenvalue spectrum chosen aims to mimic the observed red-spectrum of ocean variability, i.e., the largest and smallest eigenvalues decay a bit faster than the other eigenvalues (we note that these properties are often more pronounced in real ocean systems and the decays are faster). In the test case (as in the real ocean), the positive eigenvalues represent growing characteristics of the system whereas the negative eigenvalues represent decaying characteristics. We use trigonometric sine and cosine functions as the corresponding eigenvectors. The first six eigenvectors of matrix A are shown in figure (6-1).

Similarly, the singular values of matrix B are plotted in figure (6-2). We use Legendre polynomials as the left singular vectors and $\hat{\mathbf{e}}_{\mathbf{k}}, 1 \leq k \leq 8$ (defined by equation (3.22)) as the right singular vectors. The first six left singular vectors of matrix B are depicted in figure (6-2).

The dynamics of the system are made time-dependent by varying the largest 5 eigenvalues of matrix A in time, using trigonometric cosine functions to represent their time evolution. Eigenvalues which are positive initially become negative at a later time and vice-a-versa. Thus, eigenvectors that grow initially start decaying later, resulting in other eigenvectors becoming dominant at a later time.

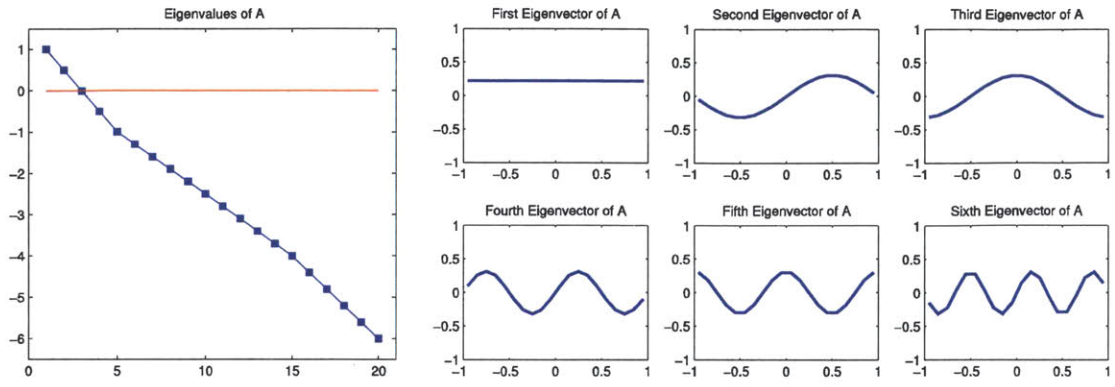

Figure 6-1: (a) Eigenvalues of matrix A for the 20-dimensional self-engineered test case (b) First six eigenvectors of matrix A for the 20-dimensional self-engineered test case

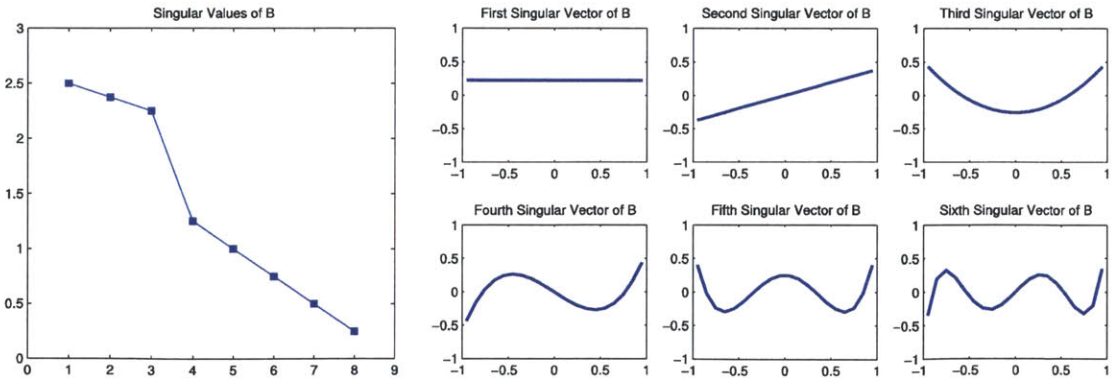

Figure 6-2: (a) Singular values of matrix B for the 20-dimensional self-engineered test case (b) First six left singular vectors of matrix B for the 20-dimensional self-engineered test case

We consider the time domain $t \in [0, 4]$ and use a time step of $\Delta t = 0.01$. The initial uncertainty is set to zero (deterministic initial condition) and the initial condition is represented as

$$\begin{bmatrix} x_1(0,\omega) \\ x_2(0,\omega) \\ \vdots \\ x_{20}(0,\omega) \end{bmatrix} = \begin{bmatrix} 1.0 \\ 1.0 \\ \vdots \\ 1.0 \end{bmatrix} \tag{6.1}$$

The stochastic mean of the entire 20-dimensional system using Monte Carlo simulations with 2×10^4 sample realizations is shown in figure (6-3). It is observed that the mean values of all the state variables follow the exact same dynamics. This is because the initial conditions project only on the first eigenvector of $A(t)$ at $t = 0$. Since in our test case the mean equation is $\frac{d\bar{x}}{dt} = A\bar{x}$, at all times, the mean will remain orthogonal to the other eigenvectors and in the direction of the state space that corresponds to that constant first eigenvector of A. Hence, all of the elements of the mean should remain equal for all times if they are equal initially. The variance of the system state estimated using the MC scheme is plotted in figure (6-4). Unlike the mean, the variances of different state variables exhibit dissimilar dynamics. This is because the variance is driven by the sustained stochastic forcing $B(X(t;\omega), t)\, dW(t;\omega)$ which is not a square matrix (it is a 20×8 matrix) and is not orthogonal to the eigenvectors of A.

To obtain more information about the system state, the MC solution is decoupled into deterministic modes and corresponding stochastic coefficients (similar to the DO scheme), using singular value decomposition (SVD) of the ensemble spread matrix (as in ESSE scheme). The singular vectors (modes) are arranged in order of decreasing variance. The variances of the first six as estimated with the MC scheme are shown in figure (6-5). By construction, the magnitude of the variances decreases significantly from the first mode to the second, from the second mode to the third, and so on. For instance, at $t = 4s$, the first mode captures around 61.8 percent of the total variance, the first two modes together capture around 92.4 percent of the total variance and the first four modes together capture around 99.2 percent of the total variance of the system. To further illustrate the dynamics of the decoupled system, a comparison of the time-evolution of

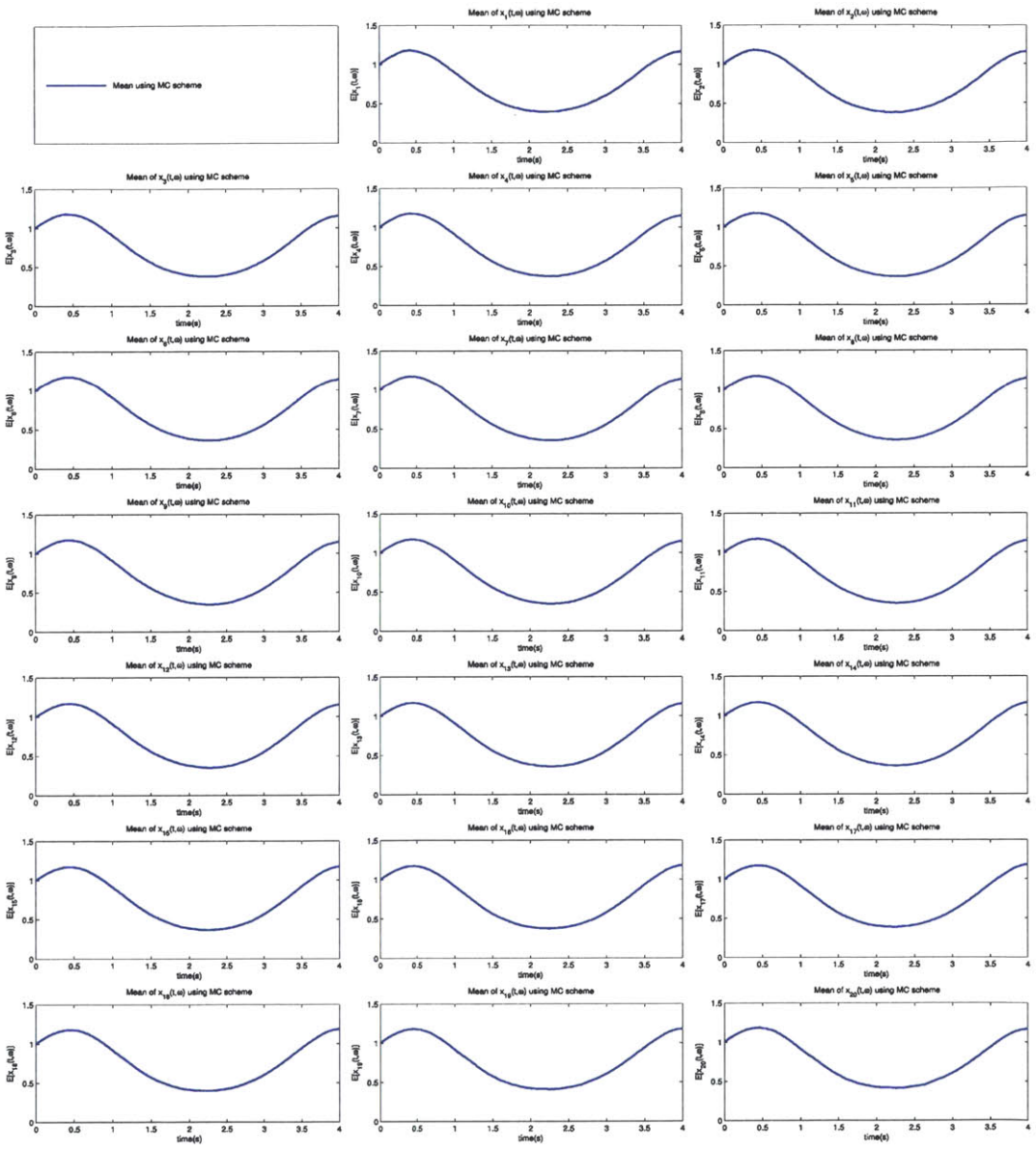

Figure 6-3: Mean of solution field $x(t;\omega)$ for the 20-dimensional self-engineered test case using the MC scheme

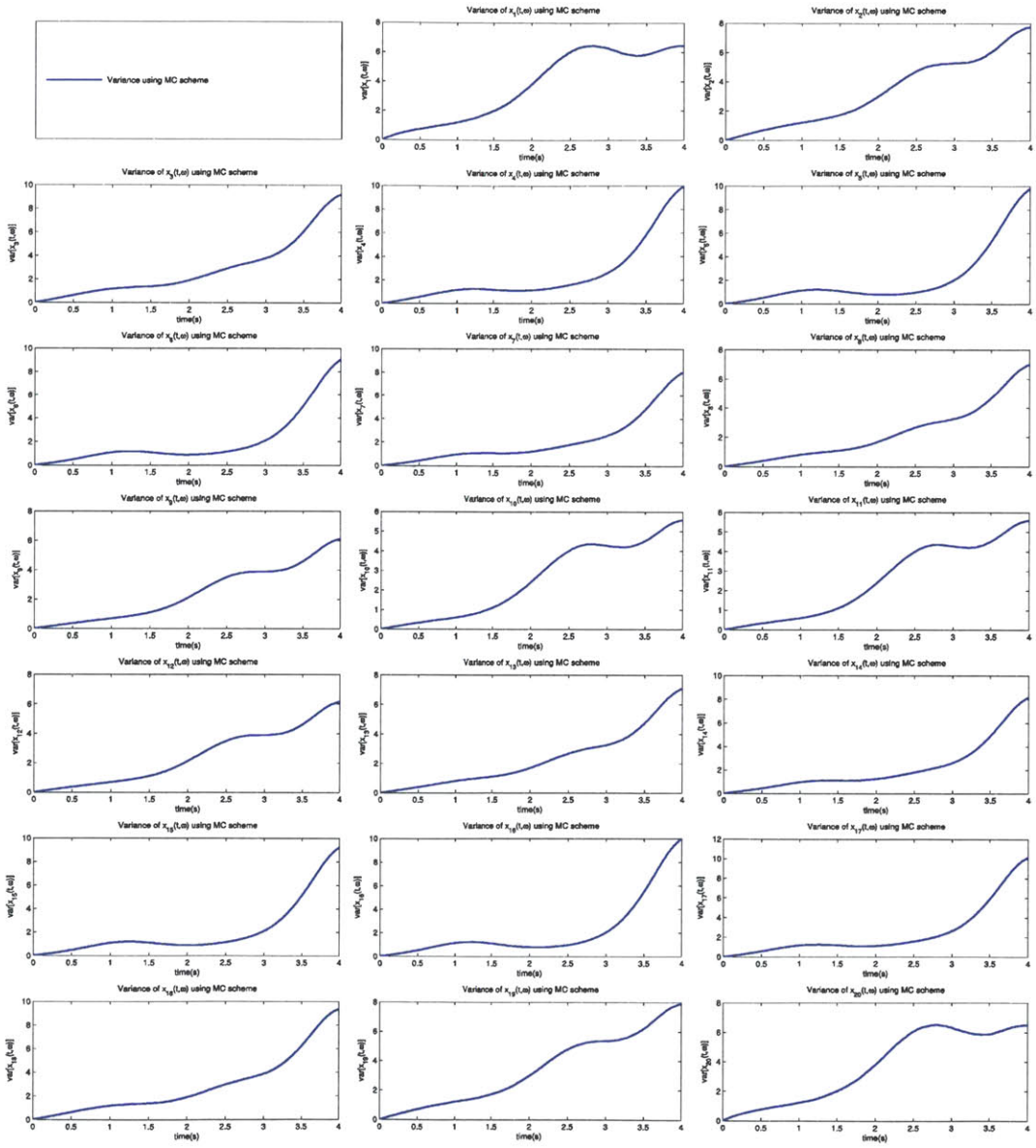

Figure 6-4: Variance of solution field $x(t;\omega)$ for the 20-dimensional self-engineered test case using the MC scheme

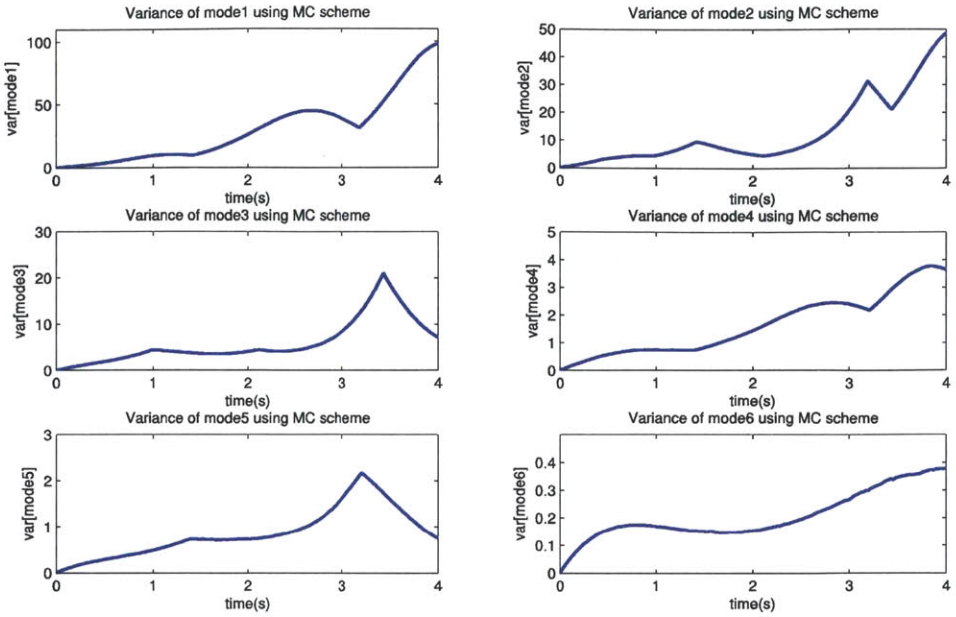

Figure 6-5: Variance of first six modes for the 20-dimensional self-engineered test case using the MC scheme

the variances of the first six singular vectors is shown in figure (6-6). We find that the evolution of eigenvalues of matrix A causes the dynamics of the decoupled system state to change in time. As the system is evolved, the variances of the modes change relative to each other, causing the modes to interchange their relative positions at certain time instances. For example, at around $t = 1.43s$, the first and second modes interchange their positions. Similarly, at around $t = 2.20s$, the second and third modes interchange their positions. The time evolution of the first three deterministic modes is depicted in figure (6-7). The interchange of relative positions of the modes is seen very clearly in this figure. In what follows, the MC solution is assumed to be the true solution.

Next, we model the self-engineered test case using the DO scheme with $s = 6$. The stochastic mean and variance of the entire system is presented in figures (6-8) and (6-9) respectively. For comparison, the corresponding MC solutions are also plotted in the same figures. From these figures, we find that the DO scheme with $s = 6$ time-integrates the mean and variance with reasonable accuracy.

The variances of the first six decoupled DO modes are shown in figure (6-10). We

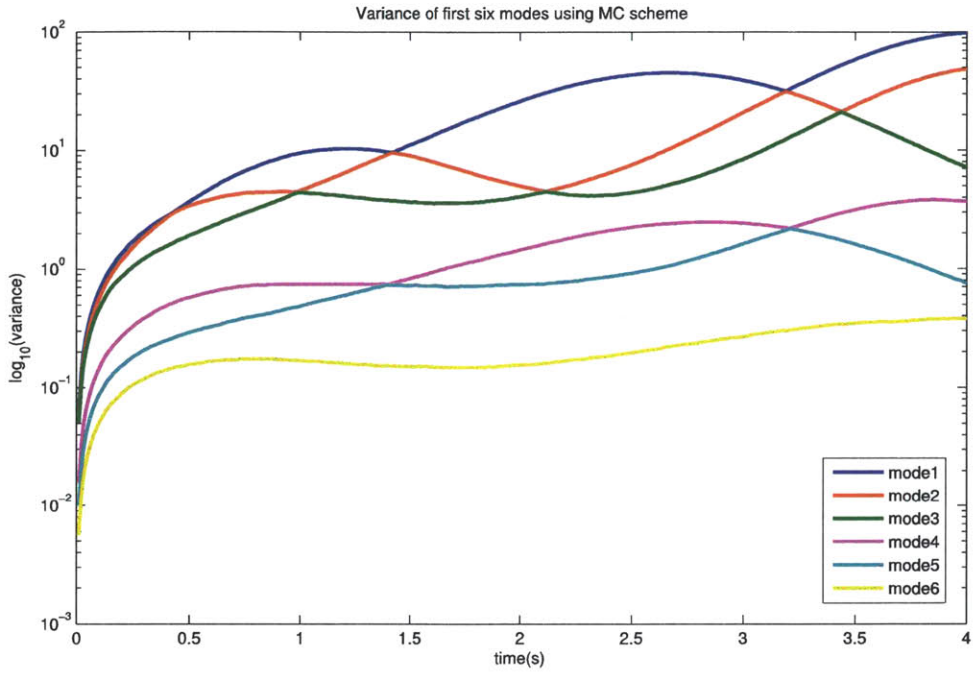

Figure 6-6: Comparison of variances of first six modes for the 20-dimensional self-engineered test case using the MC scheme

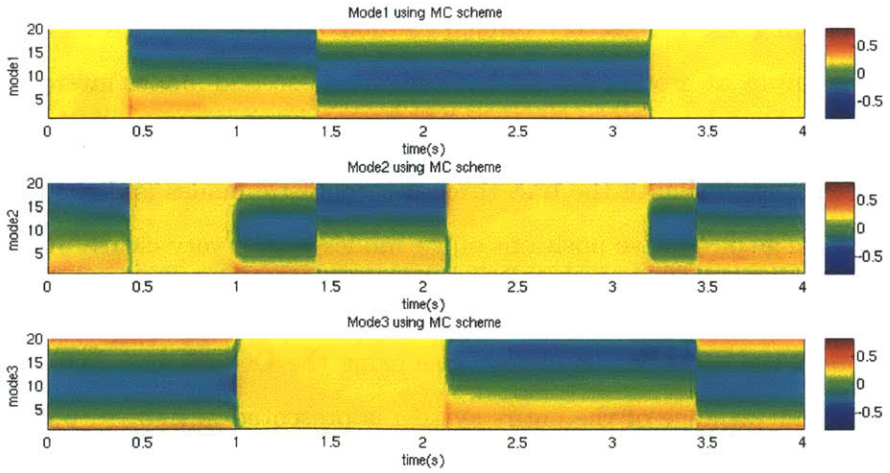

Figure 6-7: First three modes for the 20-dimensional self-engineered test case using the MC scheme

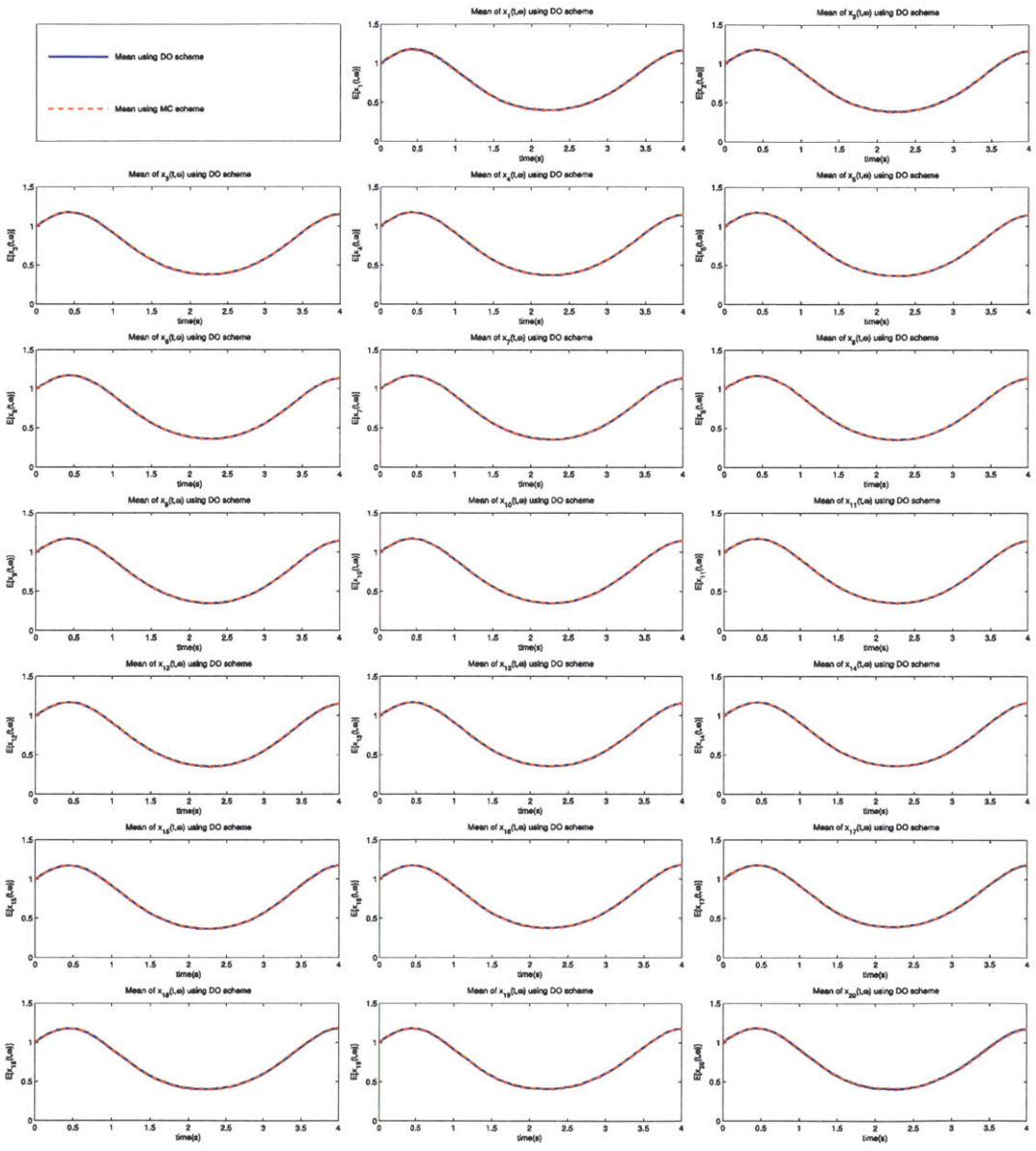

Figure 6-8: Mean of solution field $x(t;\omega)$ for the 20-dimensional self-engineered test case using the DO scheme with $s = 6$

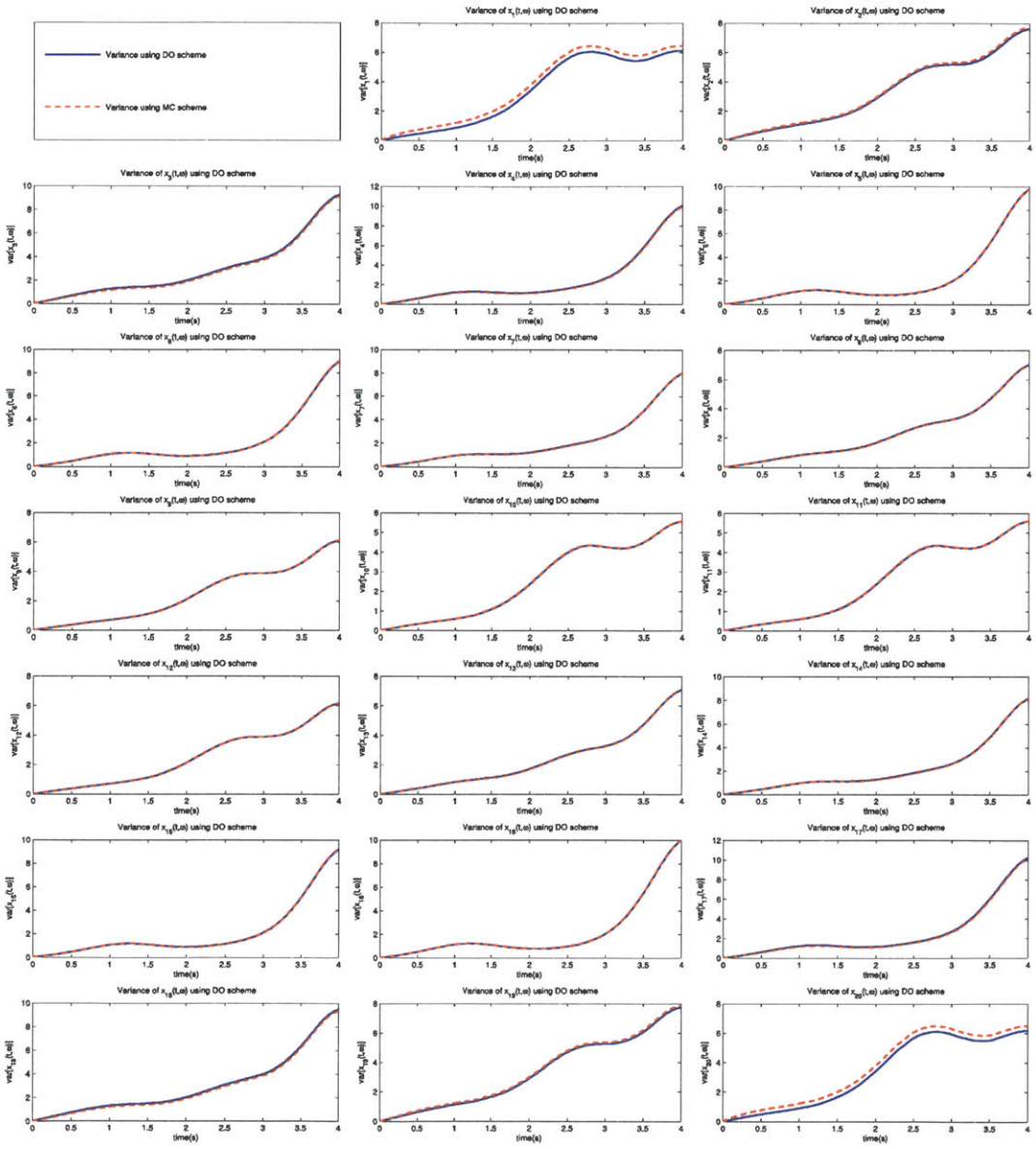

Figure 6-9: Variance of solution field $x(t;\omega)$ for the 20-dimensional self-engineered test case using the DO scheme with $s = 6$

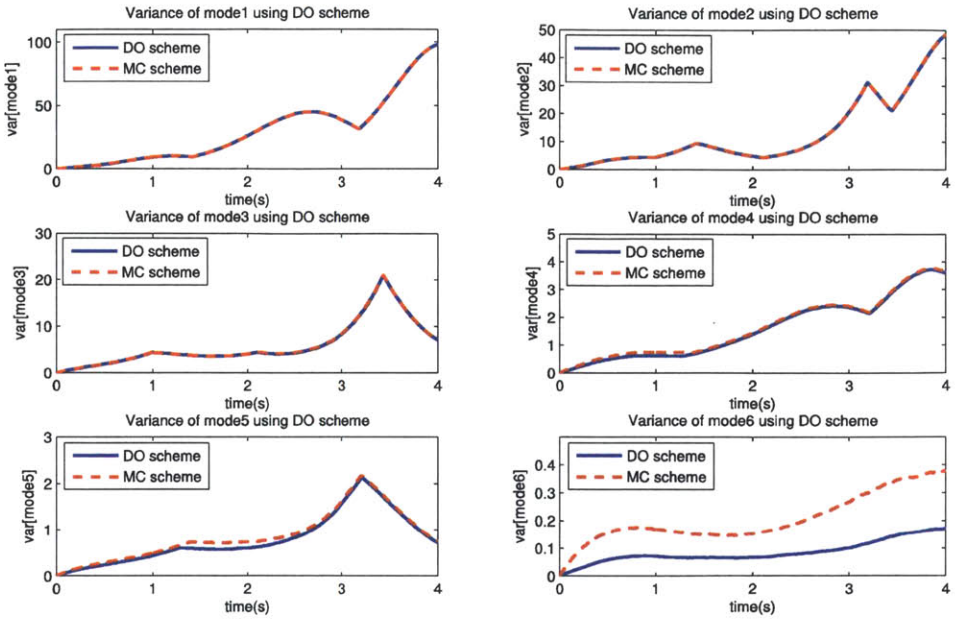

Figure 6-10: Variance of first six modes for the 20-dimensional self-engineered test case using the DO scheme with $s = 6$

find that the variances of the first three DO modes show an excellent agreement with the variances of the first three MC modes. The variance of the DO modes four and five are also very good, but that of the sixth DO mode does not show as good an agreement with the corresponding MC mode. However, the sixth and subsequent modes together account for only around 0.3 percent of the total variance of the system, and are hence not significant. The time evolution of the deterministic DO modes is illustrated in figure (6-11). The corresponding errors are also shown in the same figure. We find that apart from the short time intervals where there is a change in the relative positions of the modes, the errors are quite small in the entire time domain.

To improve the accuracy of the solution, we now model the self-engineered test case using the DO scheme with $s = 10$ modes. The corresponding stochastic mean and variance, along with the MC solutions, are plotted in figures (6-12) and (6-13) respectively. The variances of the first six decoupled DO modes are shown in figure (6-14) and the time evolution of the deterministic DO modes, along with the corresponding errors, is depicted in figure (6-15). From figures (6-12) and (6-13), we observe that the solution using the

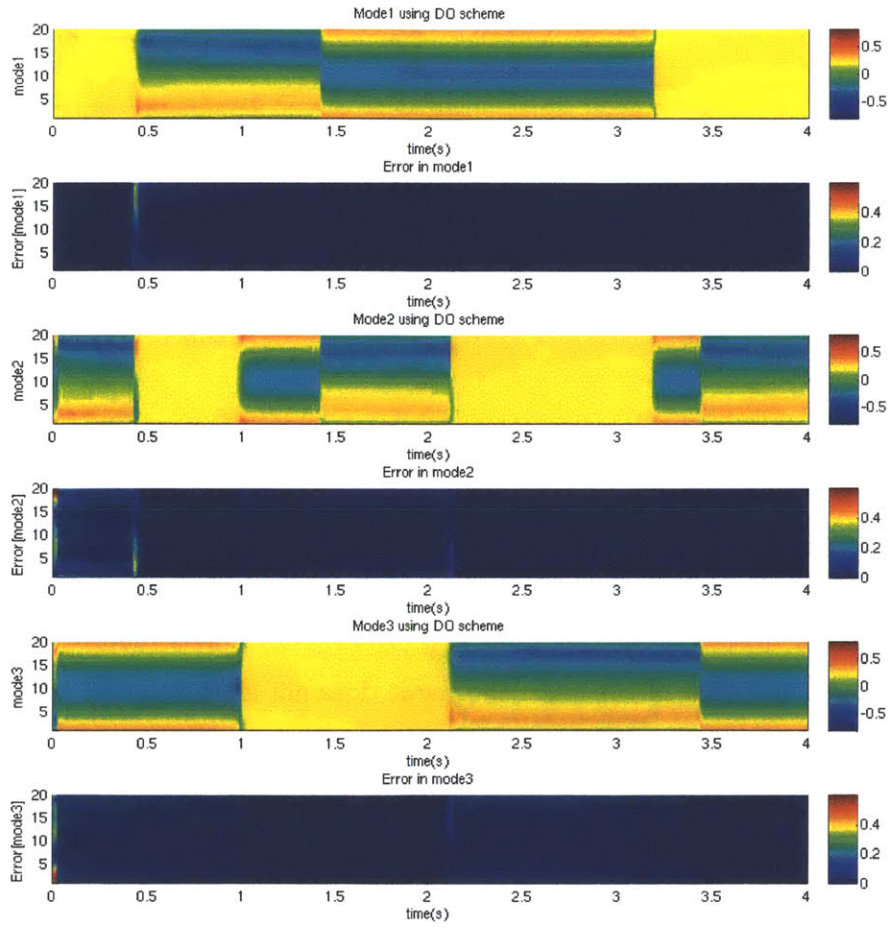

Figure 6-11: First three modes for the 20-dimensional self-engineered test case using the DO scheme with $s = 6$

DO scheme with $s = 10$ is reasonably accurate, which is as expected. Additionally, from figure (6-14), the variances of the first five DO modes show an excellent agreement with the first five MC modes. Thus, the DO scheme with $s = 10$ is able to capture as much as 99.7 percent of the total stochastic variance accurately. Moreover, from figure (6-15), we observe that for the DO scheme with $s = 10$, the errors in the evolution of the deterministic modes are extremely small over the entire time domain, including the time intervals where there is a change in the relative position of the modes. Thus, the DO scheme with $s = 10$ shows an observable improvement in accuracy compared to the DO scheme with $s = 6$.

Finally, we use our new KLgPC scheme to time integrate this dynamical test case. The KLgPC scheme is implemented on a reduced space of $\bar{r}_{red} = 6$ and using the polynomial order $p = 2$ ($s_{\text{red}} = 28$). The stochastic mean and variance of the solution field $X(t;\omega)$ using the KLgPC scheme, along with the MC solutions, is illustrated in figures (6-16) and (6-17) respectively. The comparison of the results of KLgPC and MC schemes shows that the KlgPC scheme is also accurate in modeling the evolution of uncertainty in the self-engineered test case.

To gain more insight into the KLgPC solution, it is also decoupled using SVD, similar to the DO scheme. The variances of the first six decoupled KLgPC modes are shown in figure (6-18). For comparison, the corresponding variances of the decoupled MC modes are also shown. We find that except for the sixth mode, the variances of the KLgPC modes show a good agreement with the corresponding variances of the MC modes. However, the accuracy of the KLgPC scheme in time integrating these variances is less than that of the DO scheme with $s = 10$. The time evolution of the deterministic modes for the KLgPC scheme is depicted in figure (6-19). The corresponding errors are also plotted in the same figure. It is seen that the errors in the evolution of the deterministic modes are small over the entire time domain, including the time intervals where there is a change in the relative position of the modes. Overall, for this test case, the KLgPC scheme with $\bar{r}_{red} = 6$ and $p = 2$ is more accurate than the DO scheme with $s = 6$, but slightly less accurate than the DO scheme with $s = 10$.

The run times for the different UQ schemes presented for this 20-dimensional self-

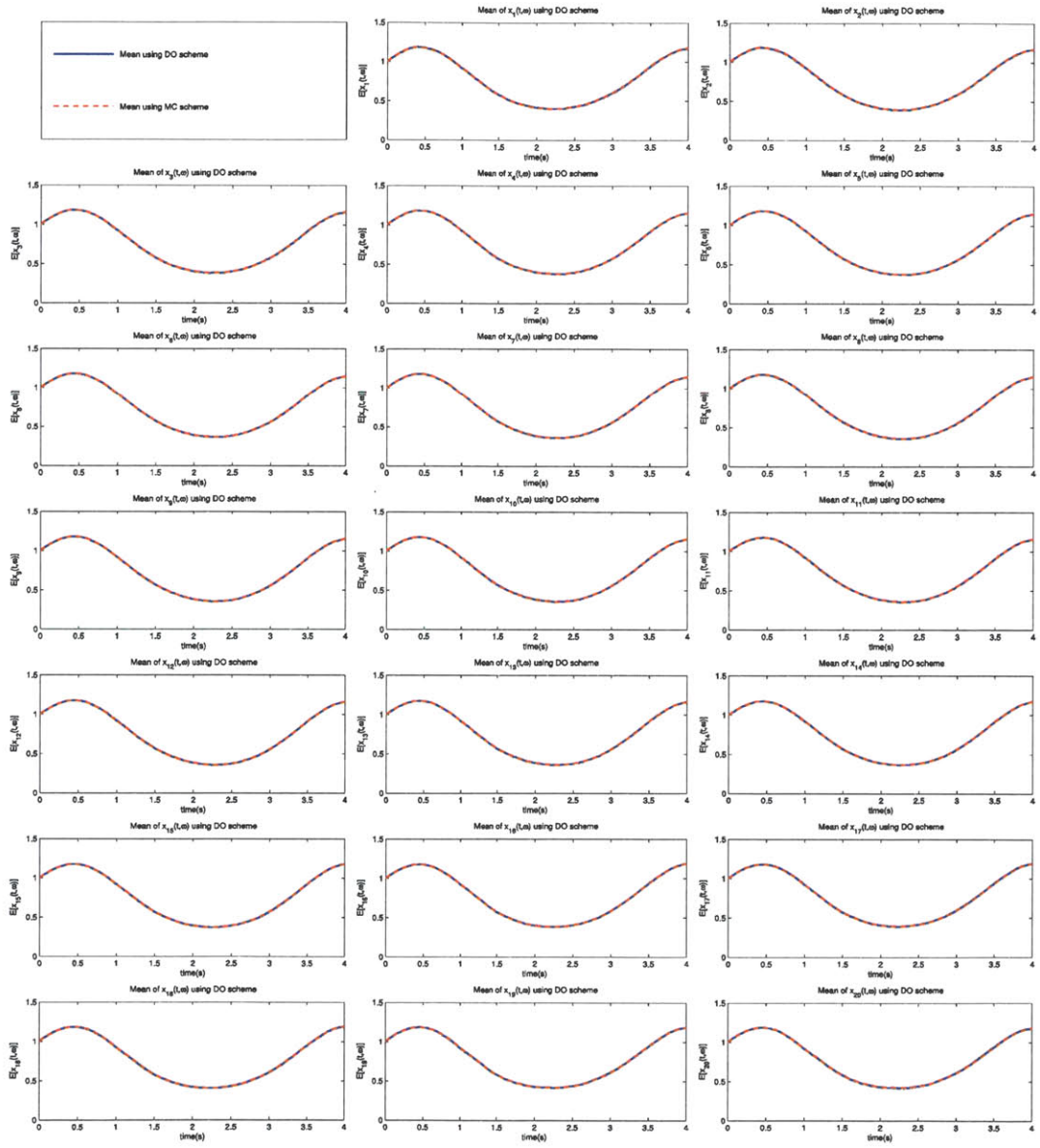

Figure 6-12: Mean of solution field $x(t;\omega)$ for the 20-dimensional self-engineered test case using the DO scheme with $s = 10$

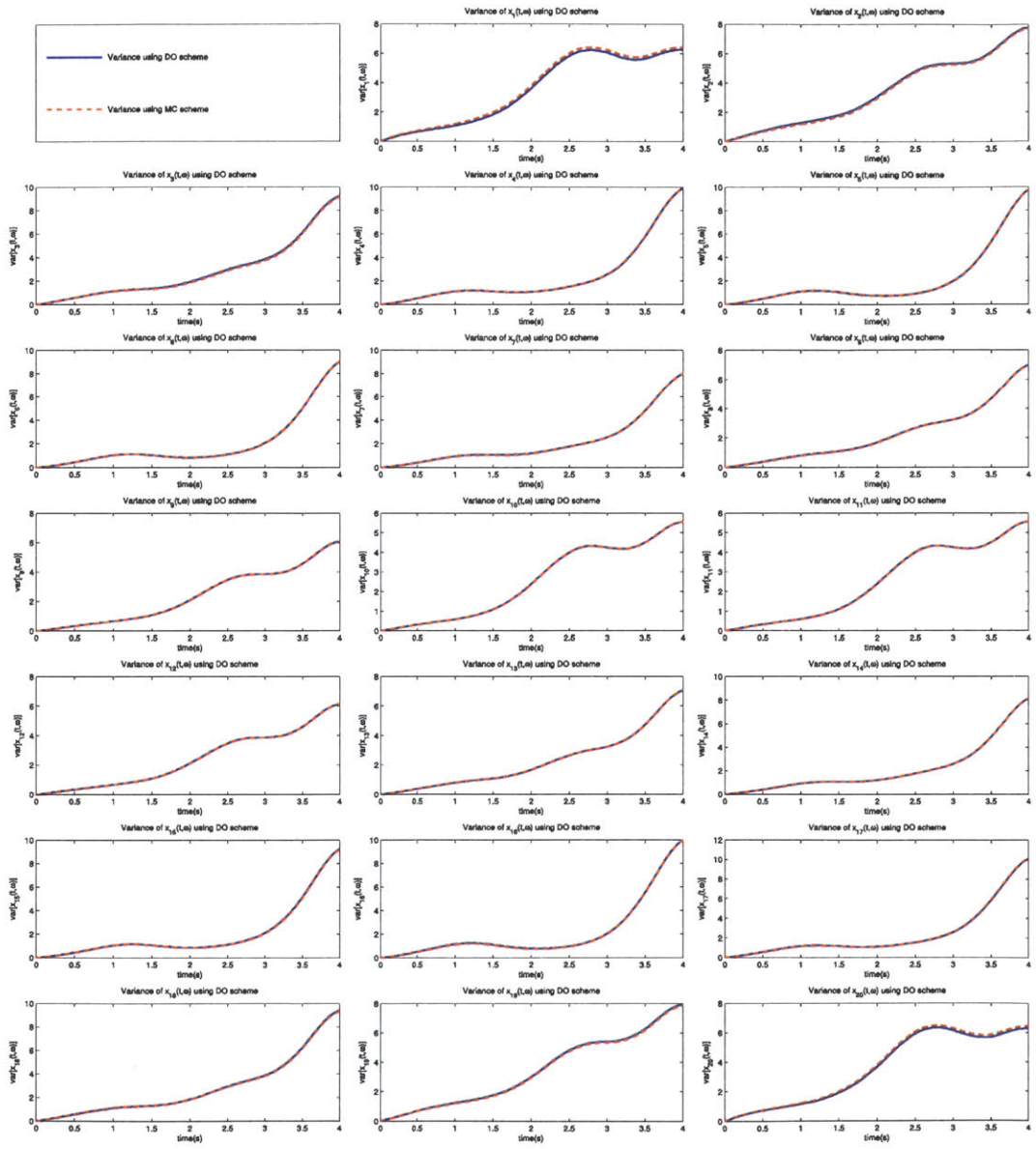

Figure 6-13: Variance of solution field $x(t;\omega)$ for the 20-dimensional self-engineered test case using the DO scheme with $s = 10$

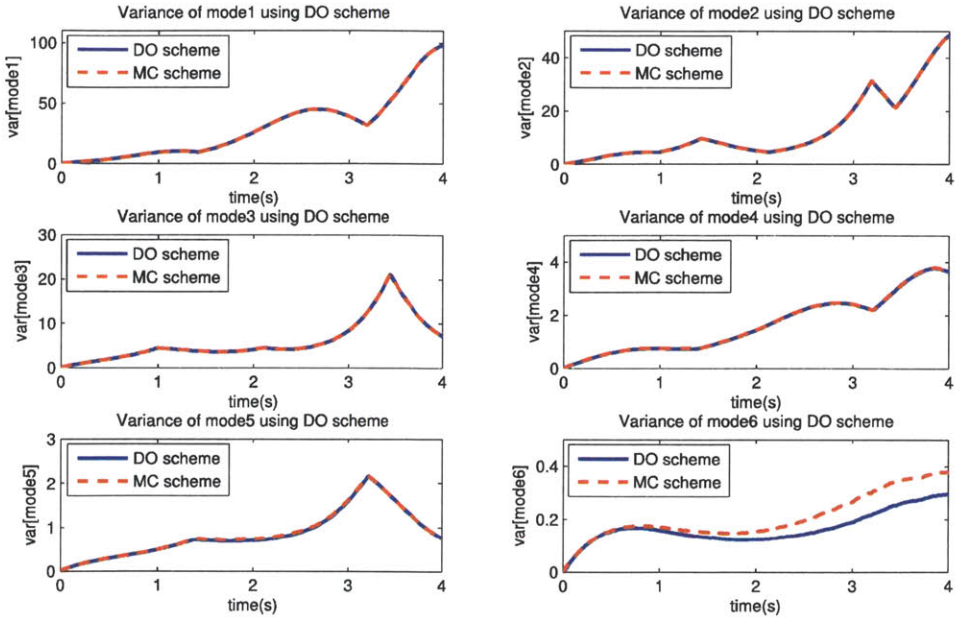

Figure 6-14: Variance of first six modes for the 20-dimensional self-engineered test case using the DO scheme with $s = 10$

engineered test case are given in table (6.1). We find that the run times for the DO scheme are significantly smaller than those of the KLgPC scheme. Even for the DO scheme with $s = 10$, which is found to be slightly more accurate than the KLgPC scheme with $\bar{r}_{red} = 6$ and $p = 2$, the run time is considerably smaller than that of the KLgPC scheme. Thus, for this stochastic test case, the DO scheme appears to be a more efficient choice. In conclusion, although the KLgPC scheme appears to be the best polynomial chaos scheme for the time-integration of uncertainty due to stochastic forcing in high dimensional stochastic systems over large time intervals, its relatively high computational cost (in comparison to the DO scheme) may prove to be a hindrance in its applicability to realistic ocean systems.

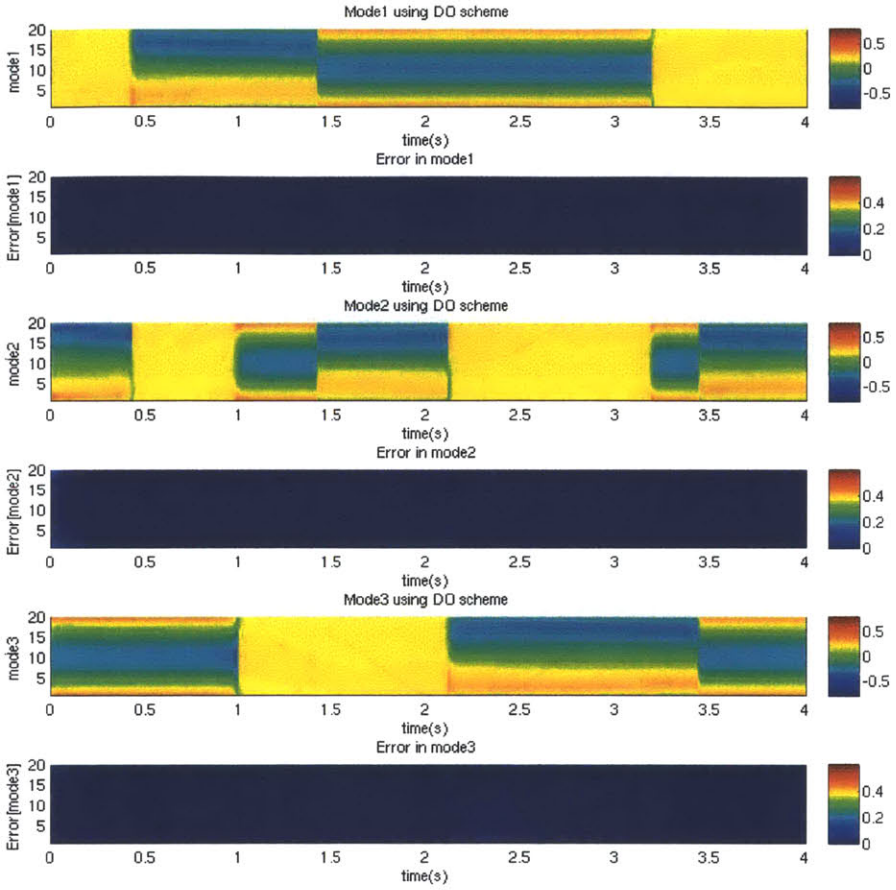

Figure 6-15: First three modes for the 20-dimensional self-engineered test case using the DO scheme with $s = 10$

Table 6.1: Run times for UQ schemes for time-integrating uncertainty in the 20-dimensional self-engineered test case

S. No.	**Uncertainty Quantification Scheme**	**Run Time**
1.	MC scheme	84.21s
2.	DO scheme with $s = 6$	75.18s
3.	DO scheme with $s = 8$	163.15s
4.	DO scheme with $s = 10$	221.31s
5.	KLgPC scheme with $\bar{r}_{red} = 6$ and $p = 2$	5271.66s

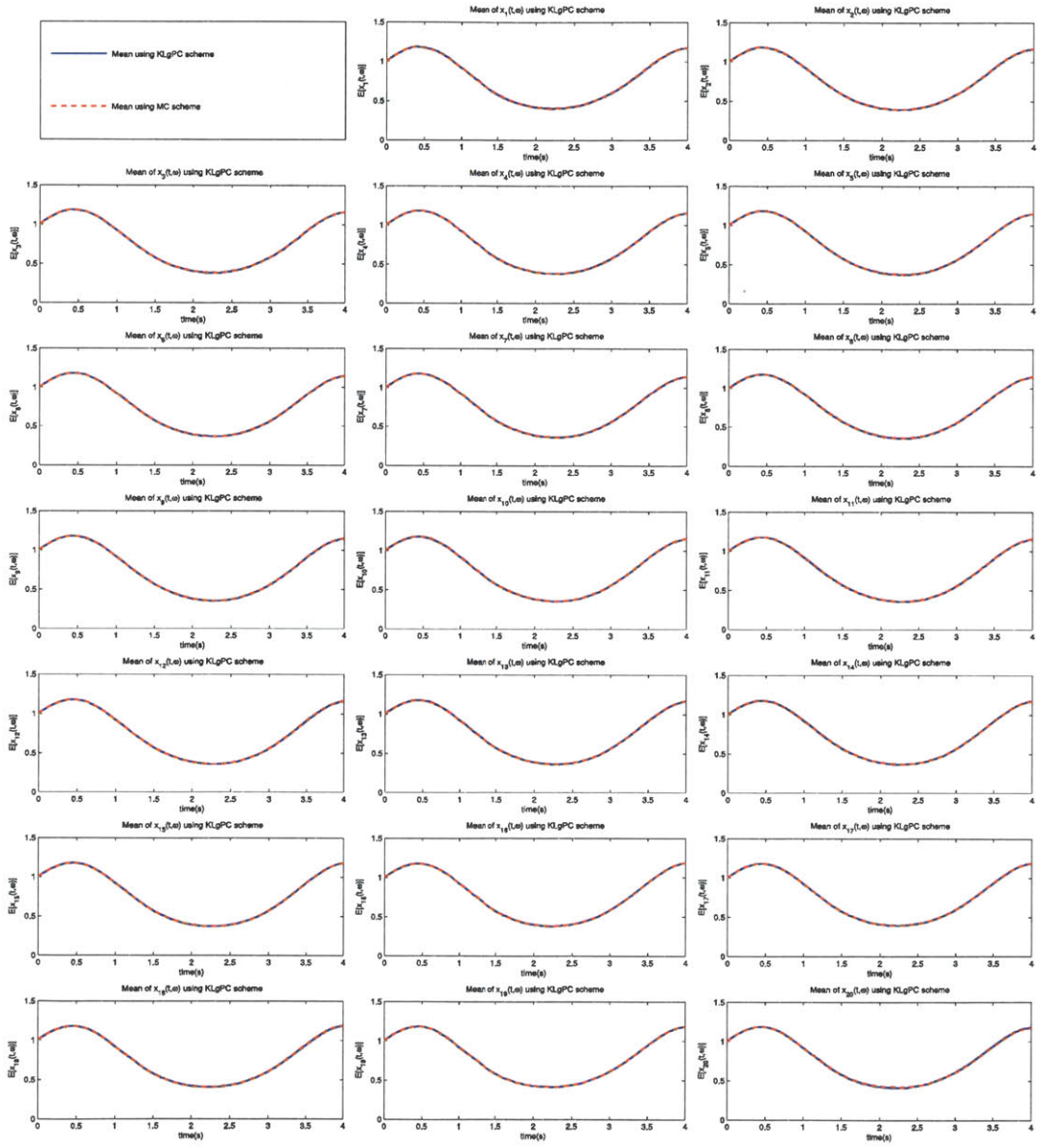

Figure 6-16: Mean of solution field $x(t;\omega)$ for the 20-dimensional self-engineered test case using the KLgPC scheme with $\bar{r}_{red} = 6$ and $p = 2$ ($s_{\text{red}} = 28$)

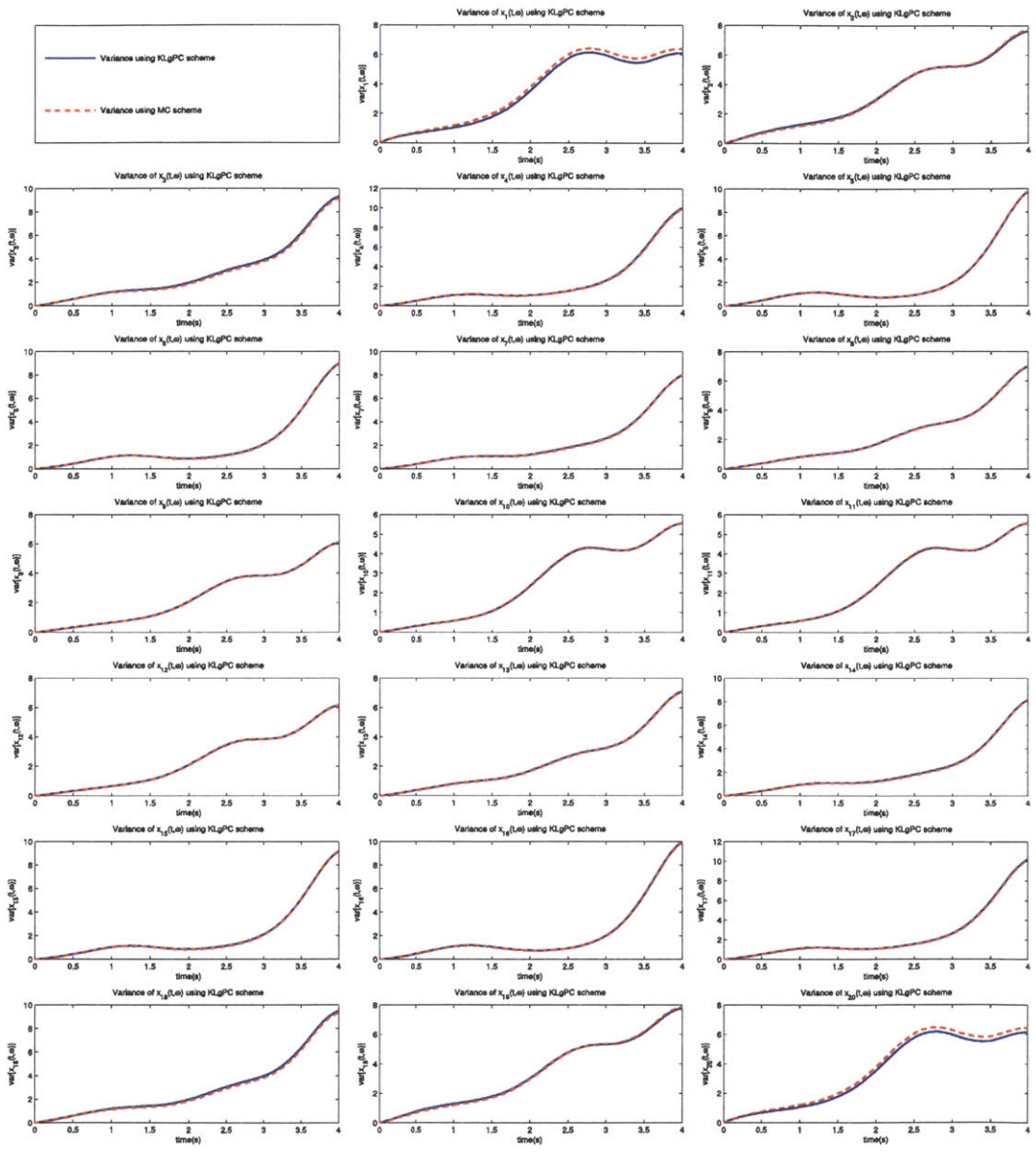

Figure 6-17: Variance of solution field $x(t;\omega)$ for the 20-dimensional self-engineered test case using the KLgPC scheme with $\bar{r}_{red} = 6$ and $p = 2$ ($s_{\text{red}} = 28$)

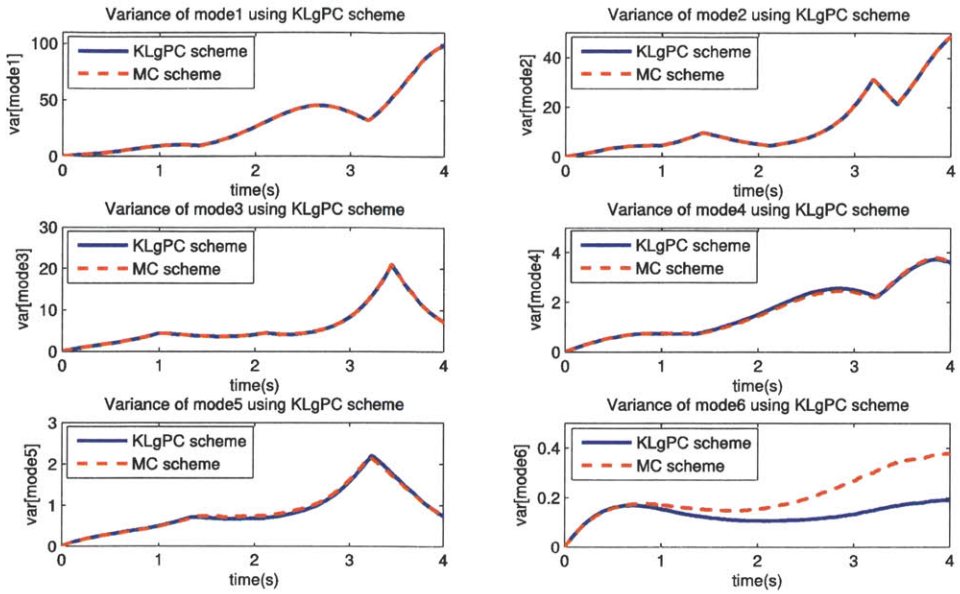

Figure 6-18: Variance of first six modes for the 20-dimensional self-engineered test case using the KLgPC scheme with $\bar{r}_{red} = 6$ and $p = 2$ ($s_{\text{red}} = 28$)

6.2 Modeling Uncertainty in Nonlinear Ocean Surface Waves

6.2.1 Introduction

Ocean surface waves are a well-known physical phenomenon and constitute an important section of ocean science. Although man has been intrigued by surface waves for a long period of time, it is only in the last 200 years, that he has been able to build a strong physical and mathematical foundation for understanding wave phenomenon. The most directly experienced and frequently occurring surface waves are the wind-driven waves, which are caused by the interaction of the wind with the ocean surface at the air-water interface. A less frequent but more catastrophic form of surface waves are the tsunamis, which are long-period oscillations caused by geologic effects such as earthquakes or landslides. Other examples of surface waves include those caused by human activity (motion of ships, explosions etc.) and marine biology.

In the present work, we focus our attention on wind-driven surface waves, that occur

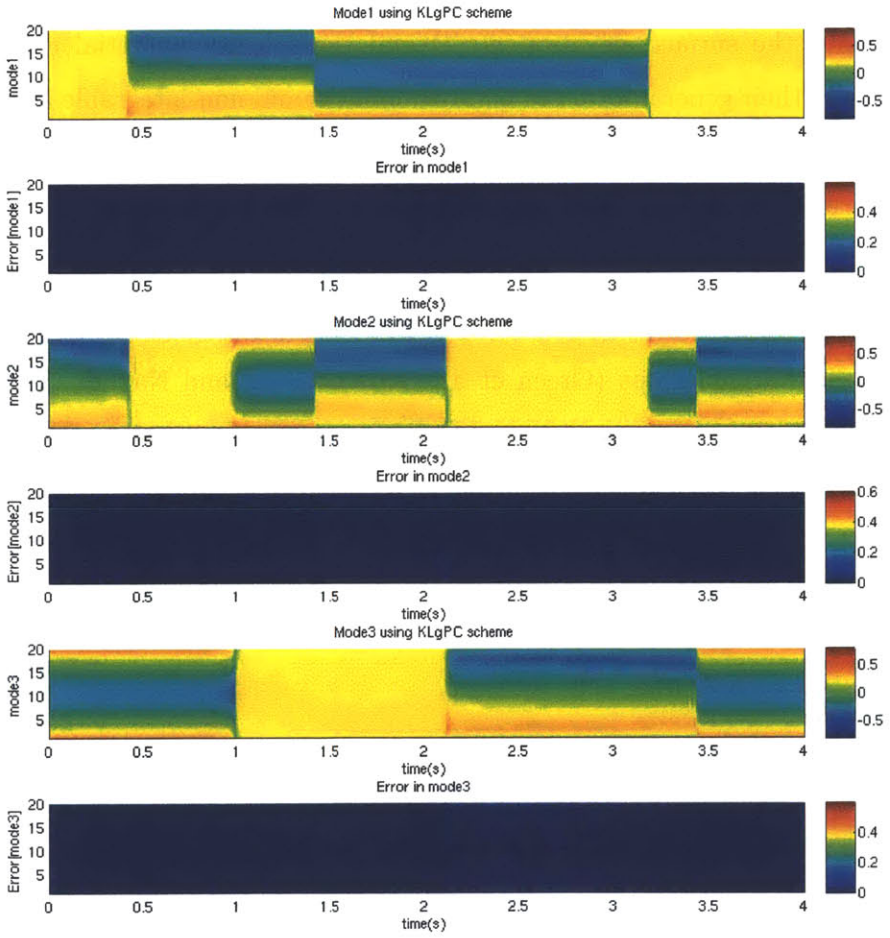

Figure 6-19: First three modes for the 20-dimensional self-engineered test case using the KLgPC scheme with $\bar{r}_{red} = 6$ and $p = 2$ ($s_{\text{red}} = 28$)

on the free surface of large water bodies (such as oceans, lakes and rivers) due to the action of the wind. Since gravity is the main restoring force in these waves, they are often referred to as wind-driven surface gravity waves. Under the assumption of irrotational and inviscid fluid flow, the governing equations of motion for these waves are the coupled and highly nonlinear Euler equations (which are derived from the Navier-Stokes equations). These equations typically involve coupled partial differential equations for two unknown variables, namely, the surface elevation $\eta(r,t)$ and the velocity potential $\phi(r,t)$. The Euler equations in their general form are highly nonlinear and non-integrable analytically. In view of their mathematical complexity, several lower order approximations to model wind-driven surface waves have been proposed over the last few decades. These models have been derived by making further simplifying assumptions on the Euler equations, by considering special cases where certain terms in the equations dominate over others.

The Green-Naghdi equations (Green et al. (1974), Green and Naghdi (1976)), also known as the Su-Gardner equations (Su and Gardner, 1969), are derived under the additional assumption that the wavelength of the surface wave (λ) is much greater than the water depth (h), i.e., $\epsilon \equiv h/\lambda \ll 1$. This assumption is typically used for studying waves in shallow water. The one-dimensional Green-Naghdi equations are given as

$$\begin{aligned} &\eta_t + [(h+\eta)u]_x = 0 \\ &u_t + uu_x + g\eta_x = \frac{1}{3(h+\eta)}[(h+\eta)^3(u_{xt} + uu_{xx} - u_x^2)]_x \end{aligned} \tag{6.2}$$

where $\eta(x,t)$ is the surface elevation and $u(x,t)$ is the depth-mean velocity field. The Green-Naghdi equations (6.2), as the Euler equations, are also highly nonlinear. If we additionally assume that the wave amplitude is much smaller than the water depth, we can simplify equation (6.2) further to obtain lower order approximations. Using the assumption that $\eta/h = O(\epsilon^2)$ and $u/(gh)^{1/2} = O(\epsilon^2)$, and dropping terms of order higher than $O(\epsilon^4)$, the Green-Naghdi equations reduce to the weakly nonlinear Boussinesq equations, which are given as

$$\begin{aligned} &\eta_t + [(h+\eta)u]_x = 0 \\ &u_t + uu_x + g\eta_x = \frac{h^2}{3}u_{xxt} \end{aligned} \tag{6.3}$$

The Boussinesq equations (6.3) represent waves of bi-directional nature and can be simplified further by assuming uni-directional waves, giving rise to the Korteweg-de Vries (KdV) equation (de Jager, 2006). The one-dimensional KdV equation is given as

$$\eta_t + c_0\eta_x + \frac{3c_0}{2h}\eta\eta_x + \frac{c_0h^2}{6}\eta_{xxx} = 0 \tag{6.4}$$

where $c_0 = \sqrt{gh}$.

The analytical solutions of many nonlinear wave equation models can be computed using a relatively new method of mathematical physics called the *inverse scattering transform* (IST), which is a generalization of the linear Fourier transform (see Osborne (2010) for details). For a given wave speed c, the analytical expression for the surface elevation $\eta(x,t)$ of a solitary wave for the Green-Naghdi equations (6.2) is given as

$$\eta(x,t)_{GN} = \frac{c^2 - c_0^2}{g}\text{sech}^2\frac{\sqrt{3(c^2-c_0^2)}(x-ct)}{2ch} \tag{6.5}$$

Similarly, the solitary wave solution for the KdV equation (6.4) is given as

$$\eta(x,t)_{KdV} = \frac{2h(c-c_0)}{c_0}\text{sech}^2\frac{\sqrt{3(c-c_0)}(x-ct)}{\sqrt{2c_0}h} \tag{6.6}$$

The relation between the speed of propagation c and the wave amplitude a is given as

$$c = c_0\left(1 + \frac{a}{2h}\right) \tag{6.7}$$

The analytical solution of the solitary wave for the Boussinesq equations (6.3) is not known (Li et al., 2004).

6.2.2 Korteweg-de Vries (KdV) Equation

A detailed historical account of the origin of the Korteweg-de Vries equation is provided by Miles (1981) and de Jager (2006). The motivation behind the development of this equation were the observations made by John Scott Russell in the Union Canal in 1834, and his subsequent experiments (Russell, 1844). He observed a round and smooth wave

moving at a constant speed in the canal without changing its form, a phenomenon which later came to be known as a solitary wave. Lord Rayleigh and Joseph Valentin Boussinesq independently developed mathematical theories to explain these observations (Rayleigh (1876), Boussinesq (1877)). The KdV equation is present implicitly in the work of Boussinesq (Boussinesq, 1872).

Diederik Johannes Korteweg was a student of J. D. van der Waals and received his doctoral degree from the University of Amsterdam in 1878. He appears to have believed that the mathematical theories of Rayleigh and Boussinesq did not properly resolve the long wave paradox (Ursell, 1953) between Russell's observations and the theory of shallow water waves proposed by George Bidell Airy (Airy, 1845). It was for this reason that he suggested this problem to his student Gustav de Vries. The first explicit appearance of the KdV equation is in the dissertation of de Vries (de Vries, 1894). Subsequently, the theory of Korteweg and de Vries was published in a paper in the Philosophical Magazine in 1895 (Korteweg and de Vries, 1895). Interest in solitary waves declined in the coming years, until the discovery of the *soliton* in 1965 (Zabusky and Kruskal, 1965). This lead to the development of inverse scattering theory (see Ablowitz and Segur (1981) for details), which was used for finding analytical solution of the KdV equation (Gardner et al., 1967), reviving academic interest in solitary waves.

The Korteweg-de Vries equation models the propagation of weakly nonlinear, weakly dispersive, incompressible, inviscid and irrotational water waves of long wavelength and small amplitude in shallow water. The physical form of the KdV equation is represented by equation (6.4). However, several other forms of the equation are also employed. Using the variable transformation $\sigma = \eta + 2h/3$, equation (6.4) reduces to the simplified form

$$\sigma_t + \frac{3c_0}{2h}\sigma\sigma_x + \frac{c_0h^2}{6}\sigma_{xxx} = 0 \tag{6.8}$$

Equation (6.8) can then be non-dimensionalized with the transformations $\zeta = 3\sigma/2h^3$ and $\tau = c_0h^2t/6$, leading to the non-dimensional form of the KdV equation, given as

$$\zeta_\tau + 6\zeta\zeta_x + \zeta_{xxx} = 0 \tag{6.9}$$

On the other hand, if we non-dimensionalize equation (6.8) using $\bar{\zeta} = 9\sigma/h^3$ and $\tau = c_0 h^2 t/6$, we get another form of non-dimensional KdV equation, represented as

$$\bar{\zeta}_\tau + \bar{\zeta}\bar{\zeta}_x + \bar{\zeta}_{xxx} = 0 \tag{6.10}$$

Finally, the sign of the nonlinear terms $6\zeta\zeta_x$ and $\bar{\zeta}\bar{\zeta}_x$ in (6.9) and (6.10) can be reversed by using a negative sign in the variable transformations of ζ and $\bar{\zeta}$ respectively.

The expression for the depth-averaged velocity field $u(x,t)$ for the KdV approximation can be obtained from conservation of mass for a homogeneous fluid, i.e., the first of the equations in (6.3), in conjunction with the KdV equation. To do so, we re-write this conservation of mass (continuity equation) as

$$\eta_t + [(h+\eta)u]_x = 0 \tag{6.11}$$

We also re-write the KdV equation (6.4) in conservative form, given as

$$\eta_t + \left[c_0\eta + \frac{3c_0}{4h}\eta^2 + \frac{c_0 h^2}{6}\eta_{xx}\right]_x = 0 \tag{6.12}$$

Comparing equations (6.11) and (6.12), we obtain

$$u = \frac{1}{h+\eta}\left[c_0\eta + \frac{3c_0}{4h}\eta^2 + \frac{c_0 h^2}{6}\eta_{xx}\right] \tag{6.13}$$

Since $\eta/h = O(\epsilon^2) \ll 1$, we can utilize a Taylor series expansion to approximate $1/(h+\eta)$. Neglecting $(\eta/h)^2$ and other higher order terms, the expression for $u(x,t)$ of equation (6.13) can be written as

$$\begin{aligned} u &\approx \frac{1}{h}\left(1 - \frac{\eta}{h}\right)\left[c_0\eta + \frac{3c_0}{4h}\eta^2 + \frac{c_0 h^2}{6}\eta_{xx}\right] \\ &= \frac{1}{h}\left[c_0\eta + \frac{3c_0}{4h}\eta^2 + \frac{c_0 h^2}{6}\eta_{xx} - \frac{c_0}{h}\eta^2 - \frac{3c_0}{4h^2}\eta^3 - \frac{c_0 h}{6}\eta\eta_{xx}\right] \end{aligned} \tag{6.14}$$

Neglecting terms of order higher than $O(\epsilon^4)$ and simplifying further, we obtain the final

expression for the depth-mean velocity field for the KdV approximation, given as

$$u = \frac{c_0}{h}\eta - \frac{c_0}{4h^2}\eta^2 + \frac{c_0 h}{6}\eta_{xx} \tag{6.15}$$

The classic KdV equations model the propagation of weakly nonlinear water waves of long wavelength and small amplitude in shallow water of constant depth. To extend their applicability to ocean waves with variable bathymetry, several modified KdV-like equations have been introduced in recent years. The class of generalized KdV-like differential equations with variable coefficients which model the propagation of ocean surface waves of small amplitude over shallow water of variable depth, is known as KdV-top equations (for more details, see the works of Van Groesen and Pudjaprasetya (1993), Dingemans (1997), Israwi (2009), Duruflé and Israwi (2012)). In what follows, we only consider the classic KdV equations, with constant bathymetry.

6.2.3 Deterministic KdV Equation: Solitary Wave Solutions

In this section, we numerically solve for and study the propagation of solitary waves using the non-dimensional form (6.9) of the one-dimensional KdV equation (6.4). As discussed earlier, a solitary wave is a smooth and rounded wave consisting of a single elevation, which propagates without a change in its form. The stability in form of a solitary wave is due to the balance between nonlinear steepening (mathematically represented by the term $6\zeta\zeta_x$) and dispersion (represented by the term ζ_{xxx}). The single soliton analytical solution of the non-dimensional KdV equation (6.9) is given by

$$\zeta(x,t) = 2\bar{\eta}^2 \mathrm{sech}^2\left[\bar{\eta}\left(x - x_0 - 4\bar{\eta}^2 t\right)\right] \tag{6.16}$$

where x_0 is the initial location of the soliton (at $t = 0$). Further, the amplitude of the solitary wave is $2\bar{\eta}^2$, its width is $1/\bar{\eta}$ and its velocity is $4\bar{\eta}^2$. Similarly, the two soliton solution of the non-dimensional KdV equation (6.9) is given as

$$\zeta(x,t) = \frac{8\left(\bar{\eta}_1^2 - \bar{\eta}_2^2\right)\left[\bar{\eta}_1^2 \cosh^2\theta_2 + \bar{\eta}_2^2 \sinh^2\theta_1\right]}{\left[\left(\bar{\eta}_1 - \bar{\eta}_2\right)\cosh\left(\theta_1 + \theta_2\right) + \left(\bar{\eta}_1 + \bar{\eta}_2\right)\cosh\left(\theta_1 - \theta_2\right)\right]^2} \tag{6.17}$$

where $\bar{\eta}_1 \geq \bar{\eta}_2$, and θ_1 and θ_2 are given by

$$\begin{aligned} \theta_1 &= \bar{\eta}_1 \left[x - x_1 - 4\bar{\eta}_1^2 t\right] \\ \theta_2 &= \bar{\eta}_2 \left[x - x_2 - 4\bar{\eta}_2^2 t\right] \end{aligned} \tag{6.18}$$

Here, for the first solitary wave, the amplitude is $2\bar{\eta}_1^2$, width is $1/\bar{\eta}_1$ and velocity is $4\bar{\eta}_1^2$, whereas for the second solitary wave, the amplitude is $2\bar{\eta}_2^2$, width is $1/\bar{\eta}_2$ and velocity is $4\bar{\eta}_2^2$. The initial locations of the two solitons are represented by x_1 and x_2 respectively.

First, we numerically solve for the 1-soliton solution of the non-dimensional KdV equation (6.9). We consider the spatial domain $x \in [-10, 20]$ and use a length scale of $\Delta x = 0.1$ for spatial discretization of the governing equation. Also, we utilize periodic boundary conditions for our numerical simulation. For time integration, we use the Zabusky-Kruskal (Z-K) numerical scheme (Zabusky and Kruskal (1965), Albowitz and Taha (1984)). The Z-K scheme is an explicit leapfrog finite difference scheme with second order convergence in space and time. The linear stability condition for the Z-K scheme has been derived by Vliegenthart (Vliegenthart, 1971) and is given as

$$\Delta t \leq \left[6\Delta x|\zeta(x,t)| + 4\left(\Delta x\right)^{-3}\right]^{-1} \tag{6.19}$$

Rose (2006) has shown that $\Delta t = \left(\Delta x\right)^3/4$ satisfies the stability condition (6.19). We consider the time domain $t \in [0, 10]$ and use a time step of $\Delta t = \left(\Delta x\right)^3/4 = 0.00025$. Herman and Knickerbocker (1993) have found that the numerical solution of the KdV equation using the Z-K scheme induces a numerical shift in the position of the solitary wave. They have proposed a correction in the velocity of the numerical KdV wave. The corrected velocity of the numerical solution is given by

$$v = \frac{dx_c}{dt} = 4\bar{\eta}^2 - \frac{4}{5}\bar{\eta}^4\left(\Delta x\right)^2 \tag{6.20}$$

The first term in equation (6.20) is the expression for the analytical velocity and the second term is a correction term due to truncation error. Our numerical solution is also adjusted to account for this truncation error.

For our example, we consider a solitary wave with $\bar{\eta} = 1.0$ and $x_0 = 0.0$. The 1-

soliton wave train for the domain $[-10, 20] \times [0, 10]$ using the Z-K numerical integration scheme with correction (6.20) is shown in figure (6-20). For comparison, the analytical 1-soliton wave train is plotted in figure (6-21). It is seen that the Z-K scheme is accurate in modeling the propagation of a single soliton. The physical form of the solitary wave at different time instances is depicted in figure (6-22). We observe that the solitary wave travels without a change in its form, which is as expected.

Next, we investigate the interaction of two solitons, still using the KdV equation (6.9). We consider the spatial domain $x \in [-10, 10]$ and as before use $\Delta x = 0.1$ for spatial discretization. We again use periodic boundary conditions for the physical domain. We consider the time domain $t \in [0, 2]$ and again choose a time step of $\Delta t = 0.00025$. We consider two solitons with $\bar{\eta}_1 = 1.2$, $\bar{\eta}_2 = 0.8$, $x_1 = -6.0$ and $x_2 = -2.0$. The numerical evolution of the 2-soliton wave train for the domain $[-10, 10] \times [0, 2]$ using the Z-K numerical integration scheme is shown in figure (6-23). For comparison, the analytical 2-soliton wave train is plotted in figure (6-24). It is found that the Z-K scheme is accurate in modeling the interaction of the two solitons. The physical form of the solution at different time instances is depicted in figure (6-25). It is observed that the solitons interact elastically, i.e., their amplitudes and physical forms are unchanged before and after the interaction. However, the interaction of two solitons induces a noticeable phase shift in their positions, as evident from the top view of the wave trains in figures (6-23) and (6-24).

6.2.4 Stochastic KdV Equation

In this section, we numerically solve for and study solutions of the Korteweg-de Vries (KdV) equation with external stochastic forcing. Starting again from the non-dimensional deterministic KdV equation (6.9), the governing equation of the resulting stochastic KdV system is then given as

$$\zeta_\tau + 6\zeta\zeta_x + \zeta_{xxx} = \epsilon\tilde{\eta}(t;\omega) \tag{6.21}$$

where $\tilde{\eta}(t;\omega)$ is stochastic noise (represented by one-dimensional Wiener process) with amplitude ϵ. For our example, we consider the spatial domain $x \in [-5, 10]$. We impose periodic boundary conditions for all simulations and consider the time domain $t \in [0, 1]$.

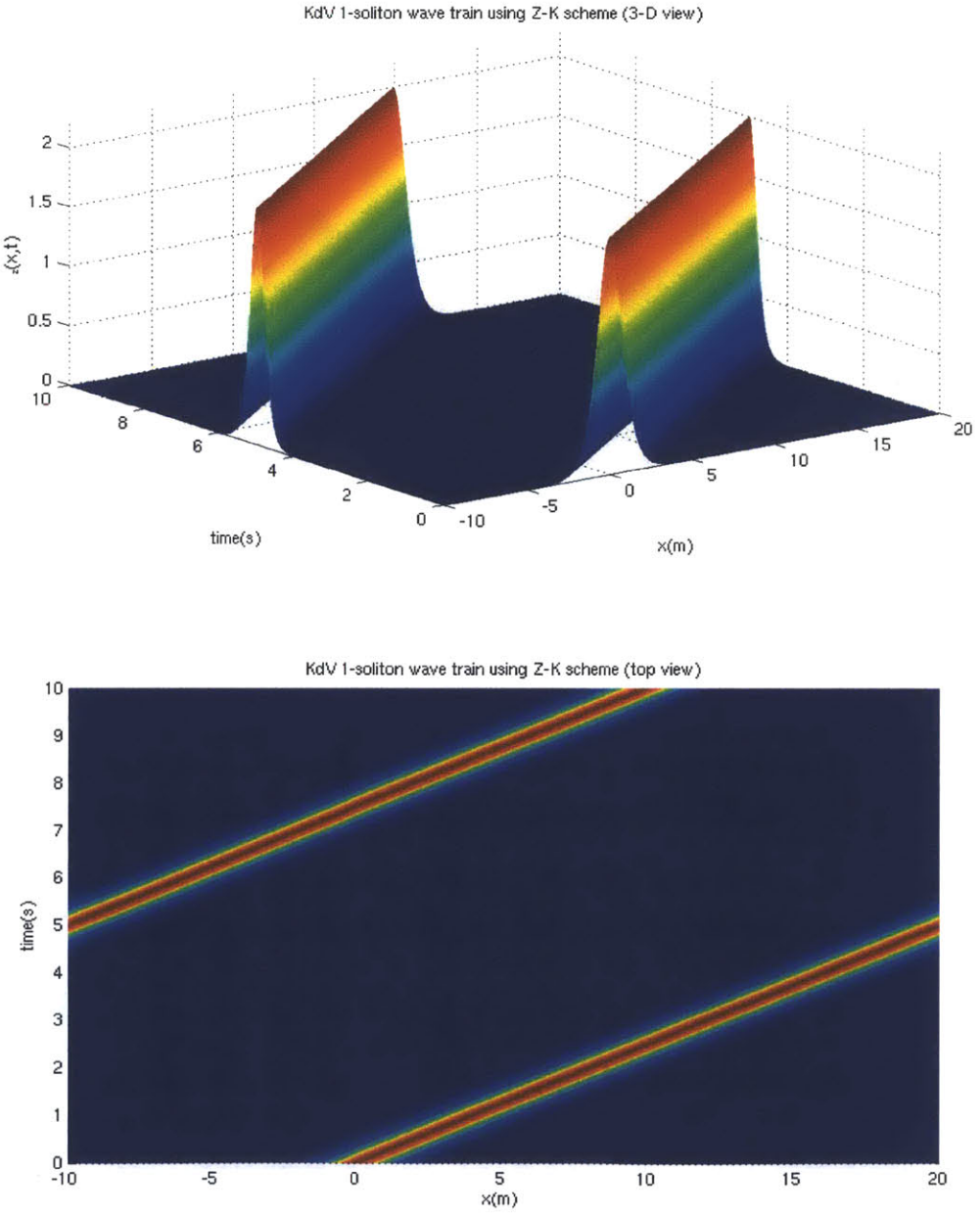

Figure 6-20: Numerical KdV 1-soliton wave train, computed using the Z-K scheme with the correction (6.20): (a) 3-D view (b) Top view

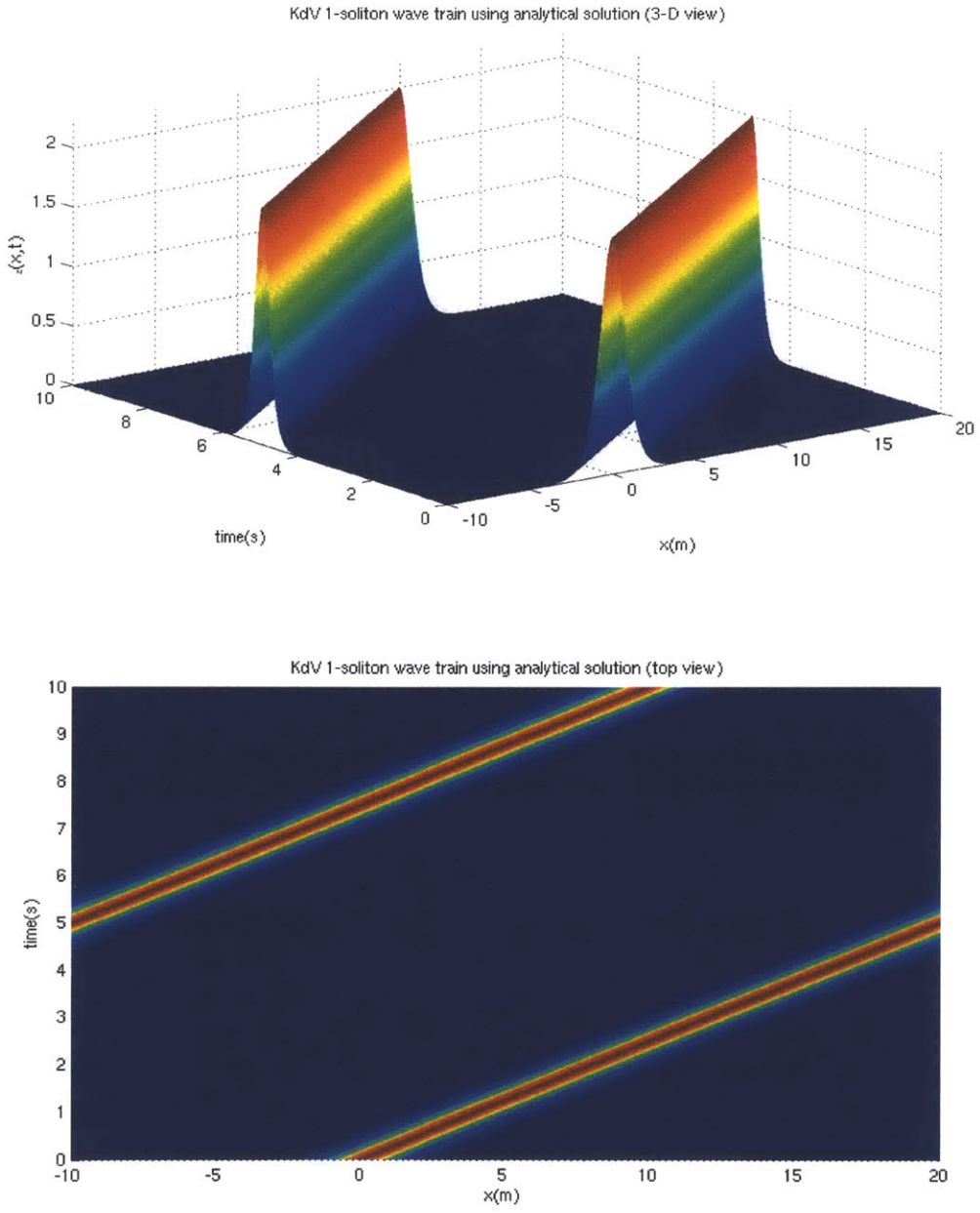

Figure 6-21: Analytical KdV 1-soliton wave train: (a) 3-D view (b) Top view

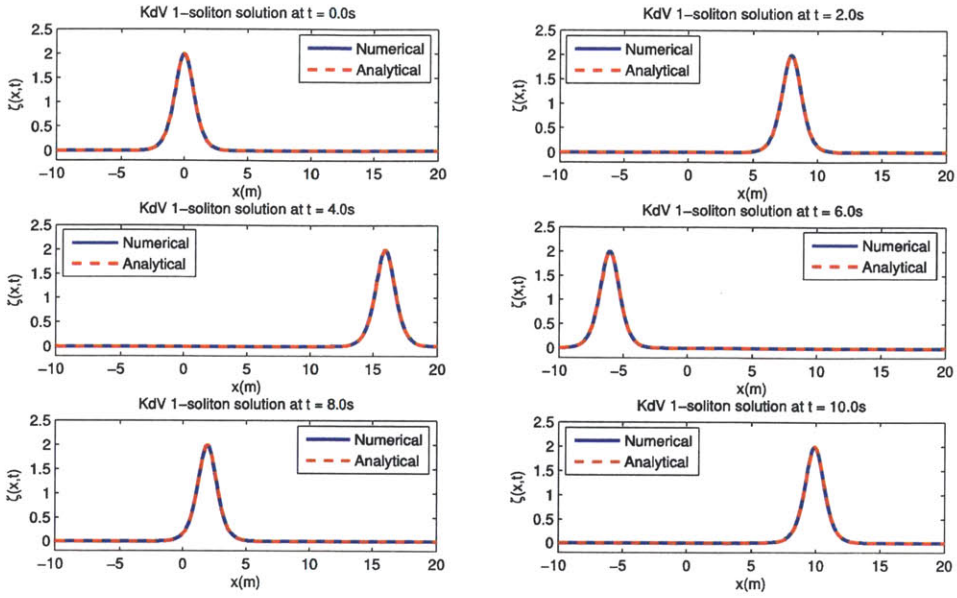

Figure 6-22: KdV 1-soliton numerical and analytical solutions at different time instances

We assume an initial solitary wave with $\bar{\eta} = 1.0$ and $x_0 = 0.0$, given by equation (6.16) with $t = 0$.

We utilize the Euler-Maruyama scheme (described in section 2.2.1) for the discretization of the stochastic PDE (6.21). We employ $\Delta x = 0.2$ for spatial discretization. Thus, the dimensionality of the spatially discretized system is $N = 75$. We compare the numerical stochastic solutions of (6.21) obtained using a Monte Carlo (MC) scheme to that obtained using the Dynamically Orthogonal (DO) equations. For the MC scheme, we utilize $M_r = 1000$ sample realizations, whereas for the DO scheme, we compare solutions using $s = 6$, $s = 10$ and $s = 14$, in each case using $M_r = 1000$ realizations for the corresponding s stochastic DO coefficients. We found that for our implementation of the DO scheme, we needed to use a substantially small time step in order to ensure numerical stability of the evolution equation for the DO modes. Hence, we employ a time step of $\Delta t = 0.005 \times (\Delta x)^3 / 4 = 0.00001$ for both the MC and DO schemes.

The evolution of the mean of the solution, as estimated using the MC scheme and using the DO scheme with three different DO subspace size s, is presented in figure (6-26). The evolution of the corresponding variance of the solution field at the same time

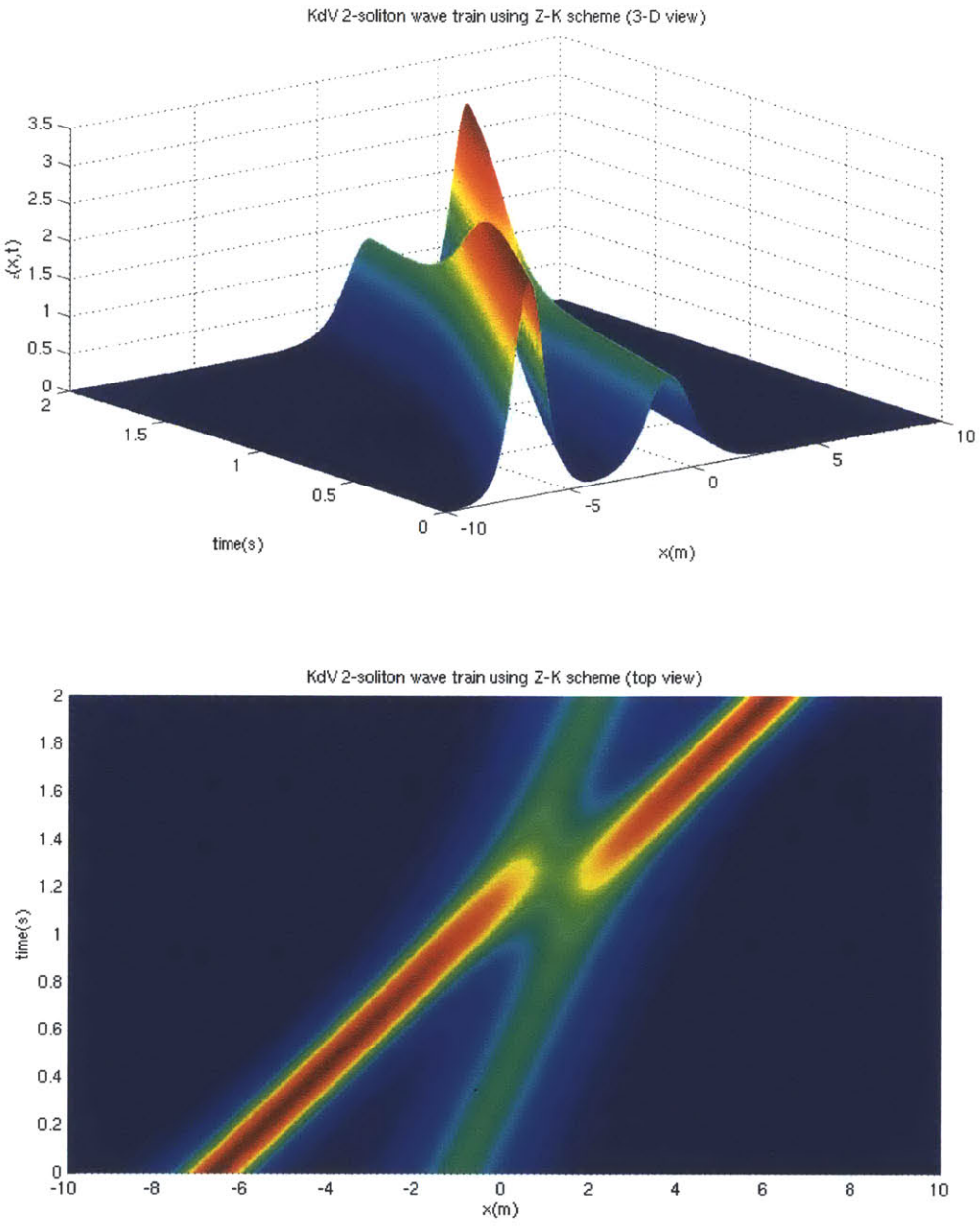

Figure 6-23: Numerical KdV 2-soliton wave train, computed using the Z-K scheme: (a) 3-D view (b) Top view

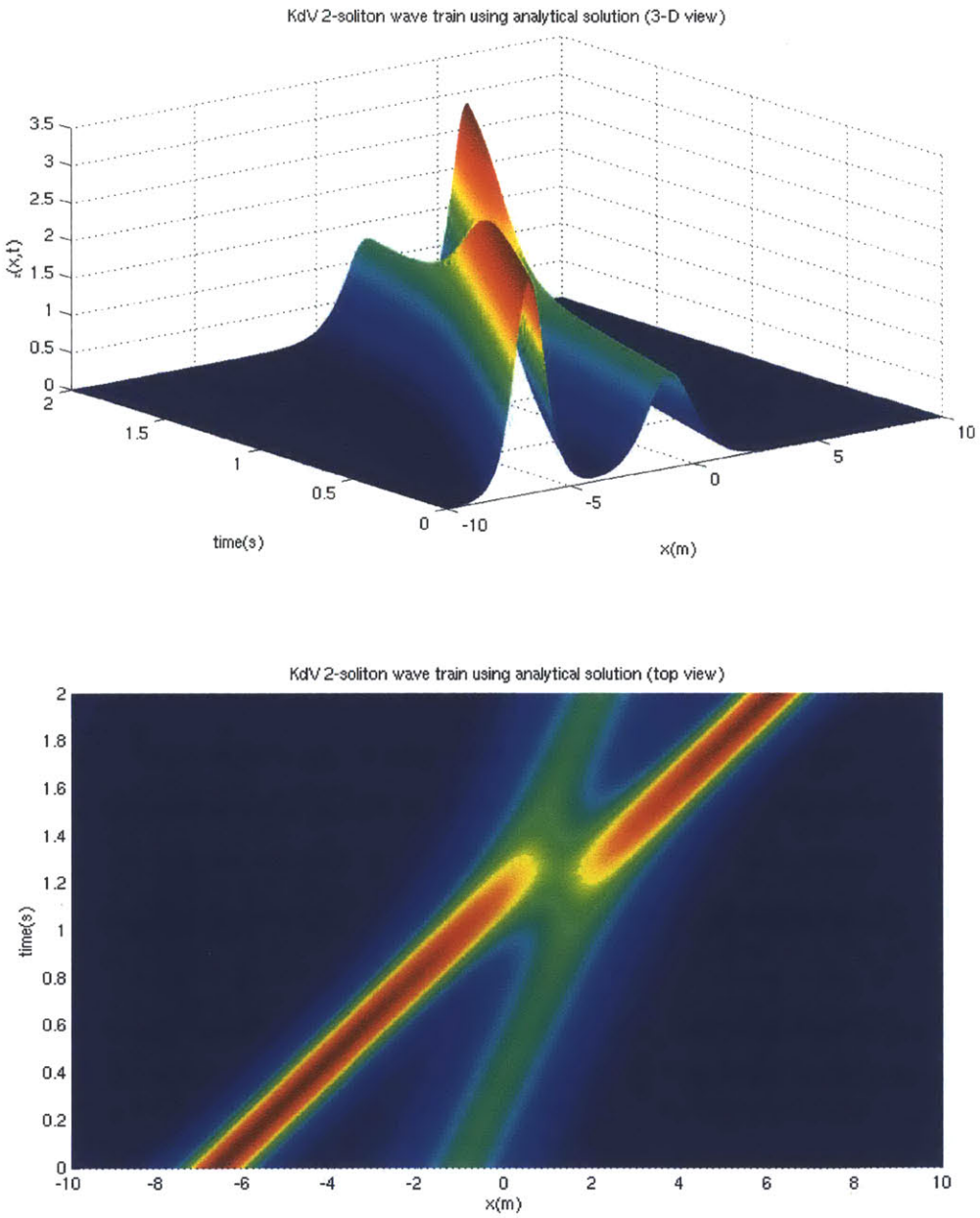

Figure 6-24: Analytical KdV 2-soliton wave train: (a) 3-D view (b) Top view

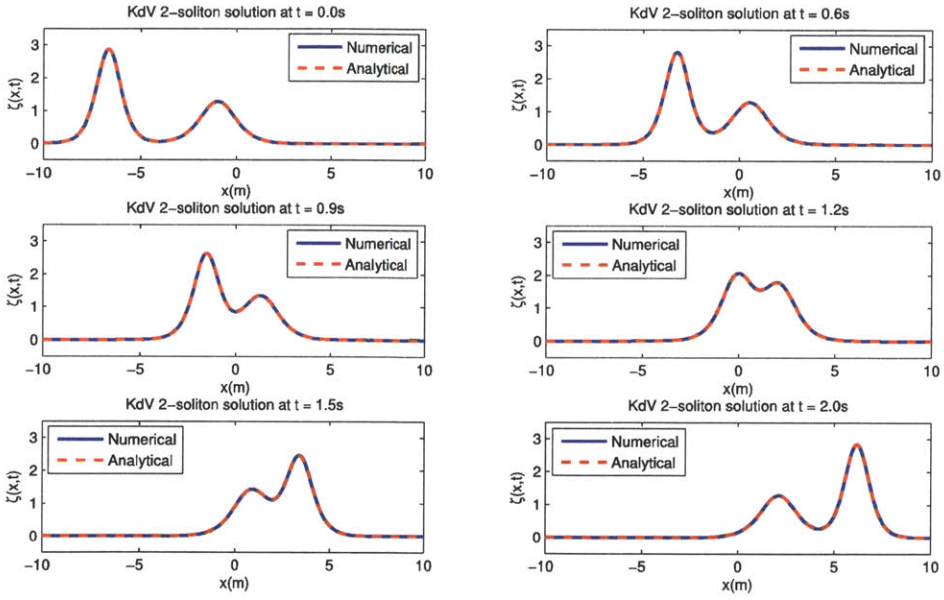

Figure 6-25: KdV 2-soliton numerical and analytical solutions at different time instances

instances using the MC and DO schemes is shown in figure (6-27). We assume that the MC solution is the true solution. From these figures, it is observed that all three DO schemes model the mean of the solution field with reasonable accuracy. However, the variance of the solution field using the DO scheme with $s = 6$ starts to deviate from the Monte Carlo solution at $t = 0.7s$, while the other two schemes (with $s = 10$ and $s = 14$) maintain their accuracy at all time instances.

In order to get a better idea of the accuracy of the numerical schemes, we investigate higher order moments of the solution field. The third and fourth central moments of the stochastic KdV solution field using the DO scheme with $s = 6$, $s = 10$ and $s = 14$, along with the corresponding MC solutions, are plotted in figures (6-28) and (6-29) respectively. Just as we expect the relative accuracy of the MC scheme with too small a sample size to decrease for higher order moments, we expect that the relative accuracy of DO schemes with too low subspace size s to decrease as we estimate higher order moments. It is observed from figures (6-28) and (6-29) that this is indeed the case, and that the relative accuracy of the DO schemes in modeling higher order moments (third and fourth moments) is lower than their accuracy in modeling the corresponding lower order moments

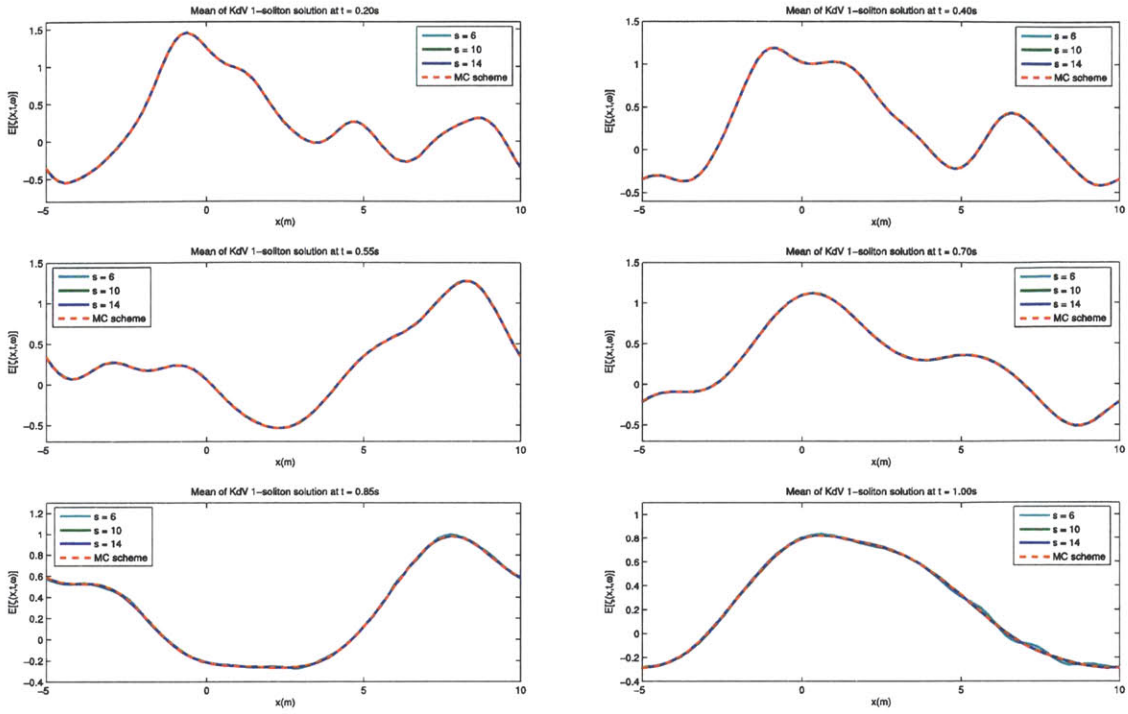

Figure 6-26: Mean of the stochastic KdV solution field at different time instances

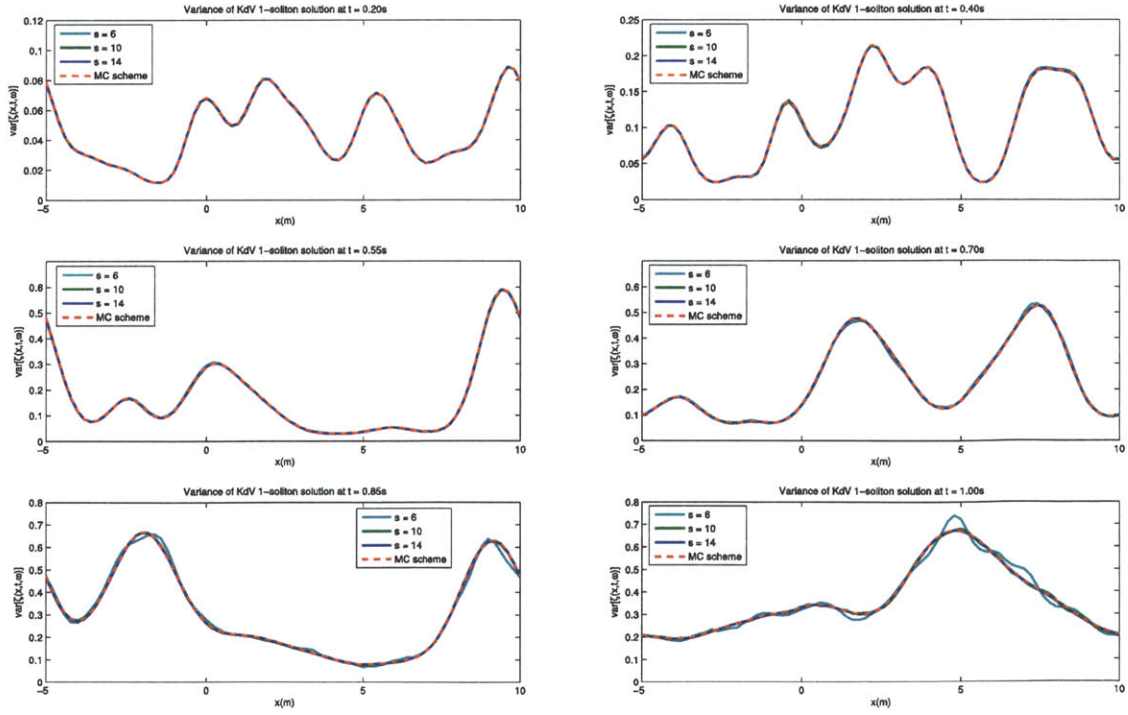

Figure 6-27: Variance of the stochastic KdV solution field at different time instances

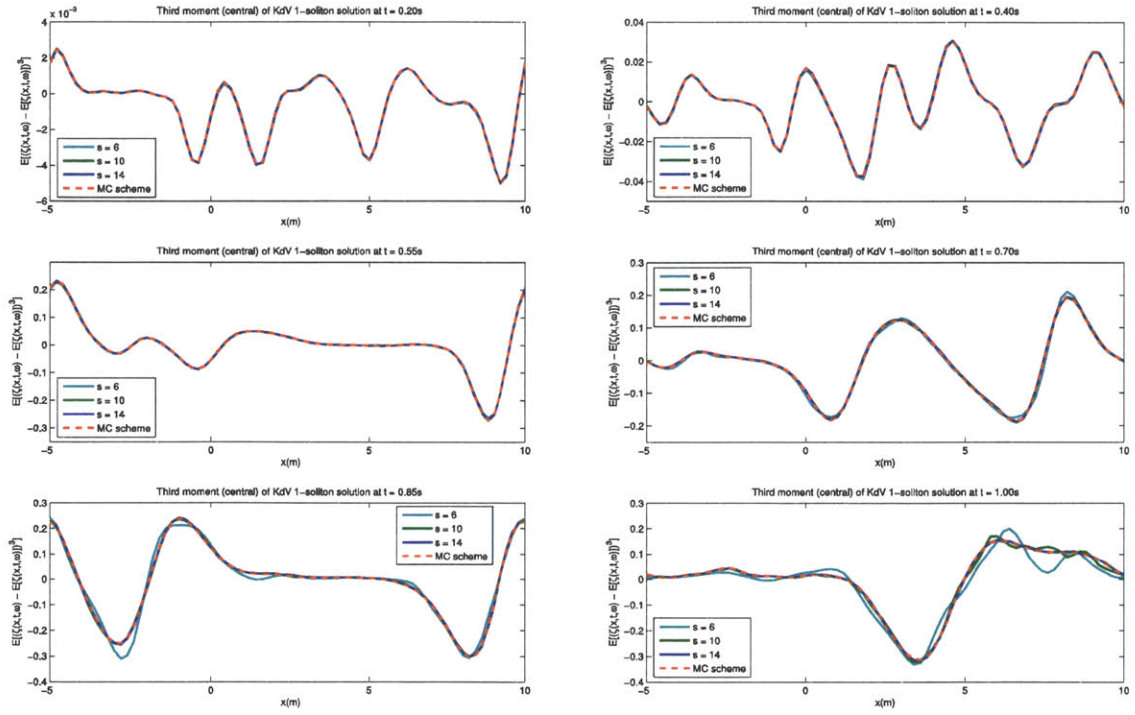

Figure 6-28: Third central moment of the stochastic KdV solution field at different time instances

(mean and variance). It is also seen that the accuracy of the DO scheme increases with an increase in the number of modes, which is as expected. The DO scheme with $s = 14$ accurately models all four moments of the solution field in the given time domain. If we allowed the simulation to run for a very long time (without data assimilation), we expect all reduced space DO schemes to eventually start losing their accuracy. However, the higher the number of modes used in the scheme, the larger the time up to which the scheme can accurately model the statistics of the solution field.

The run times for numerical integration of the KdV equation with external stochastic forcing using the different UQ schemes are presented in table (6.2). It is observed that the run time for the MC scheme is similar to the run time for DO scheme with $s = 10$. Also, the run time for DO scheme with $s = 14$ is approximately twice the run time for the MC scheme.

These observations may lead us to believe that the Monte Carlo scheme is more economical for modeling uncertainty in realistic ocean systems as compared to a DO scheme

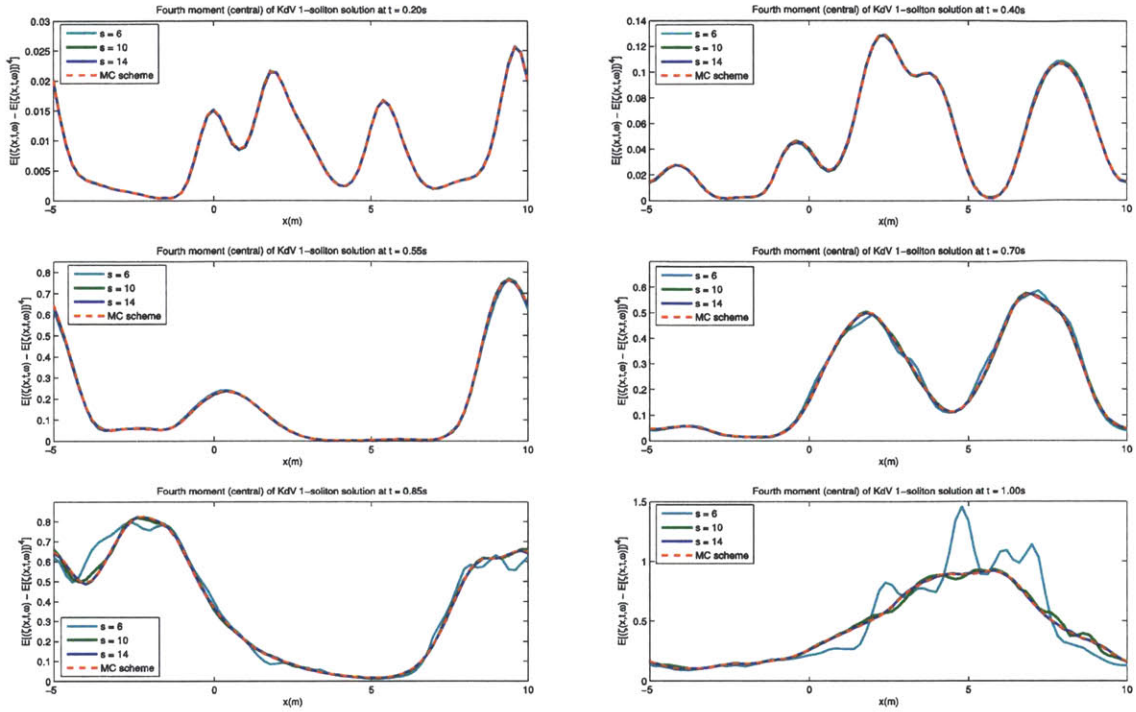

Figure 6-29: Fourth central moment of the stochastic KdV solution field at different time instances

Table 6.2: Run times for UQ schemes for time-integrating uncertainty in the KdV equation with external stochastic forcing

S. No.	Uncertainty Quantification Scheme	Run Time
1.	MC scheme	5271.68s
2.	DO scheme with $s = 4$	1829.38s
3.	DO scheme with $s = 6$	2011.18s
4.	DO scheme with $s = 8$	3599.65s
5.	DO scheme with $s = 10$	5396.80s
6.	DO scheme with $s = 12$	7709.99s
7.	DO scheme with $s = 14$	11119.24s

Table 6.3: Run times for the DO (with $s = 14$) and the MC schemes for different values of dimensionality (N) of state space

S. No.	Δx	N	Run times for DO scheme	Run times for MC scheme
1.	0.200	75	24.91s	10.46s
2.	0.150	100	25.79s	32.52s
3.	0.100	150	27.61s	53.95s
4.	0.075	200	29.76s	74.75s

of sufficiently high accuracy. However, this is not the case. All the stochastic dynamical systems that we have studied in the present work, including the stochastic KdV system, have a relatively low dimensionality (N). Most real ocean fields in two or three dimensional physical space may have a dimensionality of up to $N \sim 10^6 - 10^{10}$. From the two realistic test cases studied in this chapter, i.e., the 20-dimensional self-engineered test case and the stochastic KdV system with $N = 75$, it can be observed from tables (6.1) and (6.2) that the run times for the MC scheme increase significantly with an increase in the dimensionality of the stochastic dynamical system. The MC scheme suffers from what is known as the curse of dimensionality (Sapsis and Lermusiaux, 2012). For real ocean systems with high dimensionality, the MC scheme becomes computationally infeasible. In order to validate this argument, we run the stochastic KdV test case for different values of dimensionality N (by using different values of Δx for spatial discretization). The run times for integrating the stochastic KdV system for the first 200 time steps, using different values of N are presented in table (6.3). It is observed that the run times for the DO scheme (with $s = 14$) increase relatively slowly with an increase in N. However, the run times for the MC scheme increase significantly with an increase in dimensionality N. Hence, we conclude that the MC scheme becomes computationally infeasible for high dimensional realistic ocean systems.

Next, we investigate the sensitivity of the computational cost on the number of sample realizations (M_r). For this, we use the same example as above, but with $\Delta x = 0.15$. The run times for integrating the stochastic KdV system for the first 200 time steps, using different values of M_r are presented in table (6.4). We observe that the run times for the

Table 6.4: Run times for the DO (with $s = 14$) and the MC schemes for different number of sample realizations (M_r)

S. No.	M_r	Run times for DO scheme	Run times for MC scheme
1.	500	21.80s	15.97s
2.	1000	25.79s	32.52s
3.	2000	34.35s	65.28s

MC scheme increase linearly with an increase in the number of realizations (M_r), which is as expected. The increase in the run times for the DO scheme is marginally smaller than the increase in the run times for the MC scheme. We infer that the DO scheme is less sensitive than the MC scheme to an increase in the number of realizations and hence, is more efficient in modeling uncertainty.

In the stochastic KdV test case, we observed that the DO scheme with $s = 14$ modes was successful in integrating the stochastic differential equation with high accuracy. For most realistic high dimensional ocean systems, the number of dominant directions of uncertainty is much smaller than the dimensionality N. Thus, even large ocean systems with high dimensionality can be integrated accurately using a relatively small number of DO modes. Hence, based on the numerical examples studied in this and previous chapters, we conclude that the reduced space DO scheme is suitable for modeling realistic ocean systems with uncertainty in input parameters as well as uncertainty due to external stochastic forcing.

Chapter 7

Conclusions

This chapter presents a summary of the main results and conclusions, and identifies possible directions for future research. In this thesis, we focused our attention on a special class of non-autonomous stochastic dynamical systems, represented by equations (1.1) and (1.2). This class of systems encapsulates most systems encountered in classic nonlinear dynamics and ocean modeling, including flows modeled by Navier-Stokes equations. The main motivation behind this research was to quantify and predict uncertainty for ocean systems with external stochastic forcing.

The first goal of the present work was to develop a computationally efficient solver for time-integrating the class of non-autonomous linear and nonlinear dynamical systems (1.2), and to use this solver to study the uncertainty characteristics of stochastic ocean systems. The second objective was to investigate the use of dynamically orthogonal (DO) field equations and polynomial chaos (PC) schemes for integrating systems with uncertainty in input parameters and due to external stochastic forcing. Towards the first goal, a computationally efficient solver for the solution of the general stochastic differential equation (1.1) was developed and used to time-integrate the Korteweg-de Vries equation with stochastic forcing. Using this solver, the DO and PC schemes were intercompared in terms of accuracy of solution and computational cost. To allow time-integration of uncertainty due to external stochastic forcing over long time intervals, we derived two new polynomial schemes, namely, the reduced space KLgPC scheme and the modified TDgPC (MTDgPC) scheme.

In chapter 2, we developed the background for the current research. We studied numerical integration schemes for the weak approximation of solutions of Itô form of stochastic differential equations and investigated their convergence characteristics. Next, a literature review of UQ methods was presented and the DO and PC schemes were studied in greater detail. In chapter 3, we derived the evolution equations for the class of non-autonomous systems represented by equations (1.1) and (1.2), using DO and polynomial chaos schemes. We also introduced two new polynomial chaos schemes (KLgPC scheme and MTDgPC scheme) capable of integrating uncertainty due to external stochastic forcing over significantly large time intervals.

In chapter 4, we focused our attention on uncertainty in input parameters. Using the one-dimensional decay model and the Kraichnan-Orszag system, we studied the limitation of the gPC scheme in integrating uncertainty in nonlinear dynamical systems over large time intervals. The TDgPC scheme introduced by Gerritsma et al. (2010) was able to alleviate this limitation by re-initializing the polynomial chaos basis in time. Chapter 5 dealt with uncertainty due to external stochastic forcing. We discussed a fundamental limitation of existing classic PC schemes in time-integrating uncertainty due to external stochastic forcing. The reduced space KLgPC and the MTDgPC schemes, introduced in chapter 3, were used successfully to integrate uncertainty due to stochastic noise of both additive and multiplicative nature. However, we observed that the MTDgPC scheme utilizes the entire state space for its implementation, and would hence become computationally expensive for high dimensional systems. Thus, we concluded that the reduced space KLgPC scheme is more efficient computationally than the MTDgPC scheme for integrating uncertainty in ocean systems with stochastic forcing.

Chapter 6 dealt with uncertainty quantification and prediction of stochastic ocean systems. We engineered a 20-dimensional system to study the application of reduced space DO and KLgPC schemes on a stochastic dynamical system that concentrates most of its probability measure on a time-dependent subspace. We observed that for the same level of accuracy, the DO scheme has a significantly lower computational cost as compared to the KLgPC scheme. Next, the deterministic Korteweg-de Vries (KdV) equation was introduced and was numerically integrated using the Zabusky-Kruskal (Z-K) scheme.

Then, we time-integrated the KdV equation with external stochastic forcing using our computationally efficient stochastic solver and compared the performance of the DO and Monte Carlo schemes. Finally, based on the numerical examples studied in this work, we concluded that the reduced space DO scheme is computationally efficient for integrating stochastic ocean systems with uncertainty due to external stochastic forcing.

7.1 Future Work

In this thesis, we studied the application of reduced space DO scheme for uncertainty quantification and prediction of ocean systems with external stochastic forcing. The DO scheme has already been used with success for modeling stochastic fluid flows and other ocean related systems. However, the use of the DO scheme has so far been restricted to integrating systems with uncertainty in input parameters. A next step would be to use the DO scheme to model fluid flows and other high dimensional systems with uncertainty due to external stochastic forcing. This would greatly enhance our capabilities to model and understand the dynamics and interactions of various coupled nonlinear ocean systems which are modeled as dynamical systems with stochastic forcing. For example, the DO scheme could be used to study the uncertainty characteristics in the coupling of ocean acoustics and dynamics, or the effect of wind-driven surface waves on internal waves.

It was observed in chapter 5 that the KLgPC scheme is the most computationally efficient polynomial chaos scheme for time-integrating uncertainty due to external stochastic forcing over large time intervals. However, the computational cost of the reduced space KLgPC scheme is still much higher as compared to the reduced space DO scheme. Hence, another possible research direction could be to investigate possible ways of reducing the computational cost of the KLgPC scheme. This might involve researching ways of computing the time-dependent polynomial chaos basis either analytically or using other efficient methods.

In chapter 6, while investigating the 20-dimensional self-engineered test case, it was observed that the accuracy of the DO scheme with $s = 6$ is lower than the accuracy of the KLgPC scheme with $\bar{r}_{red} = 6$. The KLgPC scheme involves taking a singular value decomposition (SVD) of the solution field and hence represents the best possible reduced

space approximation of the stochastic field. Thus, the DO approximation of the solution field might not be the optimal one. Further research might be required to improve the DO orthogonality condition in order to obtain a better reduced space DO approximation of the solution field.

Furthermore, it was discussed in chapter 6 that the DO scheme is effective for modeling high dimensional stochastic systems because many of these dynamical systems concentrate most of their probability measure on a reduced time-dependent subspace. For such systems, as the dimensionality N of the system increases, the increase in the number of DO modes (s) required to accurately model the dynamical system is significantly lower than the corresponding increase in the dimensionality (N) of the system. Although the singular value decompositions (SVDs) of the dynamics matrices A and B give us some idea about the number of DO modes required to accurately integrate a dynamical system, further research may help us to better understand the relationship between the dimensionality of a system, its dynamics and the number of DO modes required to integrate it accurately.

Appendix A

Detailed Derivation of Evolution Equations

Here, we derive in detail, the evolution equations for the stochastic dynamical systems represented by (1.1) using DO and gPC schemes. The evolution equations for the other PC schemes are very similar in form to the evolution equations for the gPC scheme, and can be derived relatively easily building on the evolution equations for the gPC scheme, and thus have been omitted here.

A.1 Dynamically Orthogonal Equations

Consider the stochastic dynamical system represented by the differential equation (1.1). We consider a DO expansion given by equation (2.54). We omit the arguments after the mean, modes and coefficients for sake of simplicity. Substituting the DO expansion (2.54) into (1.1), we have

$$d\bar{x} + \tilde{x}_i d\phi_i + d\tilde{x}_i \phi_i = A(\bar{x} + \tilde{x}_i \phi_i)\left[\bar{x} + \tilde{x}_i \phi_i\right] dt + B(\bar{x} + \tilde{x}_i \phi_i) dW \tag{A.1}$$

Evolution equation for mean field:

Taking the mean value of equation (A.1), we get

$$\begin{aligned} d\bar{x} + \tilde{x}_i d\left[\mathrm{E}^{\omega}\left[\phi_i\right]\right] + d\tilde{x}_i \mathrm{E}^{\omega}\left[\phi_i\right] = \mathrm{E}^{\omega}\left[A(\bar{x}+\tilde{x}_i\phi_i)\left[\bar{x}+\tilde{x}_i\phi_i\right]\right] dt \\ + \mathrm{E}^{\omega}\left[B(\bar{x}+\tilde{x}_i\phi_i)dW\right] \end{aligned} \tag{A.2}$$

The stochastic noise can be considered to have zero mean value without loss of generality. Also, since $\mathrm{E}^{\omega}\left[\phi_i\right] = 0$, we have

$$d\bar{x} = \mathrm{E}^{\omega}\left[A(\bar{x}+\tilde{x}_i\phi_i)\left[\bar{x}+\tilde{x}_i\phi_i\right]\right] dt + \mathrm{E}^{\omega}\left[B(\bar{x}+\tilde{x}_i\phi_i)dW\right] \tag{A.3}$$

which is the DO evolution equation for the mean.

Evolution equation for stochastic coefficients:

Subtracting equation (A.3) from equation (A.2) and taking its projection on $\tilde{x}_k$, we get

$$\begin{aligned} &\left\langle \tilde{x}_i, \tilde{x}_k \right\rangle d\phi_i + \left\langle d\tilde{x}_i, \tilde{x}_k \right\rangle \phi_i = \\ &\qquad \left\langle A(\bar{x}+\tilde{x}_i\phi_i)\left[\bar{x}+\tilde{x}_i\phi_i\right] dt - \mathrm{E}^{\omega}\left[A(\bar{x}+\tilde{x}_i\phi_i)\left[\bar{x}+\tilde{x}_i\phi_i\right]\right] dt, \tilde{x}_k \right\rangle \\ &\qquad + \left\langle B(\bar{x}+\tilde{x}_i\phi_i)dW - \mathrm{E}^{\omega}\left[B(\bar{x}+\tilde{x}_i\phi_i)dW\right], \tilde{x}_k \right\rangle \end{aligned} \tag{A.4}$$

Imposing the DO condition $\left\langle d\tilde{x}_i, \tilde{x}_k \right\rangle = 0$ and using the condition that the modes are orthonormal, we get

$$\begin{aligned} d\phi_k = \left\langle A(\bar{x}+\tilde{x}_i\phi_i)\left[\bar{x}+\tilde{x}_i\phi_i\right] dt - \mathrm{E}^{\omega}\left[A(\bar{x}+\tilde{x}_i\phi_i)\left[\bar{x}+\tilde{x}_i\phi_i\right]\right] dt, \tilde{x}_k \right\rangle \\ + \left\langle B(\bar{x}+\tilde{x}_i\phi_i)dW - \mathrm{E}^{\omega}\left[B(\bar{x}+\tilde{x}_i\phi_i)dW\right], \tilde{x}_k \right\rangle \end{aligned} \tag{A.5}$$

which are the DO evolution equations for the stochastic coefficients.

Evolution equation for DO modes:

Multiplying equation (A.1) by ϕ_j and taking its mean value, we get

$$\begin{aligned} d\bar{x}\mathrm{E}^{\omega}\left[\phi_j\right] + \tilde{x}_i \mathrm{E}^{\omega}\left[d\phi_i\phi_j\right] + d\tilde{x}_i \mathrm{E}^{\omega}\left[\phi_i\phi_j\right] = \\ \mathrm{E}^{\omega}\left[A(\bar{x}+\tilde{x}_i\phi_i)\left[\bar{x}+\tilde{x}_i\phi_i\right]\phi_j\right] dt + \mathrm{E}^{\omega}\left[B(\bar{x}+\tilde{x}_i\phi_i)dW\phi_j\right] \end{aligned} \tag{A.6}$$

Also, multiplying equation (A.5) by ϕ_j and taking its mean value, we have

$$\begin{aligned}
&\mathrm{E}^{\omega}\left[d\phi_k\phi_j\right] = \\
&\quad \mathrm{E}^{\omega}\left[\langle A(\bar{x}+\tilde{x}_i\phi_i)\left[\bar{x}+\tilde{x}_i\phi_i\right]\phi_j dt - \mathrm{E}^{\omega}\left[A(\bar{x}+\tilde{x}_i\phi_i)\left[\bar{x}+\tilde{x}_i\phi_i\right]\right]\phi_j dt, \tilde{x}_k\rangle\right] \\
&\quad + \mathrm{E}^{\omega}\left[\langle B(\bar{x}+\tilde{x}_i\phi_i)dW\phi_j - \mathrm{E}^{\omega}\left[B(\bar{x}+\tilde{x}_i\phi_i)dW\right]\phi_j, \tilde{x}_k\rangle\right]
\end{aligned} \tag{A.7}$$

Substituting for $\mathrm{E}^{\omega}\left[d\phi_k\phi_j\right]$ from equation (A.7) in equation (A.6) and simplifying, we obtain

$$\begin{aligned}
&d\tilde{x}_i = \\
&\mathrm{E}^{\omega}\left[A(\bar{x}+\tilde{x}_k\phi_k)\left[\bar{x}+\tilde{x}_k\phi_k\right]\phi_j dt - \langle A(\bar{x}+\tilde{x}_k\phi_k)\left[\bar{x}+\tilde{x}_k\phi_k\right]\phi_j dt, \tilde{x}_m\rangle\,\tilde{x}_m\right]\left\{\mathrm{E}^{\omega}\left[\phi_i\phi_j\right]\right\}^{-1} \\
&+ \mathrm{E}^{\omega}\left[B(\bar{x}+\tilde{x}_i\phi_i)dW\phi_j - \langle B(\bar{x}+\tilde{x}_i\phi_i)dW\phi_j, \tilde{x}_m\rangle\,\tilde{x}_m\right]\left\{\mathrm{E}^{\omega}\left[\phi_i\phi_j\right]\right\}^{-1}
\end{aligned} \tag{A.8}$$

which is the DO evolution equation for the modes.

DO governing equations for quadratic-nonlinear systems

We consider the special case when matrices A and B are of the form

$$\begin{aligned}
A &= A_0 + A_1(\bar{x}+\tilde{x}_i\phi_i) \\
B &= B_0 + B_1(\bar{x}+\tilde{x}_i\phi_i)
\end{aligned} \tag{A.9}$$

where A_0 and B_0 are a function of time only and A_1 and B_1 are linear in $X = \bar{x} + \tilde{x}_i\phi_i$. Hence, we can write A and B as

$$\begin{aligned}
A &= A_0 + A_1(\bar{x}) + A_1(\tilde{x}_i\phi_i) \\
B &= B_0 + B_1(\bar{x}) + B_1(\tilde{x}_i\phi_i)
\end{aligned} \tag{A.10}$$

Substituting from equation (A.10) in equations (A.3), (A.5) and (A.8), and simplifying the resulting equations, we get the DO evolution equations for this special case, which are given as

$$d\bar{x} = A_0\bar{x}dt + A_1(\bar{x})\bar{x}dt + \mathrm{E}^{\omega}\left[A_1(\tilde{x}_k\phi_k)\tilde{x}_j\phi_j\right]dt + \mathrm{E}^{\omega}\left[B_1(\tilde{x}_k\phi_k)dW\right] \tag{A.11}$$

$$
\begin{aligned}
d\phi_i = & \langle A_0\tilde{x}_j, \tilde{x}_i\rangle \, \phi_j dt + \langle A_1(\bar{x})\tilde{x}_j, \tilde{x}_i\rangle \, \phi_j dt + \langle A_1(\tilde{x}_k\phi_k)\bar{x}, \tilde{x}_i\rangle \, dt \\
& + \langle A_1(\tilde{x}_k\phi_k)\tilde{x}_j\phi_j - \mathrm{E}^\omega\left[A_1(\tilde{x}_k\phi_k)\tilde{x}_j\phi_j\right], \tilde{x}_i\rangle + \langle B_0, \tilde{x}_i\rangle \, dW \\
& + \langle B_1(\bar{x}), \tilde{x}_i\rangle \, dW + \langle B_1(\tilde{x}_k\phi_k)dW - \mathrm{E}^\omega\left[B_1(\tilde{x}_k\phi_k)dW\right], \tilde{x}_i\rangle
\end{aligned} \tag{A.12}
$$

$$
\begin{aligned}
d\tilde{x}_i = & A_0\tilde{x}_i - \langle A_0\tilde{x}_i, \tilde{x}_j\rangle \, \tilde{x}_j dt + A_1(\bar{x})\tilde{x}_i - \langle A_1(\bar{x})\tilde{x}_i, \tilde{x}_j\rangle \, \tilde{x}_j dt \\
& + \mathrm{E}^\omega\left[A_1(\tilde{x}_k\phi_k)\bar{x}\phi_j - \langle A_1(\tilde{x}_k\phi_k)\bar{x}\phi_j, \tilde{x}_m\rangle \, \tilde{x}_m\right]\left\{\mathrm{E}^\omega\left[\phi_i\phi_j\right]\right\}^{-1} dt \\
& + \mathrm{E}^\omega\left[A_1(\tilde{x}_k\phi_k)\tilde{x}_p\phi_p\phi_j - \langle A_1(\tilde{x}_k\phi_k)\tilde{x}_p\phi_p\phi_j, \tilde{x}_m\rangle \, \tilde{x}_m\right]\left\{\mathrm{E}^\omega\left[\phi_i\phi_j\right]\right\}^{-1} dt \\
& + \mathrm{E}^\omega\left[B_0 dW\phi_j - \langle B_0 dW\phi_j, \tilde{x}_m\rangle \, \tilde{x}_m\right]\left\{\mathrm{E}^\omega\left[\phi_i\phi_j\right]\right\}^{-1} \\
& + \mathrm{E}^\omega\left[B_1(\bar{x})dW\phi_j - \langle B_1(\bar{x})dW\phi_j, \tilde{x}_m\rangle \, \tilde{x}_m\right]\left\{\mathrm{E}^\omega\left[\phi_i\phi_j\right]\right\}^{-1} \\
& + \mathrm{E}^\omega\left[B_1(\tilde{x}_k\phi_k)dW\phi_j - \langle B_1(\tilde{x}_k\phi_k)dW\phi_j, \tilde{x}_m\rangle \, \tilde{x}_m\right]\left\{\mathrm{E}^\omega\left[\phi_i\phi_j\right]\right\}^{-1}
\end{aligned} \tag{A.13}
$$

DO governing equations in vector form

We define $\tilde{X} \in \mathbb{R}^{N\times s}$ as $\tilde{X} = [\tilde{x}_1\tilde{x}_2\ldots\tilde{x}_s]$ and $\tilde{\Phi} \in \mathbb{R}^{s\times 1}$ as $\tilde{\Phi} = [\phi_1\phi_2\ldots\phi_s]^T$. Then we have the vector form of DO evolution equations, given as

$$
d\bar{x} = A_0\bar{x}dt + A_1(\bar{x})\bar{x}dt + \mathrm{E}^\omega\left[A_1(\tilde{X}\tilde{\Phi})\tilde{X}\tilde{\Phi}\right]dt + \mathrm{E}^\omega\left[B_1(\tilde{X}\tilde{\Phi})dW\right] \tag{A.14}
$$

$$
\begin{aligned}
d\tilde{\Phi} = & \tilde{X}^T A_0\tilde{X}\tilde{\Phi}dt + \tilde{X}^T A_1(\bar{x})\tilde{X}\tilde{\Phi}dt + \tilde{X}^T A_1(\tilde{X}\tilde{\Phi})\bar{x}dt \\
& + \tilde{X}^T\left[A_1(\tilde{X}\tilde{\Phi})\tilde{X}\tilde{\Phi} - \mathrm{E}^\omega\left[A_1(\tilde{X}\tilde{\Phi})\tilde{X}\tilde{\Phi}\right]\right]dt \\
& + \tilde{X}^T B_0 dW + \tilde{X}^T B_1(\bar{x})dW + + \tilde{X}^T\left[B_1(\tilde{X}\tilde{\Phi})dW - \mathrm{E}^\omega\left[B_1(\tilde{X}\tilde{\Phi})dW\right]\right]
\end{aligned} \tag{A.15}
$$

$$
\begin{aligned}
d\tilde{X} = & \left[A_0\tilde{X} - \tilde{X}\tilde{X}^T A_0\tilde{X}\right] dt + \left[A_1(\bar{x})\tilde{X} - \tilde{X}\tilde{X}^T A_1(\bar{x})\tilde{X}\right] dt \\
& + \mathrm{E}^\omega \left[A_1(\tilde{X}\tilde{\Phi})\bar{x}\tilde{\Phi}^T - \tilde{X}\tilde{X}^T A_1(\tilde{X}\tilde{\Phi})\bar{x}\tilde{\Phi}^T\right] \mathrm{P}(\tilde{\Phi})^{-1} dt \\
& + \mathrm{E}^\omega \left[A_1(\tilde{X}\tilde{\Phi})\tilde{X}\tilde{\Phi}\tilde{\Phi}^T - \tilde{X}\tilde{X}^T A_1(\tilde{X}\tilde{\Phi})\tilde{X}\tilde{\Phi}\tilde{\Phi}^T\right] \mathrm{P}(\tilde{\Phi})^{-1} dt \\
& + \mathrm{E}^\omega \left[B_0 dW\tilde{\Phi}^T - \tilde{X}\tilde{X}^T B_0 dW\tilde{\Phi}^T\right] \mathrm{P}(\tilde{\Phi})^{-1} \\
& + \mathrm{E}^\omega \left[B_1(\bar{x})dW\tilde{\Phi}^T - \tilde{X}\tilde{X}^T B_1(\bar{x})dW\tilde{\Phi}^T\right] \mathrm{P}(\tilde{\Phi})^{-1} \\
& + \mathrm{E}^\omega \left[B_1(\tilde{X}\tilde{\Phi})dW\tilde{\Phi}^T - \tilde{X}\tilde{X}^T B_1(\tilde{X}\tilde{\Phi})dW\tilde{\Phi}^T\right] \mathrm{P}(\tilde{\Phi})^{-1}
\end{aligned}
\tag{A.16}
$$

where $\mathrm{P}(\tilde{\Phi}) = \mathrm{E}^\omega \left[\tilde{\Phi}\tilde{\Phi}^T\right]$ is the covariance matrix of $\tilde{\Phi}$.

DO governing equations using realizations

Let $\tilde{\Phi}^r \in \mathbb{R}^{s\times 1}$ and $dW^r \in \mathbb{R}^{N\times 1}$ represent one specific realization of stochastic variables $\tilde{\Phi}$ and dW respectively. Then we have, for these specific realizations, the DO evolution equations for the mean, stochastic coefficients and modes, respectively, given as

$$
d\bar{x} = A_0\bar{x}dt + A_1(\bar{x})\bar{x}dt + \mathrm{E}^\omega \left[A_1(\tilde{X}\tilde{\Phi}^r)\tilde{X}\tilde{\Phi}^r\right] dt + \mathrm{E}^\omega \left[B_1(\tilde{X}\tilde{\Phi}^r)dW^r\right] \tag{A.17}
$$

$$
\begin{aligned}
d\tilde{\Phi}^r = & \tilde{X}^T A_0\tilde{X}\tilde{\Phi}^r dt + \tilde{X}^T A_1(\bar{x})\tilde{X}\tilde{\Phi}^r dt + \tilde{X}^T A_1(\tilde{X}\tilde{\Phi}^r)\bar{x}dt \\
& + \tilde{X}^T \left[A_1(\tilde{X}\tilde{\Phi}^r)\tilde{X}\tilde{\Phi}^r - \mathrm{E}^\omega \left[A_1(\tilde{X}\tilde{\Phi}^r)\tilde{X}\tilde{\Phi}^r\right]\right] dt \\
& + \tilde{X}^T B_0 dW^r + \tilde{X}^T B_1(\bar{x})dW^r \\
& + \tilde{X}^T \left[B_1(\tilde{X}\tilde{\Phi}^r)dW^r - \mathrm{E}^\omega \left[B_1(\tilde{X}\tilde{\Phi}^r)dW^r\right]\right]
\end{aligned}
\tag{A.18}
$$

$$
\begin{aligned}
d\tilde{X} = &\left[A_0\tilde{X} - \tilde{X}\tilde{X}^T A_0\tilde{X}\right]dt + \left[A_1(\bar{x})\tilde{X} - \tilde{X}\tilde{X}^T A_1(\bar{x})\tilde{X}\right]dt \\
&+ \mathrm{E}^{\omega}\left[A_1(\tilde{X}\tilde{\Phi}^r)\bar{x}(\tilde{\Phi}^r)^T - \tilde{X}\tilde{X}^T A_1(\tilde{X}\tilde{\Phi}^r)\bar{x}(\tilde{\Phi}^r)^T\right]\mathrm{P}((\tilde{\Phi}^r))^{-1}dt \\
&+ \mathrm{E}^{\omega}\left[A_1(\tilde{X}\tilde{\Phi}^r)\tilde{X}\tilde{\Phi}^r(\tilde{\Phi}^r)^T - \tilde{X}\tilde{X}^T A_1(\tilde{X}\tilde{\Phi}^r)\tilde{X}\tilde{\Phi}^r(\tilde{\Phi}^r)^T\right]\mathrm{P}((\tilde{\Phi}^r))^{-1}dt \\
&+ \mathrm{E}^{\omega}\left[B_0 dW^r(\tilde{\Phi}^r)^T - \tilde{X}\tilde{X}^T B_0 dW^r(\tilde{\Phi}^r)^T\right]\mathrm{P}((\tilde{\Phi}^r))^{-1} \\
&+ \mathrm{E}^{\omega}\left[B_1(\bar{x})dW^r(\tilde{\Phi}^r)^T - \tilde{X}\tilde{X}^T B_1(\bar{x})dW^r(\tilde{\Phi}^r)^T\right]\mathrm{P}((\tilde{\Phi}^r))^{-1} \\
&+ \mathrm{E}^{\omega}\left[B_1(\tilde{X}\tilde{\Phi}^r)dW^r(\tilde{\Phi}^r)^T - \tilde{X}\tilde{X}^T B_1(\tilde{X}\tilde{\Phi}^r)dW^r(\tilde{\Phi}^r)^T\right]\mathrm{P}((\tilde{\Phi}^r))^{-1}
\end{aligned}
\tag{A.19}
$$

Vectorized DO governing equations using realizations

We define $\tilde{\Phi}^R \in \mathbb{R}^{s\times M_r}$ as $\tilde{\Phi}^R = \left[\tilde{\Phi}^1\tilde{\Phi}^2\ldots\tilde{\Phi}^M_r\right]$ to represent M_r realizations of $\tilde{\Phi}$ and $d\tilde{W}^R \in \mathbb{R}^{N\times M_r}$ as $d\tilde{W}^R = \left[dW^1 dW^2 \ldots dW^M_r\right]$ to represent M_r realizations of dW. Then we have the vectorized form of DO evolution equations with realizations, given as

$$
d\bar{x} = A_0\bar{x}dt + A_1(\bar{x})\bar{x}dt + \mathrm{E}^{\omega}\left[A_1(\tilde{X}\tilde{\Phi}^R)\tilde{X}\tilde{\Phi}^R\right]dt + \mathrm{E}^{\omega}\left[B_1(\tilde{X}\tilde{\Phi}^R)d\tilde{W}^R\right] \tag{A.20}
$$

$$
\begin{aligned}
d\tilde{\Phi}^R = &\tilde{X}^T A_0\tilde{X}\tilde{\Phi}^R dt + \tilde{X}^T A_1(\bar{x})\tilde{X}\tilde{\Phi}^R dt + \tilde{X}^T A_1(\tilde{X}\tilde{\Phi}^R)\bar{x}dt \\
&+ \tilde{X}^T\left[A_1(\tilde{X}\tilde{\Phi}^R)\tilde{X}\tilde{\Phi}^R - \mathrm{E}^{\omega}\left[A_1(\tilde{X}\tilde{\Phi}^R)\tilde{X}\tilde{\Phi}^R\right]\right]dt \\
&+ \tilde{X}^T B_0 d\tilde{W}^R + \tilde{X}^T B_1(\bar{x})d\tilde{W}^R \\
&+ \tilde{X}^T\left[B_1(\tilde{X}\tilde{\Phi}^R)d\tilde{W}^R - \mathrm{E}^{\omega}\left[B_1(\tilde{X}\tilde{\Phi}^R)d\tilde{W}^R\right]\right]
\end{aligned}
\tag{A.21}
$$

$$
\begin{aligned}
d\tilde{X} = &\left[A_0\tilde{X} - \tilde{X}\tilde{X}^T A_0\tilde{X}\right]dt + \left[A_1(\bar{x})\tilde{X} - \tilde{X}\tilde{X}^T A_1(\bar{x})\tilde{X}\right]dt \\
&+ \mathrm{E}^{\omega}\left[A_1(\tilde{X}\tilde{\Phi}^R)\bar{x}(\tilde{\Phi}^R)^T - \tilde{X}\tilde{X}^T A_1(\tilde{X}\tilde{\Phi}^R)\bar{x}(\tilde{\Phi}^R)^T\right]\mathrm{P}((\tilde{\Phi}^R))^{-1}dt \\
&+ \mathrm{E}^{\omega}\left[A_1(\tilde{X}\tilde{\Phi}^R)\tilde{X}\tilde{\Phi}^R(\tilde{\Phi}^R)^T - \tilde{X}\tilde{X}^T A_1(\tilde{X}\tilde{\Phi}^R)\tilde{X}\tilde{\Phi}^R(\tilde{\Phi}^R)^T\right]\mathrm{P}((\tilde{\Phi}^R))^{-1}dt \\
&+ \mathrm{E}^{\omega}\left[B_0 d\tilde{W}^R(\tilde{\Phi}^R)^T - \tilde{X}\tilde{X}^T B_0 d\tilde{W}^R(\tilde{\Phi}^R)^T\right]\mathrm{P}((\tilde{\Phi}^R))^{-1} \\
&+ \mathrm{E}^{\omega}\left[B_1(\bar{x})d\tilde{W}^R(\tilde{\Phi}^R)^T - \tilde{X}\tilde{X}^T B_1(\bar{x})d\tilde{W}^R(\tilde{\Phi}^R)^T\right]\mathrm{P}((\tilde{\Phi}^R))^{-1} \\
&+ \mathrm{E}^{\omega}\left[B_1(\tilde{X}\tilde{\Phi}^R)d\tilde{W}^R(\tilde{\Phi}^R)^T - \tilde{X}\tilde{X}^T B_1(\tilde{X}\tilde{\Phi}^R)d\tilde{W}^R(\tilde{\Phi}^R)^T\right]\mathrm{P}((\tilde{\Phi}^R))^{-1}
\end{aligned}
\tag{A.22}
$$

Vectorization for optimal numerical computations

Since matrix A_1 is linear in $\tilde{x}_k\phi_k$, all the stochastic terms can be combined together. Thus, from equation (A.11), we have

$$
d\bar{x} = A_0\bar{x}dt + A_1(\bar{x})\bar{x}dt + A_1(\tilde{x}_k)\tilde{x}_j\mathrm{E}^{\omega}\left[\phi_k\phi_j\right]dt + B_1(\tilde{x}_k)\mathrm{E}^{\omega}\left[\phi_k dW\right] \tag{A.23}
$$

We define $V_1 \in \mathbb{R}^{N\times s^2}$ as $V_1 = A_1(\tilde{x}_k)\tilde{x}_j, 1 \le k,j \le s$ and $M_2(\tilde{\Phi}^R) \in \mathbb{R}^{s^2\times M_r}$ as $M_2(\tilde{\Phi}^R) = \tilde{\phi}_k^r\tilde{\phi}_j^r, 1 \le k,j \le s, 1 \le r \le M_r$. Also, we define $V_3 \in \mathbb{R}^{N\times sN}$ as $V_3 = B_1(\tilde{x}_k), 1 \le k \le s$ and $M_{n1}(\tilde{\Phi}^R, d\tilde{W}^R) \in \mathbb{R}^{sN\times M_r}$ as $M_{n1}(\tilde{\Phi}^R, d\tilde{W}^R) = \tilde{\phi}_k^r d\tilde{W}_p^r, 1 \le k \le s, 1 \le p \le n, 1 \le r \le M_r$. Then from equation (A.23), we get the final DO evolution equation for the mean, given as

$$
d\bar{x} = A_0\bar{x}dt + A_1(\bar{x})\bar{x}dt + V_1\mathrm{E}^{\omega}\left[M_2(\tilde{\Phi}^R)\right]dt + V_3\mathrm{E}^{\omega}\left[M_{n1}(\tilde{\Phi}^R, d\tilde{W}^R)\right] \tag{A.24}
$$

Similarly, from equation (A.12), we have

$$
\begin{aligned}
d\phi_i = &\left\langle A_0\tilde{x}_j, \tilde{x}_i\right\rangle\phi_j dt + \left\langle A_1(\bar{x})\tilde{x}_j, \tilde{x}_i\right\rangle\phi_j dt + \left\langle A_1(\tilde{x}_k)\bar{x}, \tilde{x}_i\right\rangle\phi_k dt \\
&+ \left\langle A_1(\tilde{x}_k)\tilde{x}_j, \tilde{x}_i\right\rangle\left(\phi_k\phi_j - \mathrm{E}^{\omega}\left[\phi_k\phi_j\right]\right)dt \\
&+ \left\langle B_0, \tilde{x}_i\right\rangle dW + \left\langle B_1(\bar{x}), \tilde{x}_i\right\rangle dW + \left\langle B_1(\tilde{x}_k), \tilde{x}_i\right\rangle\left(\phi_k dW - \mathrm{E}^{\omega}\left[\phi_k dW\right]\right)
\end{aligned}
\tag{A.25}
$$

We define $V_2 \in \mathbb{R}^{N\times s}$ as $V_2 = A_1(\tilde{x}_k)\bar{x}, 1 \le k \le s$. Using this and earlier definitions, and vectorizing equation (A.25), we get the final DO evolution equation for the stochastic

coefficients, given as

$$\begin{aligned} d\tilde{\Phi}^R = & \tilde{X}^T A_0 \tilde{X} \tilde{\Phi}^R dt + \tilde{X}^T A_1(\bar{x}) \tilde{X} \tilde{\Phi}^R dt + \tilde{X}^T V_2 \tilde{\Phi}^R dt \\ & + \tilde{X}^T V_1 \left[M_2(\tilde{\Phi}^R) - \mathrm{E}^\omega \left[M_2(\tilde{\Phi}^R) \right] \right] dt \\ & + \tilde{X}^T B_0 d\tilde{W}^R + \tilde{X}^T B_1(\bar{x}) d\tilde{W}^R \\ & + \tilde{X}^T V_3 \left[M_{n1}(\tilde{\Phi}^R, d\tilde{W}^R) - \mathrm{E}^\omega \left[M_{n1}(\tilde{\Phi}^R, d\tilde{W}^R) \right] \right] \end{aligned} \tag{A.26}$$

Furthermore, from equation (A.13), we have

$$\begin{aligned} d\tilde{x}_i = & \left[A_0 \tilde{x}_i - \langle A_0 \tilde{x}_i, \tilde{x}_j \rangle \tilde{x}_j \right] dt + \left[A_1(\bar{x}) \tilde{x}_i - \langle A_1(\bar{x}) \tilde{x}_i, \tilde{x}_j \rangle \tilde{x}_j \right] dt \\ & + \left[A_1(\tilde{x}_k) \bar{x} - \langle A_1(\tilde{x}_k) \bar{x}, \tilde{x}_m \rangle \tilde{x}_m \right] \mathrm{E}^\omega \left[\phi_k \phi_j \right] C^{-1}_{\phi_i \phi_j} dt \\ & + \left[A_1(\tilde{x}_k) \tilde{x}_p - \langle A_1(\tilde{x}_k) \tilde{x}_p, \tilde{x}_m \rangle \tilde{x}_m \right] \mathrm{E}^\omega \left[\phi_k \phi_p \phi_j \right] C^{-1}_{\phi_i \phi_j} dt \\ & + \left[B_0 - \langle B_0, \tilde{x}_m \rangle \tilde{x}_m \right] \mathrm{E}^\omega \left[dW \phi_j \right] C^{-1}_{\phi_i \phi_j} \\ & + \left[B_1(\bar{x}) - \langle B_1(\bar{x}), \tilde{x}_m \rangle \tilde{x}_m \right] \mathrm{E}^\omega \left[dW \phi_j \right] C^{-1}_{\phi_i \phi_j} \\ & + \left[B_1(\tilde{x}_k) - \langle B_1(\tilde{x}_k), \tilde{x}_m \rangle \tilde{x}_m \right] \mathrm{E}^\omega \left[\phi_k dW \phi_j \right] C^{-1}_{\phi_i \phi_j} \end{aligned} \tag{A.27}$$

where $C^{-1}_{\phi_i \phi_j} = \{ \mathrm{E}^\omega [\phi_i \phi_j] \}^{-1}$. We define $M_3(\tilde{\Phi}^R) \in \mathbb{R}^{s^2 \times s}$ as $M_3(\tilde{\Phi}^R) = \mathrm{E}^\omega \left[\tilde{\phi}^r_k \tilde{\phi}^r_p \times \tilde{\phi}^r_j \right], 1 \leq k, p, j \leq s, 1 \leq r \leq M_r$. Also define $M_{n2}(\tilde{\Phi}^R, d\tilde{W}^R) \in \mathbb{R}^{sN \times s}$ as $M_{n2}(\tilde{\Phi}^R, d\tilde{W}^R) = \mathrm{E}^\omega \left[\tilde{\phi}^r_k d\tilde{W}^r_p \times \tilde{\phi}^r_j \right], 1 \leq k, j \leq s, 1 \leq p \leq N, 1 \leq r \leq M_r$. Using this and earlier definitions and simplifying and vectorizing equation (A.27), we get the final DO evolution equation for the modes, given as

$$\begin{aligned} d\tilde{X} = & \left[A_0 \tilde{X} - \tilde{X} \tilde{X}^T A_0 \tilde{X} \right] dt + \left[A_1(\bar{x}) \tilde{X} - \tilde{X} \tilde{X}^T A_1(\bar{x}) \tilde{X} \right] dt \\ & + \left[V_2 - \tilde{X} \tilde{X}^T V_2 \right] dt + \left[V_1 - \tilde{X} \tilde{X}^T V_1 \right] M_3(\tilde{\Phi}^R) \mathrm{P}((\tilde{\Phi}^R))^{-1} dt \\ & + \left[B_0 - \tilde{X} \tilde{X}^T B_0 \right] \mathrm{E}^\omega \left[d\tilde{W}^R \tilde{\Phi}^R \right] \mathrm{P}((\tilde{\Phi}^R))^{-1} \\ & + \left[B_1(\bar{x}) - \tilde{X} \tilde{X}^T B_1(\bar{x}) \right] \mathrm{E}^\omega \left[d\tilde{W}^R \tilde{\Phi}^R \right] \mathrm{P}((\tilde{\Phi}^R))^{-1} \\ & + \left[V_3 - \tilde{X} \tilde{X}^T V_3 \right] M_{n2}(\tilde{\Phi}^R, d\tilde{W}^R) \mathrm{P}((\tilde{\Phi}^R))^{-1} \end{aligned} \tag{A.28}$$

Final form of DO governing equations

Thus, from equations (A.24), (A.26) and (A.28), we have the final form of the DO evo-

lution equations for the mean, stochastic coefficients and modes respectively, given as follows:

Mean

$$d\bar{x} = A_0\bar{x}dt + A_1(\bar{x})\bar{x}dt + V_1\mathrm{E}^{\omega}\left[M_2(\tilde{\Phi}^R)\right]dt + V_3\mathrm{E}^{\omega}\left[M_{n1}(\tilde{\Phi}^R, d\tilde{W}^R)\right] \tag{A.29}$$

Stochastic coefficients

$$\begin{aligned} d\tilde{\Phi}^R = {} & \tilde{X}^T A_0 \tilde{X}\tilde{\Phi}^R dt + \tilde{X}^T A_1(\bar{x})\tilde{X}\tilde{\Phi}^R dt + \tilde{X}^T V_2 \tilde{\Phi}^R dt \\ & + \tilde{X}^T V_1\left[M_2(\tilde{\Phi}^R) - \mathrm{E}^{\omega}\left[M_2(\tilde{\Phi}^R)\right]\right]dt \\ & + \tilde{X}^T B_0 d\tilde{W}^R + \tilde{X}^T B_1(\bar{x})d\tilde{W}^R \\ & + \tilde{X}^T V_3\left[M_{n1}(\tilde{\Phi}^R, d\tilde{W}^R) - \mathrm{E}^{\omega}\left[M_{n1}(\tilde{\Phi}^R, d\tilde{W}^R)\right]\right] \end{aligned} \tag{A.30}$$

DO Modes

$$\begin{aligned} d\tilde{X} = {} & \left[A_0\tilde{X} - \tilde{X}\tilde{X}^T A_0\tilde{X}\right]dt + \left[A_1(\bar{x})\tilde{X} - \tilde{X}\tilde{X}^T A_1(\bar{x})\tilde{X}\right]dt \\ & + \left[V_2 - \tilde{X}\tilde{X}^T V_2\right]dt + \left[V_1 - \tilde{X}\tilde{X}^T V_1\right]M_3(\tilde{\Phi}^R)\mathrm{P}((\tilde{\Phi}^R))^{-1}dt \\ & + \left[B_0 - \tilde{X}\tilde{X}^T B_0\right]\mathrm{E}^{\omega}\left[d\tilde{W}^R\tilde{\Phi}^R\right]\mathrm{P}((\tilde{\Phi}^R))^{-1} \\ & + \left[B_1(\bar{x}) - \tilde{X}\tilde{X}^T B_1(\bar{x})\right]\mathrm{E}^{\omega}\left[d\tilde{W}^R\tilde{\Phi}^R\right]\mathrm{P}((\tilde{\Phi}^R))^{-1} \\ & + \left[V_3 - \tilde{X}\tilde{X}^T V_3\right]M_{n2}(\tilde{\Phi}^R, d\tilde{W}^R)\mathrm{P}((\tilde{\Phi}^R))^{-1} \end{aligned} \tag{A.31}$$

A.2 Generalized Polynomial Chaos

We again consider the dynamical system represented by the differential equation (1.1). Consider the multi-variate polynomial chaos expansion given by equation (2.43). Substituting this expansion in equation (1.1), we have

$$d\tilde{x}_i\Psi_i = A(\tilde{x}_i\Psi_i)\left[\tilde{x}_j\Psi_j\right]dt + B(\tilde{x}_i\Psi_i)dW \tag{A.32}$$

Multiplying equation (A.32) by Ψ_k and taking expectation of the resulting equation, we get

$$d\tilde{x}_i \mathrm{E}^{\omega}\left[\Psi_i \Psi_k\right] = \mathrm{E}^{\omega}\left[A(\tilde{x}_i \Psi_i)\tilde{x}_j \Psi_j \Psi_k\right] dt + \mathrm{E}^{\omega}\left[B(\tilde{x}_i \Psi_i) dW \Psi_k\right] \tag{A.33}$$

gPC governing equations for quadratic non-linear systems

We again consider the special case here matrices A and B have the form given by equations (A.9) and (A.10). Substituting from equation (A.10) in equation (A.33) and simplifying, we get the gPC evolution equation for this special case, which is given by

$$\begin{aligned} d\tilde{x}_i = A_0 \tilde{x}_i dt + \mathrm{E}^{\omega}\left[A_1(\tilde{x}_k \Psi_k)\tilde{x}_j \Psi_j \Psi_l\right] C^{-1}_{\Psi_i \Psi_l} dt \\ + B_0 \mathrm{E}^{\omega}\left[dW \Psi_l\right] C^{-1}_{\Psi_i \Psi_l} + \mathrm{E}^{\omega}\left[B_1(\tilde{x}_k \Psi_k) dW \Psi_l\right] C^{-1}_{\Psi_i \Psi_l} \end{aligned} \tag{A.34}$$

gPC governing equation in vector form

We define $\tilde{X} \in \mathbb{R}^{N \times s}$ as $\tilde{X} = [\tilde{x}_1 \tilde{x}_2 \dots \tilde{x}_s]$ and $\tilde{\Psi} \in \mathbb{R}^{s \times 1}$ as $\tilde{\Psi} = [\Psi_1 \Psi_2 \dots \Psi_s]^T$. Then we have the vector form of gPC evolution equation, given as

$$\begin{aligned} d\tilde{X} = A_0 \tilde{X} dt + \mathrm{E}^{\omega}\left[A_1(\tilde{X}\tilde{\Psi})\tilde{X}\tilde{\Psi}\tilde{\Psi}^T\right] \mathrm{P}(\tilde{\Psi}^T)^{-1} dt \\ + B_0 \mathrm{E}^{\omega}\left[dW \tilde{\Psi}^T\right] \mathrm{P}(\tilde{\Psi}^T)^{-1} + \mathrm{E}^{\omega}\left[B_1(\tilde{X}\tilde{\Psi}) dW \tilde{\Psi}^T\right] \mathrm{P}(\tilde{\Psi})^{-1} \end{aligned} \tag{A.35}$$

where $\mathrm{P}(\tilde{\Psi}) = \mathrm{E}^{\omega}\left[\tilde{\Psi}\tilde{\Psi}^T\right]$ is the covariance matrix of $\tilde{\Psi}$.

gPC governing equation using realizations

Let $\tilde{\Psi}^r \in \mathbb{R}^{s \times 1}$ and $dW^r \in \mathbb{R}^{N \times 1}$ represent one specific realization of stochastic variables $\tilde{\Psi}$ and dW respectively. Then we have, for these specific realizations, the gPC evolution equations for the deterministic coefficients, given as

$$\begin{aligned} d\tilde{X} = A_0 \tilde{X} dt + \mathrm{E}^{\omega}\left[A_1(\tilde{X}\tilde{\Psi}^r)\tilde{X}\tilde{\Psi}^r(\tilde{\Psi}^r)^T\right] \mathrm{P}((\tilde{\Psi}^r))^{-1} dt \\ + \mathrm{E}^{\omega}\left[B_0 dW^r(\tilde{\Psi}^r)^T\right] \mathrm{P}((\tilde{\Psi}^r))^{-1} + \mathrm{E}^{\omega}\left[B_1(\tilde{X}\tilde{\Psi}^r) dW^r(\tilde{\Psi}^r)^T\right] \mathrm{P}((\tilde{\Psi}^r))^{-1} \end{aligned} \tag{A.36}$$

Vectorization for optimal numerical computations

Since matrix A_1 is linear in $\tilde{x}_k \Psi_k$, all the stochastic terms can be combined together.

Thus, from equation (A.34), we have

$$\begin{aligned} d\tilde{x}_i = A_0\tilde{x}_i dt + A_1(\tilde{x}_k)\tilde{x}_j \mathrm{E}^{\omega}\left[\Psi_k\Psi_j\Psi_l\right] C^{-1}_{\Psi_i\Psi_l} dt \\ + B_0 \mathrm{E}^{\omega}\left[dW\Psi_l\right] C^{-1}_{\Psi_i\Psi_l} + B_1(\tilde{x}_k)\mathrm{E}^{\omega}\left[\Psi_k dW\Psi_l\right] C^{-1}_{\Psi_i\Psi_l} \end{aligned} \tag{A.37}$$

We define $V_1 \in \mathbb{R}^{N\times s^2}$ as $V_1 = A_1(\tilde{x}_k)\tilde{x}_j, 1 \leq k, j \leq s$ and $M_3(\tilde{\Psi}^R) \in \mathbb{R}^{s^2\times s}$ as $M_3(\tilde{\Psi}^R) = \mathrm{E}^{\omega}\left[\tilde{\Psi}^r_k\tilde{\Psi}^r_j \times \tilde{\Psi}^r_l\right], 1 \leq k, j, l \leq s, 1 \leq r \leq M_r$. Also define $V_3 \in \mathbb{R}^{N\times sN}$ as $V_3 = B_1(\tilde{x}_k), 1 \leq k \leq s$ and $M_{n2}(\tilde{\Psi}^R, \tilde{Z}^R) \in \mathbb{R}^{sN\times s}$ as $M_{n2}(\tilde{\Psi}^R, \tilde{Z}^R) = \mathrm{E}^{\omega}\left[\tilde{\Psi}^r_k\tilde{Z}^r_j \times \tilde{\Psi}^r_l\right] \quad , 1 \leq k, l \leq s, 1 \leq j \leq N, 1 \leq r \leq M_r$. Then from equation (A.37), we get the final gPC evolution equation, given as

$$\begin{aligned} d\tilde{X} = A_0\tilde{X}dt + V_1 M_3(\tilde{\Psi}^R)\mathrm{P}((\tilde{\Psi}^R))^{-1}dt \\ + B_0\mathrm{E}^{\omega}\left[d\tilde{W}^R\tilde{\Psi}^R\right]\mathrm{P}((\tilde{\Psi}^R))^{-1} + V_3 M_{n2}(\tilde{\Psi}^R, d\tilde{W}^R)\mathrm{P}((\tilde{\Psi}^R))^{-1} \end{aligned} \tag{A.38}$$

Final form of gPC governing equation

Thus, from equation (A.38), e have the final form of the gPC evolution equation, which is given as

$$\begin{aligned} d\tilde{X} = A_0\tilde{X}dt + V_1 M_3(\tilde{\Psi}^R)\mathrm{P}((\tilde{\Psi}^R))^{-1}dt \\ + B_0\mathrm{E}^{\omega}\left[d\tilde{W}^R\tilde{\Psi}^R\right]\mathrm{P}((\tilde{\Psi}^R))^{-1} + V_3 M_{n2}(\tilde{\Psi}^R, d\tilde{W}^R)\mathrm{P}((\tilde{\Psi}^R))^{-1} \end{aligned} \tag{A.39}$$

Appendix B

Algorithm for General Stochastic Solver

Here, we discuss the details of the stochastic solver developed for efficient time integration of stochastic dynamical systems represented by (1.1) and (1.2). The numerical code for the general stochastic solver is divided into four main parts, which are as follows:

- **functions *spec_A( )* and *spec_B( )* :** used to define the matrices A and B for the class of dynamical systems governed by the differential equation (1.1)
- **script *setup_script* :** used to define the model parameters and initial conditions for the dynamical system
- **script *plot_script* :** used for plotting the final solution
- **function *main( )* :** used to perform the time integration of the system (1.1)

In what follows, we discuss each of these four parts of the stochastic solver.

B.1 Functions *spec_A( )* and *spec_B( )*

These functions use a sparse representation to define matrices A and B for stochastic dynamical systems represented by (1.1). The matrices A and B are decomposed into

state independent and state dependent parts, given as

$$\begin{aligned} A(X(r,t;\omega),t) &= A_0(r,t;\omega) + A_1(X(r,t;\omega),t) \\ B(X(r,t;\omega),t) &= B_0(r,t;\omega) + B_1(X(r,t;\omega),t) \end{aligned} \tag{B.1}$$

where $A_0(r,t;\omega)$ and $B_0(r,t;\omega)$ are functions in time, space and uncertainty (ω) only and $A_1(X(r,t;\omega),t)$ and $B_1(X(r,t;\omega),t)$ are linear in $X(r,t;\omega)$. The matrices A_0 and B_0 are defined directly whereas sparse representation is used for defining matrices A_1 and B_1. For these matrices, the array $node_1$ stores the location of non-empty entries of the matrix. Array N_1 stores which state variable is specified at the corresponding non-empty location and the array C_1 stores the corresponding coefficient to be multiplied to the state variable. For example, consider the governing equations for the Kraichnan-Orszag three mode problem, given as

$$\begin{aligned} \frac{dx_1(t;\omega)}{dt} &= x_2(t;\omega)x_3(t;\omega) \\ \frac{dx_2(t;\omega)}{dt} &= x_3(t;\omega)x_1(t;\omega) \\ \frac{dx_3(t;\omega)}{dt} &= -2x_1(t;\omega)x_2(t;\omega) \end{aligned} \tag{B.2}$$

The differential equations (B.2) can be represented non-uniquely in the form (1.1) as

$$\frac{\partial}{\partial t}\begin{pmatrix} x_1 \\ x_2 \\ x_3 \end{pmatrix} = \begin{pmatrix} 0 & x_3 & 0 \\ 0 & 0 & x_1 \\ 0 & -2x_1 & 0 \end{pmatrix}\begin{pmatrix} x_1 \\ x_2 \\ x_3 \end{pmatrix} \tag{B.3}$$

from which we have

$$A = \begin{bmatrix} 0 & x_3 & 0 \\ 0 & 0 & x_1 \\ 0 & -2x_1 & 0 \end{bmatrix} \tag{B.4}$$

Thus, we define the matrix A_0 as

$$A_0 = \begin{bmatrix} 0 & 0 & 0 \\ 0 & 0 & 0 \\ 0 & 0 & 0 \end{bmatrix} \tag{B.5}$$

Furthermore, we define the matrix A_1 using $node_1$, N_1 and C_1 as

$$\begin{aligned} node_1 &= \begin{bmatrix} 4 & 6 & 8 \end{bmatrix} \\ N_1 &= \begin{bmatrix} 3 & 1 & 1 \end{bmatrix} \\ C_1 &= \begin{bmatrix} 1 & -2 & 1 \end{bmatrix} \end{aligned} \tag{B.6}$$

A similar approach is used for defining matrix B in terms of matrices B_0 and B_1.

B.2 Script *setup_script*

This script is used for setting up the problem by defining the model parameters and the initial conditions for the dynamical system (1.1). The following model parameters are used in the numerical code:

- n : Dimension of state space
- n_noise : Dimension of driving Wiener process
- s : Dimension of the DO subspace and the number of polynomial basis functions for PC expansion of the solution state
- m : Number of Monte Carlo realizations
- delt : Time step size
- k_max : Number of time steps up to which we perform numerical time integration
- Xsi : Realizations of random variables used to define uncertainty in the dynamical system

- num_int_choice : Variable specifying the choice of numerical time integration scheme

The initial conditions are defined according to the uncertainty quantification scheme being used for integrating the stochastic differential equation.

B.3 Script *plot_script*

This script is used for saving and plotting the final solution after the numerical run is complete.

B.4 Function *main( )*

This function first evaluates *setup_script* to define the model parameters and initial conditions for the problem. Next, time integration of the evolution equations is performed based on the choice of numerical integration scheme given through the model parameter num_int_choice defined in *setup_script*. The following functions are called in *main( )* during the time integration, when using the DO scheme:

- *calc_A1* : used to calculate the matrix $A_1(\bar{x})$
- *calc_B1* : used to calculate the matrix $B_1(\bar{x})$ or $B_1(\tilde{x}_i)$ for any particular i, where $1 \leq i \leq s$
- *calc_M2Phi* : used to calculate the second moment of stochastic coefficients, i.e., $\mathbb{E}[\phi_i \phi_j]$, for all $1 \leq i, j \leq s$
- *calc_M3Phi* : used to calculate the third moment of stochastic coefficients, i.e., $\mathbb{E}[\phi_i \phi_j \phi_k]$, for all $1 \leq i, j, k \leq s$
- *calc_Mn1Phi* : used to calculate the mean value of n_{noise}-dimensional Wiener process multiplied by stochastic coefficients i.e., $\mathbb{E}[dW \phi_i]$, for all $1 \leq i \leq s$
- *calc_Mn2Phi* : used to calculate the mean value of $\mathbb{E}[dW \phi_i \phi_j]$, for all $1 \leq i, j \leq s$
- *calc_val1* : used to calculate the value of $A_1(\tilde{x}_i)\tilde{x}_j$, for all $1 \leq i, j \leq s$

- *calc_val2* : used to calculate the value of $A_1(\tilde{x}_i)\bar{x}$, for all $1 \leq i \leq s$
- *calc_val3* : used to calculate the value of $B_1(\tilde{x}_i)$, for all $1 \leq i \leq s$

Additionally, orthonormalization of the modes is performed after every time step to ensure that the modes remain numerically orthonormal. The algorithm for orthonormalization is as follows:

$$\begin{aligned} M &= \tilde{X}' * \tilde{X}; \\ [v \quad d] &= eig(M); \\ \tilde{X} &= \tilde{X} * v/sqrt(d); \\ \Phi &= v' * \Phi; \end{aligned} \tag{B.7}$$

where $\tilde{X}$ and Φ are matrices comprising of deterministic modes $\tilde{x}_i, 1 \leq i \leq s$ and $\phi_i, 1 \leq i \leq s$ respectively. Furthermore, the following other functions are called in *main( )* during the time integration step when using the MC scheme:

- *calc_mc1* : used to calculate the value of $A_1(\tilde{X}^R)\tilde{X}^R$
- *calc_mc2* : used to calculate the value of $B_1(\tilde{X}^R)dW^R$

While using the gPC scheme, the following functions are called in *main( )* during the time integration step:

- *Hermite* : used to generate Hermite polynomials up to order p
- *Legendre* : used to generate Legendre polynomials up to order p
- *calc_index* : used to calculate the multi-index for polynomial chaos expansion
- *calc_psi* : used to calculate the realizations of multi-variate polynomial basis functions
- *calc_A1* : used to calculate the matrix $A_1(\bar{x})$
- *calc_B1* : used to calculate the matrix $B_1(\bar{x})$ or $B_1(X_{mode(i)})$ for any particular spatial mode

- *calc_M3Phi* : used to calculate the third moment of stochastic coefficients, i.e., $\mathbb{E}[\Psi \cdot \Psi \cdot \Psi]$

- *calc_Mn2Phi* : used to calculate the moment of noise multiplied by square of stochastic coefficients i.e., $\mathbb{E}[Z \cdot \Psi \cdot \Psi]$

- *calc_val1* : used to calculate the value of $A_1(X_{modes}) \cdot X_{modes}$

- *calc_val3* : used to calculate the value of $B_1(X_{modes})$

In TDgPC, the new Modified TDgPC (MTDgPC) and the new KLgPC schemes, in addition to all the functions used in the gPC scheme, the function *calc_Psi_new_multi* is used during time integration to calculate the new polynomial basis numerically using Gram-Schmidt orthogonalization method (during the re-initialization step).

When the time integration step is complete, the script *plot_script* is called in order to save the solution and to plot the relevant figures.

Appendix C

Table of Runs

Here, we tabularize the systems and simulations that we have investigated in this research work, including those for the study of uncertainty in input parameters, uncertainty due to external stochastic forcing and uncertainty prediction for stochastic ocean systems.

Table C.1: Uncertainty in Input Parameters

S. No.	Test Case	Governing Equations	Model Parameters
P1	1-D Decay Model (Gerritsma et al., 2010)	$\frac{du}{dt} + ku = 0$ $u(0) = 1$ $k \sim U(-1, 1)$	Realizations $= 1 \times 10^4$ $\Delta t = 0.01, 0 \leq t \leq 30$ Scheme: RK-4
P2	K-O Problem (Gerritsma et al., 2010)	$\frac{dx_1}{dt} = x_2 x_3$ $\frac{dx_2}{dt} = x_1 x_3$ $\frac{dx_3}{dt} = -2x_1 x_2$ $x_1(0) = 0.99 + 0.01\xi_1$ $x_2(0) = 1, x_3(0) = 1$ $\xi_1 \sim U(-1, 1)$	Realizations $= 1 \times 10^4$ $\Delta t = 0.01, 0 \leq t \leq 40$ Scheme: RK-4
P3	K-O Problem (Gerritsma et al., 2010)	$\frac{dx_1}{dt} = x_2 x_3$ $\frac{dx_2}{dt} = x_1 x_3$ $\frac{dx_3}{dt} = -2x_1 x_2$ $x_1(0) = 0.995 + 0.01\xi_1$ $x_2(0) = 1, x_3(0) = 1$ $\xi_1 \sim U(-1, 1)$	Realizations $= 1 \times 10^4$ $\Delta t = 0.01, 0 \leq t \leq 40$ Scheme: RK-4
P4	K-O Problem (Gerritsma et al., 2010)	$\frac{dx_1}{dt} = x_2 x_3$ $\frac{dx_2}{dt} = x_1 x_3$ $\frac{dx_3}{dt} = -2x_1 x_2$ $x_1(0) = 0.99 + 0.01\xi_1$ $x_2(0) = 1.0 + 0.01\xi_2$ $x_3(0) = 1.0 + 0.01\xi_3$ $\xi_1, \xi_2, \xi_3 \sim U(-1, 1)$	Realizations $= 1 \times 10^4$ $\Delta t = 0.01, 0 \leq t \leq 40$ Scheme: RK-4

Table C.2: Uncertainty due to External Stochastic Forcing

S. No.	Test Case	Governing Equations	Model Parameters
P5	3-D Autonomous (additive noise)	$dX = AXdt + BdW$ $A = \begin{bmatrix} -3 & 1 & 1 \\ 2 & -5 & 1 \\ 3 & 1 & -6 \end{bmatrix}$ $B = \begin{bmatrix} 0 & 2 & 1 \\ 0 & 1 & 0 \\ 2 & 0 & 0 \end{bmatrix}$ $X(t=0) = [1\ 1\ 1]^T$	Realizations $= 2 \times 10^5$ $\Delta t = 0.01, 0 \leq t \leq 4$ Scheme: EM
P6	3-D Non-autonomous (additive noise)	$dX = AXdt + BdW$ where A and B are as defined below $X(t=0) = [1\ 1\ 1]^T$	Realizations $= 2 \times 10^5$ $\Delta t = 0.01, 0 \leq t \leq 4$ Scheme: EM
P6	$A = \begin{bmatrix} -3 + 2\cos(2\pi t) & 1 & 1 + 2\sin(2\pi t) \\ 2 & -5 & 1 \\ 3 & 1 + 3\sin(4\pi t) & -6 + +3\cos(4\pi t) \end{bmatrix}$ $B = \begin{bmatrix} 0.5\cos(2\pi t) & 2 + 0.5\sin(2\pi t) & 1 \\ 0 & 1 + \sin(2\pi t) & \cos(2\pi t) \\ 2 & 0 & 0 \end{bmatrix}$		
P7	4-D Autonomous (multiplicative noise)	$dX = AXdt + BdW$ where A and B are as defined below $X(t=0) = [1\ 1\ 1\ 1]^T$	Realizations $= 5 \times 10^4$ $\Delta t = 0.01, 0 \leq t \leq 3$ Scheme: EM
P7	$A = \begin{bmatrix} \frac{-3}{20} & \frac{1}{20} & \frac{1}{20} & \frac{1}{20} \\ \frac{1}{20} & \frac{-3}{20} & \frac{1}{20} & \frac{1}{20} \\ \frac{1}{20} & \frac{1}{20} & \frac{-3}{20} & \frac{1}{20} \\ \frac{1}{20} & \frac{1}{20} & \frac{1}{20} & \frac{-3}{20} \end{bmatrix}$ $B = \begin{bmatrix} \frac{1}{5}x_1 & \frac{1}{100}x_2 & \frac{1}{100}x_3 & \frac{1}{100}x_4 \\ \frac{1}{100}x_1 & \frac{1}{5}x_2 & \frac{1}{100}x_3 & \frac{1}{100}x_4 \\ \frac{1}{100}x_1 & \frac{1}{100}x_2 & \frac{1}{5}x_3 & \frac{1}{100}x_4 \\ \frac{1}{100}x_1 & \frac{1}{100}x_2 & \frac{1}{100}x_3 & \frac{1}{5}x_4 \end{bmatrix}$		

Table C.3: Uncertainty Prediction for Stochastic Ocean Systems

S. No.	Test Case	Governing Equations	Model Parameters
P8	20-D Non-autonomous (additive noise)	$dX = AXdt + BdW$ Self-engineered A, B $X(t=0) = [1\ 1 \ldots 1]^T$	Realizations $= 2 \times 10^4$ $\Delta t = 0.01, 0 \leq t \leq 4$ Scheme: EM
P9	KdV 1-soliton (deterministic)	$\zeta_\tau + 6\zeta\zeta_x + \zeta_{xxx} = 0$ $\bar{\eta} = 1.0, x_0 = 0.0$	$\Delta x = 0.1, x \in [-10, 20]$ $\Delta t = 0.00025, 0 \leq t \leq 10$ Scheme: Z-K
P10	KdV 2-soliton (deterministic)	$\zeta_\tau + 6\zeta\zeta_x + \zeta_{xxx} = 0$ $\bar{\eta}_1 = 1.2, \bar{\eta}_2 = 0.8$ $x_1 = -6.0, x_= - 2.0$	$\Delta x = 0.1, x \in [-10, 10]$ $\Delta t = 0.00025, 0 \leq t \leq 2$ Scheme: Z-K
P11	KdV 1-soliton (stochastic)	$\zeta_\tau + 6\zeta\zeta_x + \zeta_{xxx} = \epsilon\tilde{\eta}(t;\omega)$ $\bar{\eta}_1 = 1.0, x_0 = 0.0$	Realizations $= 1000$ $\Delta x = 0.2, x \in [-5, 10]$ $\Delta t = 0.00001, 0 \leq t \leq 1$ Scheme: EM

Bibliography

Ablowitz, M. J. and Segur, H. (1981). *Solitons and the inverse scattering transform*, volume 4. SIAM.

Airy, G. B. (1845). Tides and waves. *Encyclopaedia Metropolitana*, pages 241 396.

Albowitz, M. and Taha, T. (1984). Analytical and numerical aspects of certain nonlinear evolution equations. iii. korteweg-de vries equation. *Journal of Computational Physics*, 55(2):231 253.

Babuška, I., Nobile, F., and Tempone, R. (2007). A stochastic collocation method for elliptic partial differential equations with random input data. *SIAM Journal on Numerical Analysis*, 45(3):1005 1034.

Bachelier, L. (1900). *Théorie de la spéculation*. Gauthier-Villars.

Berkooz, G., Holmes, P., and Lumley, J. L. (1993). The proper orthogonal decomposition in the analysis of turbulent flows. *Annual review of fluid mechanics*, 25(1):539 575.

Bertsekas, D. and Tsitsiklis, J. (2002). *Introduction to probability*, volume 1. Athena Scientific Nashua, NH.

Borcea, L., Papanicolaou, G., Tsogka, C., and Berryman, J. (2002). Imaging and time reversal in random media. *Inverse Problems*, 18(5):1247.

Boussinesq, J. (1872). Th {é} orie des ondes et des remous qui se propagent le long d\'un canal rectangulaire horizontal, en communiquant au liquide contenu dans ce canal des vitesses sensiblement pareilles de la surface au fond. *J. Math. Pures Appl.*, 17(2):55 108.

Boussinesq, J. (1877). *Essai sur la théorie des eaux courantes*. Imprimerie nationale.

Branicki, M. and Majda, A. J. (2012). Fundamental limitations of polynomial chaos for uncertainty quantification in systems with intermittent instabilities. *Comm. Math. Sci*, 11.

Brown, R. (1828). Xxvii. a brief account of microscopical observations made in the months of june, july and august 1827, on the particles contained in the pollen of plants; and on the general existence of active molecules in organic and inorganic bodies. *The Philosophical Magazine, or Annals of Chemistry, Mathematics, Astronomy, Natural History and General Science*, 4(21):161 173.

Burrage, K. and Burrage, P. (1996). High strong order explicit runge-kutta methods for stochastic ordinary differential equations. *Applied Numerical Mathematics*, 22(1):81 101.

Burrage, K. and Burrage, P. (2000). Order conditions of stochastic runge kutta methods by b-series. *SIAM Journal on Numerical Analysis*, 38(5):1626 1646.

Cameron, R. H. and Martin, W. T. (1947). The orthogonal development of non-linear functionals in series of fourier-hermite functionals. *The Annals of Mathematics*, 48(2):385 392.

Cheng, M., Hou, T., and Zhang, Z. (2012). A dynamically bi-orthogonal method for time-dependent stochastic partial differential equations i: Derivation and algorithms'.

Chorin, A. J. (1974). Gaussian fields and random flow. *Journal of Fluid Mechanics*, 63:21 32.

Crow, S. and Canavan, G. (1970). Relationship between a wiener-hermite expansion and an energy cascade. *J. Fluid Mech*, 41(2):387 403.

Dashti, M. and Stuart, A. M. (2011). Uncertainty quantification and weak approximation of an elliptic inverse problem. *SIAM Journal on Numerical Analysis*, 49(6):2524 2542.

de Jager, E. (2006). On the origin of the korteweg-de vries equation. *arXiv preprint math/0602661*.

de Vries, G. (1894). *Bijdrage tot de kennis der lange golven*. PhD thesis, Universiteit van Amsterdam.

Debusschere, B., Najm, H., Matta, A., Shu, T., Knio, O., Ghanem, R., and Le Maıtre, O. (2002). Uncertainty quantification in a reacting electrochemical microchannel flow model. In *Proc. 5th Int. Conf. on Modeling and Simulation of Microsystems*, pages 384 387.

Debusschere, B., Najm, H., Pébay, P., Knio, O., Ghanem, R., and Le Maître, O. (2004). Numerical challenges in the use of polynomial chaos representations for stochastic processes. *SIAM Journal on Scientific Computing*, 26(2):698 719.

Debusschere, B. J., Najm, H. N., Matta, A., Knio, O. M., Ghanem, R. G., and Le Maître, O. P. (2003). Protein labeling reactions in electrochemical microchannel flow: Numerical simulation and uncertainty propagation. *Physics of fluids*, 15:2238.

Dingemans, M. W. (1997). *Water wave propagation over uneven bottoms: Linear wave propagation. Part 1*, volume 13. World Scientific.

Doostan, A. and Owhadi, H. (2011). A non-adapted sparse approximation of pdes with stochastic inputs. *Journal of Computational Physics*, 230(8):3015 3034.

Doucet, A., De Freitas, N., Gordon, N., et al. (2001). *Sequential Monte Carlo methods in practice*, volume 1. Springer New York.

Duruflé, M. and Israwi, S. (2012). A numerical study of variable depth kdv equations and generalizations of camassa holm-like equations. *Journal of Computational and Applied Mathematics*, 236(17):4149 4165.

Eckhardt, R. (1987). Stan ulam, john von neumann, and the monte carlo method. *Los Alamos Sci*, 15:131 143.

Einstein, A. (1905). Über die von der molekularkinetischen theorie der wärme geforderte bewegung von in ruhenden flüssigkeiten suspendierten teilchen. *Annalen der physik*, 322(8):549 560.

Ernst, O. G., Mugler, A., Starkloff, H.-J., and Ullmann, E. (2012). On the convergence of generalized polynomial chaos expansions. *ESAIM: Mathematical Modelling and Numerical Analysis*, 46(02):317 339.

Fishman, G. (1996). *Monte Carlo: concepts, algorithms, and applications*. Springer.

Frauenfelder, P., Schwab, C., and Todor, R. A. (2005). Finite elements for elliptic problems with stochastic coefficients. *Computer methods in applied mechanics and engineering*, 194(2):205 228.

Gardner, C. S., Greene, J. M., Kruskal, M. D., and Miura, R. M. (1967). Method for solving the korteweg-devries equation. *Physical Review Letters*, 19(19):1095 1097.

Gay, D. H. and Ray, W. H. (1995). Identification and control of distributed parameter systems by means of the singular value decomposition. *Chemical Engineering Science*, 50(10):1519 1539.

Gerritsma, M., Van der Steen, J., Vos, P., and Karniadakis, G. (2010). Time-dependent generalized polynomial chaos. *Journal of Computational Physics*, 229(22):8333 8363.

Ghanem, R. (1998). Probabilistic characterization of transport in heterogeneous media. *Computer Methods in Applied Mechanics and Engineering*, 158(3):199 220.

Ghanem, R. (1999a). Ingredients for a general purpose stochastic finite elements implementation. *Computer Methods in Applied Mechanics and Engineering*, 168(1):19 34.

Ghanem, R. (1999b). Stochastic finite elements with multiple random non-gaussian properties. *Journal of Engineering Mechanics*, 125(1):26 40.

Ghanem, R. G. and Spanos, P. D. (1991). *Stochastic finite elements: a spectral approach*. Springer-Verlag.

Giles, M. (2008a). Improved multilevel monte carlo convergence using the milstein scheme. *Monte Carlo and quasi-Monte Carlo methods 2006*, pages 343 358.

Giles, M. B. (2008b). Multilevel monte carlo path simulation. *Operations Research*, 56(3):607 617.

Gilks, W. R., Richardson, S., and Spiegelhalter, D. (1995). *Markov Chain Monte Carlo in practice: interdisciplinary statistics*, volume 2. Chapman & Hall/CRC.

Green, A., Laws, N., and Naghdi, P. (1974). On the theory of water waves. *Proceedings of the Royal Society of London. A. Mathematical and Physical Sciences*, 338(1612):43 55.

Green, A. and Naghdi, P. (1976). A derivation of equations for wave propagation in water of variable depth. *Journal of Fluid Mechanics*, 78(02):237 246.

Hastings, W. K. (1970). Monte carlo sampling methods using markov chains and their applications. *Biometrika*, 57(1):97 109.

Herman, R. and Knickerbocker, C. (1993). Numerically induced phase shift in the kdv soliton. *Journal of Computational Physics*, 104(1):50 55.

Higham, D. (2001). An algorithmic introduction to numerical simulation of stochastic differential equations. *SIAM review*, 43(3):525 546.

Holmes, P., Lumley, J. L., and Berkooz, G. (1998). *Turbulence, coherent structures, dynamical systems and symmetry.* Cambridge University Press.

Hou, T., Luo, W., Rozovskii, B., and Zhou, H. (2006). Wiener chaos expansions and numerical solutions of randomly forced equations of fluid mechanics. *Journal of Computational Physics*, 216(2):687 706.

Hunter, J. K. (2009). Math280: Applied mathematics. Math280 UCDavis class notes.

Israwi, S. (2009). Variable depth kdv equations and generalizations to more nonlinear regimes. *arXiv preprint arXiv:0901.3201.*

Itô, K. (1944). Stochastic integral. *Proceedings of the Japan Academy, Series A, Mathematical Sciences*, 20(8):519 524.

James, F. (2000). Monte carlo theory and practice. *Reports on Progress in Physics*, 43(9):1145 1189.

Jazwinski, A. H. (1970). *Stochastic processes and filtering theory.* Academic Press, New York.

Jolliffe, I. T. (1986). *Principal component analysis*, volume 487. Springer-Verlag New York.

Kloeden, P. and Platen, E. (2011). *Numerical solution of stochastic differential equations*, volume 23. Springer.

Kloeden, P., Platen, E., and Hofmann, N. (1995). Extrapolation methods for the weak approximation of itô diffusions. *SIAM journal on numerical analysis*, 32(5):1519 1534.

Kloeden, P. E. and Platen, E. (1989). A survey of numerical methods for stochastic differential equations. *Stochastic Hydrology and Hydraulics*, 3(3):155 178.

Knio, O. and Le Maitre, O. (2006). Uncertainty propagation in cfd using polynomial chaos decomposition. *Fluid Dynamics Research*, 38(9):616 640.

Komori, Y. (2007a). Multi-colored rooted tree analysis of the weak order conditions of a stochastic runge kutta family. *Applied numerical mathematics*, 57(2):147 165.

Komori, Y. (2007b). Weak second-order stochastic runge kutta methods for non-commutative stochastic differential equations. *Journal of computational and applied mathematics*, 206(1):158 173.

Komori, Y., Mitsui, T., and Sugiura, H. (1997). Rooted tree analysis of the order conditions of row-type scheme for stochastic differential equations. *BIT Numerical Mathematics*, 37(1):43 66.

Korteweg, D. J. and de Vries, G. (1895). On the change of form of long waves advancing in a rectangular canal, and on a new type of long stationary waves. *The London, Edinburgh, and Dublin Philosophical Magazine and Journal of Science*, 39(240):422 443.

Kraichnan, R. H. (1963). Direct-interaction approximation for a system of several interacting simple shear waves. *Physics of Fluids*, 6(11):1603 1609.

Küpper, D., Lehn, J., and Rößler, A. (2007). A step size control algorithm for the weak approximation of stochastic differential equations. *Numerical Algorithms*, 44(4):335 346.

Le Maître, O. and Knio, O. (2010). *Spectral methods for uncertainty quantification: with applications to computational fluid dynamics.* Springer.

Le Maitre, O., Knio, O., Najm, H., and Ghanem, R. (2004a). Uncertainty propagation using wiener-haar expansions. *Journal of Computational Physics*, 197(1):28 57.

Le Maitre, O., Najm, H., Ghanem, R., and Knio, O. (2004b). Multi-resolution analysis of wiener-type uncertainty propagation schemes. *Journal of Computational Physics*, 197(2):502 531.

Le Maître, O., Najm, H., Pébay, P., Ghanem, R., and Knio, O. (2007). Multi-resolution-analysis scheme for uncertainty quantification in chemical systems. *SIAM Journal on Scientific Computing*, 29(2):864 889.

Le Maitre, O. P., Reagan, M. T., Najm, H. N., Ghanem, R. G., and Knio, O. M. (2002). A stochastic projection method for fluid flow: Ii. random process. *Journal of computational Physics*, 181(1):9 44.

Lermusiaux, P. F. (1999). Data assimilation via error subspace statistical estimation. part ii: Middle atlantic bight shelfbreak front simulations and esse validation. *Monthly Weather Review*, 127(7):1408 1432.

Lermusiaux, P. F. (2006). Uncertainty estimation and prediction for interdisciplinary ocean dynamics. *Journal of Computational Physics*, 217(1):176 199.

Lermusiaux, P. F., Chiu, C.-S., Gawarkiewicz, G. G., Abbot, P., Robinson, A. R., Miller, R. N., Haley, P. J., Leslie, W. G., Majumdar, S. J., Pang, A., et al. (2006). Quantifying uncertainties in ocean predictions. Technical report, DTIC Document.

Lermusiaux, P. F. and Robinson, A. (1999). Data assimilation via error subspace statistical estimation. part i: Theory and schemes. *Monthly Weather Review*, 127(7):1385 1407.

Li, Y. A., Hyman, J. M., and Choi, W. (2004). A numerical study of the exact evolution equations for surface waves in water of finite depth. *Studies in Applied Mathematics*, 113(3):303 324.

Lumley, J. L. (2007). *Stochastic tools in turbulence*. Dover Publications.

Luo, W. (2006). *Wiener chaos expansion and numerical solutions of stochastic partial differential equations*. PhD thesis, California Institute of Technology, Department of Applied and Computational Mathematics.

Ma, X. and Zabaras, N. (2009). An adaptive hierarchical sparse grid collocation algorithm for the solution of stochastic differential equations. *Journal of Computational Physics*, 228(8):3084 3113.

Majda, A. J. and Branicki, M. (2012). Lessons in uncertainty quantification for turbulent dynamical systems. *Discrete Contin. Dyn Syst*, 32:3133 231.

Majda, A. J., Franzke, C., and Khouider, B. (2008). An applied mathematics perspective on stochastic modelling for climate. *Philosophical Transactions of the Royal Society A: Mathematical, Physical and Engineering Sciences*, 366(1875):2427 2453.

Majda, A. J., Timofeyev, I., and Vanden Eijnden, E. (2001). A mathematical framework for stochastic climate models. *Communications on Pure and Applied Mathematics*, 54(8):891 974.

Maruyama, G. (1955). Continuous markov processes and stochastic equations. *Rendiconti del Circolo Matematico di Palermo*, 4(1):48 90.

McGrath, E. J. and Irving, D. (1973). Techniques for efficient monte carlo simulation. volume iii. variance reduction. Technical report, DTIC Document.

Miles, J. W. (1981). Korteweg-de vries equation: A historical essay. *Journal of fluid mechanics*, 106:131 147.

Milstein, G. and Tretyakov, M. (2004). *Stochastic numerics for mathematical physics. Scientific Computation*. Springer-Verlag, Berlin.

Moler, C. (2004). *Numerical computing with MATLAB*. Society for Industrial Mathematics.

Müller, P. and Henyey, F. (1997). Workshop assesses monte carlo simulations in oceanography. In *Monte Carlo simulations in oceanography: proceedings, Aha Huliko a Hawaiian Winter Workshop, University of Hawaii at Manoa, January 14-17, 1997*, volume 9, page 201. School of Ocean and Earth Science and Technology.

Najm, H. N. (2009). Uncertainty quantification and polynomial chaos techniques in computational fluid dynamics. *Annual Review of Fluid Mechanics*, 41:35 52.

Najm, H. N., Debusschere, B. J., Marzouk, Y. M., Widmer, S., and Le Maître, O. (2009). Uncertainty quantification in chemical systems. *International journal for numerical methods in engineering*, 80(6-7):789 814.

Newton, N. (1991). Asymptotically efficient runge-kutta methods for a class of ito and stratonovich equations. *SIAM Journal on Applied Mathematics*, 51(2):542 567.

Niederreiter, H. (2010). *Quasi-Monte Carlo Methods.* Wiley Online Library.

Nihoul, J. and Djenidi, S. (1998). Global coastal ocean: the processes and methods. In *Global coastal ocean: the processes and methods*, volume 10, chapter Coupled physical, chemical and biological models. Harvard University Press.

Øksendal, B. (2010). *Stochastic differential equations: an introduction with applications.* Springer.

Orszag, S. A. and Bissonnette, L. (1967). Dynamical properties of truncated wiener-hermite expansions. *Physics of Fluids*, 10:2603.

Osborne, A. (2010). *Nonlinear Ocean Waves & the Inverse Scattering Transform*, volume 97. Academic Press.

Owhadi, H., Scovel, C., Sullivan, T. J., McKerns, M., and Ortiz, M. (2010). Optimal uncertainty quantification. *arXiv preprint arXiv:1009.0679.*

Rayleigh, L. (1876). On waves. *Phil. Mag*, 1(5):257 279.

Rose, A. (2006). *Numerical simulations of the stochastic KDV equation.* PhD thesis, University of North Carolina.

Rößler, A. (2004). Stochastic taylor expansions for the expectation of functionals of diffusion processes. *Stochastic analysis and applications*, 22:1553 1576.

Rößler, A. (2006). Rooted tree analysis for order conditions of stochastic runge-kutta methods for the weak approximation of stochastic differential equations. *Stochastic analysis and applications*, 24(1):97 134.

Rößler, A. (2007). Second order runge-kutta methods for stratonovich stochastic differential equations. *BIT Numerical Mathematics*, 47(3):657 680.

Rößler, A. (2009). Second order runge-kutta methods for itô stochastic differential equations. *SIAM Journal on Numerical Analysis*, 47(3):1713 1738.

Rößler, A. (2010). Runge-kutta methods for the strong approximation of solutions of stochastic differential equations. *SIAM Journal on Numerical Analysis*, 48(3):922 952.

Rümelin, W. (1982). Numerical treatment of stochastic differential equations. *SIAM Journal on Numerical Analysis*, 19(3):604 613.

Russell, J. S. (1844). Report on waves. In *14th meeting of the British Association for the Advancement of Science*, volume 311, page 390.

Sapsis, T. P. (2010). *Dynamically orthogonal field equations for stochastic fluid flows and particle dynamics.* PhD thesis, Massachusetts Institute of Technology, Department of Mechanical Engineering.

Sapsis, T. P. and Lermusiaux, P. F. (2009). Dynamically orthogonal field equations for continuous stochastic dynamical systems. *Physica D: Nonlinear Phenomena*, 238(2324):2347 2360.

Sapsis, T. P. and Lermusiaux, P. F. (2012). Dynamical criteria for the evolution of the stochastic dimensionality in flows with uncertainty. *Physica D: Nonlinear Phenomena*, 241(1):60 76.

Schwab, C. and Todor, R. A. (2006). Karhunen loève approximation of random fields by generalized fast multipole methods. *Journal of Computational Physics*, 217(1):100 122.

Shvartsman, S. Y. and Kevrekidis, I. G. (2004). Nonlinear model reduction for control of distributed systems: A computer-assisted study. *AIChE Journal*, 44(7):1579 1595.

Sirovich, L. (1987). Turbulence and the dynamics of coherent structures. i-coherent structures. ii-symmetries and transformations. iii-dynamics and scaling. *Quarterly of applied mathematics*, 45:561 571.

Soize, C. and Ghanem, R. (2004). Physical systems with random uncertainties: chaos representations with arbitrary probability measure. *SIAM Journal on Scientific Computing*, 26(2):395 410.

Sondergaard, T. (2011). Data assimilation with gaussian mixture models using the dynamically orthogonal field equations. Master's thesis, Massachusetts Institute of Technology.

Sondergaard, T. and Lermusiaux, P. F. (2013a). Data assimilation with gaussian mixture models using the dynamically orthogonal field equations. part i. theory and scheme. *Monthly Weather Review*, 141(6):1737 1760.

Sondergaard, T. and Lermusiaux, P. F. (2013b). Data assimilation with gaussian mixture models using the dynamically orthogonal field equations. part ii: Applications. *Monthly Weather Review*, 141(6):1761 1785.

Stratonovich, R. (1966). A new representation for stochastic integrals and equations. *SIAM Journal on Control*, 4(2):362 371.

Strogatz, S. (2001). *Nonlinear dynamics and chaos: with applications to physics, biology, chemistry and engineering.* Perseus Books Group.

Su, C. and Gardner, C. S. (1969). Korteweg-de vries equation and generalizations. iii. derivation of the korteweg-de vries equation and burgers equation. *Journal of Mathematical Physics*, 10:536.

Talay, D. (1990). Second-order discretization schemes of stochastic differential systems for the computation of the invariant law. *Stochastics: An International Journal of Probability and Stochastic Processes*, 29(1):13 36.

Talay, D. and Tubaro, L. (1990). Expansion of the global error for numerical schemes solving stochastic differential equations. *Stochastic Analysis and Applications*, 8(4):483 509.

Tocino, A. and Vigo-Aguiar, J. (2002). Weak second order conditions for stochastic runge kutta methods. *SIAM Journal on Scientific Computing*, 24(2):507 523.

Ueckermann, M., Lermusiaux, P., and Sapsis, T. (2013). Numerical schemes for dynamically orthogonal equations of stochastic fluid and ocean flows. *Journal of Computational Physics*, 233(0):272 294.

Ursell, F. (1953). The long-wave paradox in the theory of gravity waves. In *Mathematical Proceedings of the Cambridge Philosophical Society*, volume 49, pages 685 694. Cambridge Univ Press.

Van Groesen, E. and Pudjaprasetya, S. (1993). Uni-directional waves over slowly varying bottom. part i: Derivation of a kdv-type of equation. *Wave Motion*, 18(4):345 370.

Vliegenthart, A. (1971). On finite-difference methods for the korteweg-de vries equation. *Journal of Engineering Mathematics*, 5(2):137 155.

Wan, X. and Karniadakis, G. (2005). An adaptive multi-element generalized polynomial chaos method for stochastic differential equations. *Journal of Computational Physics*, 209(2):617 642.

Wan, X. and Karniadakis, G. (2006a). Multi-element generalized polynomial chaos for arbitrary probability measures. *SIAM Journal on Scientific Computing*, 28(3):901 928.

Wan, X. and Karniadakis, G. E. (2006b). Beyond wiener askey expansions: handling arbitrary pdfs. *Journal of Scientific Computing*, 27(1):455 464.

Wiener, N. (1923). Differential space. *Journal of Mathematical Physics*, 2:131 174.

Wiener, N. (1938). The homogeneous chaos. *Amer. J. Math*, 60(4):897 936.

Xiu, D. and Karniadakis, G. E. (2002). The wiener askey polynomial chaos for stochastic differential equations. *SIAM Journal on Scientific Computing*, 24(2):619 644.

Xiu, D. and Karniadakis, G. E. (2003). Modeling uncertainty in flow simulations via generalized polynomial chaos. *Journal of Computational Physics*, 187(1):137 167.

Zabusky, N. J. and Kruskal, M. D. (1965). Interaction of" solitons" in a collisionless plasma and the recurrence of initial states. *Physical Review Letters*, 15(6):240 243.

Zaremba, S. (1968). The mathematical basis of monte carlo and quasi-monte carlo methods. *SIAM review*, 10(3):303 314.

Zhang, Y., Henson, M. A., and Kevrekidis, Y. G. (2003). Nonlinear model reduction for dynamic analysis of cell population models. *Chemical engineering science*, 58(2):429 445.